Effects of Different Iron Species and Redox Imbalance on Iron Homeostasis, Cellular Integrity, and Neuronal Function in *Caenorhabditis elegans*

Dissertation

Zur Erlangung des Doktorgrades

der Naturwissenschaften (Dr. rer. nat.) in der Fachgruppe Chemie und Biologie

der Mathematischen Naturwissenschaftlichen Fakultät

der Bergischen Universität Wuppertal

vorgelegt von

Anna Gremme geb. Reimer

aus Greven

– 2025 –

Dekan:	Prof. Dr. Francesco Knechtli
Erste Gutachterin:	Prof. Dr. Julia Bornhorst
Zweiter Gutachter:	Prof. Dr. Martin Simon
Tag der mündlichen Prüfung:	__.___.____

Introductory Remarks

This thesis has a semi-cumulative format, consisting of three submitted or published papers in peer-reviewed journals as first or co-author (chapters 3 – 5) and unpublished data (included and annotated in chapter 3). Each co-author read the papers and their comments, as well as those of the reviewers and editors, were incorporated into the manuscripts. The published supplementary information is presented in the appendix. Chapters 1 and 2 provide a general overview of the topic of this thesis, and the data obtained are discussed in chapter 6.

To ensure consistency in figure and table numbering and citation throughout this thesis, these may differ from the published papers. Similarly, spelling, abbreviations, or nomenclature may vary across the papers.

As recommended by the NIH, human *GENES* are written in italics and uppercase letters, and human PROTEINS are written in uppercase letters without italics. *C. elegans genes* are written in lowercase italics, and their PROTEINS are written in uppercase letters without italics. A *C. elegans* strain with a loss-of-function mutation is named after the respective gene, followed by ‘Δ’.

Table of Contents

Figures

Tables

Abbreviations

4-HNE	4-hydroxy-2-nonenal
ADP	adenosine diphosphate
AMP	adenosine monophosphate
ATP	adenosine triphosphate
ARE	antioxidant response element
BCL2	B-cell lymphoma 2
BSO	buthionine sulfoximine
C. elegans	*Caenorhabditis elegans*
CE	capillary electrophoresis
CL	cardiolipin
CAT	catalase
CNS	central nervous system
Cer	ceramide
CP	ceruloplasmin
TCA	citric acid cycle
Co	cobalt
CoQ10	coenzyme Q10
Cu	copper
CTR1	copper transporter 1
DNA	deoxyribonucleic acid
DEM	diethyl maleate
DIC	differential interference contrast
DEG	differentially expressed genes
DHODH	dihydroorotate dehydrogenase
DMT1	divalent metal transporter 1
DCYTB	duodenal cytochrome b
ETC	electron transport chain
ER	endoplasmic reticulum

E. coli	*Escherichia coli*
EFSA	European Food Safety Authority
FTN	ferritin
FTH	ferritin heavy chain
FTL	ferritin light chain
FPN	ferroportin
FSP1	ferroptosis suppressor protein 1
FLD	fluorescence detector
FOXO	forkhead box 0
DGE	German Nutrition Society
GCL	glutamate cysteine ligase
GCLC	glutamate-cysteine ligase catalytic subunit
GGT	glutamyltranspeptidase
GSH	glutathione
GSSG	glutathione disulfide
GPX	glutathione peroxidase
GR	glutathione reductase
GST	glutathione-S-transferase
GFP	green fluorescence protein
GCH1	GTP cyclohydrolase 1
HCP1	heme carrier protein 1
hrg	*heme responsive genes*
HP	hephaestin
HexCer	hexosylceramide
HPLC	high pressure liquid chromatography
HFE	homeostatic iron regulator
HIF	hypoxia-inducible factor
IIS	insulin/insulin-like growth factor-1 signaling
IGF-1	insulin-like growth factor-1

ICP	ion coupled plasma
Fe	iron
IDE	iron dependent enhancer
$FeCl_2$	iron(II) chloride
FeGlu	iron(II) gluconate
FAC	iron(III) ammonium citrate
IRE	iron-responsive element
IRP	iron-responsive protein
Fe-S	iron-sulfur cluster
LIP	labile iron pool
L1	larval stage 1
Lip-1	liproxstatin-1
LPC	lysophosphatidylcholine
LPE	lysophosphatidylethanolamine
MDA	malondialdehyde
Mn	manganese
MS	mass spectrometry
mRNA	messenger ribonucleic acid
MT	metallothionein
FTMT	mitochondrial ferritin
UPR^{mt}	mitochondrial unfolded protein response
MAF	musculoaponeurotic fibrosarcoma
NGM	nematode growth medium
NADH	nicotinamide adenine dinucleotide, reduced
NAD+	nicotinamide adenine dinucleotide, oxidized
NADPH	nicotinamide adenine dinucleotide phosphate
NTBI	non-transferrin-bound iron
NRF2	nuclear factor-erythroid 2 related factor 2
NMR	nuclear magnetic resonance

OES	optical emission spectroscopy
OXPHOS	oxidative phosphorylation
PNS	peripheral nervous system
PC	phosphatidylcholine
PE	phosphatidylethanolamine
PS	phosphatidylserine
PI	phosphoinositol
PL	phospholipid
PE-O	plasmanyl-phosphatidylethanolamine
PCBP	poly(c)-binding protein
PUFA	polyunsaturated fatty acid
PCA	principal component analysis
RONS	reactive oxygen and nitrogen species
RT-qPCR	reverse transcription-quantitative polymerase chain reaction
SF	serum ferritin
SL	sphingolipid
SM	sphingomyelin
SEM	standard error of the mean
SOD	superoxide dismutase
tBOOH	*tert*-butyl hydroperoxide
BH4	tetrahydrobiopterin
TRX	thioredoxin
TIBC	total iron binding capacity
TF	transferrin
TFR	transferrin receptor
TSAT	transferrin saturation
WHO	World Health Organization
Zn	zinc
ZIP	Zrt/Irt-like protein

Summary

Iron (Fe) is the most abundant essential trace element across almost all organisms, and is involved in important biological processes such as DNA synthesis, energy production, and oxygen transport. Its redox cycling between the physiologically relevant oxidation states Fe(II) and Fe(III) is crucial for these functions, but also drives the formation of reactive oxygen and nitrogen species (RONS) through the Fenton reaction. Excessive RONS production impairs cellular function and integrity, underscoring the importance of an effective antioxidative defense system in maintaining cellular homeostasis. Glutathione (GSH), the most abundant intracellular antioxidant, plays an essential role in this defense by acting as a radical scavenger but also as an important co-enzyme in various metabolic and detoxification processes. In the general population, Fe is mainly taken up through drinking water, food, and food supplements, and in 2024, the European Food Safety Authority (EFSA) defined safe intake levels of 10 mg/day for children and 40 mg/day for adults. To investigate the consequences of elevated Fe levels in relation to different Fe species and a weakened antioxidative system, the model organism *Caenorhabditis elegans* (*C. elegans*) was used in this thesis. In a further study, the consequences of elevated copper (Cu) levels on genes involved in Fe homeostasis were investigated, highlighting potential targets of trace element interactions, especially in the case of overexposure.

To investigate the impact of excess Fe from different Fe species on Fe homeostasis, oxidative stress, and cell death, *C. elegans* was exposed via the diet to 0.5 mM or 1 mM Fe(III) ammonium citrate (FAC), Fe(II) gluconate (FeGlu), or Fe(II) chloride ($FeCl_2$) separately for either 5 h or 24 h. These treatments demonstrated that Fe bioavailability depends on both the oxidation state and ligand of the Fe compound, with FAC resulting in the lowest and $FeCl_2$ in the highest total Fe content. However, the effects on oxidative stress, cell death, and Fe homeostasis were Fe species-unspecific. In addition to increased

mitochondrial RONS, the Fe species led to increased translocation of the transcription factor DAF-16/FOXO, increased superoxide dismutase activity, and increased apoptosis in germ line cells. All tested Fe species led to decreased gene expression of the metal transporter *smf-3*/*DMT1* and increased gene expression of the Fe storage protein *ftn-1*/*FTN*. Furthermore, gene expression analysis and total Fe measurements in the corresponding deletion mutants suggest an involvement of the reductase *f55h2.5*/*DCYTB* and Cu storage protein *f21d5.3*/*CP* in Fe homeostasis, both of which have been poorly studied in *C. elegans*. In summary, this study showed that although the total Fe content varied greatly after treatment with the Fe species, the effects on the examined endpoints were similar. This could be due to tightly regulated Fe homeostasis, as several genes associated with this were differently expressed after treatment with each Fe species.

The investigations of the consequences of excess Fe in combination with GSH depletion were carried out after treating *C. elegans* L4 for 24 h with FAC and/or subsequent treatment with diethyl maleate (DEM) for 2 h or 24 h. DEM is a well-established compound used to deplete GSH levels by conjugating with the thiol group of GSH. FAC treatment led to a fivefold increase in total Fe compared to untreated control, which was still three times increased 24 h later without additional FAC supply. Unchanged Fe(II) levels and increased gene expression of *ftn-1* indicate storage of Fe as Fe(III). Nevertheless, FAC treatment led to increased levels of subclasses of phospho- (PL) and sphingolipids (SL) and the neurotransmitter acetylcholine. The binding product of DEM and GSH could be determined using HPLC-MS/MS, revealing that the 2 h DEM treatment resulted in a 70% depletion of GSH. In addition, this treatment led to a 15% decrease in survival rate and an increase in Fe(II) level. Differently regulated genes associated with Fe homeostasis underscore the impact of DEM treatment on Fe homeostasis. In addition, DEM decreased mitochondrial mass after both treatment times, increased the levels of several subclasses of PL and SL after

24 h treatment, and had an effect on neurotransmitter metabolism. These findings were further supported by altered gene expression levels of genes associated with these pathways, as revealed by transcriptomic analysis. The combined treatment with FAC and DEM had no further effect on the tested endpoints compared to treatment with FAC or DEM alone. Additional treatment with the ferroptosis inhibitor liproxstatin-1 (Lip-1) led to a slight increase in survival rate after FAC and DEM treatment, but was unable to raise it to the level of the untreated control. In addition, Lip-1 had no impact on the effects caused by FAC and DEM. Since only one ferroptosis marker was examined, it is difficult to conclude whether ferroptosis plays a role after treatment with FAC and DEM and requires further investigations. Nevertheless, this study revealed that both FAC and DEM affected endpoints relevant for cellular and organismal integrity and function. In addition, counter-regulation and long-lasting effects were demonstrated in this study.

Both Fe-related studies showed that metal homeostasis may play an important role, which is further emphasized in the study investigating the consequences of dysfunctional Cu homeostasis. Cu dyshomeostasis was modeled by using deletion mutants of the Cu chaperone *atox-1* and Cu storage protein *f21d5.3*/*CP*. This study revealed that the deletion of the Cu chaperone *atox-1* after treatment of *C. elegans* L4 for 24 h with $CuSO_4$ led to changes in energy nucleotides, neurotransmitter levels, and increased levels of malondialdehyde (MDA), a byproduct of lipid peroxidation. In the *f21d5.3*/*cp*Δ mutant, the same treatment also led to alterations in energy nucleotide, MDA, and cardiolipin (CL) levels, but even without $CuSO_4$ treatment, neuronal endpoints were altered compared to wild type worms. The MDA levels could be reliably measured by optimizing and validating the measurement in this thesis using HPLC-FLD. Overall, this study demonstrated that functional Cu homeostasis is important for cellular functions and neuronal stability.

Taken together, this thesis demonstrates that the Fe species matters, and that despite the regulated expression of Fe homeostasis genes, likely due to counter-regulatory mechanisms, the treatments affected endpoints related to oxidative stress and cell death. Furthermore, it was shown that *C. elegans* is a suitable model organism for investigating Fe homeostasis. In addition, it is shown that an impaired redox system can lead to alterations in mitochondria, lipidome, and neurological endpoints. All three studies suggest that metal homeostasis plays a crucial role in maintaining organismal viability.

Chapter 1 – Motivation and Scope of the Thesis

Chapter 1 – Motivation and Scope of the Thesis

Motivation of the Thesis

Iron (Fe) is an essential trace element and crucial for many biological processes. In the general population, Fe is mostly associated with a deficiency of this element, but few people are aware that an accumulation or excess intake of Fe may lead to adverse effects. It has been known since 1894 that Fe can lead to the excessive formation of reactive oxygen and nitrogen species (RONS) via the Fenton reaction and that excess Fe levels are associated with oxidative stress, cell death, and neurodegenerative diseases.[1] These negative effects are the reason why the European Food Safety Authority (EFSA) has defined safe intake levels for Fe of 10 mg/day for children and 40 mg/day for adults in 2024.[2] Fe occurs in natural and fortified foods, food supplements, and drinking water in a variety of Fe compounds, and various Fe species are used in scientific studies associated with Fe. Even though it has been shown before that different Fe species have varying bioavailability, there is still a lack of studies investigating effects of Fe compounds at the cellular level. In addition, it is not fully understood which pathways are involved in Fe toxicity, particularly in relation to the Fe-dependent cell death, ferroptosis.[3] In this context and in relation to neurodegenerative diseases, the involvement of glutathione (GSH) is discussed as an antioxidant but also as a complexing molecule in the labile iron pool (LIP).[4] However, studies investigating the consequences of elevated Fe levels in combination with GSH deficiency in living organisms are limited.

This thesis aimed to fill these gaps in knowledge and uncover more about possible pathways linked to elevated Fe levels, caused by different Fe species and GSH depletion, using *Caenorhabditis elegans* (*C. elegans*) as a model organism. To investigate the involvement of different genes, *C. elegans* deletion mutants were used, and RT-qPCR and transcriptomic analysis were performed. Furthermore, various analytical instrumentation, dye assays, and behavioral assays were used to investigate detailed metabolic processes.

Scope of the Thesis

- Comparison of the impact of different Fe species on Fe homeostasis, oxidative stress, and cell death in *C. elegans*
- Investigations of an impaired redox system in *C. elegans* regarding Fe homeostasis, oxidative stress, lipidome, neurotransmitters, and whether these lead to ferroptotic cell death
- Optimization and validation of a MDA measurement method via HPLC-FLD for measurement in *C. elegans* samples and application in studies investigating Fe and Cu homeostasis

Chapter 2 – General Background Information

Chapter 2 – General Background Information

2.1 Iron (Fe)

Fe is the fourth most abundant element in the earth crust, the most abundant trace element in the human body, and essential for almost all organisms, from bacteria to plants, animals, and humans.[5,6] Essential processes such as oxygen transport, energy production, and DNA synthesis and repair are dependent on Fe as a key compound.[7,8] From a chemical point of view, Fe is the 26th element in the periodic table of elements and therefore a transition metal, which is thermodynamically most stable in the oxidation states Fe(II) and Fe(III).[9] These forms are physiologically most relevant and are taken up by humans generally complexed or bound to biomolecules like proteins, mainly through drinking water, food, and food supplements. Food rich in Fe includes red meat, legumes, and nuts, but whole grain products and vegetables are also important sources.[10] In 2024, the EFSA estimated that, based on the Fe content of consumed food, adult men take up to 13.7 mg Fe/day and women 10.9 mg Fe/day. Furthermore, the EFSA established a safe level of Fe intake of 40 mg/day for all adults, using the occurrence of black stools as an endpoint.[2] In addition, the German Nutrition Society (DGE) recommended in 2023 a daily Fe uptake of 11 mg for men and 14 – 16 mg for women, making a distinction between pre-menopausal and post-menopausal women and giving an additional recommendation for pregnant women of 27 mg/day.[11] These studies indicate that in the general population, adult men tend to take in slightly more Fe than recommended, and women slightly less. Still, it should be noted that the bioavailability of Fe from different food sources can vary a lot.[12] In addition to other Fe species, meat and seafood mainly contain heme Fe, which has a higher bioavailability than nonheme Fe.[13] Drinking water and plant-based foods and food supplements contain only nonheme Fe, mainly Fe(III), which have a lower bioavailability per se and can be exacerbated when bound to plant components such as phytate.[14] In addition, there are foods fortified with nonheme Fe worldwide, such as rice, flour, and

cereals, which are intended to prevent Fe deficiency in the general population or target groups such as children.[15]

The absorption of orally supplied Fe occurs primarily in the duodenum and proximal jejunum, where mainly enterocytes form the epithelial layer. While 15 – 35% of heme Fe is absorbed, the absorption rate of nonheme Fe is less than 10%.[12] As there is no active excretion mechanism for Fe in humans, only small amounts are excreted through sweat, urine, bleeding, and shed enterocytes in the intestinal lumen.[16–18]

2.1.1 Iron Homeostasis

To maintain a balance between essential and excessive amounts of Fe, the regulation of Fe-homeostasis is of major importance. While nonheme Fe(II) is mainly imported into the enterocytes via divalent metal transporter 1 (DMT1), Fe(III) has to be reduced to Fe(II) by a reductase such as duodenal cytochrome b (DCYTB) or by reducing compounds such as ascorbic acid from food (Figure 1).[19] It is assumed that heme Fe is imported into the enterocytes via endocytosis, i.e., via cell membrane-enclosed vesicles and a membrane transporter, but this is not yet fully elucidated. The involvement of heme carrier protein 1 (HCP1) was discussed for a long time, but has been rejected, as it turned out to have a high affinity for folate.[20] Within the cell, Fe can be stored as less reactive Fe(III) in the cytosolic storage protein ferritin (FTN), which in humans consists of the two subunits ferritin heavy (FTH) and light chain (FTL). Together, the subunits form a cavity, and while FTH has ferroxidase activity for oxidizing Fe(II) to Fe(III), FTL is the storage site for up to 4500 Fe ions.[21] The copper (Cu) storage protein ceruloplasmin (CP) also shows ferroxidase activity and is discussed to be involved in Fe storage in ferritin.[22] In case of low Fe within the cell, ferritinophagy can degrade ferritin, and the Fe ions can be released into the cytosol.[23] Here, a small part of the intracellular Fe forms the LIP, consisting of Fe(II) complexed to low molecular weight molecules, such as GSH, and Fe chaperons, like poly C-binding proteins (PCBPs).[4,24] It is still under discussion

whether, in the form of these complexes, Fe is delivered intracellularly to FTN, apoenzymes, and other cell organelles such as mitochondria and the endoplasmic reticulum (ER).[24] However, mitoferrin 1 and 2 are probably mainly responsible for Fe import into the mitochondria.[25] The transport in this organelle is of particular importance, as this is the main synthesis site for Fe-sulfur (Fe-S) cluster and Fe-porphyrin complexes, also known as heme. These are the main structures in which Fe is incorporated into proteins to function as an important cofactor.[26] To maintain Fe homeostasis within the mitochondria, mitochondrial ferritin (FTMT) controls the availability of Fe.[27] At the basolateral membrane of the cell, Fe export is carried out by the transport of Fe(II) via ferroportin (FPN) into the bloodstream and conversion to Fe(III) by the membrane-associated Cu dependent ferroxidases hephaestin (HP) or CP.[28,29] In the bloodstream, Fe(III) occurs bound to FTN, the Fe transport protein transferrin (TF), or as non-transferrin-bound Fe (NTBI).[30–32] Fe-loaded TF can bind to transferrin receptors (*TFR*) of other cells and is taken up via endocytosis, followed by a pH-dependent intracellular Fe(II) release through DMT1.[26] On the basolateral side of enterocytes and other organs, such as liver, pancreas, and heart, NTBI can be imported via DMT1 or the Zrt/Irt-like proteins (ZIP) ZIP8 and ZIP14.[33,34]

To adapt these intracellular processes depending on the Fe status, i.e., a deficiency or repletion, there are several regulatory factors. An important one is the activation or inactivation of iron-responsive proteins (IRP), which regulate post-transcriptionally the synthesis or degradation of, for example, DMT1, FTN, FPN, and TF by binding to iron-responsive elements (IRE) of the untranslated region of the respective mRNA.[35] In addition, systemic Fe homeostasis is regulated by binding of the peptide hormone hepcidin to FPN, resulting in occlusion or degradation of this exporter.[36] However, synthesis of hepcidin is not only stimulated by Fe, but also by inflammation.[37] In the event of Fe or oxygen deficiency, transcription factors called hypoxia-inducible factors (HIFs) are activated, which are involved in the regulation of DCYTB, DMT1, TF, CP,

FPN, and hepcidin.[38] Especially, HIF2α plays an important role in the intestinal absorption of Fe.[39]

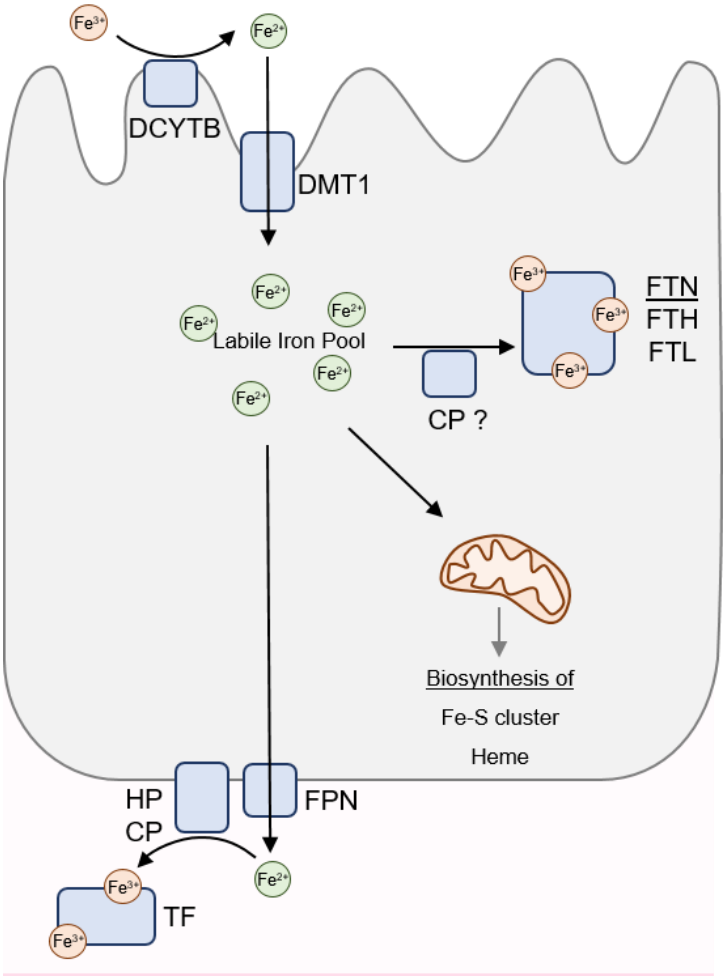

Figure 1. Simplified illustration of the Fe homeostasis in human enterocytes. [Adapted and modified from Galy et al.][26]

2.1.2 Physiological Relevance

Due to the interconversion between Fe(II) and Fe(III), Fe is an important biological catalyst and thus an essential cofactor of several proteins and enzymes. Hemoglobin and myoglobin, which are involved in oxygen transport, build the largest proportion of these proteins.[40] Bound to hemoglobin, the central Fe(II) reversibly binds oxygen from the lungs for transport through the bloodstream to all organs, or it binds to carbon monoxide, nitric oxide, alkyl

isocyanide, and nitroso-compounds to transport them out of the organism.[41] If the Fe ion is oxidized to Fe(III), these molecules no longer bind to the so-called methemoglobin, but other molecules such as H_2O, cyanide, or azide can bind to it.[41] Myoglobin is found in the heart and red muscle cells, where it stores oxygen and facilitates its transport intracellularly to the oxygen-consuming mitochondria.[42] Within the mitochondria, complexes I – IV contain Fe as a cofactor, which are parts of the mitochondrial respiratory chain, and Fe is therefore involved in the energy production in the form of adenosine triphosphate (ATP). Fe enables electron transport between the complexes, through to complex IV (cytochrome c oxidase), where reduction of O_2 to H_2O takes place.[43,44] In deoxyribonucleic acid (DNA) replication and repair, the activity of several proteins, such as polymerases, primases, and helicases, is dependent on Fe-S clusters.[8] In addition, there are ribonucleotide reductases, which are involved in the synthesis of deoxyribonucleotides, which are dependent on Fe as Fe(II) tyrosyl radical.[45]

2.1.3 Fe Deficiency and Overload

There are a number of diseases that are associated with either Fe deficiency or elevated Fe levels. An Fe deficiency can be caused, among others, by insufficient absorption through diet, chronic blood loss, or a high Fe requirement, e.g., during pregnancy or in high-performance athletes.[46–48] Insufficient absorption through diet can be caused by low-Fe food but also by malabsorption, i.e., illness or disorders of the gastrointestinal tract.[49] Probably the best-known consequences of an Fe deficiency are reduction in erythrocytes and low hemoglobin concentrations, the most common causes of anemia.[50] The resulting impaired transport of oxygen to organs and the decreased activity of Fe-dependent proteins can lead to non-specific symptoms such as fatigue, weakness, and reduced concentration, often causing the condition to remain undiagnosed.[50] Severe Fe deficiency can cause adverse consequences such

as heart diseases, restless leg syndrome, and impaired child neurocognitive development.[46]

The most common genetically caused disease worldwide leads to an excess of Fe, often due to low hepcidin concentration, and is called hemochromatosis.[37] The most prevalent cause is a homozygous mutation of the *homeostatic Fe regulator* (*HFE*), but other mutations as of *FPN1* and *TFR2,* can also lead to this disease.[51] Affected individuals can prevent this excess Fe by regular phlebotomy, as untreated hemochromatosis can lead to severe liver damage and diabetes.[52] The homozygous mutation of *CP* leads to aceruloplasminemia, associated with Fe deficiency in the plasma and thus to anemia, but also with cellular Fe overload.[53] In addition, there are non-genetically caused diseases, such as chronic liver diseases, which can lead to secondary Fe overload.[54]

For clinical indications of a Fe deficiency or overload in humans, certain biomarkers like serum ferritin (SF), transferrin saturation (TSAT), total Fe binding capacity (TIBC), and the ratio of soluble transferrin receptor to ferritin can be measured in the serum.[2] Even though SF is often measured and used as an indicator of Fe deficiency, this value can be increased by various factors such as infections or inflammation.[55] In 2020, the World Health Organization (WHO) released thresholds for SF in healthy men (> 200 µg/L), menstruating women (> 150 µg/L), and non-healthy individuals (> 500 µg/L) that, if exceeded, may indicate an Fe overload. According to the WHO, SF values < 12 µg/L in children and < 15 µg/L in adults are indicative of Fe deficiency. In the presence of inflammation or infection, the thresholds are raised to < 30 µg/L or < 70 µg/l, respectively. However, the WHO also indicates that further markers should be included for a reliable diagnosis.[56] The TSAT could be measured as well, since it remains unchanged if SF falsely indicates Fe overload. TSAT values over 40% indicate systemic Fe overload and are often the first indication of hemochromatosis.[2]

2.2 Oxidative Stress

The main risk of excessive Fe amounts is its ability to promote oxidative stress. As early as 1894, Fenton described the oxidation of tartaric acid in the presence of Fe(II) and hydrogen peroxide.[1] Nowadays, it is known that Fe(II) has a reducing effect and can therefore form RONS as shown in Figure 2.[57] In low concentrations, RONS are important signaling molecules and are involved in cellular processes such as proliferation, migration, and the regulated cell death, apoptosis.[58] However, as these species have unpaired valence electrons or unstable bonds, they have an oxidative effect and react with biomolecules such as proteins, lipids, and DNA.[59] These adverse modifications can lead to profound consequences for cellular function, integrity, and even cell death.[60] In addition to Fe, other metals such as Cu and cobalt (Co) also have the property of causing Fenton-like reactions.[61] Further sources of RONS can also be cellular processes, such as oxidative phosphorylation in the mitochondrial respiratory chain.[60] Under optimal conditions, cells have a large number of molecules, proteins, and signaling pathways that have antioxidative effects and prevent or repair damage caused by reactive species.[62] However, if there is an imbalance between the reactive species and the antioxidants, for example, in case of excessive RONS production, that is defined as oxidative stress.[63] Several diseases, such as cancer, cardiovascular diseases, and neurodegenerative diseases, are associated with excessive RONS production and oxidative stress.[64]

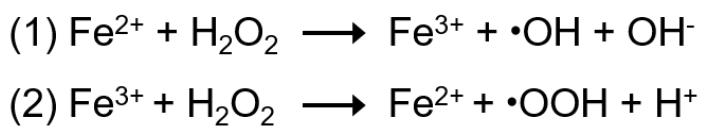

Figure 2. Fe-catalyzed formation of reactive oxygen species via the Fenton reaction. [Adapted and modified from Meng et al.][65]

2.2.1 Antioxidative System

In principle, the antioxidative system against Fe-derived RONS involves Fe homeostasis-associated proteins, since FTN and TF bind the element as less reactive Fe(III).[66] Additionally, the IRP/IRE system can be regulated by RONS and thus impact the availability of reactive Fe(II) as well.[35] RONS can also activate transcription factors, which can lead to increased formation of antioxidative proteins. One of the most important factors is nuclear factor-erythroid 2 related factor 2 (NRF2), which accumulates in the nucleus in response to oxidative stress. Bound to small musculoaponeurotic fibrosarcoma proteins (MAF), the heterodimer binds to antioxidant response element (ARE)/electrophile responsive element of cytoprotective genes such as superoxide dismutase (SOD), catalase (CAT), and glutathione peroxidase (GPX) and thus stimulates their transcription.[67] SOD and CAT convert reactive species such as oxygen anions and hydrogen peroxide to less reactive compounds.[68,69] In this process, SOD is dependent on Cu, zinc (Zn), and manganese (Mn), whereby Cu/Zn-SOD is mainly found in the cytosol and Mn-SOD exclusively in the mitochondria.[68] In plants and certain bacteria, cytosolic Fe-SOD also exists.[70] GPX4, as one representative of the GPX family, reduces the lipid hydroperoxides in cell membranes, formed by RONS, to alcohols. For this, GPX4 requires the peptide GSH as a cofactor, which is discussed in more detail in 2.3.1.1. Other GPX orthologs also have antioxidative effects and can reduce H_2O_2 and fatty acid hydroperoxides in the cytosol.[71] Along with GPX, Glutathione-S-transferases (GSTs) are part of the antioxidative system by binding GSH to xenobiotics or byproducts of lipid peroxidation.[72] Equally important transcription factors are the four proteins of the Forkhead box 0 (FOXO) family. In addition to RONS-suppressing enzymes such as SOD and CAT, target genes of FOXO are further involved in metal homeostasis, such as CP and metallothionein (MT), and genes involved in the repair of biomolecules like thioredoxin (TRX).[73]

2.2.1.1 Glutathione

GSH is the most abundant antioxidative molecule in human cells, which itself serves as a radical scavenger and an important cofactor of several enzymes.[74] Intracellular ATP-dependent GSH synthesis occurs in the cytosol from the three amino acids glutamate, cysteine, and glycine, whereby the availability of cysteine and the activity of glutamate cysteine ligase (GCL), the first step of GSH synthesis, are the rate-limiting factors.[75] Since cysteine is extracellularly unstable, it is imported as cystine through the antiporter system x_c^- and reduced to cysteine in the cytosol.[76] GSH contained in food or the bloodstream cannot be absorbed by cells and must first be degraded into the amino acids by γ-glutamyltranspeptidase (GGT).[75] 80 – 85% of the cellular GSH stays in the cytosol, 10 – 15% is found in the mitochondria, and < 1% is in the ER. [77] When scavenging radicals or as a co-enzyme of GPX4, GSH reacts with another GSH molecule to form its oxidized form, glutathione disulfide (GSSG) (Figure 3). However, GSSG can be reduced back to two GSH molecules by glutathione reductase (GR).[78] In addition to its antioxidative function, GSH is bound to xenobiotics by GST in phase II of the xenobiotic metabolism to achieve water solubility and excretion of the substances.[72]

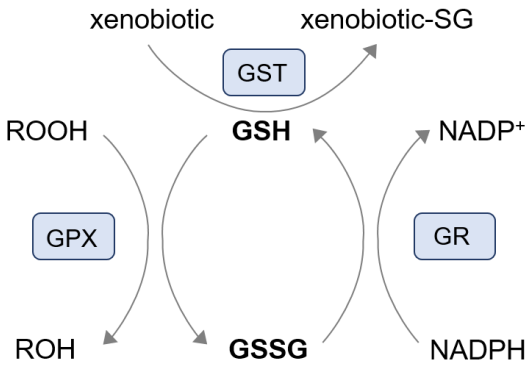

Figure 3. Schematic overview of GSH-dependent enzymes. [Adapted and modified from Johnson et al.][79]

As GSH is involved in many important processes, a deficiency is associated with several diseases such as cancer, neurodegenerative diseases, and

cardiovascular diseases.[80] Since cysteine is a semi-essential amino acid, GSH deficiency can be caused by disrupted cysteine metabolism or a low-cysteine/cystine diet. Ageing can also be a risk factor for low GSH amounts, as the metabolism can be impaired.[81,82] In rare cases, there are inborn defects in the enzymes associated with GSH synthesis, which can also lead to a deficiency of this peptide.[80] There are several ways to induce GSH depletion in the laboratory and thus investigate mechanistic consequences, with diethyl maleate (DEM) and buthionine sulfoximine (BSO) being the most commonly used molecules. DEM binds spontaneously or through GSTs to the thiol group of GSH, thereby preventing it from acting as an antioxidant (Figure 4).[83] BSO, on the other hand, inhibits GCL and thus suppresses GSH synthesis.[84]

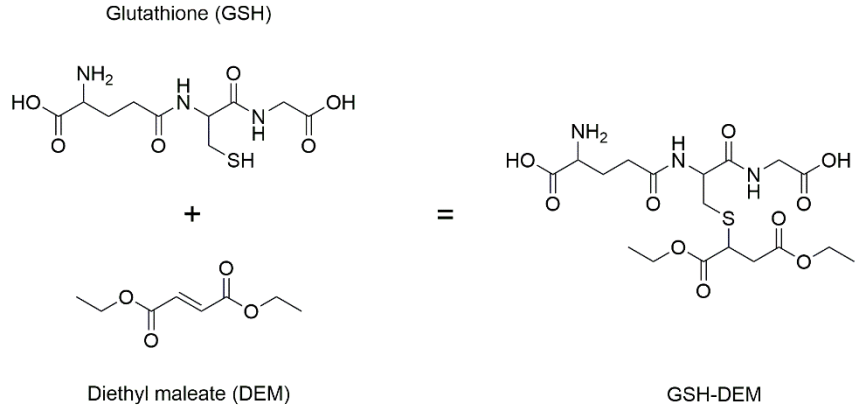

Figure 4. Simplified scheme of the reaction between GSH and DEM. [Adapted and modified from Kubal et al.][83]

2.2.2 Mitochondrial RONS Homeostasis

The mitochondria play a crucial role not only in energy production but also in cell signaling and, thus, in the maintenance of cellular homeostasis.[85] More than 90% of cellular energy is produced in the form of ATP via an interplay of citric acid cycle (TCA), electron transport chain (ETC), and oxidative phosphorylation (OXPHOS) in the mitochondria.[86] However, this crucial process also leads to the formation of RONS, which are mainly generated as superoxide anions ($O_2^{\bullet}$) and hydrogen peroxide (H_2O_2) by electrons released from complex I and III of

the ETC.[87] Fe, which is present in high quantities in the mitochondria due to its incorporation into the Fe-dependent co-factors, also contributes to RONS formation. In addition, it is being discussed whether Fe is increasingly transported into the mitochondria during oxidative stress, as was observed in cardiomyocytes when tert-butyl hydroperoxide (tBOOH) was applied.[88] For these reasons, mitochondria are supposed to be highly vulnerable to oxidative stress, which can lead to mitochondrial fragmentation, swelling, or shortening.[87] Various factors, including oxidative stress, activate the mitochondrial unfolded protein response (UPR^{mt}), which initiates a transcriptional program in the mitochondria and nucleus to ensure mitochondrial function.[89] These include fusion and fission processes to ensure that the pro-inflammatory content of impaired mitochondria does not enter the cytosol in an uncontrolled manner. While damaged mitochondria are repaired by further mitochondria during fusion, the mitochondrion is divided during fission, and the damaged part is degraded by mitophagy.[90] The integrity, functionality, and amount of this organelle are often used as oxidative stress markers and are discussed in context of cell death and neurodegenerative diseases.[91,92] However, a small non-damaging amount of mitochondrial RONS can act as secondary messengers and alter signal transduction by oxidizing proteins like phosphatases, kinases, proteases, and transcription factors. Mitochondrial RONS can therefore also be positively involved in the regulation of growth factors, cell proliferation and differentiation, cellular oxygen sensing, and hypoxia.[87] To maintain a balance, there are, as already mentioned, high concentrations of GSH and mitochondrial-specific enzymes like Mn-SOD, GPX4, and FTMT.[27,77,93]

2.2.3 Lipidome as Target of Oxidative Stress

In addition to proteins and DNA, lipids are common targets of RONS, with lipids localized in cell membranes being widely discussed in this context.[94] The variety of different structures of the lipids due to the composition of the hydrophilic head group and the degree of unsaturation in the lipophilic fatty acids enables

adapted forms of the bilayer membranes, but also the incorporation and interaction with a wide range of proteins.[95] Phospholipids (PL) such as phosphatidylcholine (PC) and phosphatidylethanolamine (PE), along with cholesterol, are the most abundant lipids of cell membranes, although sphingolipids (SL) are also important constituents.[96] However, the electron-rich double bonds make a higher-grade unsaturated fatty acid more vulnerable to the reaction with RONS.[97] In this reaction, the lipid radical formed at the beginning reacts with oxygen to form a lipid peroxyl radical, which can react with further unsaturated fatty acids to form a lipid hydroperoxide and simultaneously trigger a chain reaction.[97,98] These hydroperoxides can be converted by GPX to a less reactive alcohol, but can react further to the cleavage of reactive aldehydes such as malondialdehyde (MDA) and 4-hydroxy-2-nonenal (4-HNE).[71,99] This not only leads to a reorganization of the lipid composition through the formation of less unsaturated and shorter fatty acids, but also to the formation of adducts between the aldehydes and other biomolecules.[99] The oxidized lipids, as well as the aldehydes themselves and their formed adducts, are often used as markers for oxidative stress. However, 4-HNE is further involved as a signaling molecule in stress response pathways and regulates NRF2, among others.[100] The antioxidant α-tocopherol, known as vitamin E, plays a crucial role *in vivo*, as its lipophilic structure allows it to be incorporated into cell membranes and thus prevents lipid peroxidation.[101] While some lipid classes like PC and PE are present in high amounts in every type of cell membrane, other lipids such as cardiolipins (CL) are found exclusively in the mitochondrial membrane and thus serve as markers for changes in this organelle.[96,102]

2.3 Cell Death

Every day, probably 10^{11} cells undergo a programmed cell death in a human body, which already plays an important role in the fetus in the formation of organs and structures, for example, in the separation of fingers.[103,104] If the

damage to a dysfunctional, infected, or mutated cell becomes too severe and can no longer be repaired, programmed cell death is initiated. This allows a controlled degradation of the cell, preventing further proliferation and the uncontrolled release of pro-inflammatory contents.[105] Cell proliferation balances cell death, whereby an imbalance with enhanced proliferation can lead to diseases such as cancer, and with increased cell death to degenerative diseases, e.g., neurodegeneration.[106] In addition to genetically programmed cell deaths such as apoptosis, necroptosis, and pyroptosis, there are also types, such as necrosis or ferroptosis, that occur in an uncontrolled manner.[107]

2.3.1 Apoptosis

To date, it is one of the most studied types of cell death, which is mainly triggered by two pathways, the intrinsic and the extrinsic. Both pathways activate a cascade of caspases, with intracellular causes such as impaired homeostasis or DNA damage in the intrinsic pathway and extracellular signaling often by lymphocytes in the extrinsic pathway.[108]

In the intrinsic pathway, oligomerization of proteins of the B-cell lymphoma 2 (BCL2) family leads to pores in the outer mitochondrial membrane, resulting in permeabilization and the release of cytochrome c.[109,110] This leads to the formation of apoptosomes, which are a complex including cytochrome c and procaspase-9, and activate the apoptosis initiator caspase-9. This starts the cascade and leads to the activation of caspase-3 and -7, which in turn activate further procaspases through cleavage.[111] An important proapoptotic regulator of this pathway is the transcription factor p53, which triggers the expression of several BCL2 proteins in response to DNA damage.[108,112]

The extrinsic pathway involves the activation of death receptors like Fas on the cell surface, which oligomerize by binding ligands and lead to activation of caspase-8 and -10.[113] These are parts of the death-inducing signaling complex, which in turn leads to activation of the effector caspases-3, -6, and -7.[108]

This caspase then leads to apoptotic cell death, which is characterized by breakdown of the nuclear membrane and genomic DNA, cleavage of intracellular proteins, and membrane blebbing.[108] In addition, among others, nucleosomes and apoptotic extracellular vesicles are released, and phosphatidylserine (PS) is delocalized to the outer cell membrane as an “eat me” signal. This enables phagocytotic cells to recognize the dying cell and engulf it to avoid the release of pro-inflammatory contents.[114] To identify apoptotic cells, there are several assays based on the detection of membrane permeability, mitochondrial damage, caspase activity, p53 activity, and DNA fragmentation.[115]

2.3.2 Ferroptosis

In 2008, first studies were published on Fe-dependent cell death, although studies on non-apoptotic cell death with special characteristics had already been published years earlier.[116,117] Ferroptosis, in contrast to apoptosis, is a spontaneous and non-genetically induced form of cell death, characterized by the peroxidation of polyunsaturated fatty acids in membrane-bound PL and the subsequent disruption of the plasma membrane.[117,118] In general, ferroptosis is discussed as age-related cell death, which is associated with Fe accumulation in the brain. Hepcidin is also discussed to play a crucial role, as inflammation increases in aging, leading to increased hepcidin synthesis and intracellular accumulation of Fe.[119] Due to the ability of Fe to catalyze the Fenton reaction and thus generate RONS, labile Fe(II) is thought to play a crucial role in both the initiation of lipid peroxidation and the reaction of lipid hydroperoxides to lipid alkoxyl radicals.[118] Due to the release of Fe from ferritin in the lysosomes and the high demand for Fe in the mitochondria, lipid peroxidation in the membranes of these organelles is often discussed in the context of ferroptosis.[120–122] The ER also appears to have a role in this cell death, as it is rich in polyunsaturated fatty acids (PUFAs), and structural alterations in the organelle have been observed in ferroptotic cells.[3] The ability of GPX4 to convert hydroperoxides from PL and

cholesterol into the corresponding alcohols makes this enzyme perhaps the most important in the suppression of ferroptosis.[123,124] This in turn also means that a malfunction of this enzyme, e.g., due to cysteine or GSH deficiency, can lead to the induction of this cell death. Since GPX4 is a selenium-dependent enzyme, a deficiency of this element is also discussed as promoting ferroptosis.[125,126] In addition, ferroptosis can be suppressed by ferroptosis suppressor protein 1 (FSP1)/Coenzyme Q10 (CoQ_{10}), dihydroorotate dehydrogenase (DHODH), and GTP cyclohydrolase 1 (GCH1)/ tetrahydrobiopterin (BH_4).[3] In research, ferroptosis inhibitors are used to identify this type of cell death. These include Liproxstatin-1 (Lip-1) and Ferrostatin-1, which act as radical scavengers, preventing lipid peroxidation.[127,128] In addition, more than one marker should be used to identify this cell death, including shrunken mitochondria and lipid peroxidation by lipidomics or aldehyde byproducts.[3] In contrast, there is also evidence that ferroptosis may play an ubiquitous role in metal toxicity. This is based on studies, which showed that other metals like Mn, Zn, Cu, or arsenic, may be involved in Fe dyshomeostasis or changes in GSH synthesis and GPX4 activity, thus inducing ferroptosis.[129]

2.4 The Nervous System

The nervous system can be divided into the central (CNS) and peripheral (PNS) nervous system, with the CNS comprising the spinal cord and brain, and the PNS the nerves to other organs. Together they form a crucial, sensitive network that responds to external and internal stimuli through chemical and electrical signal transmission.[130] Neurons are the signal-transmitting cells, which consist of a cell body (soma) with extensions (dendrites) connected with an axon, including synaptic end bulbs. The dendrites receive chemical signals via the synaptic cleft through the end bulbs of another cell, which in turn can be transmitted as electrical signals through the axon to the end of the cell.[131] Neurotransmitters, which are stored in vesicles of the presynaptic cell, serve as chemical signals. The electrical signal and the associated change in the action

potential result in the opening of Ca^{2+} channels. The incoming Ca^{2+} ions bind to vesicle fusion proteins, which ultimately lead to exocytosis and release of the neurotransmitters into the synaptic cleft.[132] In addition to storing neurotransmitters in synaptic vesicles, presynaptic neurons also express neurotransmitter importers to regulate neurotransmitter concentrations in the synaptic cleft. This regulation is essential for effective and reliable signal transmission.[133] Furthermore, the neurotransmitters can bind specific receptors of the postsynaptic cell and thus lead to signal transmission via electrical impulses. The most important neurotransmitters include acetylcholine, dopamine, γ-aminobutyric acid, and serotonin.[134] The second major cell type, neuroglia cells, support and protect neurons and also regulate the homeostasis of the neuronal extracellular fluid. These include astrocytes, oligodendrocytes, microglia, and ependymal cells in the CNS and Schwann and satellite cells in the PNS. These processes require a lot of energy, which means that the brain needs 25% of the glucose available in the body. Therefore, cells of the CNS and PNS are rich in mitochondria.[135] However, this also exposes the neuronal cells to increased RONS production and oxidative stress.[136] In addition, metals such as Fe and Cu accumulate in the brain with age, which can also contribute to increased RONS production. This increase the risk of cell death and loss of neurons, which is thought to be involved in neurodegenerative diseases such as Alzheimer's or Parkinson's diseases.[137] Other hallmarks of neurodegenerative diseases include disrupted neurotransmitter homeostasis, mitochondrial dysfunction, protein aggregation, fragmentation of the Golgi apparatus, dysfunctional cellular/axonal transport, and neuroinflammatory processes.[134,138,139]

2.5 Other Trace Elements

The main focus of this work is on Fe, but due to similar chemical properties and their co-presence in food, the trace elements can interact or are even dependent on each other.[140] Mn is probably one of the elements that interacts with most of the proteins involved in Fe homeostasis. Like Fe, Mn is biologically relevant as Mn(II) and Mn(III) species and is taken up through food such as nuts, grains, and rice.[141] The trace element is an important cofactor of several enzymes, including CAT and SOD.[142,143] Fe and Mn are transported via DMT1, which leads to overexposure of Mn in studies with Fe-deficient models.[144,145] Furthermore, Mn increased IRP activity in lung carcinoma cells, which was associated with decreased ferritin levels. It was assumed that the cause was an Fe deficiency caused by competition for DMT1.[146] In addition, Mn can be exported via ferroportin and transported via transferrin in cases of overexposure.[147–149]

Cu is biologically relevant as Cu(I) and Cu(II) species and is most commonly present in nuts, legumes, and fish. The trace element is a cofactor of several enzymes and, like Fe, is part of cytochrome c oxidase and involved in antioxidant defense as Cu-SOD.[150] Cu is probably also imported in small amounts via DMT1, but primarily as Cu(I) through copper transporter 1 (CTR1), following the reduction of dietary Cu(II) by membrane-bound reductases like Fe.[151,152] Apart from this interaction, Fe and Cu compete less, but as already mentioned, Fe homeostasis is dependent on Cu as a cofactor of hephaestin and CP. This also reflects the impact of aceruloplasminemia on Fe deficiency in plasma with simultaneous systemic Fe overload.[53] In addition, a study with Fe-overloaded rats showed decreased Cu and CP levels in the liver and spleen.[153]

In contrast to the elements already mentioned, Zn is only biologically relevant as Zn(II) and is found in meat, cereals, and legumes, among other foods.[154] Zn is the second most abundant trace element, a cofactor in over 300 enzymes, and plays a crucial role in antioxidant and anti-inflammatory systems.[155] Although Zn is not imported via DMT1, it has been shown in Caco-2 cells that

Zn treatment leads to increased Fe level and DMT1 expression, probably via IRP-2 induction.[156] In addition, it is presumed that ZIPs are also involved in Fe import at the basolateral side of enterocytes and other organs.[34] Several studies showed a correlation between Zn deficiency and Fe overload, regardless of whether the Zn deficiency or the Fe overload was initiated first.[157–159]

2.6 *Caenorhabditis elegans*

C. elegans is a transparent nematode that has been used as a model organism for over 50 years, in almost all biological fields.[160] The well-studied organism is used for the 3R principle to replace, reduce, and refine animal testing.[161] Due to its maximum size of 1 mm, the simple *in vitro* model is easy to handle, and its relatively short life cycle enables many studies to be conducted at the same stage of life in a short period.[162] The fact that over 99% of a *C. elegans* population are hermaphrodites has the great advantage of a genetically identical culture. A single hermaphrodite consists of 959 somatic cells and can produce up to 300 progeny.[163,164] In addition, the nematode was the first multicellular organism whose entire genome was sequenced.[165] The 6 chromosomes of hermaphrodites contain around 20,000 protein-coding genes, of which 60 – 80% have orthologs in humans.[166,167] This knowledge enables the relatively simple manipulation of the genome in the form of deletion of a section or fusion of small fluorescent proteins with target genes. The transparency of the worm is a further advantage here, as the inside of the nematode and fluorescence-tagged proteins can also be evaluated in a living organism using simple microscopy. This makes it possible to study the properties of certain genes due to incomplete or missing function and altered expression or localization of the corresponding proteins due to the fluorescence.[168] Using analytical methods, e.g., macromolecules, metabolites, or even metal contents can be measured in just one experimental approach in hundreds to thousands of genetically identical individuals. In addition, the worm is also used for behavioral, developmental, and lifespan studies, which can be evaluated using microscopy. All this makes

C. elegans a suitable model organism for toxicological studies, including metal toxicological investigations.[169,170]

The anatomy of the worms is quite simple compared to mammals. The pharynx is a pumping system through which the nematodes take up food. Not only do absorption and excretion of food components take place in the intestine, but also processes such as xenobiotic metabolism, which in humans takes place in the liver.[162,170] In hermaphrodites, the reproductive system consists of two gonadal arms that converge at the spermatheca and lead into the uterus. The pharynx, intestine, and reproductive system are surrounded by pseudocoelomic space, to which the body muscle, dorsal and ventral nerve, and neurons are connected. The entire worm is surrounded by a cuticle, through which substances from the environment can also be absorbed to a small extent.[162]

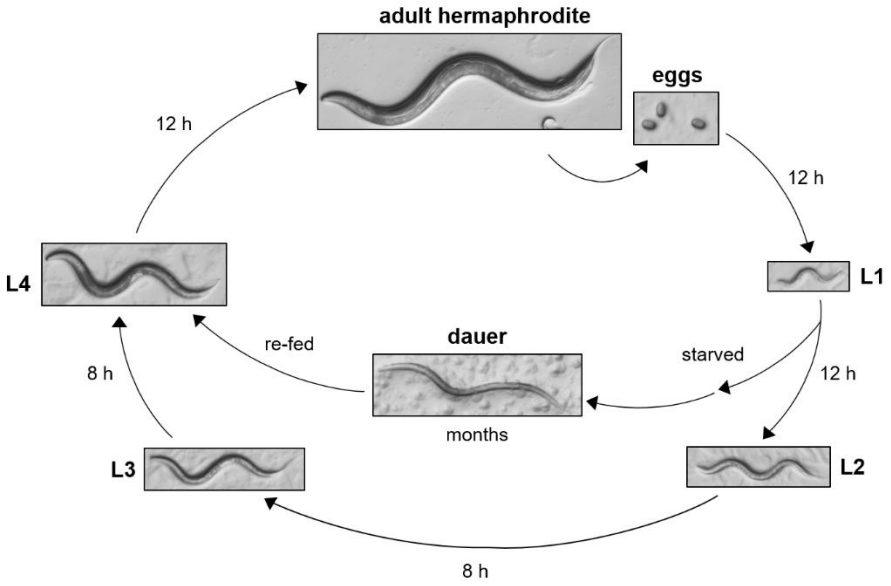

Figure 5. Life cycle of a hermaphroditic *C. elegans* wild type at 20 °C. Images were taken with a Leica MZ10 F stereo microscope at 50X magnification. [Adapted and modified from Kimble et al.][171]

In the laboratory, the nematodes are cultivated either in buffer or on agar plates at temperatures between 16 and 25 °C. *E. coli* is used as a food source, with OP50 and NA22 strains being the most commonly used.[160] Treating the worms with a bleach solution for a few minutes is one option to get a synchronized

population, as only the eggs remain intact, and L1 larvae only continue to grow in contact with food.[172] This ensures that the worms are at the same stage of development for experiments to improve comparability. When the worms carry eggs after around 3 days at 20 °C, they are considered to be adults (Figure 5).[162] This period refers to the wild type N2 and may vary in other *C. elegans* strains. A special characteristic of *C. elegans* is the dauer stage into which worms develop after the L1 stage in an adverse environment, for example, in the absence of food. This is a survival stage, in which the nematode forms a thicker cuticle and adapts its metabolism and behavior to ensure survival for several months. In addition, the worms can be cryopreserved at this stage and stored at -80 °C for years. After thawing and providing food, the worms grow slowly at first, but later continue to grow as usual.[173]

2.6.1 Iron Homeostasis in *Caenorhabditis elegans*

Among the many orthologous genes between humans and *C. elegans* are several genes conserved related to Fe homeostasis. In *C. elegans*, Fe can be taken up as both heme and nonheme Fe, whereby it is dependent on heme from food, as the nematode is a heme auxotroph.[174] *C. elegans* possesses three orthologous genes to DMT1 for nonheme Fe import, of which the proteins SMF-1 and SMF-3 are highly expressed at the apical membrane of the nematodes intestine, and SMF-2 is mainly cytoplasmic expressed (Figure 6).[175] The study by Romney et al. suggests that SMF-3 is mainly responsible for the intestinal uptake of Fe, as *smf-3* deletion mutants showed decreased Fe levels and *smf-3* was transcriptionally upregulated during Fe deficiency.[176] Although several studies showed elevated Fe levels after treatment with Fe(III) species, it is unknown if and how these species are reduced and if it is taken up via SMF.[177–179] However, F55H2.5 could function as a Fe(III) reducing enzyme, as it is considered to be an ortholog of *DCYTB*.[180] The *heme responsive genes* (*hrg*) are involved in heme transport in *C. elegans*, with mainly *hrg-4* being responsible for intestinal import at the apical membrane.[174,181] In *C. elegans*,

FTN-1 and FTN-2 are the orthologs of the Fe storage proteins FTH and FTL, whereby both show ferroxidase activity to store Fe as Fe(III) species in the nematode.[182–184] While FTN-1 is mainly expressed in the intestine, FTN-2 shows high expression in the pharynx, body muscle, and hypodermis.[185] Although FTN-2 purified from *C. elegans* showed a faster reaction with Fe at the ferroxidase site, probably due to structural properties, FTN-1 can store around 1550 Fe atoms/ferritin, and FTN-2 only 225 Fe atoms/ferritin in the Fe core.[184] *C. elegans* has three ferroportin orthologous genes, *fpn-1.1*, *fpn-1.2*, and *fpn-1.3*, the latter being a pseudogene.[180] While their functions in Fe export in the nematodes are still poorly understood, a study by Chakraborty et al. showed that FPN-1.1 also functions as a Mn exporter.[186] The CP ortholog F21D5.3 is probably also involved in the export of Fe in *C. elegans*.[180,187] However, the gene is insufficiently characterized, also about its ferroxidase activity and its function in storing Fe in ferritin. Recently, Weishaupt et al. showed increased labile Cu levels in *f21d5.3* deletion mutants and increased mRNA levels after Cu treatment in wild type worms.[188]

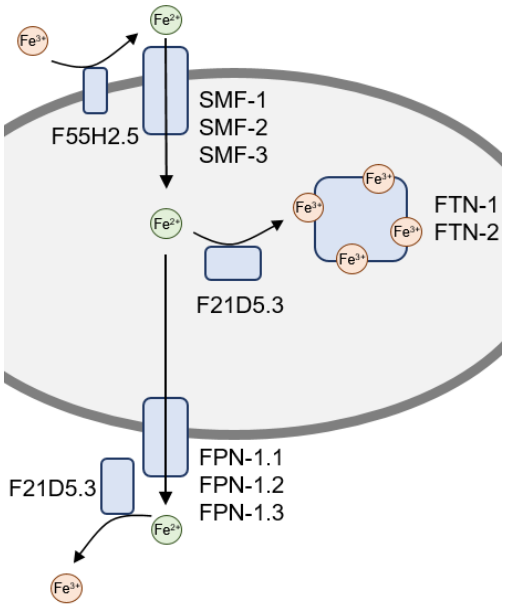

Figure 6. Overview of the Fe homeostasis in *C. elegans*. [Adapted and modified from a previously published paper][189]

The regulation of Fe metabolism in *C. elegans* is regulated by HIF-1, an ortholog of HIF1α and HIF2α, and initiates the binding to Fe-dependent enhancer (IDE) of the promoters of *ftn* and *smf*.[176,190–192] In addition, the insulin/insulin-like growth factor-1 (IGF-1) signaling (IIS) pathway can also regulate *ftn* expression via the translocation of the FOXO ortholog DAF-16 into the nucleus.[192] While some Fe homeostasis associated pathways are conserved in the nematode, not all pathways are completely understood.

2.6.2 Further Conserved Pathways in *Caenorhabditis elegans*

Due to many orthologous genes associated with oxidative stress, *C. elegans* is also a suitable organism for studies in this field.[193] In the nematodes, the main source of RONS is also the OXPHOS in the mitochondria.[194] For detoxification, *C. elegans* possesses five SOD orthologs, of which SOD-1 and SOD-5 (Cu/Zn SOD) are localized in the cytosol, SOD-2 and SOD-3 (Mn SOD) in the mitochondria, and SOD-4 (Cu/Zn SOD) in the extracellular matrix.[195] Catalase orthologs are located in the cytosol (CTL-1) and the peroxisomes (CTL-2, CTL-3), as in humans.[196] Additionally, GSH synthesis (*gcs-1*/*GCLC*, *gss-1*/*GSS*) and reduction (*gsr-1*/*GR*) genes have orthologs in *C. elegans*.[197] More than 50 orthologs of the detoxification enzyme GST have been identified in the nematode.[198] Analogous to FOXO and NRF2, the orthologous transcription factors DAF-16 and SKN-1, respectively, are conserved in *C. elegans* and are activated in response to oxidative stress via the IIS pathway.[193]

Furthermore, many genes associated with cell death are conserved in *C. elegans,* and the organism was already used in 1994 or earlier for the mechanistic understanding of apoptosis, for which Horvitz, Brenner, and Sulston were awarded the Nobel Prize in Physiology or Medicine in 2002.[199] The ortholog of BH3-only, a member of the *BCL2* family, is *egl-1*, which is activated by oxidative stress or by the p53 ortholog *cep-1*.[200,201] Caspase activation by CED-3 occurs via several steps, which involve the BCL2 ortholog CED-9. Unlike in humans, mitochondria do not play an essential role in this type of cell death

in the nematode.[202] In *C. elegans*, the PS signature of an apoptotic cell can be recognized by CED-1 of a neighboring somatic cell.[200] This activates one of the engulfing pathways, which involves CED-1, CED-6, CED-7, and DYN-1.[203] Due to the transparency of the worm, apoptotic cells can be visualized with bright field light or by fluorescence fusion proteins, e.g., with CED-1 in the living organism under the microscope.[200,204]

To elucidate further mechanistic pathways in ferroptosis, *C. elegans* has been used in several studies. Eight GPX orthologs are conserved in the nematode, which do not contain Se in the active center, but a cysteine residue.[197] Sakamoto et al. hypothesize that GPX-1, GPX-2, GPX-6, and GPX-7 together have the same function as human GPX4 and are involved in the suppression of lipid peroxidation.[205] Jenkins et al. showed that with increasing age of *C. elegans,* GSH levels decrease and Fe(II) levels increase, which would promote ferroptosis.[206]

In *C. elegans*, over 70% of lipid homeostasis-associated genes have orthologous genes in humans, making the organism suitable for several mechanistic lipid-related studies.[207] Compared to humans, PL and SL are present in all cellular membranes of the nematode, with PE and PC making up the largest fraction. Cardiolipins are only present in the mitochondrial membrane.[208] While humans depend on essential omega-3 and omega-6 fatty acids from the diet, *C. elegans* can synthesize them itself.[209]

With only 302 neurons, the neuronal network of *C. elegans* is relatively small, but all neurons have been identified, and the network can be analyzed as a whole.[210,211] The important neurotransmitter systems involving acetylcholine, dopamine, γ-aminobutyric acid, and serotonin are highly conserved in the nematode.[212] In *C. elegans*, fluorescent fusion proteins are used to examine the morphology of specific neurons with the microscope in the living organism, while behavioral assays are used to examine alterations in their function. In addition,

analytical methods can be used to measure, for example, neurotransmitter levels.[213]

2.6.3 Limitations using *Caenorhabditis elegans* as a model organism

Besides the several orthologous genes and the mentioned advantages of *C. elegans*, it also has its limitations, like any other model organism. The nematode is a simple model organism that, as an invertebrate, lacks some of the characteristics needed to compare it with higher organisms. The absence of organs such as the heart, liver, kidneys, and lungs restricts some organ-specific investigations. In addition, the intestine in *C. elegans* has a neutral pH value, whereas it is slightly acidic in the human duodenum, which can affect the absorption of molecules and ions.[214,215] Further, the nematode has limitations regarding Fe homeostasis as it lacks an orthologous gene for *TF* and *hepcidin*. In addition, a simple neuronal network cannot answer all questions relating to the complex human network. Nevertheless, *C. elegans* can contribute to our understanding of biological mechanisms, from behavior down to the molecular level. Studies on the nematode thus provide preliminary evidence and may also contribute to our understanding of human diseases and therapeutic approaches.

Abstract

Iron (Fe) is present in foods and food supplements in a wide variety of Fe species. Caution needs to be paid in the case of overdosing on this essential trace element, as adverse effects like neurodegenerative diseases are associated with increased iron levels in the brain. However, knowledge regarding the species-specific effects of nutritionally relevant Fe species is limited. Therefore, we treated the nematode *Caenorhabditis elegans* (*C. elegans*) with an overdose of the Fe species iron(III) ammonium citrate (FAC), iron(II) gluconate (FeGlu), and iron(II) chloride ($FeCl_2$) for 5 and 24 h. While the bioavailability of Fe was highest with $FeCl_2$ and lowest with FAC, the effects on tested endpoints, such as superoxide dismutase activity, translocation of the transcription factor DAF-16 (human FOXO3), mitochondrial reactive oxygen and nitrogen species, and apoptotic cells were similar. This study provides further insights into Fe-species-specific effects on genes related to Fe homeostasis of *C. elegans* by studying gene expression and investigating *C. elegans* mutants lacking *smf-3*, *ftn-1*, *ftn-2*, *dcytb* (*f55h2.5*), and *cp* (*f 21d5.3*). Thus, these findings underline the significance of the oxidation state and ligand of Fe species with respect to bioavailability while also identifying the key genes involved in Fe homeostasis in *C. elegans*.

Chapter 3

Is Ferric the Same as Ferrous? Effect of Nutritionally Relevant Iron Species in *C. elegans*: Bioavailability, Iron Homeostasis, Oxidative Stress, and Cell Death

Based on

Anna Gremme, Zainab Al-Timimi Safa Flaih, Johannes Scholz, Emely Gerisch, Alicia Thiel, Gawain McColl, Heiko Hayen, Bernhard Michalke, and Julia Bornhorst

Journal of Agriculture and Food Chemistry, **2025**

DOI: 10.1021/acs.jafc.4c10463

Keywords

iron species, iron homeostasis, oxidative stress, *C. elegans*

Chapter 3 – Is Ferric the Same as Ferrous? Effect of Nutritionally Relevant Iron Species in *C. elegans*: Bioavailability, Iron Homeostasis, Oxidative Stress, and Cell Death

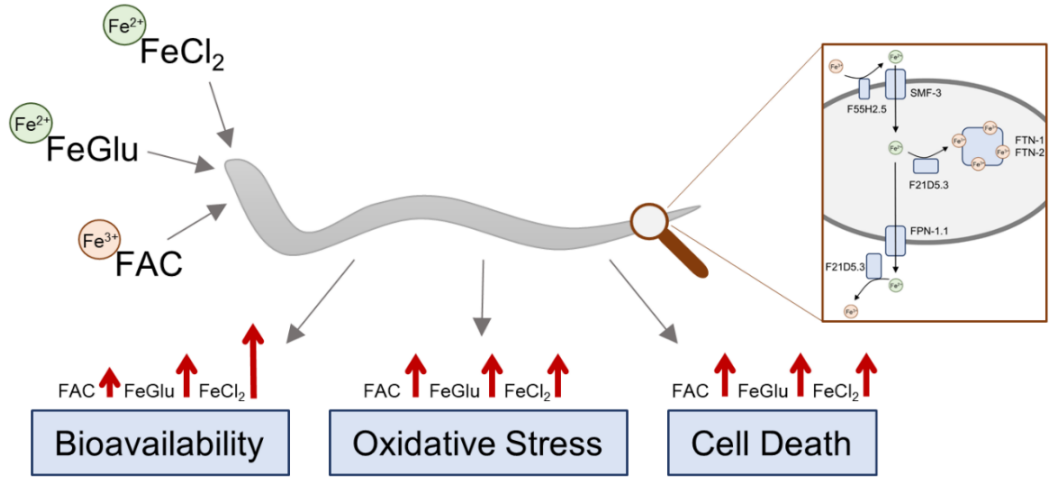

Figure 7. Graphical abstract of: Is Ferric the Same as Ferrous? Effect of Nutritionally Relevant Iron Species in *C. elegans*: Bioavailability, Iron Homeostasis, Oxidative Stress, and Cell Death

3.1. Introduction

In the general population, iron (Fe) is taken up as an essential trace element through food (natural and fortified), drinking water, and food supplements. The species vary across sources with respect to the oxidation state Fe(II) (i.e., ferrous) and Fe(III) (i.e., ferric) as well as the potential ligand. While meat and seafood contain heme and nonheme Fe, plants and plant-derived food supplements contain nonheme Fe only. With the growing popularity of vegetarian and vegan diets, nonheme Fe is becoming increasingly important in the diet. In addition, the German Nutrition Society (DGE) recommends that a healthy and environmentally friendly diet should consist of 75% plant-based food.[216] Several Fe(II) and Fe(III) compounds, including iron(III) ammonium citrate (FAC) and iron(II) gluconate (FeGlu), are permitted as additives in food and food supplements in the EU.[217] The European Food Safety Authority (EFSA) just released updated intake assessment data in April 2024. The panel

notes that the 95th percentile-estimated background intake of Fe from natural food sources (excluding food supplements) across surveys is up to 23.1 mg/day in adult (≥18 to ≤65 years) males and up to 18.6 mg/day in females.[2]

In living organisms, Fe is an important key component in various biological processes due to its redox interconversion between oxidation states Fe(II) and Fe(III). These include essential processes such as oxygen transport, energy production, and DNA synthesis and repair.[7,8] Fe deficiency is associated with severe health consequences and, if prolonged, may progress to anemia.[50] However, Fe overdosing is associated with various health issues, including cardiovascular, neurodegenerative, and cancer diseases.[218] The underlying mechanisms of Fe toxicity upon overexposure are still not conclusively clarified, with a particular lack of knowledge regarding different Fe species. An often-discussed mechanism of Fe-induced toxicity is oxidative stress. Overexposure to Fe can result in the excessive formation of reactive oxygen and nitrogen species (RONS) via the Fenton reaction, which can cause adverse modification of macromolecules such as DNA, proteins, and lipids.[219,220] This can result in negative consequences for cellular function and integrity, including cell death.[221]

In the case of Fe-induced oxidative stress, the antioxidant system may serve to minimize RONS. For example, certain transcription factors can be activated by RONS, which upregulates genes of enzymes such as catalases, superoxide dismutases (SOD), and glutathione peroxidases (GPX).[73] The tripeptide glutathione (GSH) functions as a cofactor for GPX, whereby it is oxidized to glutathione disulfide (GSSG).[71] Additionally, GSH exhibits radical scavenging activities and can thus neutralize reactive species such as hydroxyl radicals.[222]

Due to the lack of knowledge regarding species-specific effects of nutritionally-relevant Fe species, especially with regard to Fe bioavailability and homeostasis, this study aimed to investigate species-specific effects of overexposure to the Fe compounds FAC, FeGlu, and iron(II) chloride ($FeCl_2$) with respect to bioavailability, Fe homeostasis, oxidative stress, and cell death. It is generally known that ferrous Fe is more bioavailable than ferric Fe, but the

cellular species-specific consequences remain poorly understood. In the current study, we used the nematode *Caenorhabditis elegans* (*C. elegans*) as an *in vivo* invertebrate model organism. While many studies perform Fe treatment in liquid media in the absence of food, we provide the nematode with nutritionally relevant Fe species via the food source. Due to many orthologous genes to the mammalian, including genes of Fe homeostasis, antioxidant defense, and cell death pathways, the nematode is a suitable model organism to study Fe homeostasis and toxicity.[169] In 2014, Anderson et al. published a comprehensive review on the conserved genes of Fe homeostasis in *C. elegans*, which also pointed out gaps in knowledge regarding, e.g., duodenal Cytochrome b (DCYTB) or hephaestin orthologues.[190] In our study, we aim to fill some of these gaps by investigating several genes in Fe homeostasis following Fe overdosing.

3.2. Materials and Methods

3.2.1. *C. elegans* Handling and Fe Treatment

C. elegans strains Bristol N2 (wild type), ok1035 (*smf-3*Δ), ok3611 (*f55h2.5*, *dcytb*Δ), TJ356 (*daf-16*::gfp), and MD701 (*ced-1*::gfp) were obtained from the Caenorhabditis Genetics Center (CGC). The ceruloplasmin and hephaestin mutant tm14205 (*f21d5.3*, *cp*Δ) was obtained from the Mitani laboratory at Tokyo Women's Medical University. The ferritin null strain [*ftn-2*(*ok404*);*ftn-1*(*ok3625*)] (GMC005, *ftn-1;ftn-2*ΔΔ) has been previously described.[177] The strains and functions of the respective genes were described previously, and an overview is shown in Figure 9.

The worms were cultivated at 20 °C on 8P agar plates coated with NA22 *E. coli*, as previously described.[160] Synchronization to perform all experiments in larval stage 4 (L4) worms was carried out, as described previously.[223] The Fe species FAC (reagent grade, Sigma-Aldrich), FeGlu (98%, Sigma-Aldrich), and $FeCl_2$ (99.99%, Sigma-Aldrich) were freshly dissolved in bidistilled water before each experiment. They were then added separately to inactive OP50 *E. coli* and

distributed on Nematode Growth Medium (NGM) agar plates. To inactivate the *E. coli*, it was heated for 4 h in a 70 °C water bath.[224] L4 worms were treated for 5 or 24 h on Fe-enriched plates. All concentrations treated were nonlethal, and no behavioral changes of the worms were observed after both treatment times.

3.2.2. Protein Determination via BCA Assay

As described in the respective assay sections, some results were normalized to the protein content. The protein amount was determined using the bicinchoninic acid (BCA) assay, as described previously.[225]

3.2.3. Quantification of Total Fe, Mn, Cu, and Zn via ICP-OES

Total element contents of Fe, Mn, Cu, and Zn were quantified via inductively coupled plasma-optical emission spectrometry (ICP-OES) (Avio 220 Max, PerkinElmer), using Yttrium (Y) as an internal standard. After Fe treatment, 1500 worms per condition were pelletized and prepared for analysis as described previously.[188] In short, after Y was added to the pellets, they were homogenized using a freeze–thaw cycle, followed by sonication (UP100H, Hielscher). Subsequently, the pellets were dried and ashed with a 1:1 mixture of HNO3 (Suprapur, Merck KGaA) and H2O2 (for ultratrace analysis, Sigma-Aldrich) at 95 °C. The residue was redissolved in 2% HNO3. Instrumental analysis was also carried out according to this protocol with the following parameters: Plasma power: 1500 W, cooling gas: 8 L/min, auxiliary gas: 0.2 L/min, nebulizer (MicroMist) gas: 0.7 L/min, and the following element lines: Fe–259.939 nm, Mn–257.610 nm, Cu–327.393 nm, Zn–206.200 nm, and Y–371.029 nm. Results were normalized to the protein content.

3.2.4. Gene Expression via Taqman Real-Time qPCR Analysis

Gene expression was determined on the AriaMx Real-Time PCR System using TaqMan gene expression assay probes (Applied Biosystems, Thermo Fisher Scientific).[188] Total RNA was isolated using the TRIzol method, as described by Bornhorst et al.[226] Transcription of 1 µg of isolated RNA was performed using the High-Capacity cDNA Reverse Transcription Kit (Applied Biosystems,

Thermo Fisher Scientific), as described by the manufacturer. The following probes were used: *smf-3* (Ce02461545_g1), *dcytb* (Ce02451148_g1), *ftn-1* (Ce02477612_g1), *ftn-2* (Ce02415799_g1), *cp* (Ce02456979_m1), *daf-16* (Ce02422838_m1), fpn-1.1 (Ce02414545_m1), sod-4 (Ce02451138_g1), *sod-3* (Ce02404515_g1), *skn-1* (Ce02407447_g1), *gcs-1* (Ce02436725_g1), and *gst-4* (Ce02458730_g1).[224] Normalization was carried out according to the comparative 2–ΔΔCt method using the afadin (*AFDN*) orthologue *afd-1* (Ce02414573_m1) as the housekeeper gene.[227]

3.2.5. Mitochondrial Membrane Potential and Mitochondrial-Derived RONS via MitoTracker Red CM-H2Xros

Mitochondrial membrane potential and mitochondrial-derived RONS were assessed using MitoTracker Red CM-H2XRos (Thermo Fisher Scientific).[228] After Fe treatment, worms were washed with NaCl solution (85 mM NaCl, 0.01% Tween 20) by allowing the young adult worms to sink to the bottom of the tube and removing the supernatant. 2250 worms per condition were incubated in the dark for 2 h with 50 µM MitoTracker. After washing off the dye, worms were placed on NGM plates coated with active OP50 *E. coli* and left to excrete the dye from the intestine for 1 h in the dark. Following washing, an aliquot was taken for protein determination, and the fluorescence was measured in triplicate using a microplate reader (Infinite M Plex Tecan) (excitation: 560 nm, emission: 599 nm).

3.2.6. DAF-16 Translocation

As a further endpoint for oxidative stress, translocation of the transcription factor DAF-16 (abnormal dauer formation 16, orthologue of human FOXO3 (forkhead box O3)) was evaluated in the DAF-16::GFP strain by fluorescence microscopy (DM6 B fluorescence microscope, Leica Microsystems GmbH). In this strain, the *daf-16* gene is fused with a green fluorescent protein (GFP) gene, resulting in the formation of a green fluorescent DAF-16 fusion protein.[229] Worms were anesthetized with levamisole (5 mM, Sigma-Aldrich) on 4% agarose pads

following Fe treatment. Translocation in about 30 worms per condition was assessed with the LAS X software (Leica Microsystems GmbH) and categorized as (1) DAF-16::GFP in the cytosol and (2) DAF-16::GFP as an intermediate or in the nucleus. As a positive control, L4 worms were treated with 150 mM paraquat for 24 h.[230]

3.2.7. Total SOD Activity via WST-1-Based SOD Inhibition Assay

Total SOD activity was determined using a WST-1-based SOD Inhibition Assay Kit (Dojindo Molecular Technologies) according to manufacturer's protocol. Following Fe treatment, 750 worms per condition were washed with NaCl solution and once with ice-cold dilution buffer from the kit, as described in Section 3.2.5. The worms were disrupted three times in 200 µL of dilution buffer using the freeze–thaw cycle method (1 min liquid nitrogen, 1 min 37 °C water bath) and afterward homogenized twice with zirconia beads in a bead ruptor (20 s, high, Biolab Products). After centrifugation (5 min, 9500 rcf, 4 °C), SOD activity and protein content were determined in the supernatant. SOD activity was evaluated in duplicates using external calibration with SOD from bovine erythrocytes (Sigma-Aldrich), as described previously.[231] Paraquat was used as a positive control, as described in Section 3.2.6.

3.2.8. GSH and GSSG Quantification via LC–MS/MS

The levels of reduced (GSH) and oxidized (GSSG) glutathione were quantified by liquid chromatography–tandem-mass spectrometry (LC–MS/MS), as previously published by Thiel et al.[232] After Fe treatment, 750 worms per condition were washed as described in Section 2.5 and frozen in 50 µL of 85 mM NaCl at −80 °C until analysis. GSH and GSSG amounts were normalized to protein content.

3.2.9. Phospholipid Determination via SFC–TIMS–MS/MS

Phospholipids were quantified utilizing a modified Agilent Technologies SFC system, which was hyphenated to a timsTOF fleX (Bruker Daltonics GmbH & Co. KG) mass spectrometer. The employed chromatographic conditions, as well

as the mass spectrometric parameters in positive ionization mode, can be found in the previous publication and were adopted here.[223] Phosphatidylethanolamines (PE) and phosphatidylcholines (PC) were extracted from the nematodes via a modified protocol by Folch et al.[223,233] Relative lipid concentrations were determined by integration of peak areas and normalization to protein content. The peak areas were integrated by MetaboScape software (version 2023b, Bruker Daltonics GmbH & Co. KG). The shorthand notation of Liebisch et al. was used for lipid nomenclature.[234] The total fatty acid composition of a phospholipid (PL) is described by the total number of carbon atoms (X) and double bonds (Y), for instance, PC 32:0 (PL X:Y).

3.2.10. CED-1::GFP Location in Apoptotic Germ Cells

Apoptotic germ cells were evaluated via a CED-1::GFP reporter by fluorescence microscopy (DM6 B fluorescence microscope, Leica Microsystems GmbH). The sample pads were prepared, as described in Section 3.2.6. The engulfment of apoptotic cells can be recognized by circular GFP fluorescence and was scored in about 10 worms per condition in both gonadal arms.

3.2.11. Statistical Analysis

GraphPad Prism 6 (GraphPad software) was used for statistical analysis. A t test with $\alpha = 0.05$ was used with the following significance levels: *$p \leq 0.05$, **$p \leq 0.01$, and ***$p \leq 0.001$.

3.3. Results

3.3.1. Fe Bioavailability Depends on the Oxidation State and the Ligand of the Fe Compound

Different studies have demonstrated that bioavailability differs between various Fe compounds.[235–237] To verify whether treatment with FAC, FeGlu, and $FeCl_2$ in *C. elegans* leads to a species-specific Fe overdosing after 5 and 24 h, Fe bioavailability was quantified via ICP-OES. As an essential trace element, Fe was quantified in the untreated control with a Fe basal level of 0.31 ± 0.01 ng/µg protein after 5 h and 0.33 ± 0.02 ng/µg protein after 24 h. Each Fe species

applied led to increased Fe levels compared with the untreated control at both treatment times (Figure 8). While no Fe species-specific effect was observed after 5 h, at 24 h, the Fe level was lowest with FAC (0.59 ± 0.06 ng/µg protein), followed by FeGlu (1.07 ± 0.15 ng/µg protein), and highest with $FeCl_2$ (2.98 ± 0.30 ng/µg protein) treatment (Figure 8). Thus, an Fe species-specific bioavailability was observed not only between the ferric and ferrous Fe species but also between the two Fe(II) species. The bioavailability of Fe by FeGlu and $FeCl_2$ was time dependent, whereas no difference was observed between the two treatment times of FAC.

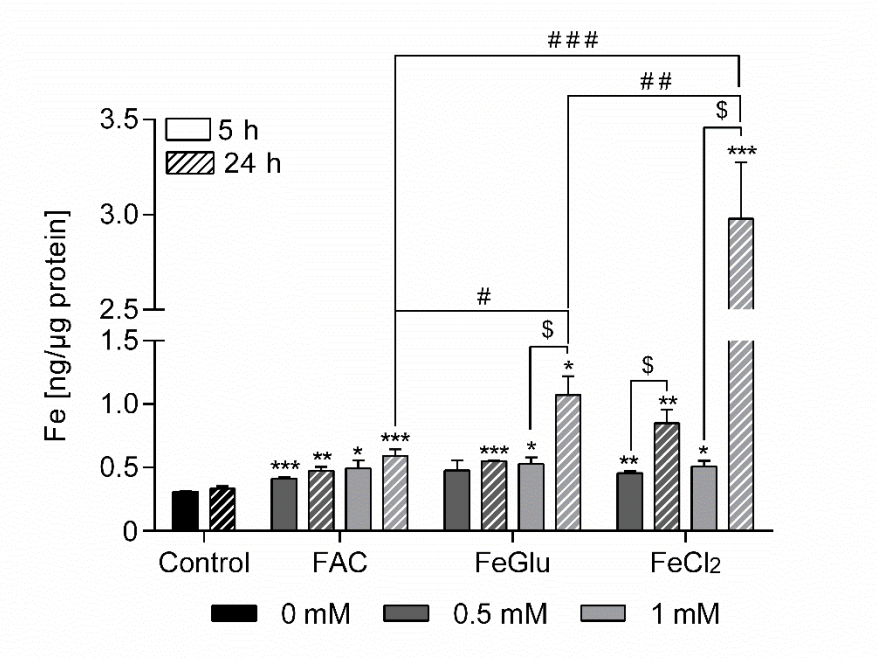

Figure 8. Bioavailability of Fe after treatment for 5 or 24 h with Fe species [ng/µg protein]. Total Fe was normalized to protein content. Shown are mean + SEM of n ≥ 3 independent experiments. Significance is depicted as * compared to untreated control, # compared to other Fe species, and $ compared to other treatment times.

3.3.2. Effect on Fe Homeostasis: Gene Expression and Bioavailability in Mutants Lacking Fe-Associated Proteins

To investigate whether there is an Fe species-specific effect on genes related to Fe homeostasis, the relative gene expression was measured in wild-type worms via qPCR. To address the consequences of lacking these proteins for Fe

bioavailability, the Fe content in the respective deletion mutant was quantified. An overview of the genes investigated is shown in Figure 9. It is known that in *C. elegans*, the divalent metal transporter 1 (*DMT-1*) orthologue *smf-3* (yeast SMF (divalent cation transporter) homologue) is involved in the regulation of Fe homeostasis,[190] but little is known about its expression in response to different Fe species. The gene expression of *smf-3* decreased after 5 h of treatment with each Fe species, while after 24 h, no effect was observed (Figure 10A). In addition, the deletion of *smf-3* led to a lower Fe basal level. Each species led to a species-unspecific increased Fe level in *smf-3*Δ, but the amount differs significantly from that of the wild type (Figure 10E). This effect was highest after $FeCl_2$ treatment as only 12% Fe could be measured after 1 mM $FeCl_2$ treatment compared to the wild type (Table 1). In the case of FAC and FeGlu exposure in the *smf-3* mutant, about 40% Fe was taken up compared to wild-type worms applying the same dose.

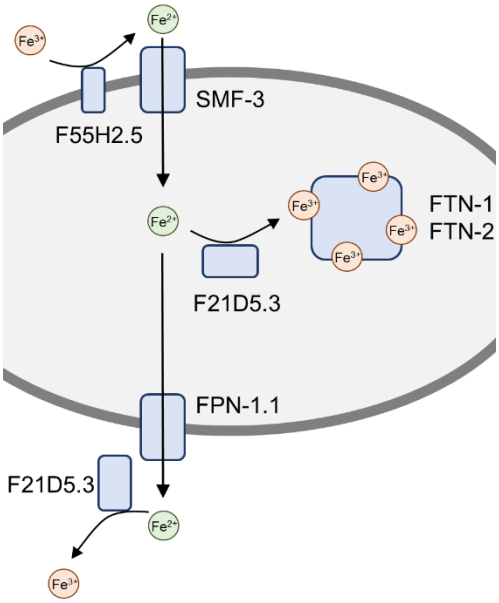

Figure 9. Schematic overview of the investigated genes involved in Fe homeostasis in *C. elegans*. SMF-3 (orthologue of human DMT-1) is involved in Fe import, while F55H2.5 (orthologue of human DCYTB) is involved in the reduction of Fe(III) to Fe(II). Intracellularly, Fe(II) can be oxidized to Fe(III) by F21D5.3 (orthologue of human CP and hephaestin) and stored in FTN-1 and FTN-2 (orthologue of human FTH and FTL). FPN-1.1 (orthologue of human FPN) mediates Fe export. Extracellularly, Fe(II) can be oxidized to Fe(III) by F21D5.3.

The gene *dcytb* (*f55h2.5*) in *C. elegans* is the orthologue of human *DCYTB*.[180] While none of the Fe species led to an alteration in the gene expression of *dcytb* (Figure 10B), the Fe basal level and Fe content were decreased in worms lacking the respective protein compared to wild-type worms (Figure 10F). In comparison with the wild type, the difference after $FeCl_2$ treatment was greater than after FAC and FeGlu treatment (Table 1).

Table 1. Differences in the Bioavailability of Fe in *smf-3*Δ, *dcytb*Δ, *ftn-1;ftn-2*ΔΔ, and *cp*Δ Compared to Wild Type After Incubation for 24 h With Fe Species [%] [a,b]

	Differences in bioavailability of Fe compared to wild type [%]			
	*smf-3*Δ	*dcytb*Δ	*ftn-1;ftn-2*ΔΔ	*cp*Δ
control	25 ± 2	63 ± 9	51 ±4	65 ± 5
0.5 mM FAC	41 ± 1	67 ± 6	78 ± 7	106 ± 17
1 mM FAC	43 ± 3	72 ± 1	67 ± 6	79 ± 3
0.5 mM FeGlu	38 ± 7	67 ± 6	88 ± 20	135 ± 38
1 mM FeGlu	42 ± 8	66 ± 16	49 ± 4	54 ± 11
0.5 mM $FeCl_2$	25 ± 2	42 ± 1	52 ± 2	55 ± 7
1 mM $FeCl_2$	12 ± 1	38 ± 13	33 ± 4	23 ± 3

[a] The Fe content of wild-type worms was set to 100%, and the values provided represent the percentage relative to the wild type.

[b] Shown are mean ± SEM of n ≥ 3 independent experiments.

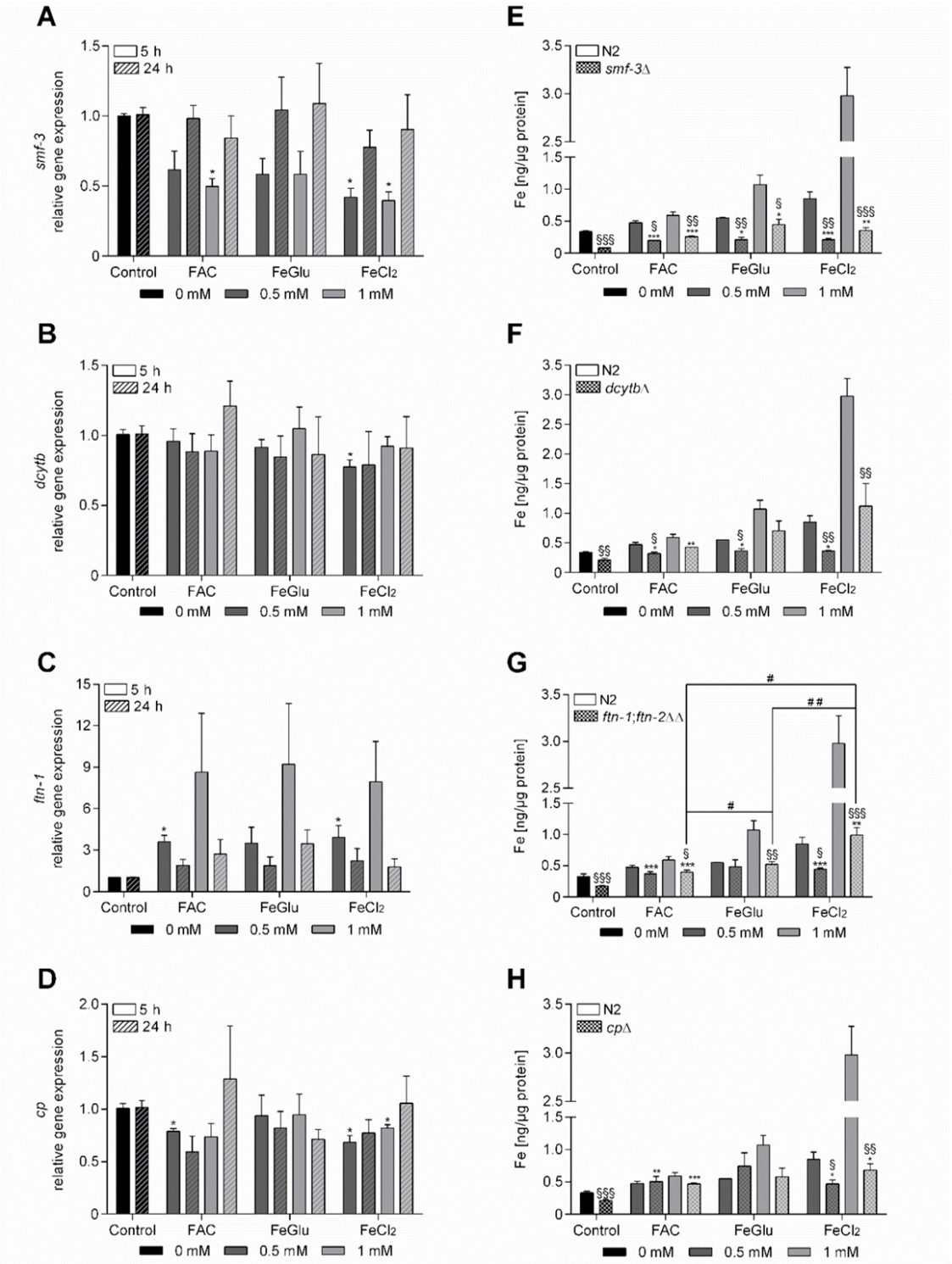

Figure 10. Relative gene expression of (A) *smf-3*, (B) *dcytb*, (C) *ftn-1*, and (D) *cp* in wild type after treatment for 5 or 24 h with Fe species. Bioavailability of Fe in (E) *smf-3*Δ, (F) *dcytb*Δ, (G) *ftn-1;ftn-2*ΔΔ and (H) *cp*Δ compared to wild type after treatment for 24 h with Fe species [ng/µg protein]. Total Fe was normalized to protein content. Shown are mean + SEM of n ≥ 3 independent experiments. Significance is depicted as * compared to untreated control, # compared to other Fe species, and $ compared to wild type.

In *C. elegans*, the two genes *ftn-1* and *ftn-2* (ferritin) encode two Fe storage proteins.[190] Both orthologues have ferroxidase activity, comparable to the human ferritin heavy chain (*FTH*), and can store Fe like the human ferritin light chain (*FTL*).[184] Following 5 h of Fe treatment, the gene expression of *ftn-1* increased in a species-unspecific manner (Figure 10C), while none of the Fe species led to an alteration in the gene expression of *ftn-2* (Supplementary Figure 37). The deletion of the genes of both Fe storage proteins led in *ftn-1;ftn-2*ΔΔ to a lower Fe basal level and a lower Fe level after treatment with each species compared to the wild type (Figure 10G, Table 1).

The *C. elegans* gene *cp* (*f21d5.3*) is an orthologue to human *ceruloplasmin* (*cp*) and *hephaestin*.[180] Treatment with the Fe species led to a slight downregulation of *cp* gene expression (Figure 10D). Although the Fe basal level was lower in *cp*Δ, there was no difference in the Fe level after FAC treatment compared to that of the wild type (Figure 10H). Only treatment with 1 mM FeGlu and both concentrations of $FeCl_2$ showed lower Fe levels compared to the wild type (Figure 10H and Table 1).

3.3.3. Species-Specific Fe-Induced Oxidative Stress and Response

Since the high occurrence of oxygen and Fe within the mitochondria can lead to the formation of RONS, both mitochondrial-derived RONS and mitochondrial membrane potential were determined using MitoTracker Red CM-H2Xros. The results indicated that each species contributes species-unspecifically to the formation of RONS following 5 and 24 h of Fe treatment by up to 80% (Figure 11A).

In humans, a response to the increased level of formation of RONS may be the translocation of transcription factors Forkhead box O-class proteins (FoxO) from the cytosol to the nucleus. In the nucleus, FoxO regulates downstream genes with an impact on stress resistance, energy metabolism, and DNA repair.[238] The translocation of the FOXO3 orthologue DAF-16 can be visualized in the nematode strain DAF-16::GFP under the fluorescence microscope

(Figure 11C). Increased translocation into the nucleus was observed after treatment with each Fe species (Figure 11B). Translocation following 5 h of treatment was higher with $FeCl_2$ treatment compared to FeGlu, but only at concentrations of 0.5 mM. Gene expression of *daf-16* was slightly downregulated by each species (Supplementary Figure 38).

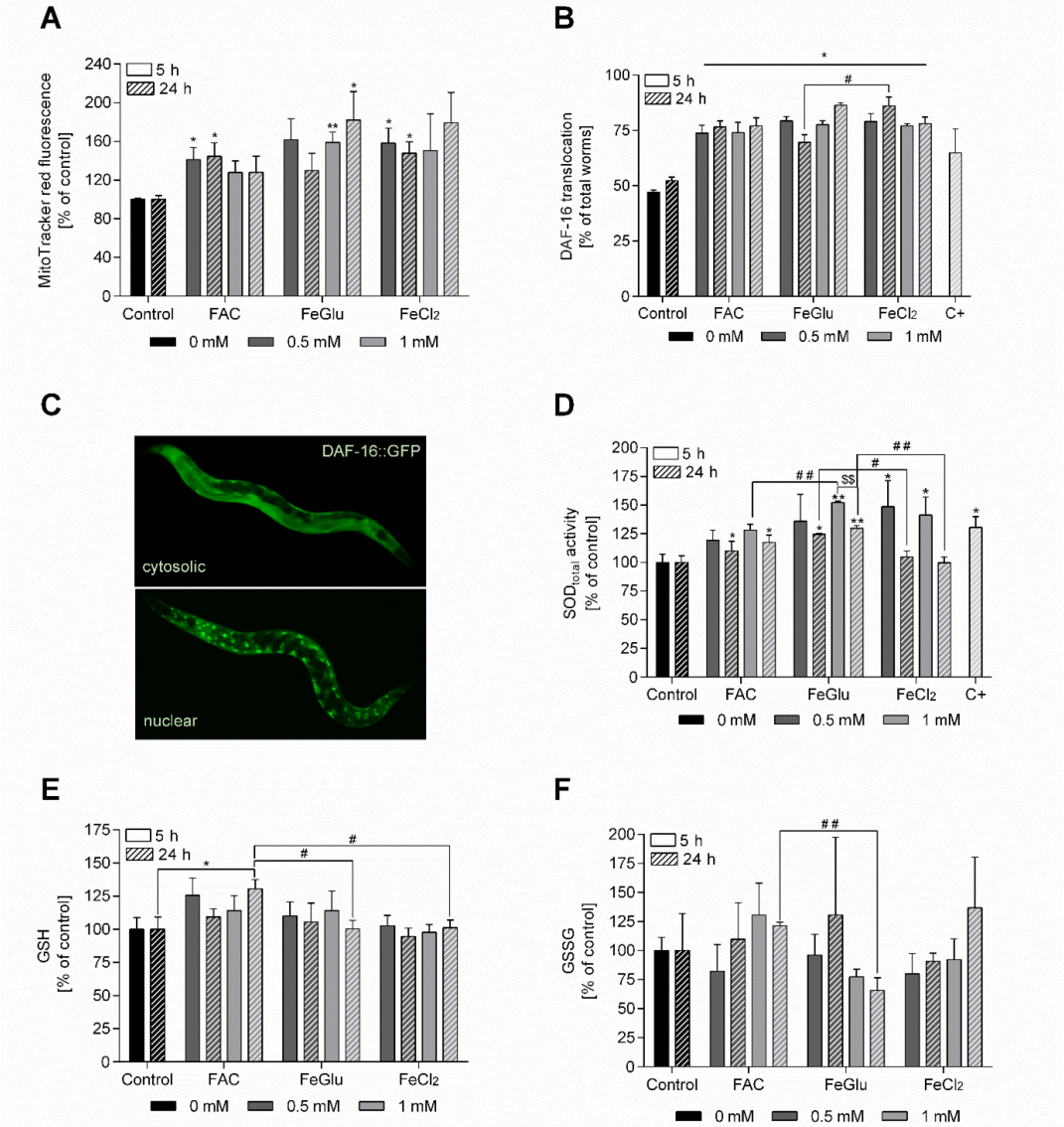

Figure 11. (A) MitoTracker red fluorescence compared to untreated control [%]. (B) DAF-16 translocation from cytosol to nucleus in DAF-16::GFP strain [% of total worms]. (C) Fluorescence images of DAF-16::GFP strain with cytosolic or nuclear localized DAF-16. (D) Total SOD activity compared to untreated control [%]. (E) GSH and (F) GSSG compared to untreated control [%]. Shown are mean + SEM after treatment for 5 or 24 h with Fe species of n ≥ 3 independent experiments. Paraquat was used as a positive control (C+). Significance is depicted as * compared to untreated control, # compared to other Fe species, and $ compared to other treatment times.

Various enzymes, including SOD, by detoxifying superoxide, are involved in counteracting oxidative stress.[239] To verify whether the treatment with the Fe species leads to an effect on SOD, the activity of the total SOD was measured. While the total SOD activity after 5 h of treatment was 6.7 ± 0.8 U/mg protein in the untreated control, after 24 h, the activity was 13.0 ± 1.3 U/mg protein. Each Fe species led to increased SOD activity after 5 h of treatment, whereby the activity was higher with 1 mM FeGlu than after 1 mM FAC treatment (Figure 11D). After 24 h of treatment, $FeCl_2$ had no effect on SOD activity, resulting in a significant difference compared to FeGlu treatment (Figure 11D). Treatment with the Fe species did not lead to any alteration in the gene expression of *sod-3* (human *SOD-2*) and *sod-4* (human *SOD-3*) (Supplementary Figure 38).

In addition to enzymes, molecules such as GSH are involved in oxidative stress defense, either as radical scavengers or as cofactors of enzymes. The oxidation of GSH leads to the formation of GSSG, which is used as a marker for oxidative stress.[240] After both treatment times, the GSH level in the untreated control was 3.1 ± 0.3 ng/µg of protein, and the GSSG level was 4.0 ± 0.5 pg/µg of protein. Only 1 mM FAC led to an increase in GSH level by 30% after 24 h of treatment (Figure 11E). However, treatment with 1 mM FeGlu led to a reduced GSSG level by 35% after 24 h of treatment (Figure 11F).

Cellular membranes, such as the plasma membrane or mitochondrial membrane, have a specific composition of lipids and proteins to maintain their function. Phospholipids, such as PE and PC, represent the largest fraction in human and *C. elegans* cellular membranes, whereby a change in the composition can lead to a disruption in the functionality of the membrane.[241,242] Unsaturated fatty acids, in particular, can be targets for RONS, which can alter the composition of the cell membrane.[243] However, treatment with the three Fe species for 24 h did not result in significant changes in the degree of saturation or the ratio of these two lipid classes (Figures 12 and Supplementary Figure 39).

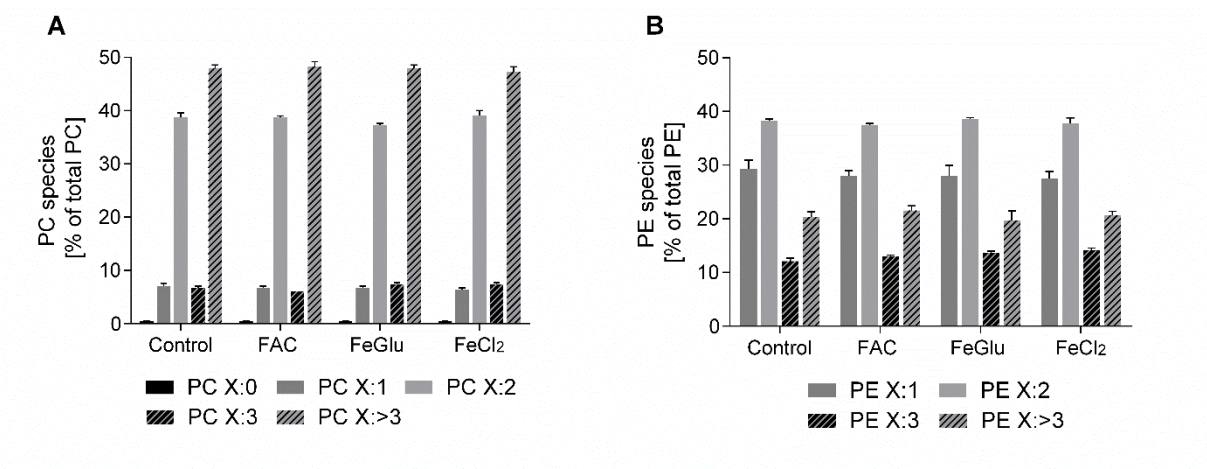

Figure 12. Distribution of PL based on the degree of saturation of PC (A) and PE (B) after treatment with Fe species for 24 h. Shown are mean + SEM of n ≥ 3 independent experiments, and PC X:0 represents, e.g., the sum of the measured saturated PC.

3.3.4. Treatment with the Fe Species Leads to an Increase in Apoptotic Cells

In the somatic cells of *C. elegans*, the receptor orthologue CED-1 is expressed, which engulfs apoptotic germ line cells in the nematode (Figure 13A).[244] The number of apoptotic germ line cells can be evaluated in the strain CED-1::GFP under a fluorescence microscope (Figure 13C). After 5 h of treatment, an average of 18 ± 1 apoptotic cells per worm were counted in the untreated control, compared with 11 ± 1 after 24 h. Treatment with each Fe species increased the number of apoptotic germ line cells by up to 50% after 5 and 24 h (Figure 13B). However, after 5 h, more apoptotic cells could be observed after treatment with 1 mM $FeCl_2$ than after 1 mM FAC.

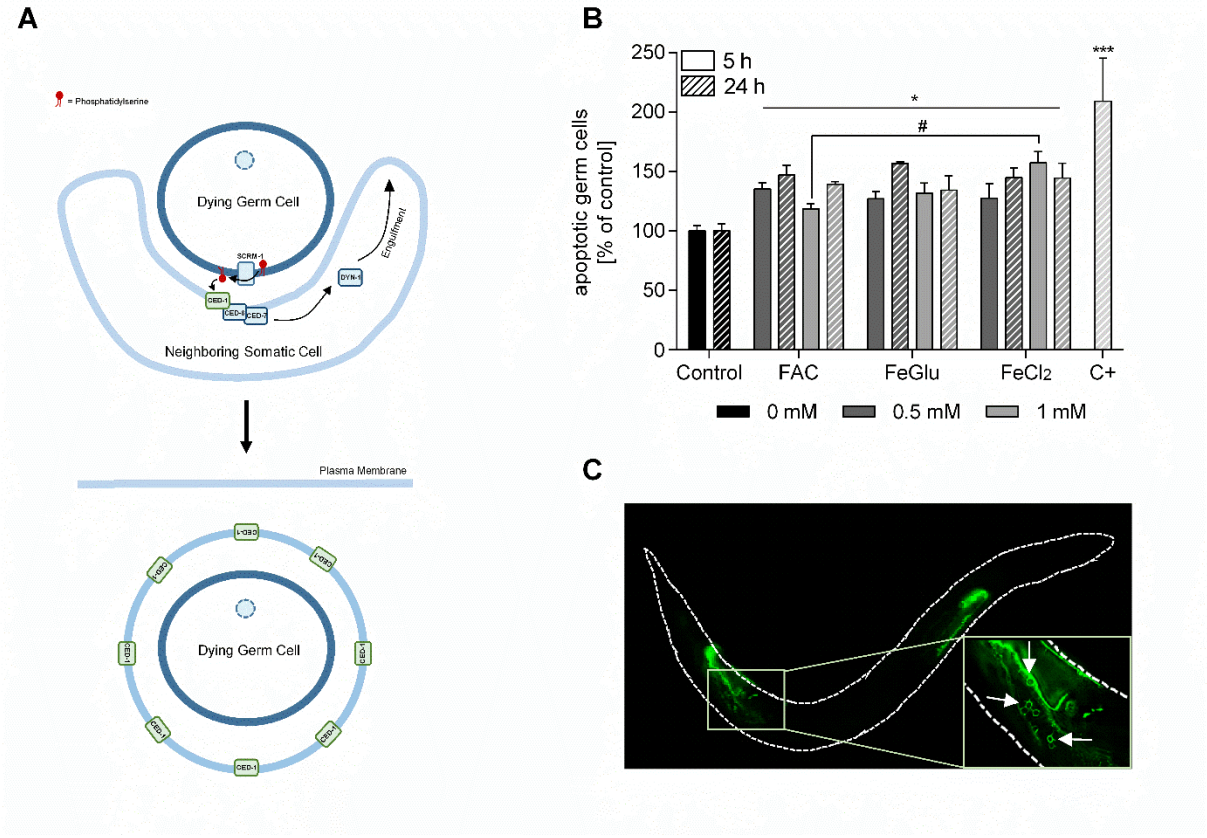

Figure 13. (A) Schematic engulfment of an apoptotic germ line cell by a neighboring somatic cell. (B) Apoptotic germ line cells compared to untreated control [% of control] after treatment for 5 and 24 h with Fe species. Shown are mean + SEM of n ≥ 3 independent experiments. (C) Fluorescence image of CED-1::GFP strain with circular apoptotic germ line cells, shown by white arrows. Significance is depicted as * compared to untreated control and # compared to other Fe species.

3.4. Discussion

Although Fe is the most biologically abundant transition metal, it is highly toxic in cases of overdose. In 2024, the EFSA released safe levels, such as 10 mg/day for children aged 1–3 years and 40 mg/day for adults.[2] Therefore, attention must be paid to avoid overdosing of Fe from food supplements and fortified foods. Regarding the Fe species in food and food supplements, knowledge about Fe species-specific effects is limited, and studies that directly compare bioavailability, effects on Fe homeostasis, and cellular consequences within the same study and model are lacking. A comparison under the same

experimental conditions is crucial due to factors influencing Fe absorption, such as age, dietary factors, and genetics.

This study confirmed that the bioavailability of Fe is dependent on both the Fe oxidation state and the Fe ligand of the Fe species used for exposure.[236,245] In contrast to FAC, $FeCl_2$ treatment for 24 h resulted in five times more Fe, and FeGlu treatment resulted in almost twice as much Fe in the nematode. While both Fe(II) species were taken up in a time-dependent manner, the uptake of Fe by FAC appeared to be time limited in *C. elegans*. In *C. elegans*, there is no known direct way to import ferric Fe. This first has to be reduced to ferrous Fe to be taken up via divalent metal transporters.[246] The time limitation may indicate a limitation of the reduction capacity of the involved reductases or reducing compounds. In 2024, the EFSA reported that the only indicator for an Fe dose–response was the occurrence of black stool, indicating the presence of unabsorbed Fe in the gastrointestinal tract. It is not considered an adverse event per se but may lead to systemic Fe overload and was used as a basis for the assessment of a safe Fe intake.[2] The importance and variability of bioavailability were also demonstrated in a study involving participants with various diets. While dietary Fe amounts were similar, omnivores showed better Fe status (measured as ferritin) than flexitarians, vegetarians, or vegans.[247] This underlines the importance of the choice of Fe compound and the importance of knowledge about the bioavailability and uptake of certain Fe species.

Nevertheless, there are some limitations associated with the model organism used in this study that limit the transfer of the findings to humans. Despite sharing numerous orthologous genes, *C. elegans* lacks transferrin, a protein for serum Fe transport in humans, and hepcidin, which plays a critical role in Fe metabolism and intestinal uptake. Additionally, while most Fe in humans is taken up in the duodenum at an acidic pH, the intestinal pH of *C. elegans* is nearly neutral.[214]

The increased gene expression of *smf-3* and the lower Fe levels in *smf-3*Δ indicated the involvement of this gene in the Fe homeostasis of all three Fe

species. Notably, the most prominent effect was detected in the $FeCl_2$-exposed worms since lacking *smf-3* showed severely reduced Fe content of 10–20% compared to $FeCl_2$-treated wild-type worms. However, despite the loss of function of SMF-3, an increase in Fe content could be achieved by treating with the Fe species; consequently, there must be additional ways of Fe uptake in *C. elegans*. Au et al. showed that the *DMT-1* orthologue *smf-2* is also involved in Fe import.[175] Another often-discussed Fe importer is ZIP14, which is also involved in the import of Zn and Mn.[248] The reductase *dcytb* also had an impact on the bioavailability of Fe by each of the Fe species as lower Fe levels were measured in *dcytb*Δ. The gene *f55h2.5* (*dcytb*) is reported as an orthologue for human *DCYTB*, but to our knowledge, the impact of this gene on metal homeostasis has not yet been published. The deletion of both ferritin-encoding genes led to lower but species-specific Fe levels. Due to the loss of function of the Fe storage proteins, Fe can be stored less or not at all as redox-inactive ferric Fe. FPN can export Fe(II) out of the cell, but no systemic excretion mechanism for Fe from the organism is known in humans and in *C. elegans*. Therefore, the loss of function of ferritin could have an impact on Fe import and thus lead to lower Fe levels.[249] The role of *cp* in oxidizing ferrous to ferric Fe is most commonly discussed in Fe homeostasis in relation to Fe export. The complete absence of *cp* leads to Fe accumulation in the neurodegenerative disease aceruloplasminemia.[250] In our study, the deletion of *cp* led to a lower Fe basal level and after treatment with $FeCl_2$ to a lower Fe level compared to that of the wild type. By FAC and 0.5 mM FeGlu treatment, a similar Fe level as in the wild type could be reached, although the Fe basal level is lower. This may indicate a higher accumulation of Fe in the absence of *cp* after treatment with FAC and FeGlu. A closer look at the regulation of gene expression related to Fe homeostasis genes following 5 and 24 h of exposure clearly highlights the importance of the 5 h exposure after treatment with all three Fe species. Thus, the Fe homeostasis-associated genes showed a response to the increased Fe level after a short treatment period, which is essential for maintaining Fe

homeostasis. The early regulation could possibly impact the uptake of Fe by FAC since in contrast to the ferrous Fe species, a similar amount of Fe was measured after 24 h as after 5 h of treatment. However, no conclusion can be made about the respective protein levels in this study, and this should be investigated in further studies.

The increase in MitoTracker Red fluorescence, DAF-16::GFP translocation, and SOD activity after treatment with FAC, FeGlu, and $FeCl_2$ indicated the formation of RONS and a response to oxidative stress Fe species-unspecific. We identified that the gene expression of *ftn-1* was upregulated after 5 h of treatment but have no direct evidence of the amount of ferritin-bound Fe and the amount of labile Fe. We cannot make a direct assessment of the reactivity of the increased Fe levels in our study, but the response in the oxidative stress endpoints indicates the presence of labile reactive Fe after treatment with all three Fe species. Abbasi et al. showed that after 48 h of treatment with FAC in HepG2 cells, labile Fe was 10-fold and total Fe was 3-fold higher than in the untreated control. Along with these data, RONS were also increased.[251] The increased gene expression of *ftn-1* could be associated with enhanced DAF-16 translocation, potentially to mitigate oxidative stress by reactive Fe. Ackerman et al. demonstrated that *daf-16* is involved in the regulation of *ftn-1*, as evidenced by decreased *ftn-1* gene expression in a *daf-16* RNAi mutant.[192] The increased translocation of DAF-16 in our study suggests that a variety of genes related to oxidative stress may be affected by the tested Fe species. Although the Fe content after 24 h by 1 mM $FeCl_2$ was five times and by FeGlu almost twice as high as after FAC treatment, no difference in MitoTracker fluorescence and DAF-16 translocation could be observed between the Fe species. The response of these two endpoints was the same after both treatment times. However, no changes in SOD activity could be measured after 24 h of treatment with 1 mM $FeCl_2$. In a study with HepG2 cells, treatment with ferrous sucrose and ferrous dextran resulted in a concentration-independent increase in RONS, as measured by DCF fluorescence. Only ferric gluconate led to increased

fluorescence at higher concentrations, resulting in a Fe species-specific difference.[252] Although increased Fe levels and oxidative stress are associated with increased GSSG, no elevation was detected by either Fe species at either treatment time. However, Piloni et al. showed that injection of Fe-dextran increased the Fe content in the brain of rats 4-fold, which was accompanied by lower GSH levels and increased GSSG and malondialdehyde (MDA) levels.[253] In our study, the markedly increased gene expression of *ftn-1* indicates detoxification by minimizing reactive Fe(II) and thus also the formation of RONS. While the MitoTracker measures RONS and increased DAF-16 translocation and SOD activity are responses to this reactive species, lipid peroxidation may be a consequence of RONS. We hypothesize that the regulation of Fe homeostasis and antioxidative defense could be sufficient to keep the effects on GSH and GSSG low at the measured time points in this study. Furthermore, it was investigated whether overdosing with the three Fe species affects the degree of saturation or PE/PC ratio as an alteration can lead to negative consequences on the mitochondria or the endoplasmic reticulum.[241] No alterations were observed for these endpoints compared to the untreated control.

Along with the oxidative stress endpoints, apoptotic germ cells were also increased after treatment with all three species. Lyamzaev et al. showed that FAC in rat cardiomyocyte H9c2 cells led to mitochondrial RONS and lipid peroxidation, in addition to reduced cell viability. As the mitochondrial-targeted antioxidant SkQ1 restored these effects to the level of the untreated control, it was concluded that the mitochondrial changes contributed to cell death.[254] Since we measured increased mitochondrial RONS and SOD activity, which are also expressed in the mitochondria, these changes could be involved in the increased formation of apoptotic cells. In the study by Senchuk et al., the function of *daf-16* was investigated in long-lived mitochondrial *C. elegans* mutants. Increased translocation of DAF-16 and upregulation of its targeted genes were observed in these strains. The conclusion was that mild impairment

of mitochondrial function via DAF-16 positively affects longevity.[255] This indicates that mitochondrial changes can also affect the regulation of DAF-16 in our study.

Overall, we were able to show in this study that both the oxidation state and the ligand were particularly relevant in terms of bioavailability when it comes to the choice of Fe species. In addition, we gained further insights into relevant genes of Fe homeostasis in *C. elegans*. We demonstrated that the poorly studied genes *dcytb* (*f55h2.5*) and *cp* (*f21d5.3*) are involved in Fe homeostasis and affected the bioavailability of Fe. Although treatment with FAC, FeGlu, and $FeCl_2$ led to increased RONS formation and oxidative stress response, these effects were Fe species-unspecific, even though we measured species-specific Fe amounts. The upregulation of *ftn-1* gene expression indicated Fe detoxification, but further studies would be necessary to investigate ferritin-bound Fe and the amount of reactive Fe(II). Another consequence of Fe overdosing was the increased number of apoptotic cells in *C. elegans*, which was determined in a species-unspecific manner.

3.5 Acknowledgment

C. elegans strains N2, *smf-3*Δ, *dcytb*Δ, *daf-16*::gfp and *ced-1*::gfp were provided by CGC, which is funded by NIH Office of Research Infrastructure Programs (P40 OD010440). Strain *cp*Δ was provided by Mitani laboratory at Tokyo Women's Medical University.

3.6 Funding sources

This project was supported by the DFG Research Unit TraceAge (FOR 2558, BO4103/4-2).

Abstract

Although the redox active essential trace element iron (Fe) is involved in many important biological processes, an overexposure can lead to the excessive formation of reactive oxygen and nitrogen species (RONS). Thus, Fe accumulation, as for example observed in neurodegenerative diseases or diseases as hemochromatosis, can lead to adverse consequences, especially if the antioxidant system is weakened. This system, and especially the most abundant antioxidant in organisms, glutathione (GSH), can be impaired by excess RONS levels, which is relevant during aging and in the context of neurodegenerative diseases. In this study, we demonstrate the consequences of Fe overdosing or/and GSH depletion in *Caenorhabditis elegans* (*C. elegans*) on Fe homeostasis, mitochondrial mass, phospho- and sphingolipidome, and on the neurotransmitter levels of acetylcholine, serotonin, dopamine, and γ-aminobutyric acid. Therefore, we treated L4 nematodes with Fe(III) ammonium citrate (FAC) for 24 h or/and diethyl maleate (DEM) for 2 h or 24 h. While FAC treatment alone did not affect mitochondrial mass and cardiolipin content, it increased the amount of several lipid classes and the neurotransmitter acetylcholine. Treatment with DEM alone resulted in GSH depletion by 70% and was associated with decreased mitochondrial mass and increased Fe(II), lipid, acetylcholine, and serotonin levels. Transcriptomic analysis revealed that genes involved in GSH biosynthesis, Fe homeostasis, mitochondrial stress response, lipid biosynthesis, and neurotransmitter regulation are differentially expressed after DEM treatment. In addition, we were able to determine the GSH-DEM product in the nematode using HPLC-MS/MS. Although FAC treatment increased total Fe content in the nematode fivefold, the combined treatment with DEM showed no further effects compared to treatment with FAC or DEM alone. Together, these findings highlight the consequences of an impaired intracellular redox system on mitochondria, lipidome, and neurological endpoints, and identify several pathways, metabolites, and potential counter regulation as well as long lasting effects.

Chapter 4

Iron Up and Glutathione Down: An Imbalance Impacting Iron Homeostasis, Mitochondria, Lipidome, and Neurotransmitters in *C. elegans*

Based on

Anna Gremme, Emely Gerisch, Dominik Wieland, Julia Hillebrand, Franziska Drews, Marcello Pirritano, Ann-Kathrin Weishaupt, Janina Fuss, Vera Schwantes, Johannes Scholz, Vivien Michaelis, Alicia Thiel, Gawain McColl, Bernhard Michalke, Martin Simon, Heiko Hayen, Julia Bornhorst

Submitted to: *Redox Biology*

Highlights

- FAC affected phospho- and sphingolipidome, and acetylcholine level

- Glutathione-diethyl maleate could be measured via HPLC-MS/MS

- Diethyl maleate increased Fe(II) and affected genes associated with Fe homeostasis

- Diethyl maleate impaired the mitochondria and upregulated the stress response gene *hsp-6*/*HSPA-9*

- Diethyl maleate affected phospho- and sphingolipid, serotonin, and acetylcholine metabolism

Keywords

iron, glutathione, mitochondria, lipids, neurotransmitters, *C. elegans*

Chapter 4 – Iron Up and Glutathione Down: An Imbalance Impacting Iron Homeostasis, Mitochondria, Lipidome, and Neurotransmitters in *C. elegans*

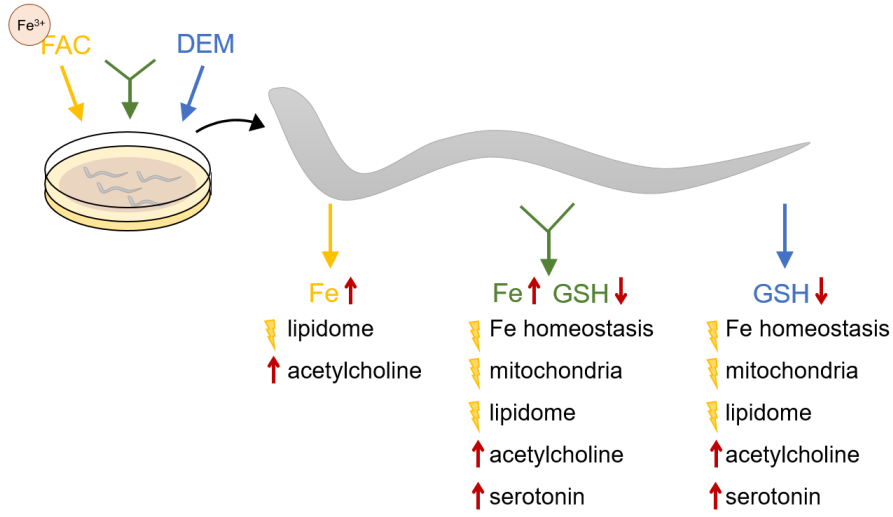

Figure 14. Graphical abstract of: Iron Up and Glutathione Down: An Imbalance Impacting Iron Homeostasis, Mitochondria, Lipidome, and Neurotransmitters in *C. elegans.*

4.1. Introduction

Iron (Fe), an essential trace element, is involved in many cellular processes, including energy production, DNA synthesis, and oxygen transport [7,8]. These functions rely on the continuous redox cycling between Fe(II) and Fe(III), which may, in excess, lead to adverse consequences such as the enhanced formation of reactive oxygen and nitrogen species (RONS) via the Fenton reaction [220]. Higher levels of RONS increase the risk of adverse modifications to biomolecules such as lipids, proteins, and DNA [219]. Therefore, a particular perturbation of cellular function and integrity arises if Fe levels are increased, as it has been observed in aging human brains and diseases like hemochromatosis or diabetes mellitus [218]. Fe accumulation in the brain is further associated with cognitive impairments and even neurodegenerative diseases such as Alzheimer's (AD) and Parkinson's diseases, but the underlying mechanisms are

not fully understood [218,256]. Due to health risks associated with excessive Fe intake from food and food supplements, the European Food Safety Authority (EFSA) has defined safe intake levels of 10 mg/day for children and 40 mg/day for adults in 2024 [2]. Under optimal conditions, cells possess a robust antioxidative system to prevent excessive RONS production and oxidative stress. However, antioxidative capacity can be depleted by enhanced RONS production, toxins, or by aging, which can lead, aside from others, to a deficiency of the important antioxidant glutathione (GSH) [257]. This endogenous tripeptide is one of the most abundant intracellular antioxidants, as it functions as a radical scavenger and as a co-enzyme for several enzymes like glutathione peroxidases (GPX), glutaredoxins, and glutathione-S-transferases (GST) [74]. As a co-enzyme of GPX, GSH is crucial for the conversion of lipid hydroperoxides, which are discussed in the context of the Fe-dependent cell death, ferroptosis [258]. Additionally, GSH plays an important role in Fe homeostasis, as it forms the major complex of the labile Fe pool (LIP). Thereby, free Fe is prevented from accumulating while ensuring its rapid availability, for example, for incorporation into Fe-dependent enzymes [4]. The biosynthesis of heme and Fe-sulfur clusters primarily takes place in the mitochondria, leading to higher amounts of Fe in this organelle [259]. This, combined with the high production of superoxide radicals during energy production in the form of adenosine triphosphate (ATP), increases the potential for mitochondrial oxidative stress and requires enhanced antioxidant defense [260]. Since neurons have a high energy demand, they are rich in mitochondria, and impairments of these organelles are often discussed in the context of neuronal dysfunction and neurodegenerative diseases [261]. This underlines the importance of a balanced Fe homeostasis and cellular redox system.

The question arises about consequences for an organism in case of Fe overexposure and GSH depletion. To gain further mechanistic insights, we established a model organism showing increased Fe amounts, decreased GSH levels, or a combination of both. For this purpose, we treated the nematode

Caenorhabditis elegans (*C. elegans*) with iron(III) ammonium citrate (FAC) or/and the GSH binding molecule diethyl maleate (DEM) [83,206]. In this study, L4 worms were treated with FAC for 24 h, followed by short-term (2 h) and long-term (24 h) treatment with DEM. These two time points resemble acute or long-term effects, with the latter more relevant for adverse effects from chronic exposure. *C. elegans* is an established model organism for toxicological and Fe homeostasis studies, as it has many orthologous genes to those in mammals, which include genes associated with oxidative stress, cell death, neurological functions, and Fe homeostasis [169].

4.2. Materials and Methods

4.2.1 *C. elegans* handling and treatment with FAC and DEM

The *C. elegans* strains Bristol N2 (wild type) and OH7193 (*him-8* (*e1489*)) were obtained from the *Caenorhabditis* Genetics Center (CGC).

The worms were cultivated on 8P agar plates coated with NA22 *E. coli* at 20 °C, as described previously [160]. To ensure all experiments were performed using worms at larval stage 4 (L4), the nematodes were synchronized following established methods and subsequently grown on nematode growth medium (NGM) coated with OP50 *E. coli* [223]. L4 worms were treated for 24 h with FAC (reagent grade, Sigma Aldrich), which was freshly dissolved in bidistilled water and added to inactive *E. coli* on NGM agar plates before each experiment. Since the chemical formula of FAC ($xFe{\cdot}yNH_4C_6H_7O_8$) is semi defined, we determined a Fe content of 14.8 ± 0.3% by weight (n = 3) using inductively coupled plasma-optical emission spectrometry (ICP-OES) (instrumental parameters in 4.2.3) in the FAC batch used. The 20 mM FAC used in this study is equivalent to 5.3 mg/mL FAC. The *E. coli* was inactivated as described previously [189]. Following 24 h FAC treatment, day 1 adult nematodes were treated with DEM (Sigma Aldrich) for either 2 h in 85 mM NaCl solution or for 24 h on NGM plates prepared in the same manner as for FAC treatment. DEM was diluted in DMSO,

and the final concentration of DMSO was adjusted to 1% v/v under all conditions. DEM treatment did not involve additional FAC exposure.

4.2.2 Protein determination via BCA Assay

To normalize metal content, GSH, GSSG, nucleotides, lipids, malondialdehyde (MDA), and neurotransmitter levels to protein content, the protein amount was determined using bicinchoninic acid (BCA) assay as described previously [225].

4.2.3 Quantification of total Fe and Zn via ICP-OES

Quantification of total Fe and Zn was performed using ICP-OES (Avio 220 Max, Perkin Elmer) as previously described [189]. The instrument parameters were as follows: Plasma power: 1500 W, cooling gas: 8 L/min, auxiliary gas: 0.2 L/min, nebulizer (MicroMist™) gas: 0.7 L/min. The analysis was performed using Yttrium (Y) as internal standard and the following element lines: Fe – 259.939 nm, Zn – 206.200 nm, Y – 371.029 nm. The element contents were normalized to protein amount.

4.2.4 Determination of GSH, GSSG, and GSH-DEM levels via HPLC-MS/MS

Quantification of reduced (GSH) and oxidized (GSSG) glutathione levels was performed using high performance liquid chromatography-tandem mass spectrometry (HPLC-MS/MS, Agilent 1290 Infinity II, Sciex QTrap 6500+ triple quadrupole MS) as described by Thiel et al. [232]. The product S-(α,β-bis(ethoxycarbonyl)ethyl)glutathione (GSH-DEM) of the reaction of GSH with DEM was previously characterized by Kubal et al. using ^{1}H NMR analysis [83]. We adapted the method of Thiel et al. to include the determination of this molecule, with specific parameters detailed in the supplementary table (Supplementary Material for Chapter 4). GSH and GSSG were quantified using external calibration and normalized to protein content. To estimate the formation of the GSH-DEM product, the GSH-DEM/GSH ratio was calculated based on the integrated peak areas.

4.2.5 Transcriptomic analysis

For transcriptome analysis, RNA was isolated from 750 day 1 and day 2 worms in 1 mL TRIreagent® (Sigma-Aldrich) using the phenol/chloroform extraction method as previously described [226]. Isolated RNA was purified with the RNA clean and concentrator™-5 Kit (Zymo Research) according to the manufacturer's instructions. The integrity of the RNA was verified using gel electrophoresis. Library preparation was performed with 300 ng RNA using the NEBNext® Ultra™ II directional RNA library prep kit for Illumina® in conjunction with Poly(A) mRNA magnetic isolation (#E7760S, #E7490S, New England Biolabs) with 14 PCR cycles according to the manufacturer's instructions.

Library concentration was verified using the Qubit™ 1xdsDNA HS Assay Kit (#Q33230, Thermo Fisher Scientific) and the Qsep1 Bio-Fragment Analyzer (BiOptic Inc.) with a Standard DNA Cartridge Kit (catalogue no.: C105201) was used to check the library for adapter contamination and size distribution.

Libraries were pooled and sequenced using a S4 Flowcell on the NovaSeq 6000 Illumina platform (Illumina) in 100 bp paired-end sequencing mode. De-multiplexing, quality trimming, and adapter removal were performed using TrimGalore (version 0.6.5, www.bioinformatics.babraham.ac.uk), which uses cutadapt [262]. Reads were randomly subsampled using seqtk (https://github.com/lh3/seqtk) and single-end reads were mapped onto the *C. elegans* Bristol N2 genome using the bowtie2 plugin for Geneious Prime version 2025.1.2. Expression values of annotated genes were calculated using the "calculate expression values" function of Geneious Prime. Differences between the sample groups were visualized by PCA based on transcripts per million (TPM) expression level data using the prcomp and ggbiplot visualization function in R. Differentially expressed genes (DEGs) were calculated using the DESeq2 Plugin for Geneious Prime with a threshold of p-value <0.01 and $\log_2$ fold change >1/<-1 for DEG characterization [263]. Term analysis of DEGs was performed using the geneontology.org website [264,265] which uses PANTHER [266].

For visualization, an R-script from [267] was used. All sequencing data are available in the ArrayExpress database (http://www.ebi.ac.uk/arrayexpress) under accession number E-MTAB-15180.

4.2.6 Determination of survival rate

Survival rate was assessed to evaluate the lethality of DEM and combined FAC and DEM treatment. For this purpose, 20 – 30 worms were transferred to a 3.5 cm NGM agar plate coated with OP50 *E. coli* following 24 h FAC and 2 h DEM treatment. After 24 h, the percentage of worms still moving and thus surviving was determined.

4.2.7 Determination of labile Fe^{2+} via FerroOrange dye

To assess the cytosolic labile Fe^{2+} status after FAC and DEM treatment, 2250 day 1 and day 2 adult worms were treated with the BioTracker FerroOrange dye (Sigma-Aldrich). Following FAC and DEM treatment, the nematodes were washed three times with NaCl solution (85 mM, 0.01 % Tween® 20) to remove eggs and L1 worms by allowing the adult worms to sink to the bottom of the tube and removing the supernatant. The FerroOrange dye was freshly dissolved in DMSO just before each experiment, and the worms were treated with a final concentration of 10 µM dye for 2 h in the dark with gentle shaking. The worms were washed again three times with NaCl solution and transferred to NGM plates coated with OP50 *E. coli* for 1 h in the dark to excrete the dye from the intestine. After repeated washing and removal of the *E. coli*, the fluorescence of the dye (excitation: 540 nm, emission: 575 nm) and the auto-fluorescence of the worms (excitation: 405 nm, emission: 455 nm) for normalization were measured with a microplate reader (Infinite M Plex, Tecan).

4.2.8 Determination of mitochondrial mass via MitoTracker™ Green FM

The mitochondrial mass was determined using MitoTracker™ Green FM (Thermo Fisher Scientific) [228]. This assay was carried out in *Pdat-1::mCherry* + P*ttx-3::mCherry* worms. Therefore, OH7193 worms were outcrossed and treated with FAC and DEM. The dye was dissolved in DMSO at a final

concentration of 2.5 mM, and aliquots were stored at -20 °C. After FAC and DEM treatment, the worms were treated with 1 µM MitoTracker™ Green for 1 h in the dark with gentle shaking. After the worms had been washed to remove the dye, they were transferred to NGM plates coated with OP50 *E. coli* to excrete the dye from the intestine for 1 h. The fluorescence of the MitoTracker™ dye (excitation: 485 nm, emission: 525 nm) and the red fluorescence of the worms (excitation: 560 nm, emission: 599 nm) were measured using a microplate reader (Infinite M Plex, Tecan). The green fluorescence of the MitoTracker Green FM was normalized to the worm number, which was measured as the red fluorescence of the worms. As a positive control, day 1 adult worms were treated for 1 h with 100 µM sodium azide (≥ 99.5%, Sigma Aldrich) [268].

4.2.9 Quantification of energy-related nucleotides via HPLC-DAD

The energy-related nucleotides ATP, adenosine diphosphate (ADP), adenosine monophosphate (AMP), nicotinamide adenine dinucleotide phosphate (NADPH), and nicotinamide adenine dinucleotide (NADH, NAD^+) were quantified using HPLC with a diode array detector (DAD) according to Bornhorst et al. [269]. Following treatment with FAC and DEM, 150 µL KOH (0.5 M) was added to 1500 day 1 and day 2 adult worms suspended in 100 µL NaCl solution. Immediately afterwards, the samples were homogenized with zirconia beads in a bead ruptor (40 sec, high, Biolab Products), and exactly 60 s after the addition of KOH, neutralized with 30 µL H_3PO_4 (10%). After centrifugation (20 min, 18620 rcf, 4 °C), the nucleotides and the protein content were measured from the supernatant. Detection was carried out at 259 nm, and quantification was performed using an external calibration for each nucleotide. Sodium azide was used as a positive control as described in 4.2.8. Nucleotide levels were normalized to protein content.

4.2.10 Determination of cardiolipins (CL) via 2D heart-cut HPLC-MS/MS

To determine CL, 4500 day 1 and day 2 adult worms were washed in 1 mL NaCl solution, and 50 µL was taken for protein determination. The worm pellet was

resuspended in 100 µL NaCl solution for lipid extraction. Prior to lipid extraction, according to a protocol based on Matyash et al., all samples underwent three freeze-thaw cycles followed by sonication in an ultrasonic processor for cell disruption [243,270]. The detailed protocol is provided in the Supporting Information (Supplementary for Chapter 4).

For the determination of CL distribution, 2D heart-cut HPLC-MS/MS (Vanquish Flex Duo UHPLC-system, Q Exactive Plus; Thermo Scientific) was performed (Supplementary for Chapter 4). Chromatographic data analysis and CL identification were carried out with the open-source software MZmine 4 (version 4.2.0; mzio GmbH) (Supplementary for Chapter 4) [271]. To analyze CL distribution, relative peak areas of the identified CL species were determined (Supplementary Figure 45). The sums of CL were normalized to the internal standard CL 64:4 and the protein content. Absolute quantification was not performed.

4.2.11 Determination of phospho- (PL) and sphingolipid (SL) composition

For the determination of PL and SL compositions, worm pellets and lipid extraction were conducted as stated above (see 4.2.10). Mass spectrometric measurements, including ion mobility spectrometry, were performed on a timsTOF fleX (Bruker Daltonics GmbH & Co. KG) mass spectrometer after reversed-phase HPLC separation utilizing an UltiMate 3000 UHPLC system (Thermo Fisher Scientific GmbH). Data processing and evaluation were carried out with the Metaboscape 2023b software (Bruker Daltonics GmbH). Details regarding mass spectrometric and chromatographic methodologies are provided in the Supporting Information (Supplementary for Chapter 4).

4.2.12 Quantification of MDA via HPLC-FLD

MDA was quantified using HPLC with fluorescence detection (HPLC-FLD, Agilent 1260 Infinity II) according to Weishaupt et al. [272]. After treatment with FAC and DEM, 1500 day 1 and day 2 adult worms were pelletized and

processed for analysis within one week. Results were normalized to protein content.

4.2.13 Quantification of neurotransmitter level via HPLC-MS/MS

The neurotransmitters acetylcholine, serotonin, dopamine, and γ-aminobutyric acid were quantified via HPLC-MS/MS (Agilent 1290 Infinity II, Sciex QTrap 6500+ triple quadrupole MS) as described previously by Weishaupt et al. [213]. For analysis, 1500 day 1 and day 2 adult worms were pelleted following FAC and DEM treatment, and neurotransmitters were quantified using deuterated internal standards [213]. The results were normalized to protein content.

4.2.14 Aldicarb sensitivity assay

To investigate the synaptic transmission of cholinergic neurons, the aldicarb-sensitivity assay according to Mahoney et al. was performed [273]. Aldicarb (Sigma-Aldrich) was dissolved in 70% ethanol and added to NGM agar at a final concentration of 2 mM. The assay was performed as previously described, and the number of non-paralyzed worms was counted every 60 min for 360 min [213].

4.2.15 Statistical analysis

Statistical analysis was performed using GraphPad Prism 6 (GraphPad Software). T-test with $\alpha = 0.05$ was used with the following significance levels: $*p \leq 0.05$, $**p \leq 0.01$, $***p \leq 0.001$.

4.3. Results

4.3.1 FAC increased the total Fe level and DEM bound to GSH

To verify the total Fe content of the worms after FAC and DEM treatment, Fe was determined using ICP-OES. 24 h treatment with 20 mM FAC increased the total Fe content in the nematodes 5-fold (Figure 15A), and even 24 h post Fe treatment, the Fe content was 3 times higher compared to untreated control (Figure 15E). While Fe levels were increased, the Zn content was decreased at both time points (Supplementary Figure 42). DEM had no effect on the Fe content after both treatment times. HPLC-MS/MS measurement revealed that the short-term treatment of 2 h with DEM decreased GSH level to 30 %

(Figure 15B), while the ratio of GSH-DEM to GSH was between 1 and 2 (Figure 15C). Whereas DEM treatment alone had no impact on GSSG level, it was markedly decreased after FAC treatment alone and combined with DEM (Figure 15D). Although long-term treatment with DEM for 24 h showed no impact on GSH levels (Figure 15F), a ratio of 0.015 ± 0.002 and 0.037 ± 0.004 of GSH-DEM to GSH could be determined depending on the DEM concentration (Figure 15G). In contrast to the short-term treatment, GSSG levels were decreased after 24 h treatment with 75 mM DEM (Figure 15H). Based on this and the higher GSH-DEM to GSH ratio, solely 75 mM DEM was used in the investigation of further endpoints for the long-term treatment.

4.3.2 Transcriptomic analysis

Transcriptomic analysis was performed to get an overview of the mechanistic consequences at the level of gene expression after FAC or/and DEM treatment. The principal component analysis (PCA) shows variances in the gene expression pattern between the untreated controls and the samples treated with DEM, both alone and in combination with FAC, in both treatment scenarios (Figure 16A, B). FAC-treated samples showed almost no variance compared to untreated control at both times measured (2 h or 24 h post FAC treatment). However, the combined treatment with FAC and DEM partially shows other differentially expressed genes (DEGs) compared to untreated control than the treatment with DEM alone. Only 74% of the genes overlap after 2 h DEM treatment and 59% after 24h DEM treatment (Supplementary Figure 43).

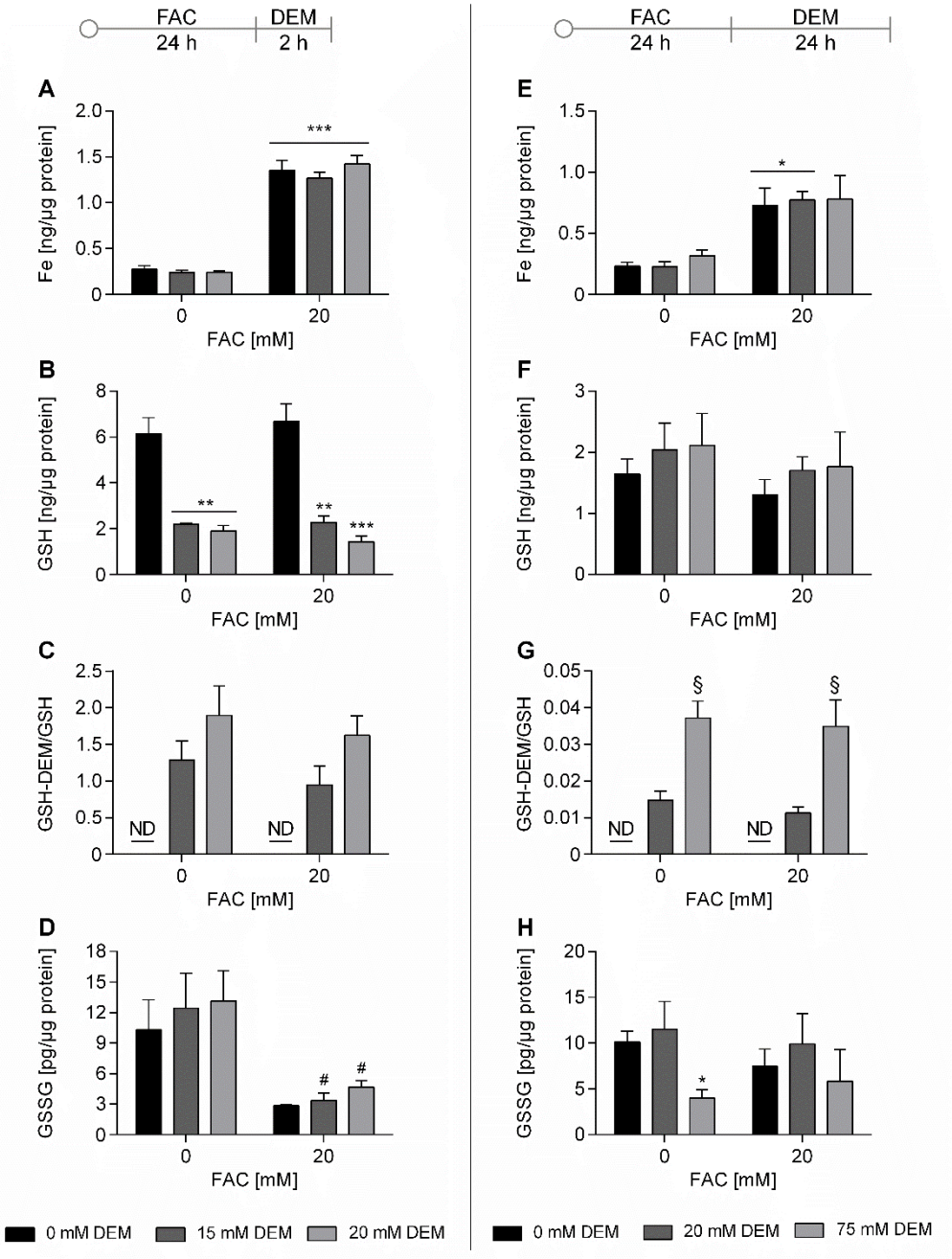

Figure 15. Increased Fe levels and glutathione status after treatment with FAC and 2 h (A-D) or 24 h (E-H) treatment with DEM. A, E) Total Fe was measured via ICP-OES. B, F) GSH levels, C, G) GSH-DEM/GSH ratio, and D, H) GSSG levels were measured via HPLC-MS/MS. Total Fe, GSH, and GSSG levels were normalized to protein content. Shown are the mean + SEM of ≥ 3 independent experiments. Significance is depicted as * compared to untreated control, § compared to other DEM concentrations, and # to DEM treatment only.

Transcriptomic analysis further indicates that DEM and the combined treatment with FAC led to changes in the expression of genes involved in GSH synthesis and GSH-dependent enzymes (Figure 16C). In addition to the genes shown here, several GST genes were also differentially expressed after DEM treatment for 2 h and 24 h, which are represented by the Gene Ontology (GO) term 'glutathione transferase activity' (Figure 17). Furthermore, several additional GO terms, such as iron ion binding, catalytic activity, oxidoreductase activity, and molecular function, were enriched among the DEGs, particularly after short-term treatment with DEM.

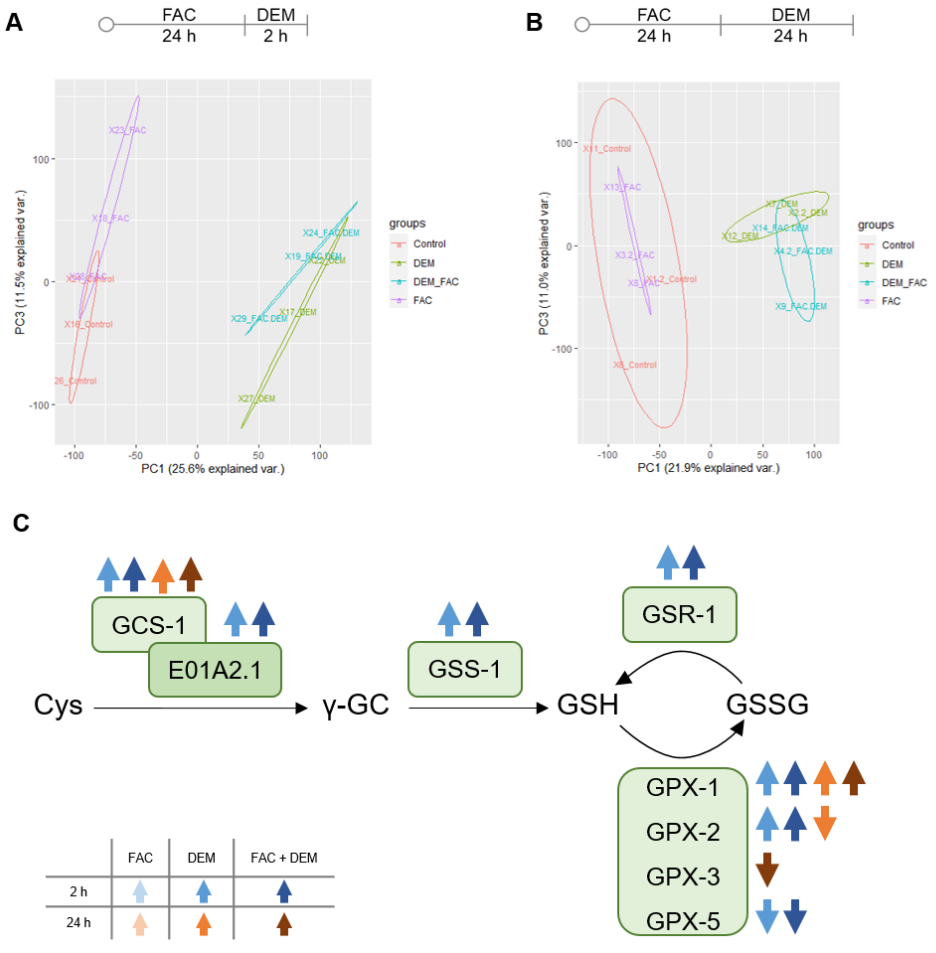

Figure 16. Principal component analysis (PCA) of PC1 and PC3 after treatment with FAC and 2 h (A) or 24 h (B) with DEM. C) Proteins encoded by DEGs of GSH metabolism. *C. elegans*/human orthologue: GCS-1/GCLC: glutamate-cysteine ligase; E01A2.1/GCLM: glutamate-cysteine ligase catalytic subunit; GSS-1/GSS: glutathione synthase; GSR-1/GSR: glutathione disulfide reductase; GPX-1/2/GPX-4: glutathione peroxidase; GPX-3/5/GPX-3: glutathione peroxidase.

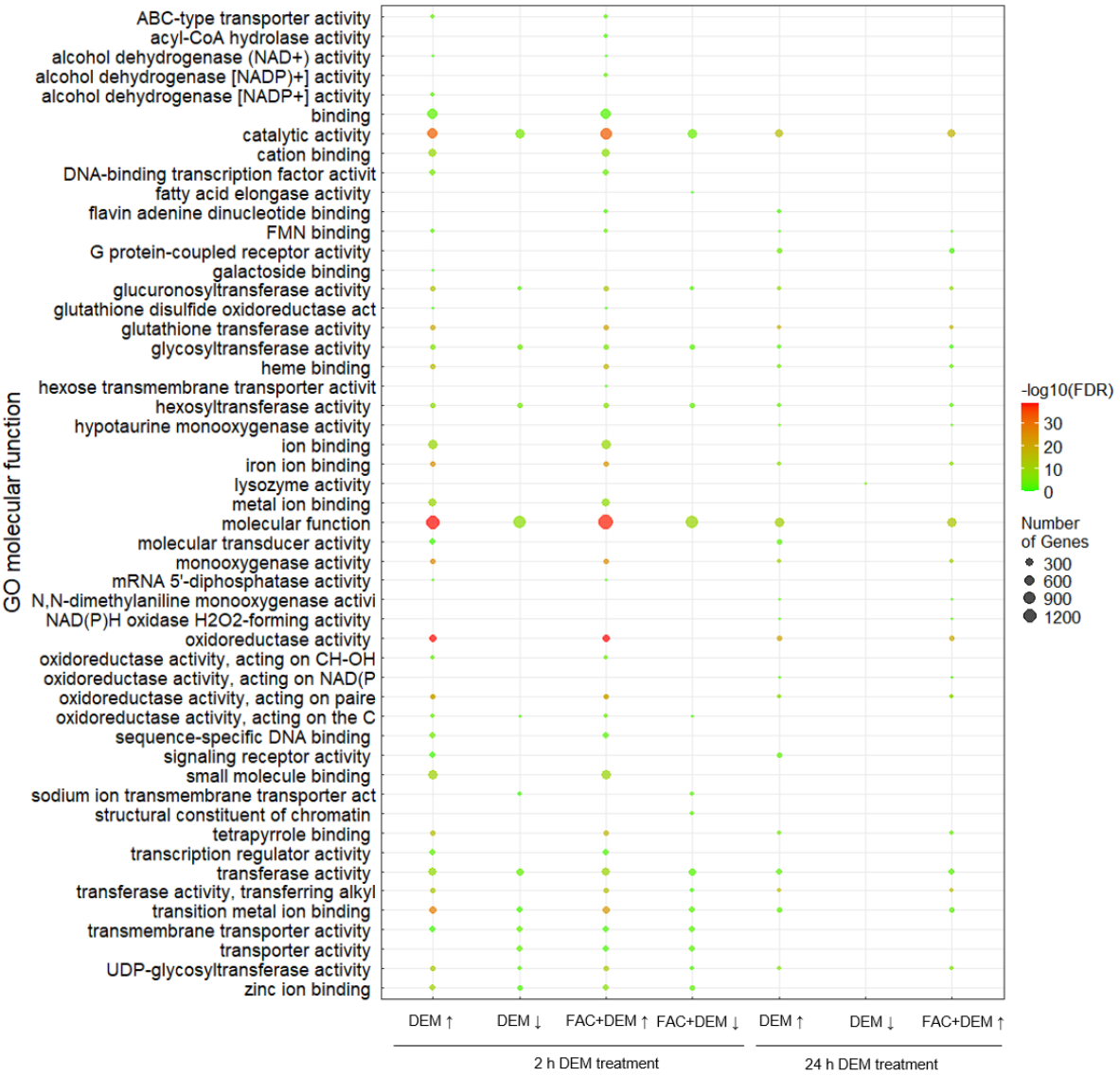

Figure 17. Heat map of a selection of Gene Ontology (GO) terms related to molecular function enriched among the up-(↑) and down-(↓) regulated DEGs after treatment with FAC and 2 h or 24 h DEM. No GO terms could be formed from the DEGs after treatment with FAC alone, and the down-regulated genes after the combined treatment with FAC and 24 h DEM.

4.3.3 DEM affects survival rate, Fe redox status, and genes of Fe homeostasis

To investigate the toxicity of FAC and DEM, the survival rate was examined 24 h after treatment. While short-term treatment with 15 mM DEM had no impact on the survival rate, 20 mM DEM alone led to a decrease of 15 % (Figure 18A). The prior treatment with FAC for 24 h had no impact on this effect. Due to the slight toxicity of 20 mM DEM, this concentration was further used for short-term treatment. Long-term treatment with DEM did not lead to a reduction in the survival rate (data not shown).

For the investigation of the Fe redox status, we treated the nematodes with FerroOrange following FAC or/and DEM treatment. This dye, also known as RhoNox-4, enables the detection of cytosolic labile Fe(II) through the irreversible reaction, resulting in a fluorescent compound (Figure 18D) [274]. Even though the total Fe content increased markedly after FAC treatment, no alterations in the Fe(II) level could be observed by FAC only (Figure 18B, C). However, the Fe(II) level increased significantly after short-term treatment with DEM, both alone and combined with FAC, to the same extent (Figure 18B). Long-term treatment with DEM did not lead to any alterations (Figure 18C).

Besides the redox status of Fe, changes in gene expression of Fe homeostasis genes also indicate an impact of DEM on Fe homeostasis (Figure 18E). This includes the downregulation of the Fe-importers *smf-2* and *smf-3*, and of the ferroxidase *f21d5.3*. Interestingly, the Fe-exporter *fpn-1.1* is upregulated, while another exporter, *fpn-1.2*, is downregulated. FAC alone and 24 h treatment with DEM led to increased gene expression of the Fe storage protein FTN-1, which stores Fe as Fe(III) species.

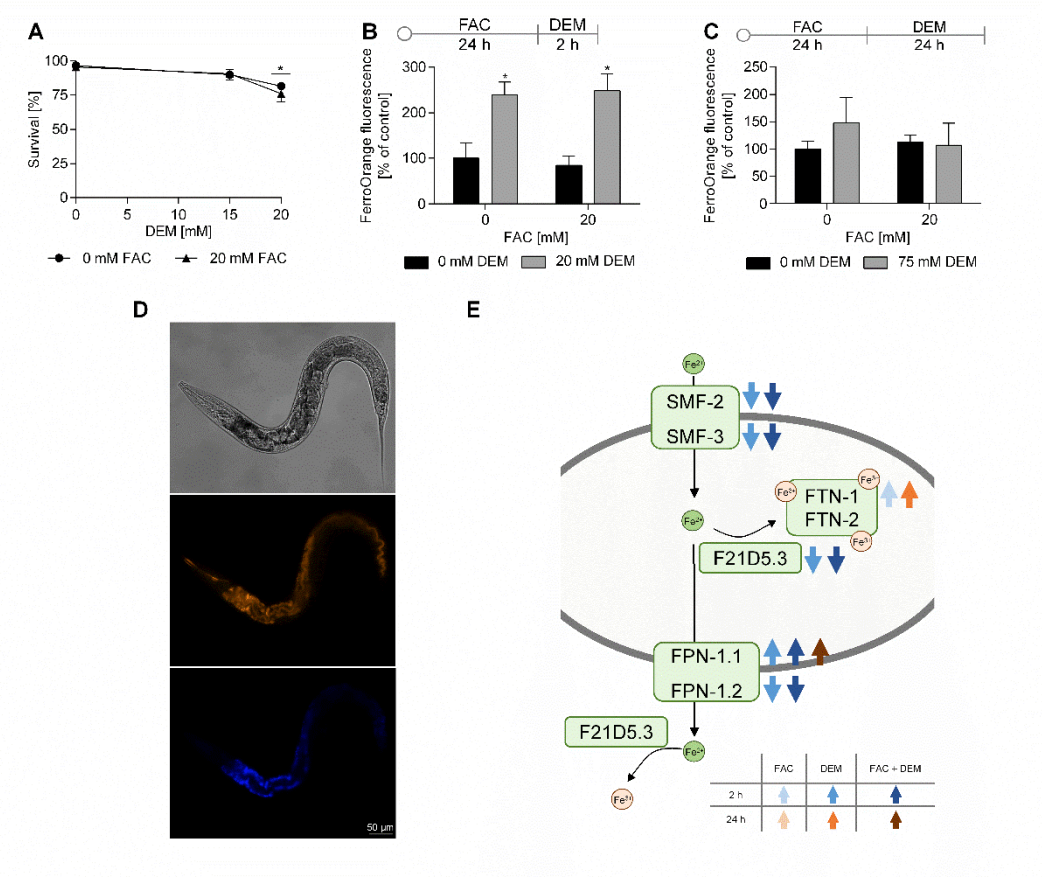

Figure 18. A) Survival rate after 24 h following FAC and 2 h DEM treatment. B, C) labile Fe(II) levels measured as FerroOrange fluorescence after treatment with FAC and 2 h (B) or 24 h (C) treatment with DEM were normalized to worm autofluorescence and untreated control. D) Representative Bright field, FerroOrange fluorescence (orange), and auto fluorescence (blue, excitation: 405 nm, emission: 455 nm) images of wild type worms after treatment with FerroOrange dye. E) Proteins encoded by DEGs of Fe-homeostasis after treatment for 2 h and 24 h with FAC, DEM, and FAC + DEM compared to untreated control. Shown are the mean + SEM of ≥ 3 independent experiments. Significance is depicted as * compared to untreated control. *C. elegans*/human orthologue: SMF-2/3/DMT-1: divalent metal transporter; FTN-1/-2/FTH and FTL: ferritin; F21D5.3/DCYTB: duodenal cytochrome B; FPN 1.1/1.2/FPN: ferroportin.

4.3.4 DEM led to mitochondrial impairment

We used the MitoTracker™ Green FM dye to determine the mitochondrial mass to explore the impact of FAC or/and DEM on the mitochondrial number and activity. The fluorescence dye accumulated in the mitochondrial matrix in living worms, whereby the intensity of the fluorescence is evaluated as proportional to the mitochondrial mass (Figure 19A) [275]. While treatment with FAC led to no

alterations, DEM led to decreased mitochondrial masses alone and combined with FAC in both short-term and long-term treatments (Figure 19B, C). In addition, transcriptomic data revealed that short-term treatment with DEM alone and in combination with FAC resulted in an upregulation of *hsp-6*, which is involved in the mitochondrial stress response (Table 2) [276]. Although the mitochondria are the main source of the energy nucleotide ATP, none of the treatments led to alterations in the overall cellular energy balance, calculated as energy charge value (AEC) (Supplementary Figure 44). The PL subclass cardiolipin (CL) was determined via 2D heart-cut HPLC-MS/MS. This class is exclusively located in the mitochondrial membrane and showed a trend toward reduced levels after 24 h DEM treatment, both alone and combined with Fe treatment (Figure 19E). In addition, the distribution of CL was primarily affected by the 24 h treatment with DEM alone and in combination with FAC (Supplementary Figure 45).

Table 2. Upregulated gene expression of *hsp-6* after treatment with 2 h DEM, both alone and in combination with FAC.

	DEM (2 h)	**FAC + DEM (2 h)**	**DEM (24 h)**	**FAC + DEM (24 h)**
stress response	*hsp-6* ↑	*hsp-6* ↑	-	-

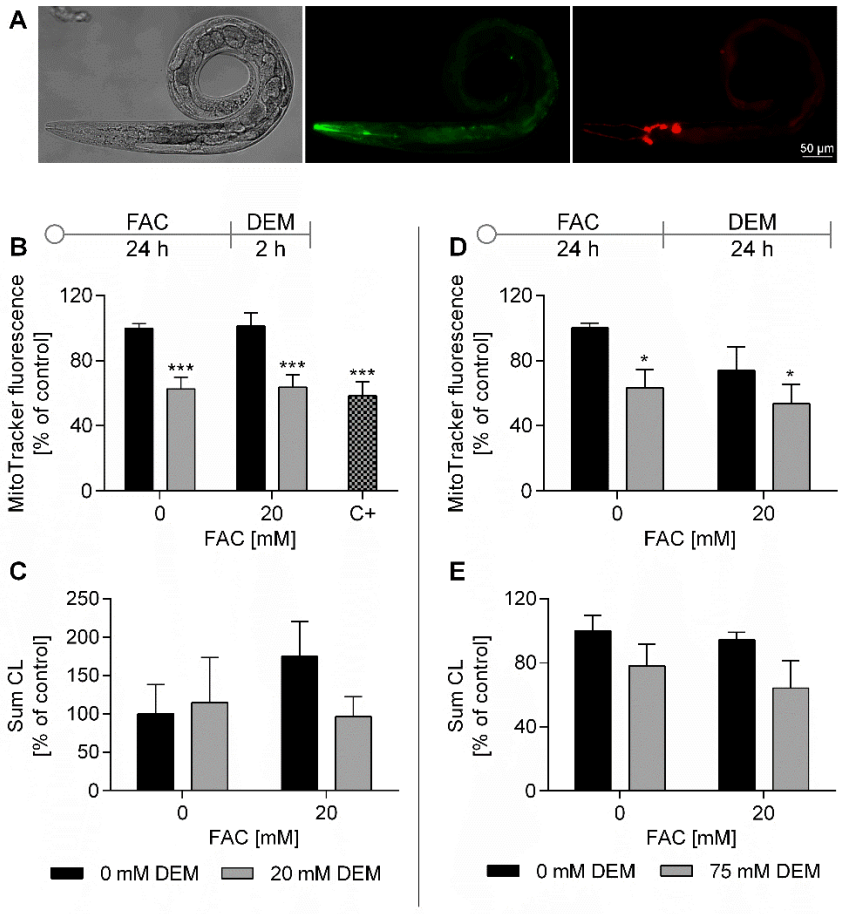

Figure 19. A) Representative Bright field, MitoTracker™ Green FM (green), and mCherry fluorescence (red) images of P*dat-1::mCherry* + P*ttx-3::mCherry* worms after treatment with MitoTracker™ Green FM dye. MitoTracker fluorescence and the sum of cardiolipins (CL) were measured after treatment with FAC and 2 h (B, C) or 24 h (D, E) DEM. MitoTracker fluorescence (B, D) was normalized to mCherry fluorescence and untreated control. CL (C, E) were determined via 2D heart-cut HPLC-MS/MS and normalized to internal standard (S3), protein content, and untreated control. Shown are the mean + SEM of ≥ 3 (CL: 2 h DEM n = 2) independent experiments. Significance is depicted as * compared to untreated control. C+: 1 h treatment with 100 µM sodium azide as positive control.

4.3.5 FAC and DEM treatment led to changes in the lipidome

In addition to CL, numerous PL and SL are part of cellular and cell organelle membranes, as well as involved in several signal transduction processes related to stress response, cell death, and neuronal function. The distributions of the 9 PL and 3 SL subclasses, measured in untreated control at both treatment times, are shown in Supplementary Figure 46. While no changes in total content of the different lipid classes could be observed after 2 h DEM treatment (Figure 20A),

FAC, DEM, and the combined treatment after 24 h led to a similar extent to increased levels of certain PL and SL subclasses (Figure 20B). After the long-term treatment, phosphatidylethanolamine (PE), plasmanyl-PE (PE-O), lyso-PE (LPE), lysophosphatidylcholine (LPC), sphingomyelin (SM), ceramide (Cer), and hexosyl-Cer (HexCer) were affected. In addition, treatment with FAC alone and in combination with DEM led to alterations in the distribution of the number of double bonds in PE and PC (Supplementary Figure 47).

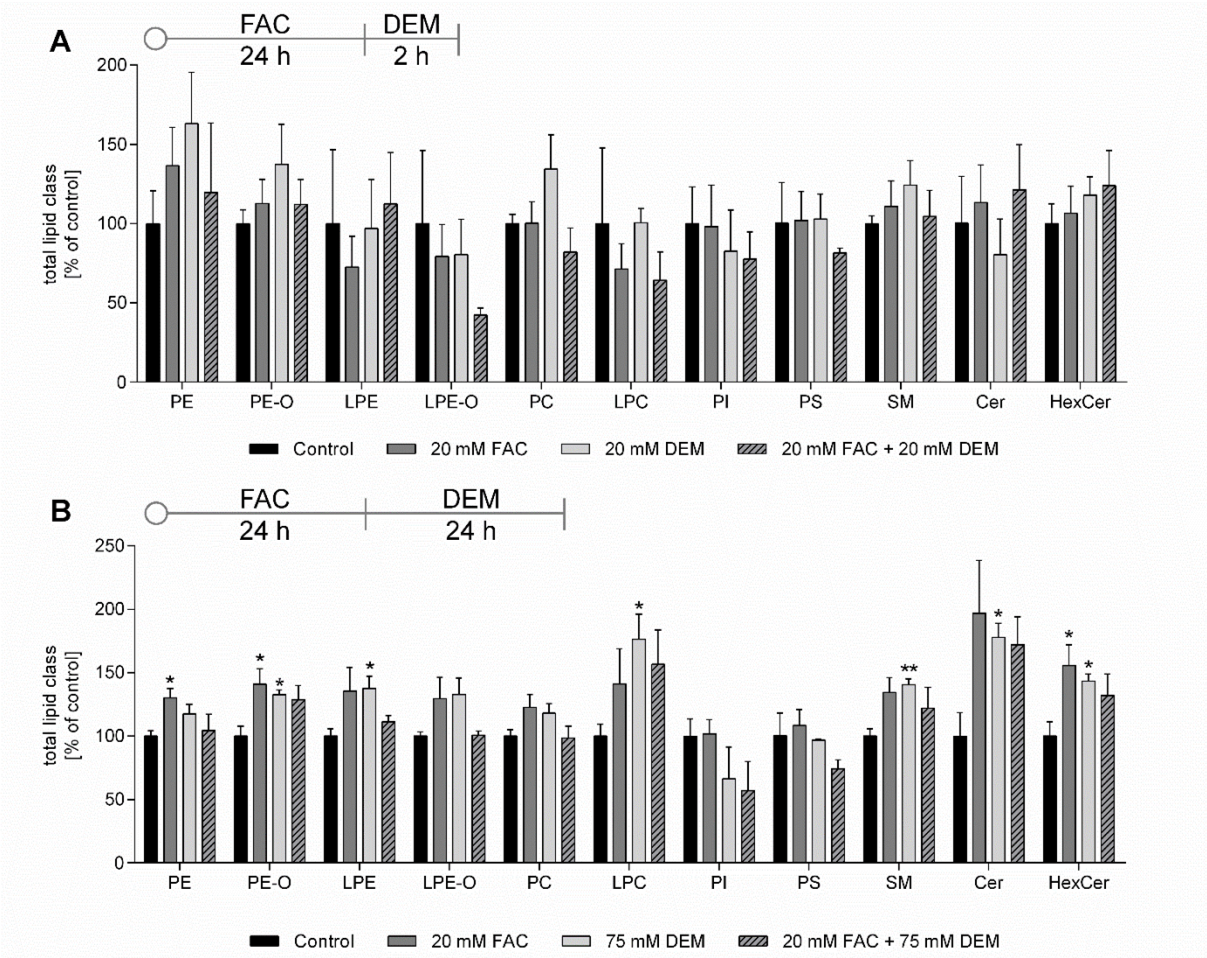

Figure 20. Relative distribution of phospho- (PL) and sphingolipid (SL) subclasses determined from the peak areas. Measurement followed after treatment with FAC and 2 h (A) or 24 h (B) DEM, and areas were normalized to protein content and untreated control. Shown are the mean + SEM of ≥ 3 independent experiments. Significance is depicted as * compared to untreated control. Abbreviations: PE phosphatidylethanolamine; PE-O plasmanyl-phosphatidylethanolamine; LPE lysophosphatidylethanolamine; PC phosphatidylcholine; LPC lysophosphatidylcholine; PI phosphatidylinositol; PS phosphatidylserine; SM sphingomyelin; Cer ceramide; HexCer hexosylceramide.

However, no changes in MDA content, which is a byproduct of lipid peroxidation, could be measured in our study (Supplementary Figure 48). The transcriptome analysis shows that several genes of the biosynthesis of Cer, HexCer, SM, PE, and PC are affected by DEM treatment, especially after 2 h (Figure 21).

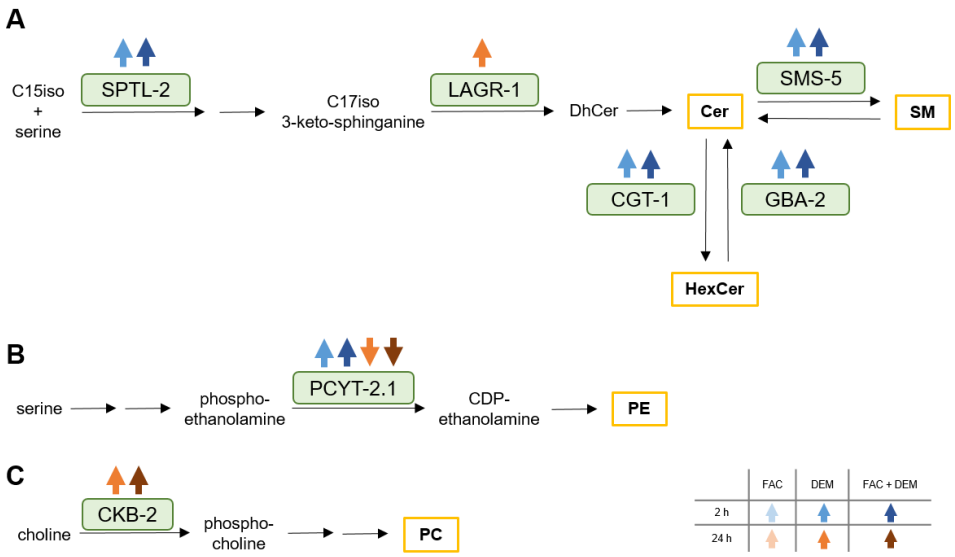

Figure 21. Proteins encoded by DEGs after treatment with FAC and DEM from the biosynthetic pathways of A) Ceramide (Cer), hexosylceramide (HexCer), and sphingomyelin (SM), B) phosphatidylethanolamine (PE), and C) phosphatidylcholine (PC). *C. elegans*/human orthologue: SPTL-2/SPTLC-2: serine palmitoyl transferase; LAGR-1/CERS-1: sphingosine N-acyltransferase; SMS-5/SMS-1: sphingomyelin synthase; CGT-1/UGCG: ceramide glucosyltransferase; GBA-2/GBA-1: glucosylceramidase; PCYT-2.1/PCYT-2: ethanolamine-phosphate cytidylyltransferase; CKB-2/CHKB: choline kinase.

4.3.6 FAC and DEM affected neuronal endpoints

Since neurons require a lot of energy and are therefore rich in mitochondria, we investigated whether FAC and DEM affect neurotransmitter levels. Treatment with FAC led to an increase in acetylcholine levels (Figure 23A), which recovered to control levels 24 h post FAC treatment (Figure 23D). While short-term treatment with DEM led to an increase in serotonin levels (Figure 23B), both serotonin and acetylcholine levels were elevated after long-term treatment (Figure 23D, E). None of the exposure conditions affected dopamine and γ-aminobutyric acid levels (Supplementary Figure 49).

Since FAC and DEM affected acetylcholine levels, we investigated whether the synaptic transmission rate of acetylcholine in the neuromuscular junction was also altered. Therefore, we examined the sensitivity to the acetylcholinesterase inhibitor aldicarb, which leads to paralysis of the worms when applied over a longer period [273]. The short-term treatment with DEM led to a slightly earlier paralysis of the worms compared to untreated control (Figure 23C), but this may also be due to the lower survival rate (Figure 18A), as no distinction could be made between paralyzed and dead worms. Following long-term treatment with DEM, a trend for resistance to aldicarb could be observed, which would indicate a lower transmission rate of acetylcholine compared to untreated control (Figure 23F). Treatment with FAC alone did not lead to any changes in aldicarb sensitivity. Short-term treatment with DEM alone and in combination with FAC led to DEGs of acetylcholinesterase, acetylcholine receptors, and serotonin biosynthesis compared to untreated control (Figure 22).

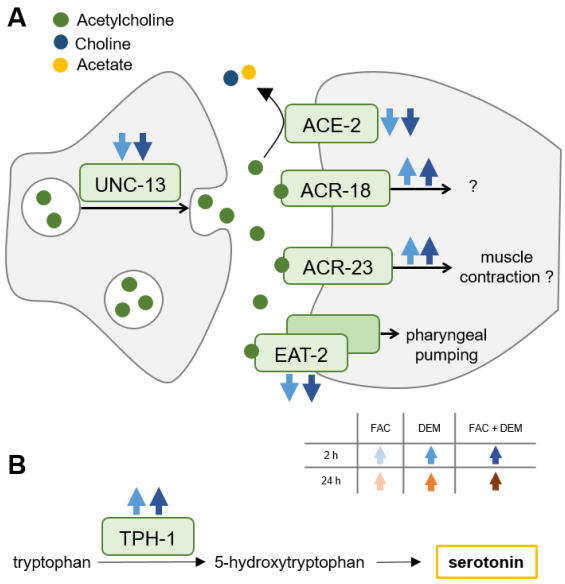

Figure 22. Proteins encoded by DEGs after short-term treatment with DEM and in combination with FAC of A) acetylcholine and B) serotonin-associated genes. *C. elegans*/human orthologue: UNC-13/UNC-13; ACE-2/BCHE: acetylcholinesterase; ACR-18/23: acetylcholine receptor; EAT-2/CHRNA-1: subunit of nicotinic acetylcholine receptor; TPH-1/TPH-1/2: tryptophan hydroxylase.

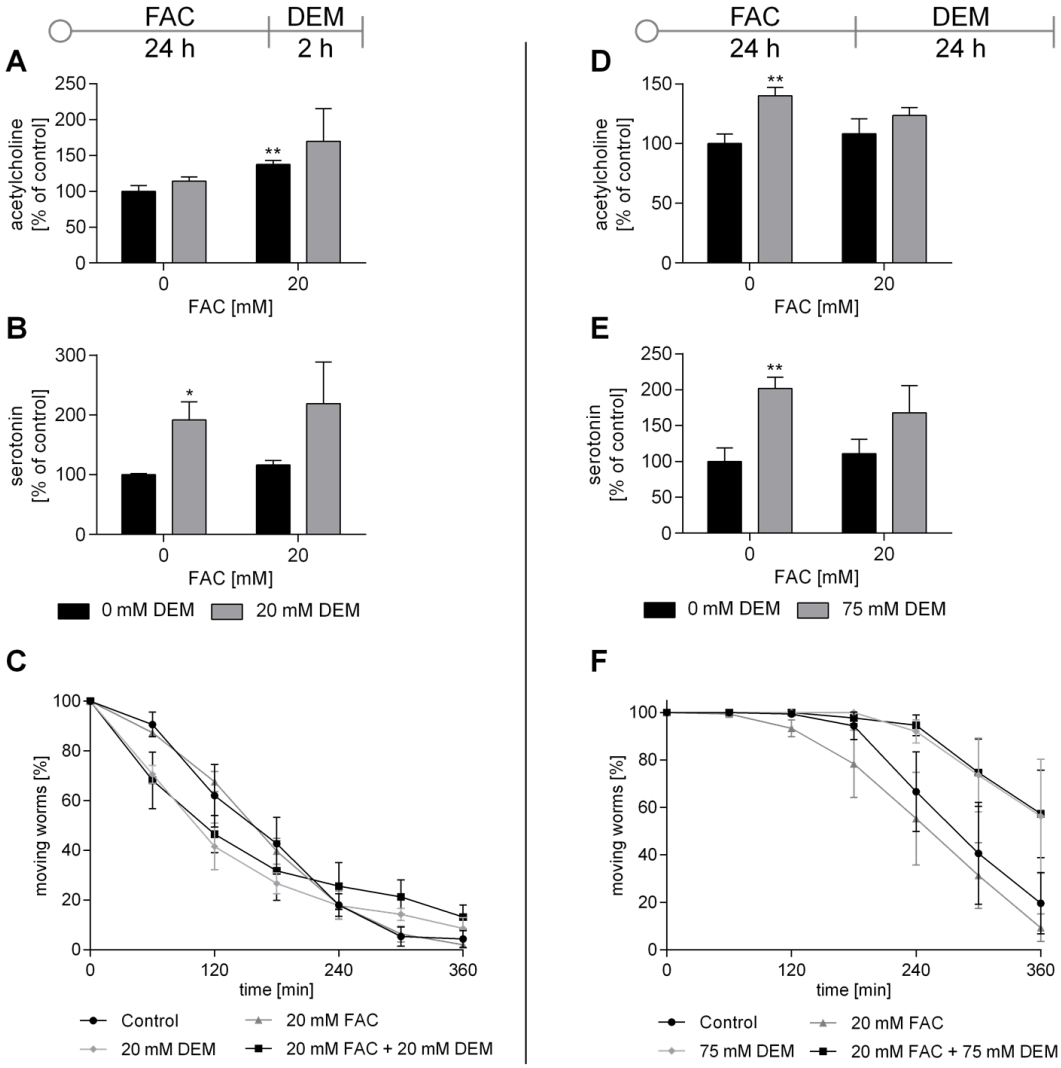

Figure 23. Neurotransmitter levels and moving worm fraction of the aldicarb-sensitivity assay after treatment with FAC and 2 h (A-C) or 24 h (D-F) treatment with DEM. A, D) Acetylcholine and B, E) serotonin levels were measured via HPLC-MS/MS and normalized to internal standard, protein content, and untreated control. C, F) Fraction of moving worms after treatment with aldicarb. Shown are the mean + SEM of ≥ 3 independent experiments. Significance is depicted as * compared to untreated control.

4.4. Discussion and conclusions

Fe is essential for various biological processes, but in terms of overdosage, it is also discussed in context of several diseases, like neurodegenerative diseases, particularly those linked to aging. This could be associated with age-related weakening of various cellular systems, such as antioxidant defense [81]. However,

there is a lack of studies addressing the effects of Fe overdosage and a decreased antioxidant capacity, especially in terms of affected mechanisms and potential counter regulating effects in a living organism.

First of all, we were able to confirm that FAC treatment led to excess Fe level in *C. elegans,* and we identified adverse effects upon the treatment. By treating L4 worms with 20 mM FAC for 24 h, we could gain a fivefold enrichment of total Fe content compared to untreated control. Although the difference was smaller 24 h post FAC treatment, it was still threefold higher compared to control, which is probably due to the lack of an active excretion mechanism of Fe [249]. Valentini et al. treated *C. elegans* eggs until young adults with 9 mM FAC and measured a twofold increase of free Fe(III) using electron paramagnetic resonance. The treatment had no effect on lifespan, but increased *ftn-1::gfp* expression and led to decreased resistance to *tert*-butyl hydroperoxide [179]. James et al. achieved approximately 50% increased Fe levels after 48 h treatment with 5 mg/mL FAC in young adult worms and showed that *ftn-2* plays a dominant role in Fe storage in *C. elegans*. FAC treatment resulted in increased FTN-2 stored Fe in this study and led to a reduced lifespan in *ftn-2* null worms [177,277]. The differential expression of *ftn-1* and the unchanged Fe(II) content after FAC treatment in our study suggests that the high amounts of Fe were stored at least to a large extent as Fe(III) in this storage protein, which can contain up to 1500 Fe atoms in *C. elegans* [184]. Even though no altered gene expression of *ftn-2* was measured in the transcriptomic analysis, FTN-2 is also expected to be involved in storing the excess Fe in our study. PCA analysis shows little variance between the FAC treated samples and the untreated controls. This suggests that FAC exposure is well buffered and needs only minor changes in gene expression. Nevertheless, 24 h post FAC treatment, nematodes showed significantly increased PE and PE-O amounts and trends toward higher amounts of SM, Cer, and HexCer. These two PL subclasses together form the largest lipid fraction in the cell membrane and are therefore important for its function and integrity, whereby ether lipids in particular are essential for the fluidity and function of

membrane proteins [242]. The three SL subclasses are also located in the cell membrane and are found primarily in lipid rafts, where they are essential for the function of receptors and signaling proteins [278]. The composition of lipids is therefore of great importance, and changes are often discussed in the context of neurodegenerative diseases such as AD. While several studies have measured decreased PE levels in the brains of AD patients, some studies have found increased SM and Cer levels [279]. Wang et al. showed effects of FAC on lipid metabolism in *C. elegans*, as FAC treatment led to increased fatty acid uptake by the fatty acid transmembrane transporter ACS-20 and lipid accumulation [280]. Fe accumulation is also discussed in the context of AD, which can become problematic with aging, when Fe homeostasis is no longer well-regulated [281]. Furthermore, FAC treatment led to a slight increase in the neurotransmitter acetylcholine, which was at the same level as the untreated control 24 h post FAC treatment. Studies in rat brains and *in vitro* indicate that Fe treatment can inhibit acetylcholinesterase activity, which could lead to an increase of the neurotransmitter [282,283]. In our study, however, FAC does not affect the transmission rate of acetylcholine in the neuromuscular junction, as no difference between FAC-treated and untreated nematodes could be observed in the behavioral assay with aldicarb. In addition to its function as an excitatory neurotransmitter in important processes such as muscle contraction, acetylcholine is also discussed as a neuromodulator [284].

We could further identify DEM as a suitable substance to model a lower antioxidant capacity in nematodes. With the short-term DEM treatment for 2 h, we decreased the GSH level with 20 mM DEM to 30% compared to untreated control. Although no alterations could be measured after long-term treatment for 24 h, the GSH-DEM product was still detected in the samples, as with short-term treatment. The fact that there are numerous GST genes among the DEGs after both treatment times indicates that they catalyze the binding of DEM to GSH in *C. elegans*, which has also been shown *in vitro* by Kubal et al. [83]. The DEGs showed upregulated genes of GSH synthesis after both treatment times.

This may indicate an increase in GSH production, which could lead to no difference in GSH level between long-term DEM treatment and untreated control due to counter regulation. While short-term treatment with DEM led to a twofold increase in Fe(II) content, this effect could not be observed after long-term treatment, when GSH levels were similar to untreated control. Jenkins et al. also showed an increase of Fe(II) in *C. elegans* by treatment with DEM for 6 h and described a buffer limit of the organism when 30% of the Fe is present as Fe(II), while the Fe(II) content was 41% higher than in untreated control [206]. The GSH depletion not only promotes the presence of reactive Fe-species but also impairs the antioxidant defense, with cells less capable of repairing damage caused by RONS. The fact that two out of seven GPX orthologues were upregulated after short-term DEM treatment could also be due to increased reactive Fe(II) species at this time point, as these may lead to lipid peroxidation [258]. Although we could not measure alterations in the content of the lipid peroxidation byproduct MDA, there were changes in the total contents of PE-O, LPE, LPC, SM, Cer, and HexCer, especially after long-term treatment with DEM. Transcriptomic analysis showed that DEM treatment led to DEGs in the biosynthesis of PE, PC, SM, Cer, and HexCer. Additionally, we detected a slight decrease in CL content, which may be associated with slightly lower mitochondrial masses after DEM treatment. Since up to 15% of cellular GSH is found in the mitochondria and these organelles are exposed to the constant formation of RONS, GSH depletion could lead to mitochondrial impairment and thus to mitophagy [77]. Cornell et al. showed that the mitochondrial stress response in the form of unfolded protein response (UPR^{mt}) in *C. elegans* is coordinated by the neurotransmitters γ-aminobutyric acid and acetylcholine signaling. They showed that UPR^{mt} induction, measured as HSP-6 expression, is associated with the lack of acetylcholinesterase and with elevated systemic acetylcholine levels [276]. In our study, short-term treatment with DEM led not only to decreased mitochondrial masses but also to upregulation of *hsp-6*, while long-term treatment resulted in elevated acetylcholine levels and altered aldicarb

sensitivity. Additionally, Cornell et al. showed that the lack of the acetylcholinesterases *ace-1* and *ace-2* increased mitochondrial fragmentation, and in our study, short-term treatment with DEM led to lower expression of the *ace-2* gene [276].

Interestingly, the combined treatment, which was associated with a combination of low GSH and increased total Fe and Fe(II) levels, did not lead to significant effects compared to DEM or FAC alone for any of the endpoints investigated in this study.

To sum up, *C. elegans* treatment with FAC affects the acetylcholine level as well as PL and SL distributions even after prolonged time without further Fe treatment. In addition, it could be shown that increased total Fe levels do not necessarily lead to increased reactive Fe(II) species, but treatment with DEM and presumably GSH depletion increased Fe(II) species in *C. elegans*. Furthermore, the DEM treatment led to changes in the mitochondria, the PL and SL, and the neurotransmitters acetylcholine and serotonin. The transcriptomic analysis could support to identify possible key genes involved up or down stream in these effects. Overall, we were able to show that *C. elegans* is a suitable organism to model Fe overdosage by FAC and lower antioxidant capacity by DEM treatment. The two DEM treatment times indicate acute and long-lasting effects. Even if the long-term DEM treatment is not reducing GSH levels due to counter regulation, we could identify long-lasting adverse consequences for the nematodes.

4.5 Credit authorship contribution statement

Anna Gremme: Conceptualization, Methodology, Visualization, Formal analysis, Investigation, Writing – Original Draft, Writing – Review & Editing; Emely Gerisch: Investigation, Writing – review & editing; Dominik Wieland: Methodology, Investigation, Writing – review & editing; Julia Hillebrand: Investigation, Writing – review & editing; Franziska Drews: Formal analysis, Visualization, Writing – review & editing; Marcello Pirritano: Formal analysis,

Visualization, Writing – review & editing; Ann-Kathrin Weishaupt: Methodology, Investigation, Writing – review & editing; Janina Fuss: Investigation; Vera Schwantes: Methodology, Investigation; Johannes Scholz: Writing – review & editing; Vivien Michaelis: Methodology, Writing – review & editing; Alicia Thiel: Methodology, Writing – review & editing; Gawain McColl: Writing – review & editing; Bernhard Michalke: Writing – review & editing; Martin Simon: Writing – review & editing; Heiko Hayen: Writing – review & editing, Supervision; Julia Bornhorst: Project administration, Methodology, Investigation, Funding acquisition, Conceptualization, Writing – review & editing.

4.6 Acknowledgements

C. elegans strains were provided by CGC, which is funded by the NIH Office of Research Infrastructure Programs (P40 OD010440).

4.7 Funding

This project was supported by the DFG Research Unit TraceAge (FOR 2558, BO4103/4-2) and by the DFG Research Infrastructure NGS CC (project 407495230) as part of the Next Generation Sequencing Competence Network (project 423957469). NGS analyses were carried out at the Competence Centre for Genomic Analysis (Kiel).

Further work – The Impact of Lip-1 on Endpoints Altered by FAC and DEM

4.8 Introduction

Ferroptosis is a non-genetically induced cell death characterized by increased Fe(II) levels and associated lipid peroxidation.[285] Fe is believed to initiate lipid peroxidation and to be involved in the reaction of the resulting hydroperoxides to alkoxyl radicals.[118] Among other GSH-dependent enzymes, GPX4 plays a key role in the reaction of lipid hydroperoxides to less reactive alcohols, which is why GSH deficiency is also discussed in the context of ferroptosis.[125] Compared to other types of cell death, such as apoptosis and necrosis, ferroptosis is less understood, and more research is needed to understand the complete mechanism. However, some characteristics are known, including the lipid peroxidation and the involvement of GPX4, as well as changes in mitochondrial morphology, expression levels of certain genes, and TFR1 mobilization.[3] To identify ferroptotic cell death, several markers should be investigated, including markers of lipid peroxidation, but also the suppression of this oxidation and thus the prevention of cell death by using ferroptosis inhibitors. The arylamine Lip-1 is a synthesized molecule that is highly effective in inhibiting ferroptosis as an antioxidant, which has been shown already in several studies from human cells, to mice, and *C. elegans*.[206,286,287] The mechanism is based on Lip-1 preventing lipid peroxidation by trapping chain-carrying peroxyl radicals.[128]

To investigate whether Lip-1 can rescue the survival rate decreased by FAC and DEM, we combined Lip-1 with FAC and DEM treatment. In addition, we investigated whether Lip-1 treatment reduces the effects of the combined FAC and DEM treatment on the different endpoints. Therefore, as in chapter 4, we treated L4 worms with FAC for 24 h and 2 h or 24 h with DEM. In addition, we added Lip-1 to the combination of FAC and DEM throughout the whole treatment time.

4.9 Materials and Methods

4.9.1 Lip-1 treatment

Lip-1 (99.88%, Selleck Chemicals) was dissolved in DMSO, and 100 mM aliquots were stored at -80 °C. Lip-1 was applied simultaneously with FAC or DEM, using 100 µM Lip-1 for 24 h and 40 µM Lip-1 for 2 h treatment. The final concentration of DMSO was adjusted to 1% v/v under all conditions. DMSO was also added to the control worms, which are referred to as untreated controls in the following sections.

All experiments were performed as described in chapter 4.2.

4.9.2 Statistical analysis

Statistical analysis was performed using GraphPad Prism 6 (GraphPad Software). T-test with $\alpha = 0.05$ was used with the following significance levels: $^{*}p \leq 0.05$, $^{**}p \leq 0.01$, $^{***}p \leq 0.001$.

4.10 Results and Discussion

To investigate whether the decreased survival rate after FAC and 2 h DEM treatment can be increased by Lip-1, we treated Lip-1 throughout the combined treatment period. Survival rate was determined 24 h after treatment and was slightly increased after the triple treatment, but still significantly decreased compared to untreated control (Figure 24A). Jenkins et al. observed a decreased survival rate in day 4 adult *C. elegans* after 6 h DEM treatment, which could be slightly rescued by Lip-1. In their study, L4 worms were treated with 200 µM Lip-1 for 4 days before being transferred to DEM-containing NGM plates for 6 h. In addition, there was no effect of Lip-1 on the decreased GSH levels achieved by DEM, and they concluded that ferroptosis was inhibited by Lip-1 downstream of GSH depletion. However, Lip-1 treatment in their study prevented the age-related increase in Fe(II) levels, measured via X-ray absorption near edge structure spectroscopy.[206] In our study, Lip-1 did not affect elevated Fe(II) levels after FAC and 2 h DEM treatment, which we investigated using FerroOrange dye (Figure 24B, C). Cañeque et al. showed that Lip-1

accumulates in the kidneys of mice and that labeled Lip-1 (cLip-1) co-localized intracellularly with a lysosomal marker. In addition, Lip-1 formed complexes with $FeCl_3$ *in vitro* in an acidic environment, as it is found in lysosomes, and cyclic voltammetry indicated that Lip-1 alters the redox potential of Fe. They concluded that lysosomes, with their acidic environment and reactive Fe species, have high potential to catalyze the oxidation of membrane PL and thus play a crucial role in ferroptotic cell death.[122]

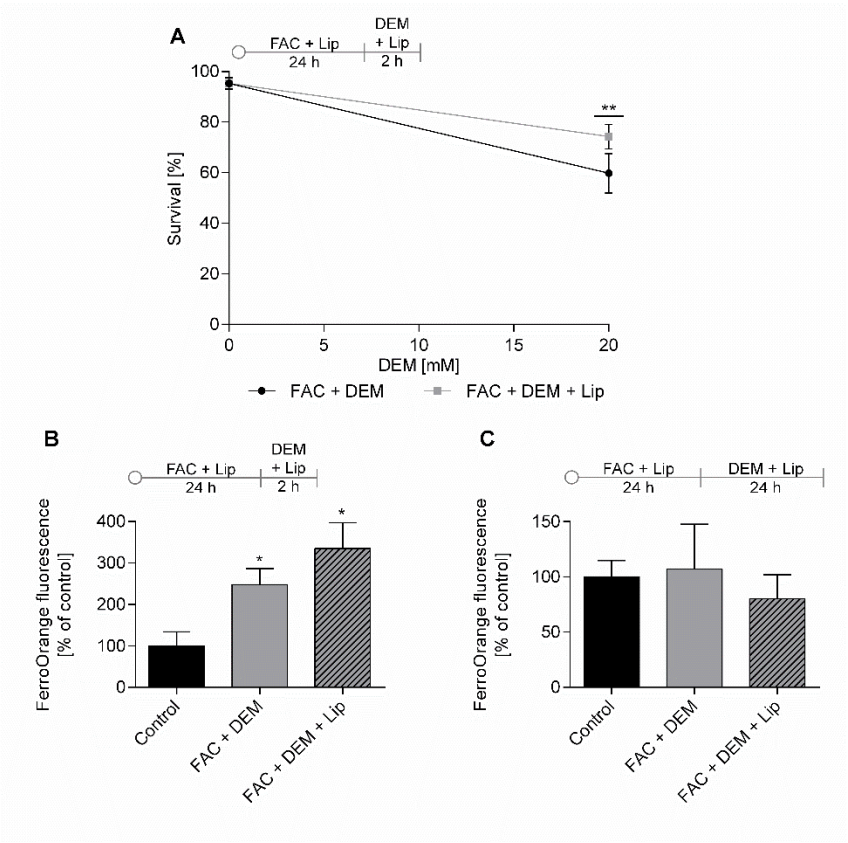

Figure 24. A) Survival rate after 24 h following combined treatment with Lip-1, FAC, and 2 h DEM. B, C) labile Fe(II) levels measured as FerroOrange fluorescence after combined treatment with Lip-1, FAC, and 2 h (B) or 24 h (C) DEM were normalized to worm autofluorescence and untreated control. Shown are the mean + SEM of ≥ 3 independent experiments (B) FAC + DEM + Lip n = 2). Significance is depicted as * compared to untreated control.

Transcriptomic analysis was performed to investigate whether Lip-1 has an impact on gene expression altered by FAC and DEM treatment. After short-term treatment, PCA shows no variance between FAC and DEM-treated samples and

the combined treatment with Lip-1 (Figure 25A). However, a variance between these samples can be observed after long-term treatment (Figure 25B). A comparable enrichment of several GO terms from the DEGs was observed with and without Lip-1 treatment (Figure 26). However, it is noticeable that GO terms associated with ion, cation, and metal binding were enriched among the upregulated genes after short-term treatment with FAC and DEM, but not in combination with Lip-1. Notably, the GO term ‘iron binding’ is also enriched in combination with Lip-1 (Figure 26). This term also includes *ftn-1*, which is upregulated following the combined short- and long-term treatment with Lip-1, but not with FAC and DEM alone (Figure 18E). However, Lip-1 had no impact on Fe(II) levels at the respective time points (Figure 24B, C).

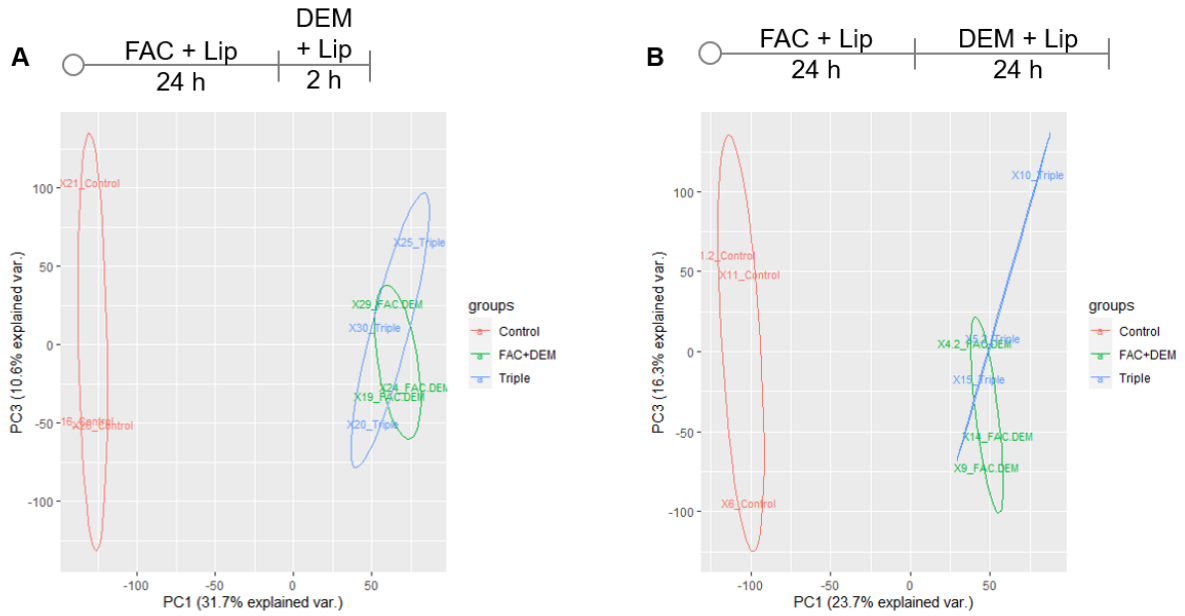

Figure 25. Principal component analysis (PCA) of PC1 and PC3 after combined treatment with Lip-1, FAC, and 2 h (A) or 24 h (B) DEM.

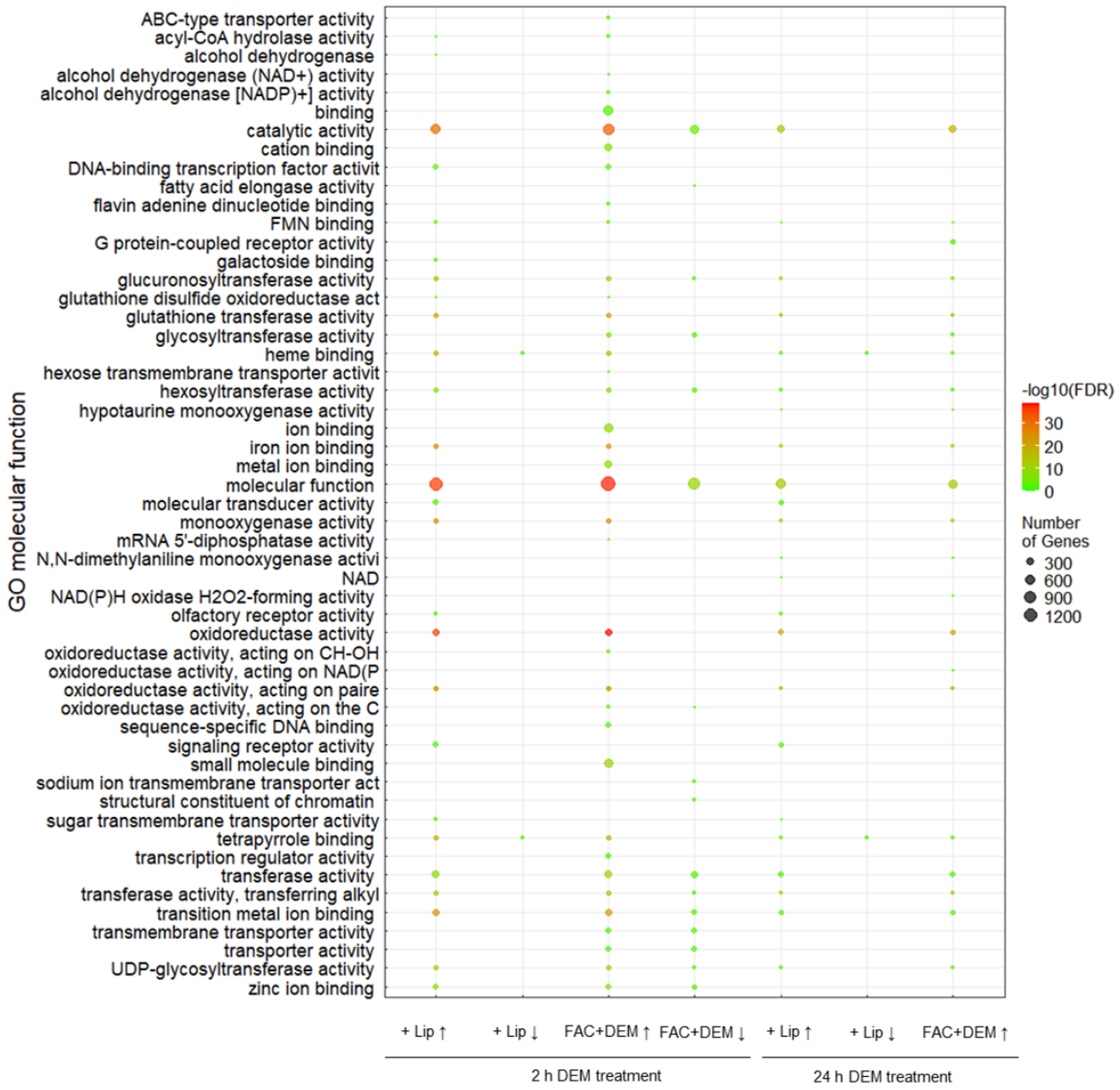

Figure 26. Heat map of a selection of GO terms related to molecular function enriched among the up-(↑) and down-(↓) regulated DEGs compared to untreated control after combined treatment with Lip-1, FAC, and 2 h or 24 h DEM. No GO term could be formed from the down-regulated genes after the combined treatment with FAC and 24 h DEM.

Since ferroptotic cell death is associated with mitochondrial alterations, we determined the mitochondrial mass using MitoTracker™ green and CL levels using a 2D heart-cut HPLC-MS/MS method after triple treatment. Lip-1 treatment could not rescue the decreased mitochondrial mass after short-term FAC and DEM treatment, and the slightly decreased CL levels after long-term

FAC and DEM treatment (Figure 27). Since initial measurements showed no effect after long-term treatment with Lip-1 on mitochondrial mass, it was not investigated further (data not shown). However, CL levels were slightly elevated after short-term triple treatment compared to untreated control (Figure 27B). Li et al. showed in mouse neuronal hippocampal cells that lipopolysaccharide led to mitochondrial fragmentation, which was protected by Lip-1.[288] In addition, Chen et al. demonstrated in mice morphine-induced shrunken mitochondria in soma and axons of spinal cord neurons, which was also protected by Lip-1.[289] In both studies, the substances led to total Fe accumulation in the neuronal cells, which was not observed by additional treatment with Lip-1.[288,289] Since the endpoints were measured in the whole organism in our study, similar effects on certain regions of the worm could not be detected.

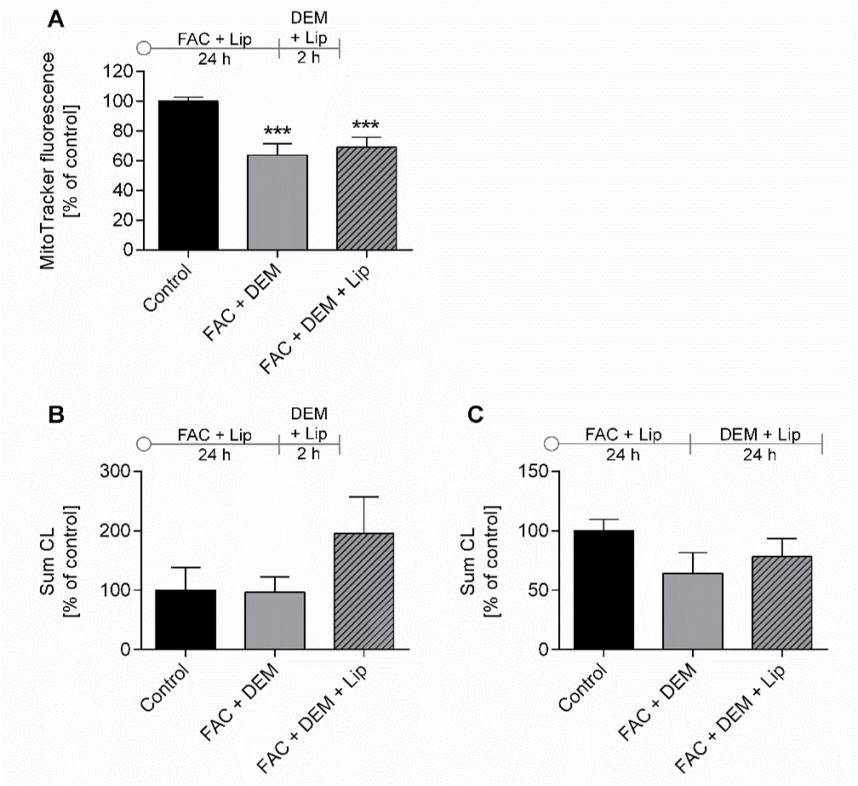

Figure 27. A) MitoTracker™ green fluorescence after combined treatment with Lip-1, FAC, and 2 h DEM was normalized to mCherry fluorescence and untreated control. B, C) CL were determined via 2D heart-cut HPLC-MS/MS following combined treatment with Lip-1, FAC, and 2 h (B) or 24 h (C) DEM and normalized to internal standard, protein content, and untreated control. Shown are the mean + SEM of ≥ 3 independent experiments. Significance is depicted as * compared to untreated control.

Measurement of PL and SL revealed no effect of Lip-1 on most of the lipid classes (Figure 28). However, the slightly decreased PS levels after FAC and 24 h DEM treatment were at control levels after combined treatment with Lip-1 (Figure 28B). PE and PC are the most abundant lipid subclasses of the measured PL and SL. The combined treatment with FAC and DEM led to slight alterations in the distribution of double bonds in both classes (Figure 29A – D). After short-term treatment with FAC and DEM, both PEs and PCs had slightly decreased lipid levels in the 7 double bonds group (Figure 29A, C), and after long-term treatment, there were slightly decreased levels of PCs with 9 double bonds (Figure 29D). On the other hand, there was a slight increase in lipids with few double bonds, which, after short-term treatment, were PCs with one double bond (Figure 29C) and, after long-term treatment, PEs with 3 and PCs with 0 double bonds were also increased (Figure 29B, D). The triple treatment with Lip-1 had no impact on these effects. The decrease of higher PUFAs could be caused by lipid peroxidation, as these are more susceptible to it than lipids with fewer double bonds.[290] However, no alterations of MDA levels were measured after FAC and DEM treatment (Supplementary Figure 48), and the unaltered lipid levels after Lip-1 treatment also indicated a different mechanism.

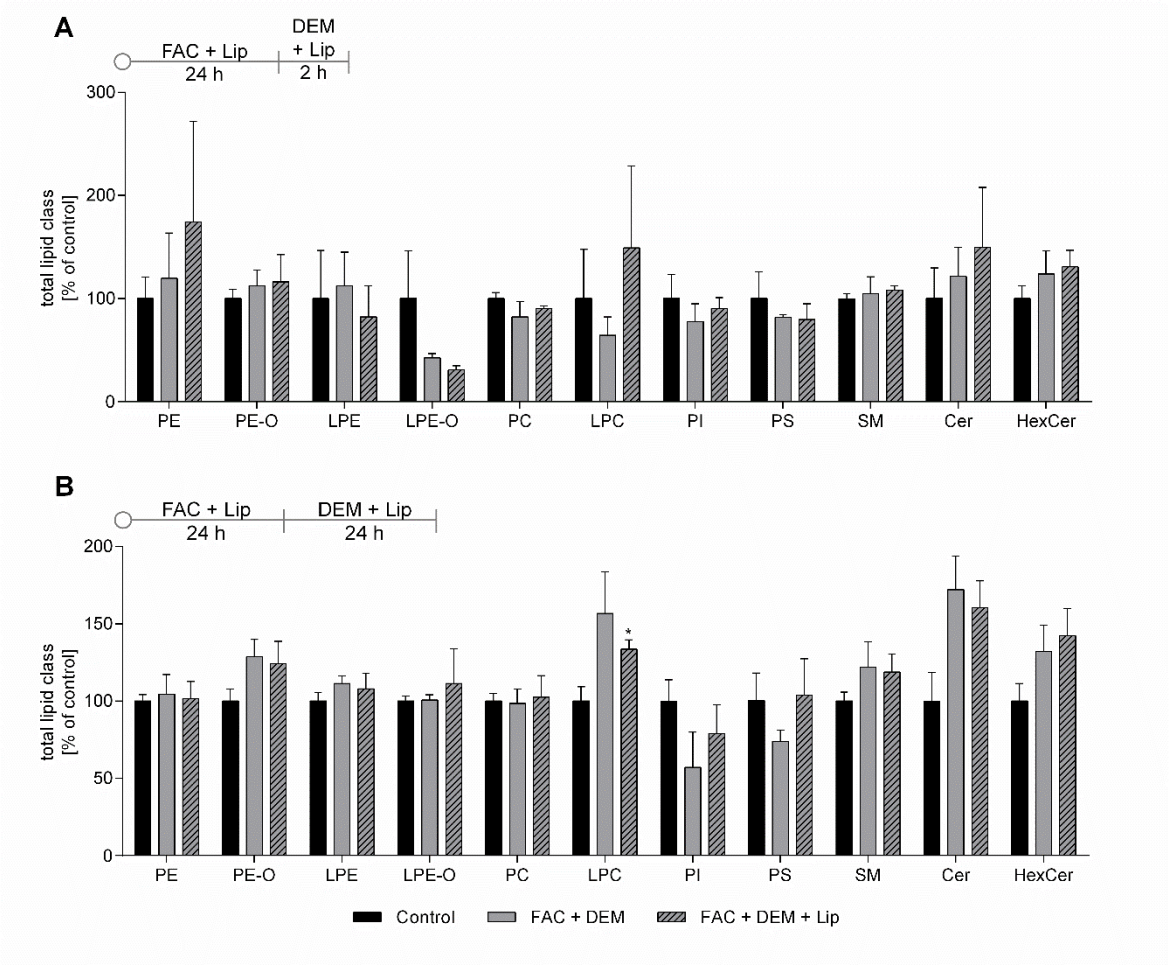

Figure 28. A, B) Relative distribution of PL and SL subclasses determined from the peak areas. Measurement followed combined treatment with Lip-1, FAC, and 2h (A) or 24 h (B) DEM, and areas were normalized to protein content and untreated control. Shown are the mean + SEM of ≥ 3 independent experiments. Significance is depicted as * compared to untreated control. Abbreviations: PE phosphatidylethanolamine; PE-O plasmanyl-phosphatidylethanolamine; LPE lysophosphatidylethanolamine; PC phosphatidylcholine; LPC lysophosphatidylcholine; PI phosphatidylinositol; PS phosphatidylserine; SM sphingomyelin; Cer ceramide; HexCer hexosylceramide.

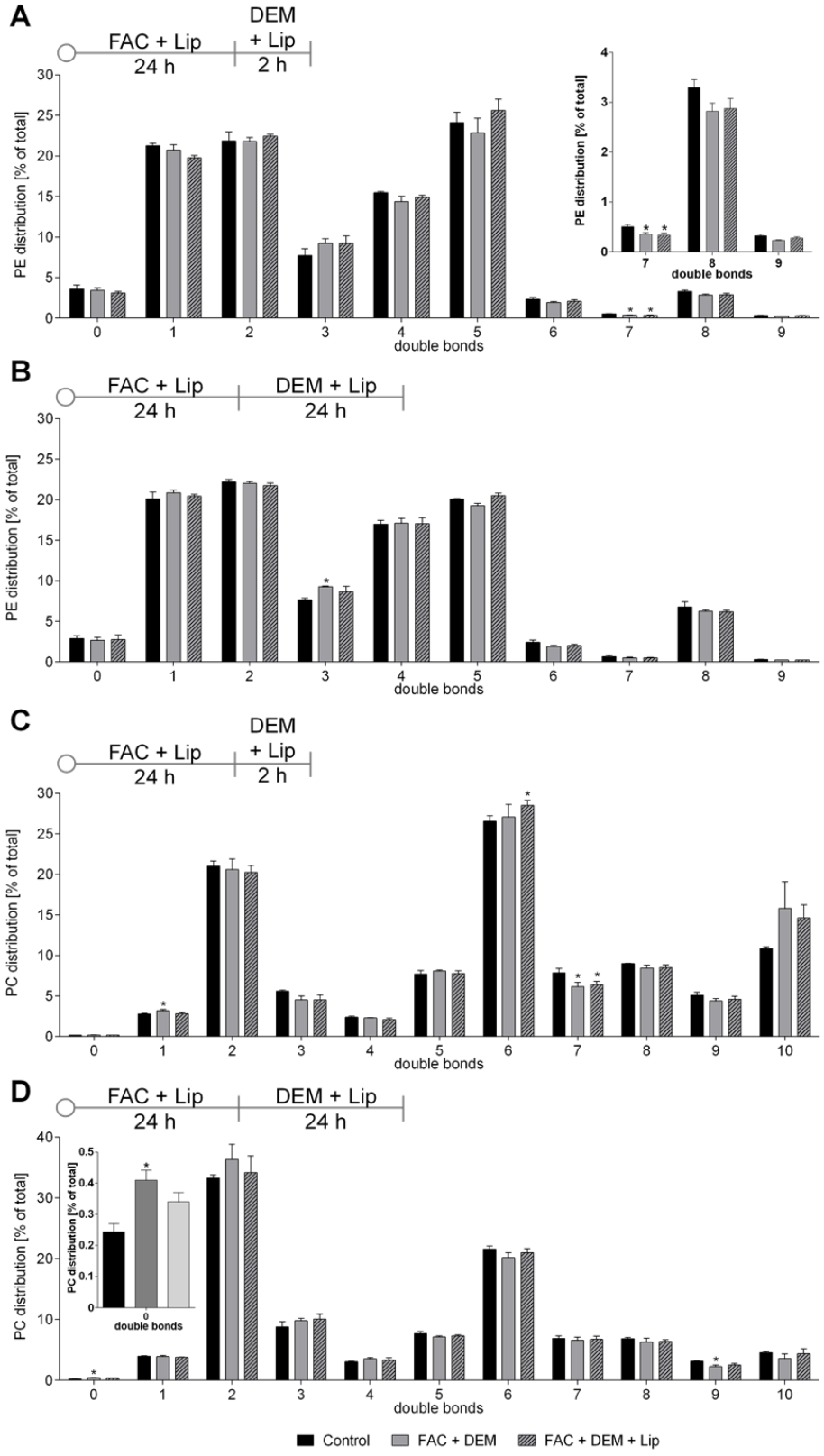

Figure 29. Distribution of PE (A, B) and PC (C, D) based on the degree of saturation after combined treatment with Lip-1, FAC, and 2 h (A, C) or 24 h (B, D) DEM. Shown are the mean + SEM of ≥ 3 independent experiments. Significance is depicted as * compared to untreated control.

Treatment with FAC and DEM led to DEG of elongases (*elo-2*, *elo-9*), desaturases (*fat-5*, *fat-6*), and acetyl-CoA synthetases (*acs-2*, *acs-3*, *acs-6*) after both treatment times (Table 3). The combined treatment with Lip-1 additionally altered the gene expression of *acs-6* and *acs-7* after short-term treatment (Table 3). Elongases extend the carbon chain of fatty acids (FA), thereby providing the potential for additional double bonds, whereas desaturases introduce double bonds into the FA structure.[291] Acetyl-CoA synthetases, on the other hand, modify FA so that they can be incorporated into lipid classes such as PL and SL.[292] Alterations in gene expression suggest that both the distribution of lipid classes and the number of double bonds could be at least partly genetically regulated.

Table 3. Up- and downregulated gene expression of elongases, desaturases, and acetyl-CoA synthetases after FAC and DEM alone (FAC + DEM) or combined with Lip-1 treatment (FAC + DEM + Lip-1) and compared to untreated control.

Gene expression	**short-term**		**long-term**	
	FAC + DEM	**+ Lip**	**FAC + DEM**	**+ Lip**
up-regulated	*elo-9*	*elo-9* *acs-6*	*fat-6* *acs-6*	*fat-6* *acs-6*
down-regulated	*elo-2* *fat-5* *acs-3*	*elo-2* *fat-5* *acs-3* *acs-7*	*acs-2*	-

Neurotransmitter levels, measured via HPLC-MS/MS, were unchanged after triple treatment compared to combined short- and long-term treatments with FAC and DEM (Figure 30). Yong et al. demonstrated that Lip-1 can positively impact the behavior of *C. elegans* models of AD. In their study, L1 worms of the strain CL4176 (expressing human Aβ1-42 in its muscle cells) were treated with 200 µM Lip-1 for 24 h, and the paralysis rate was determined, which was decreased after Lip-1 treatment compared to untreated control. In the BR5270 strain (over-expression of the F3 pro aggregation fragment of human Tau

protein), 48 h treatment with Lip-1 resulted in the same slowing rate as in the control, which was lower in the BR5270 strain.[293] Sarparast et al. showed no effect of Lip-1 on age-related degeneration of dopaminergic neurons in *Pdat-1::gfp* expressing worms, but a rescuing effect of Lip-1 on the degeneration caused by treatment with dihomo gamma linolenic acid. However, they also showed that apoptotic cell death also plays a role here, as the knockout of *ced-3* and the resulting lack of apoptosis led to less degeneration in the dopaminergic neurons and was fully rescued by Lip-1. Treatment was carried out in L4 until day 1 or day 8 adult worms on NGM plates coated with 250 µM Lip-1 and active OP50 *E. coli*.[294] These studies demonstrated that Lip-1 may have a positive effect at neuronal level, but did not measure the effect on neurotransmitter levels.

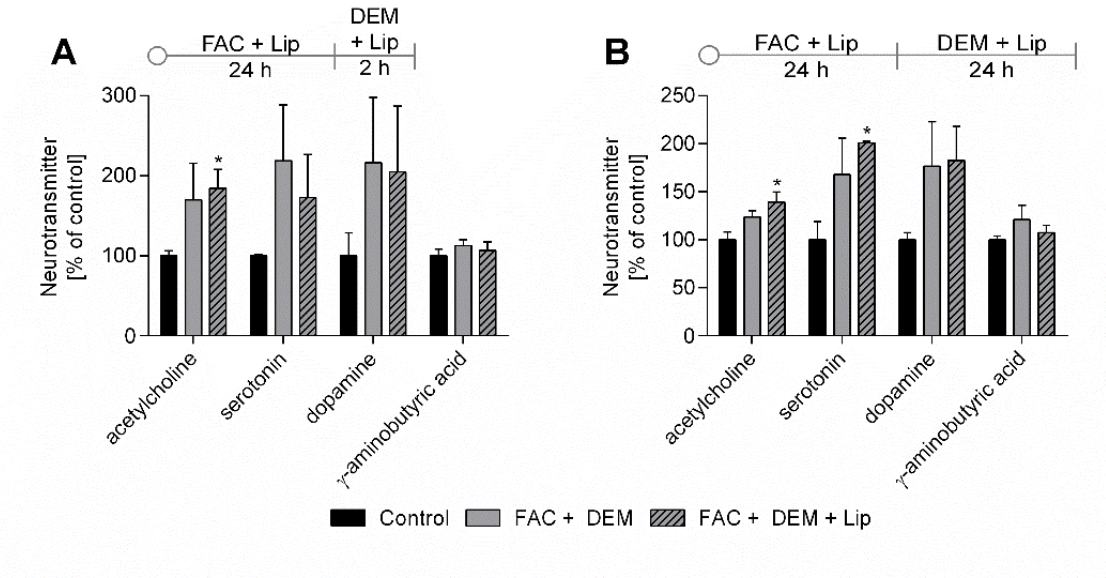

Figure 30. A, B) Neurotransmitter levels measured via HPLC-MS/MS following combined treatment with Lip-1, FAC, and 2 h (A) or 24 h (B) DEM were normalized to internal standards, protein content, and untreated control. Shown are the mean + SEM of ≥ 3 independent experiments. Significance is depicted as * compared to untreated control.

4.11 Conclusion and further perspectives

The combined treatment with FAC and DEM led to alterations in survival rate, Fe(II) level, mitochondrial mass, PL and SL distribution, and neurotransmitter level. Changes in most of these endpoints are discussed in the context of ferroptosis.[3] Nevertheless, lipid peroxidation is one of the most important hallmarks of ferroptosis, and the associated formation of MDA was not altered after FAC and DEM treatment in our study (Supplementary Figure 48). We investigated whether treatment with FAC and DEM and the associated Fe overdosage and GSH depletion led to ferroptotic cell death and which endpoints may be involved. The well-established ferroptosis inhibitor Lip-1 slightly increased the survival rate, reduced by FAC and DEM, which could indicate a partial role of ferroptosis. Nevertheless, Lip-1 did not significantly rescue any of the effects we investigated. This could also be because ferroptosis is not the only or main type of cell death in our study that led to a reduced survival rate. It is often observed that several types of cell death can occur simultaneously.[106] Although Lip-1 has been shown to impact Fe(II) levels, mitochondrial morphology, and neuronal endpoints in other studies, these studies often used other organisms, substances to induce ferroptosis, or treatment conditions for Lip-1. For further investigation, additional ferroptosis markers such as peroxidized lipids, 4-HNE, or GPX expression could be examined. Studies on other types of cell death could also provide further insight into the consequences of Fe overdosage and GSH depletion.

Abstract

While copper (Cu) is an essential trace element for biological systems due to its redox properties, excess levels may lead to adverse effects partly due to overproduction of reactive species. Thus, a tightly regulated Cu homeostasis is crucial for health. Cu dyshomeostasis and elevated labile Cu levels are associated with oxidative stress and neurodegenerative disorders, but the underlying mechanisms have yet to be fully characterized. Here, we used *Caenorhabditis elegans* loss-of-function mutants of the Cu chaperone atox-1 and Cu storage protein ceruloplasmin to model Cu dyshomeostasis, as they display a shifted ratio of total Cu towards labile Cu. We applied highly selective and sensitive techniques to quantify metabolites associated to oxidative stress with focus on mitochondrial integrity, oxidative DNA damage and neurodegeneration all in the context of a disrupted Cu homeostasis. Our novel data reveal elevated oxidative stress, compromised mitochondria displaying reduced ATP levels and cardiolipin content. Cu dyshomeostasis further induced oxidative DNA damage and impaired DNA damage response as well as neurodegeneration characterized by behavior and neurotransmitter analysis. Our study underscores the essentiality of a tightly regulated Cu homeostasis as well as mitochondrial integrity for both genomic and neuronal stability.

Chapter 5

Dysfunctional Copper Homeostasis in *Caenorhabditis elegans* affects neuronal and genomic stability

Based on:

Ann-Kathrin Weishaupt, Anna Gremme, Torben Meiners, Vera Schwantes, Karsten Sarnow, Alicia Thiel, Tanja Schwerdtle, Michael Aschner, Heiko Hayen and Julia Bornhorst

Redox Biochemistry and Chemistry, **2024**

DOI: 10.1016/j.rbc.2024.100043

Keywords

Copper dyshomeostasis, oxidative stress, mitochondrial impairment, cardiolipins, genomic and neuronal instability

Chapter 5 – Dysfunctional Copper Homeostasis in *Caenorhabditis elegans* affects neuronal and genomic stability

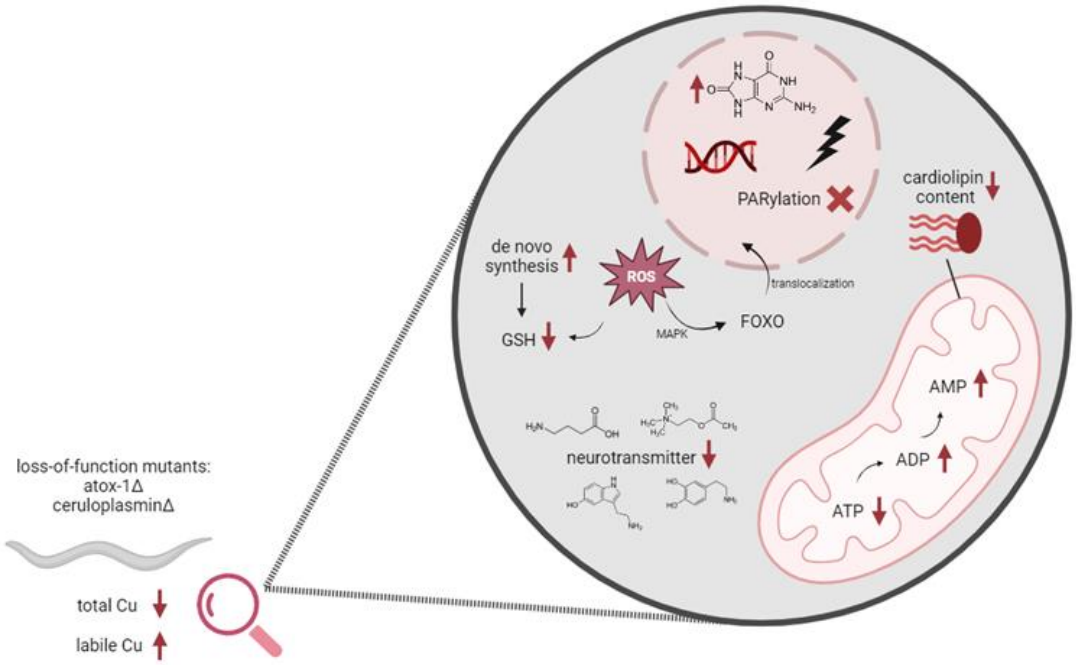

Figure 31. Graphical abstract of: Dysfunctional Copper Homeostasis in *Caenorhabditis elegans* affects neuronal and genomic stability

5.1. Introduction

Copper (Cu) is an essential trace element and micronutrient, participating in many physiological pathways as an enzyme cofactor [295]. Due to the overuse of Cu-containing chemicals and fungicides in industry and agriculture, Cu is increasingly introduced into the environment, leading to a global concern [296]. When exceeding the physiological range, Cu leads to the formation of reactive oxygen and nitrogen species (RONS) due to its redox activity, which may affect macromolecules such as lipids or the DNA [297]. Therefore, a tightly regulated Cu homeostasis is crucial, since a Cu imbalance has been reported to induce oxidative stress as well as neurodegeneration [298,299]. In a previous study, we demonstrated that a dysregulated Cu homeostasis results in elevated labile Cu levels in *Caenorhabditis elegans* (*C. elegans*) [188]. Besides total Cu levels and

the activity of the Cu storage protein ceruloplasmin, labile Cu is discussed to be an additional marker for Cu status, as it is readily available for cellular uptake [300]. As previously shown, a Cu imbalance leads to a shift from bound Cu towards pools of labile Cu [188], which is associated with the loss of antioxidant defense, impaired energy production and in turn mitochondrial deficits [298]. Indeed, Alzheimer's disease (AD) has been posited to result from Cu imbalance based on a correlation between brain Cu levels and the prevalence of AD [301]. The underlying mechanisms remain unknown, but are often linked to oxidative stress, which is induced by an imbalance of RONS and antioxidants [302]. Cells are equipped with a variety of enzymes and small molecules for antioxidative defenses [197]. Reduced and oxidized glutathione are key markers for oxidative stress [197,302]. As previously stated, RONS can damage macromolecules, such as lipids. Malondialdehyde (MDA), a degradation product of lipid peroxidation of polyunsaturated fatty acids is a common biomarker of oxidative stress [303]. A unique type of phospholipid class, exclusively present in mitochondria, are cardiolipins (CL) [304]. CLs have recently emerged in the focus of neurodegenerative diseases, as a reduction in CL levels has been linked to oxidative stress and mitochondrial dysfunction in AD [305]. Wilson's disease (WD), a Cu metabolism disorder resulting in neurological deficits, is characterized by a mutation in the *Atp7b* gene. This results in non-expression of the Cu exporter protein Atp7b, thereby leading to Cu accumulation, primarily in the liver, but also in the brain [299]. Studies reveal a progressive degradation of CLs in liver mitochondria of a WD mouse model (*Atp7b*$^{-/-}$) [306], which underlines the link between CLs and the pathogenesis of neurodegenerative diseases [304]. Massive RONS formation induced by Cu may further increase DNA lesions. An induction of DNA damage in response to elevated brain Cu levels was observed in AD, Parkinson's disease (PD), as well as in WD [307]. However, the mode of action of Cu-induced toxicity and neurotoxicity is still under debate.

This study aims to investigate the molecular mechanisms of labile Cu redox biology using the model organism *C. elegans*. The nematode is a well-established model to examine metal-induced oxidative stress and neurotoxicity [213]. In addition, *C. elegans* conserved similar proteins related to the mammalian Cu metabolism, making it suitable for its investigation. Furthermore, we recently demonstrated that the nematode can model Cu homeostasis. Our previous study revealed that deletion mutants lacking the intracellular Cu chaperone atox-1 and the Cu storage protein ceruloplasmin take up less total Cu, but display elevated levels of labile Cu compared to wildtype worms [188]. Our aim is to elucidate the toxic mechanisms upon a disrupted Cu homeostasis regarding oxidative stress, with special focus on mitochondrial integrity in terms of energy-related nucleotides such as ATP, as well as total CL levels and the CL profile. Furthermore, the consequences of oxidative stress on genomic and neuronal stability due to Cu dyshomeostasis in *C. elegans* will be investigated.

5.2. Material and Methods

5.2.1. *C. elegans* handling and treatment

C. elegans strain Bristol N2 (wildtype) and TJ356 (daf-16::GFP) were obtained from the Caenorhabditis Genetics Center (CGC, Minneapolis, USA), which is funded by the National Institutes of Health Office of Research Infrastructure Programs. Additionally, deletion mutants (Δ) tm1220 (atox-1Δ) and tm14205 (ceruloplasminΔ) were obtained from the Mitani Lab at Tokyo Women's Medical University. All strains were cultivated on 8P and NGM agar plates, which have been coated with *Escherichia coli* (*E. coli*) and maintained at 20 °C as previously described [160]. All experiments were performed using synchronous worms [308], which were placed on NGM agar plates until L4 larval stage. L4 stage worms were treated with Cu-enriched inactivated *E. coli* ($CuSO_4$ ≥99.99%, Sigma Aldrich) on NGM plates for 24 h up to 2 mM for every experiment as previously shown [188]. Optionally, 100 mM paraquat (PQ)-enriched *E. coli* for 24 h (Sigma

Aldrich) or 6.5 mM *tert*-butyl hydroperoxide (*t*-BOOH) (Sigma Aldrich) for 1 h in 85 mM NaCl solution were used as positive controls, but in wildtype worms only to verify assay procedures.

5.2.2. daf-16 translocalization in daf-16::GFP mutants

Worm strain daf-16::GFP was used to assess daf-16 translocalization by fluorescence microscopy. After Cu treatment, worms were transferred to 4% agarose pads on microscope slides and anesthetized using 5 mM levamisole (Sigma-Aldrich). Analysis was performed using DM6 B fluorescence microscope and the Leica LAS X software (Leica Microsystem GmbH). GFP localization was assessed and categorized as 1) present in cytosol, 2) as intermediate or 3) localized into nucleus. For each experiment, ~ 25 worms were analyzed for each condition.

5.2.3. Gene expression via quantitative real-time PCR analysis

For gene expression assessment, RNA was isolated in pellets containing 500 worms as previously published using the Trizol method [226], which was transcribed using the High Capacity cDNA Reverse Transcription Kit (Applied Biosystems, Thermo Fisher Scientific) as stated in the manufacturer's protocol. Quantitative real-time PCR was carried out using TaqMan Gene Expression Assay probes (Applied Biosystems, Thermo Fisher Scientific) on an AriaMx Real-Time PCR System (Agilent). For normalization by the comparative $2^{-\Delta\Delta Ct}$ method, we used *AFDN* homolog *afd-1* as housekeeping gene [227]. The following probes were used: *afd-1* (Ce0241573_m1), *sod-1* (Ce02434432_g1), *sod-4* (Ce02451138_g1), *skn-1* (Ce02434432_g1), *bli-3* (Ce02413442_m1), *mpk-1* (Ce02445290_m1), *pmk-1* (Ce02456381_g1), *nsy-1* (Ce02432208_g1), *daf-16* (Ce02422838_m1), *gcs-1* (Ce02436726_g1), *pme-1* (Ce02415136_m1) and *pme-2* (Ce02437339_g1).

5.2.4. Glutathione (GSH and GSSG) levels quantification by HPLC-MS/MS

Reduced (GSH) and oxidized (GSSG) glutathione levels were assessed by liquid-chromatography tandem-mass spectrometry (HPLC-MS/MS). Following

Cu treatment, pellets were prepared by centrifugation of 1000 worms in 100 µL 85 mM NaCl. Sample preparation and GSH/GSSG analysis was performed as previously published [232].

5.2.5. HPLC-DAD analysis of energy-related adenine and pyridine nucleotides

Sample preparation as well as analysis by ion-pair reversed phase HPLC were performed according Bornhorst et al. [269]. 2000 worms were pelletized per condition in 100 µL 85 mM NaCl and immediately prepared as stated. The analysis was performed on an Agilent 1260 Infinity II liquid chromatography system with a photodiode array detector (DAD). Nucleotide contents were evaluated by external calibration of standard solutions of adenosine triphosphate (ATP), adenosine diphosphate (ADP), adenosine monophosphate (AMP), nicotinamide adenine dinucleotide phosphate (NADPH) and nicotinamide adenine dinucleotide (NADH and NAD^+). Detection by DAD was performed at 259 nm and data analysis was carried out using the OpenLab (version 3.6) software (Agilent).

5.2.6. Quantification of malondialdehyde

Unbound and bound MDA were determined by high performance liquid chromatography with fluorescence detection (HPLC-FLD). The sample preparation was based on Grintzalis et al. [309] and optimized for *C. elegans* matrix. Phosphate buffer (3.54 g/L KH_2PO_4, 7.24 g/L Na_2HPO_4, pH 7.0) was stored at 4 °C. Following pelletizing of 2000 worms in 100 µL 85 mM NaCl, 200 µL phosphate buffer and 1.5 µL 0.1 M 2-and-3-*tert*-butyl-4-hydroxyanisol (BHA) (Sigma Aldrich) were added and the pellet was stored at -80 °C up to one week. Samples were homogenized by 3 × freeze-thaw cycles (1 min liquid nitrogen,

1 min 37 °C), 3 × sonication with an ultrasonic probe (20 sec, cycle 1, amplitude 100%; UP100H, Hielscher) and in an ultrasonic bath (5 min). After centrifugation (5 min, 18620 rcf, 4 °C), 30 µL were transferred for protein measurement. 63 µL

of 100 % trichloroacetic acid (TCA) (Carl Roth) were added, following 5 min incubation on ice. Samples were centrifuged (15 min, 20000 rcf, 4 °C) and the entire supernatant (unbound MDA fraction) was transferred to a new tube and stored on ice until further use. For alkaline hydrolysis, 250 µL 1 M NaOH were added to the remaining pellet and incubated for 30 min at 60 °C. The hydrolyzed samples (bound MDA fraction) were cooled on ice and 25 µL conc. HCl was added. 1,1,3,3-Tetramethoxypropane (TMP) (Sigma Aldrich) was used for external calibration (20 – 500 nM), which forms an MDA-TBA product by derivatization with 2-Thiobarbituric acid (TBA) (Sigma Aldrich). For derivatization, 12.5 g/L TBA solution was prepared just before use by mixing solution A (100 % TCA, conc. HCl, ratio 5:1) and solution B (25 g/L TBA in 0.2 M NaOH) in a ratio of 1:1. 50 µL 12.5 g/L TBA and 3 µL 0.1 M BHA were added to 200 µL of each a) unbound, b) bound MDA sample and c) TMP calibration solution. All solutions were heated at 100 °C for 20 min and 300 µL butanol was added after cooling. Following centrifugation (5 min, 20 000 rcf, 4 °C), MDA levels were analyzed in an aliquot of the 1-butanol phase. Settings for the HPLC-FLD analysis as well as method validation parameters are listed in the Supplementary.

5.2.7. Cardiolipin levels and distribution by 2D-LC-HRMS

Cardiolipins were analyzed by 2D-HPLC-HRMS analysis. A detailed overview of the sample preparation and instrument parameters is listed in the Supplementary.

5.2.8. 8oxodG measurement via ELISA

8-oxoguanine (8oxodG) has been quantified by the OxiSelect^{TM} Oxidative DNA Damage ELISA kit (Cell Biolabs). 2000 worms were treated with Cu and pelletized as stated above. In the first step, DNA was isolated of each sample using the Qiagen Tissue and Blood DNA extraction kit, following the manufacturer's instruction. The amount of DNA was quantified by NanoDrop measurements and portioned in 40 µg aliquots, which were dried. In the second

step, DNA was hydrolyzed by enzymes to obtain mononucleotides as described by Nicolai et al. [310]. As third step, 8-oxodG measurement was performed according the above-mentioned manufacturer's kit instructions.

5.2.9. HPLC-MS/MS analysis of PARylation levels

Sample preparation for poly-(ADP-ribose) (PAR) extraction was done in pellets of 1000 worms and according [310]. Analysis was performed by HPLC-MS/MS using an Agilent 1290 Infinity II liquid chromatography system (Agilent, Waldbronn, Germany), which is coupled to a Sciex QTRAP 6500+ triple quadrupole mass spectrometer (Sciex, Darmstadt, Germany). PAR quantification was assessed as described in [310], with minor changes in chromatography: Chromatographic separation was performed using a Hypersil Gold aQ 150 x 2.1 mm and corresponding 10 x 2.1 mm pre-column. Elution was carried out with bidistilled water + 0.1% formic acid (FA) and acetonitrile + 0.1% FA and a flow of 0.3 mL/min. Total run time was 5 min, starting with 0 – 25% of ACN in 2.5 min, to 100% ACN in 0.5 min, 100% ACN for 1 min, following re-equilibration to 0% ACN. Results were normalized to DNA content determined by Hoechst method [228].

5.2.10. Neurotransmitter quantification via HPLC-MS/MS

Dopamine, serotonin, γ-amino butyric acid and acetylcholine levels were determined by HPLC-MS/MS. Pellets of 1000 worms per 50 µL 85 mM NaCl were prepared after Cu incubation. Samples were added with 100 µL extraction buffer, processed and analyzed according to [213]. Results were normalized to protein content analyzed by BCA assay (Sigma-Aldrich).

5.2.11. Aldicarb-induced paralysis assay

The assay is based on Mahoney et al. [311] and was performed as previously published [213]. Plates with 2 mM aldicarb (stock solution in 70% EtOH) were always prepared fresh and the assay was performed as a blinded experiment at all times.

5.2.12. Statistical analysis

Statistical analysis was carried out using GraphPad Prism 6 (GraphPad Software, La Jolla, USA) using 2-way ANOVA with Tukey's multiple comparison or impaired t-test for one-to-one comparison. Significance level with $\alpha = 0.05$: *: $p \leq 0.05$; **: $p \leq 0.01$ ***: $p \leq 0.001$ compared to untreated control and §: $p \leq 0.05$ §§: $p \leq 0.01$ and §§§: $p \leq 0.001$ compared to wildtype in same condition.

5.3. Results

5.3.1. daf-16 translocation visualized by daf-16::GFP fluorescence microscopy and mRNA levels of mitogen-activated protein kinases

Protein kinases activated by stress, such as c-Jun N-terminal kinases (JNK) and p38 mitogen-activated kinases (MAPK), can stimulate Forkhead box O-class proteins (FoxO) expression and translocation from cytosol to nucleus, where it acts as transcription factor participating in DNA repair, RONS detoxification and apoptosis (Figure 32A) [238]. The homolog of human FOXO4 is daf-16 in *C. elegans*, which can be visualized in the transgenic strain daf-16::GFP by fluorescence microscopy (Figure 32B). 24 h treatment with $CuSO_4$ or PQ used as positive control leads to a significant translocation of daf-16 from cytosol into the nucleus (Figure 32C). Furthermore, we examined mRNA levels of *daf-16/FOXO4* itself, but also representatives of MAPK's subgroups p38, JNK and ERK1/2 (extracellular signal-regulated kinases): *pmk-1/MAPK11*, *nsy-1/MAP3K5* and *mpk-1/MAPK1*. Gene expression of *daf-16/FOXO4* as well as of the p38 and JNK kinases *pmk-1/MAPK11* and *nsy-1/MAP3K5* are not altered due to Cu treatment (Supplementary Figure 51), while ERK1/2 MAP kinase *mpk1/MAPK1* is upregulated in wildtype worms in a dose-dependent manner (Figure 32D). Cu does not elevate mRNA levels of *mpk-1/MAPK1* in atox-1 and ceruloplasmin-deficient worms, but basal levels are already increased to the level of Cu-treated wildtype worms.

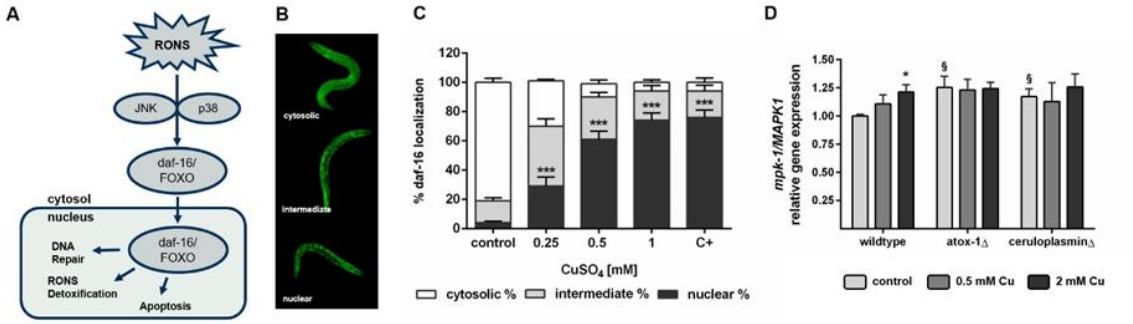

Figure 32. (A) Schematic daf-16 translocation from cytosol into the nucleus under oxidative stress conditions. (B) Exemplary fluorescence images of worms displaying cytosolic, intermediate or nuclear localized daf-16 in mutant worm daf-16::GFP. (C) daf-16 localization [%] of worms treated 24 h with CuSO4 or PQ as positive control (C+). Presented are mean values of n = 3 (N = 25) independent experiments + SEM. (D) Relative mRNA levels of mpk-1/MAPK1 following 24 h Cu incubation. Data presented are mean values of n = 4 independent experiments + SEM.

5.3.2. Reduced and oxidized glutathione, *gcs-1/GCLC* mRNA levels and energy-related nucleotides

As a marker for the antioxidative capacity, reduced (GSH) and oxidized (GSSG) glutathione were quantified by HPLC-MS/MS. Cu exposure (2 mM) significantly reduced GSH levels by 23% in wildtype worms, 34% in atox-1 and 38% in ceruloplasmin deletion mutants (Figure 33A). Inversely, Cu elevates oxidized GSSG levels in all strains (Figure 33B), however, ceruloplasmin-deficient worms display significantly lower GSSG levels after 2 mM Cu treatment compared to wildtype worms. *Gcs-1/GCLC*, which is involved in GSH synthesis, is not altered upon Cu incubation in *C. elegans*, but mutants with impaired Cu homeostasis display elevated mRNA levels (Figure 33C). Energy-related nucleotides of interest, namely ATP, ADP, AMP, NADPH, NADH and NAD^+ were assessed by HPLC-DAD analysis (Figure 33D-I). For all analytes tested, no alterations were detected by Cu treatment in wildtype worms. On the other hand, altered nucleotide levels were observed for the mutants displaying Cu dyshomeostasis, with ceruloplasmin-deficient worms seem to be specifically affected. Ceruloplasmin deletion mutants displayed reduced ATP levels compared to

wildtype worms, which are further reduced following Cu incubation. Furthermore, ADP and AMP levels were increased by Cu in atox-1 as well as ceruloplasmin mutants. While NADPH levels were elevated in atox-1-deficient worms, they were significantly reduced in ceruloplasmin-deficient worms. Moreover, both mutants contained lesser NADH levels compared to wildtype worms, and this effect was more pronounced in ceruloplasmin-deficient worms and was further exacerbated by Cu treatment. In addition, ceruloplasmin-deficient worms showed increased NAD^+ levels following Cu treatment.

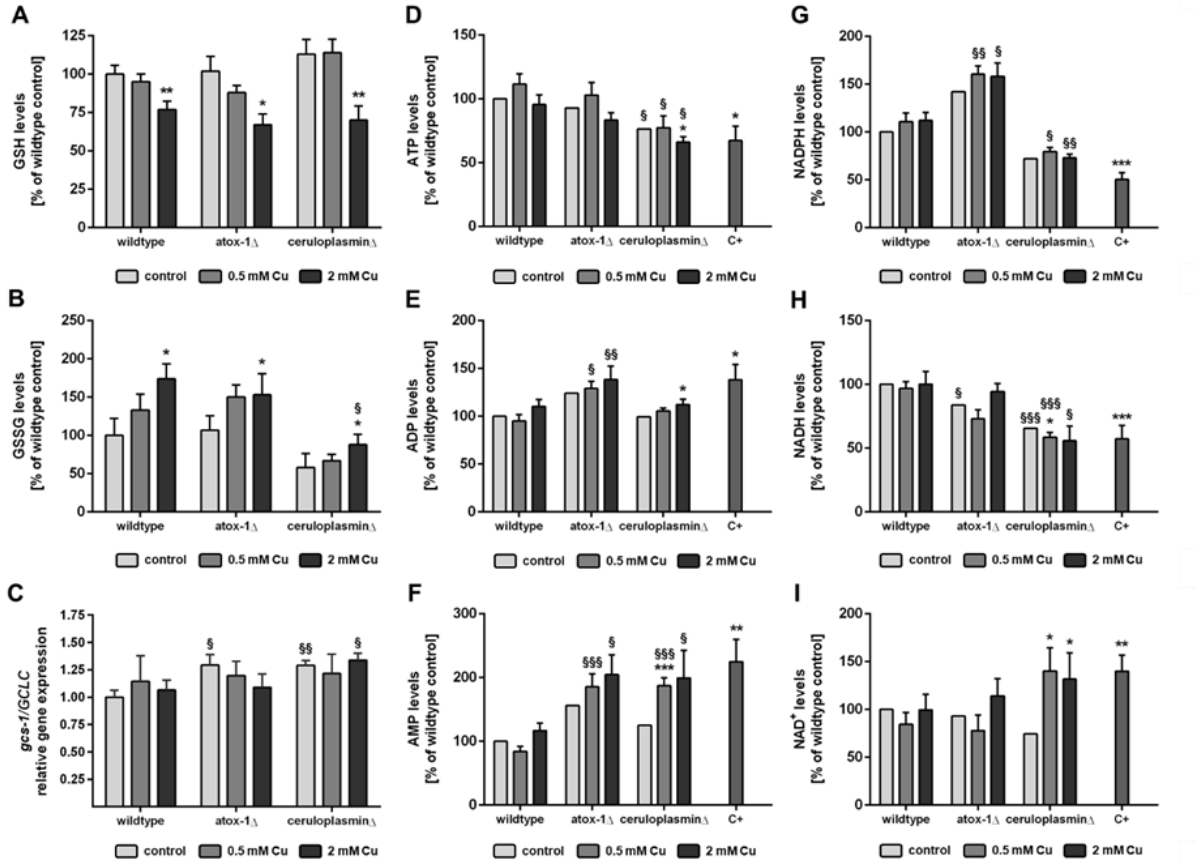

Figure 33. (A) GSH and (B) GSSG levels normalized to wildtype control [%]. (C) Relative mRNA levels of gcs-1/GCLC. Levels of (D) ATP, (E) ADP, (F) AMP, (G) NADPH, (H) NADH and (I) NAD+ compared to wildtype control [%]. PQ was used as positive control (C+) in wildtype worms. Data presented are mean values of n ≥ 4 independent experiments + SEM.

5.3.3. Malondialdehyde quantification and total cardiolipin levels and distribution

Using alkaline hydrolysis, unbound MDA as well as bound MDA, for example bound to proteins or DNA, were assessed. Our data reveal no alterations induced by Cu or *t*-BOOH on the amount of bound MDA (Supplementary Figure 53). However, unbound MDA levels increased significantly by *t*-BOOH in wildtype worms as well as by Cu treatment in the deletion mutants atox-1 and ceruloplasmin (Figure 34A). CLs are exclusively found in mitochondria and are fundamental for the mitochondrial membrane [305]. Our data showed no significant alterations in the CL profile induced by Cu supplementation in the tested worm strains but of the total CL content in the deletion mutant ceruloplasmin was reduced compared to wildtype worms (Figure 34B). Furthermore, our data revealed no alterations induced either by Cu supplementation or genetic Cu dyshomeostasis on the relative distribution of CL species with respect to chain length and the degree of saturation (Figure 34C and Supplementary Figure 54).

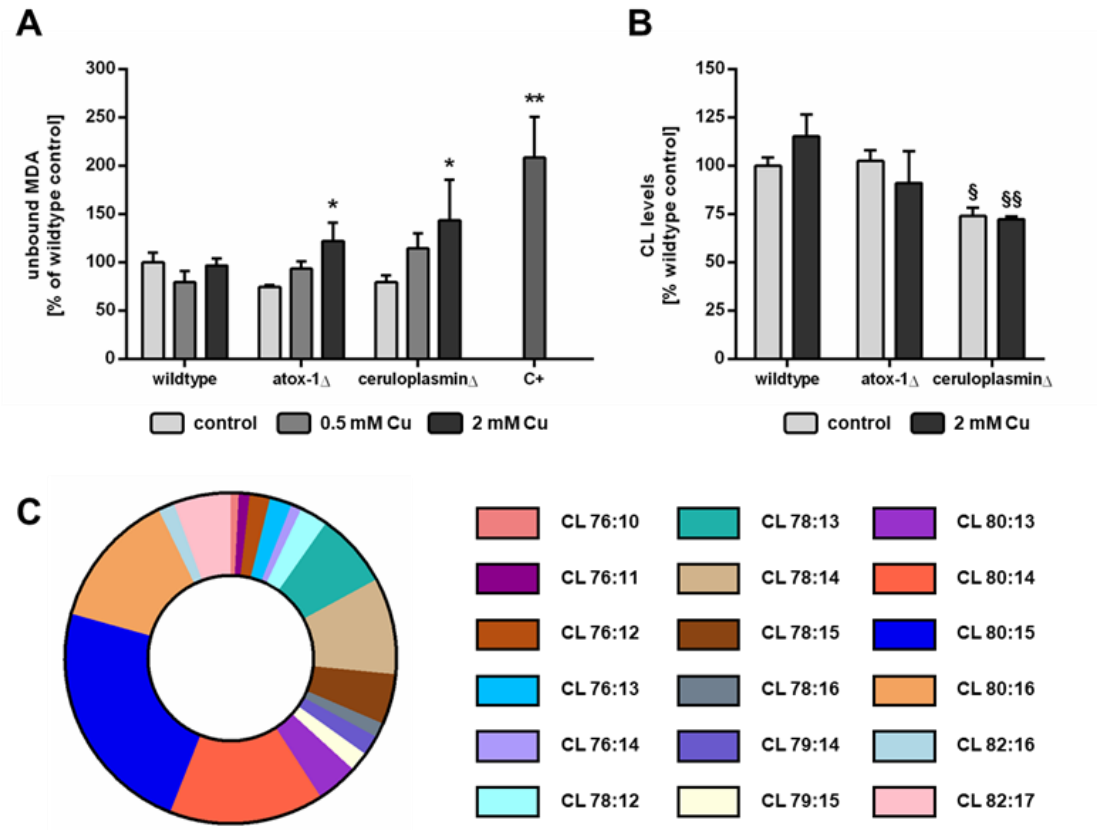

Figure 34. (A) MDA levels (unbound) normalized to wildtype control [%].(B) Total CL levels normalized to protein content and to wildtype control [%]. Data presented are mean values of n ≥ 3 independent experiments + SEM. (C) Representative distribution of CL species in terms of chain length and degree of saturation for untreated wildtype worms. *t*-BOOH was used as positive control (C+) in wildtype worms.

5.3.4. Oxidative DNA damage (8oxodG), DNA damage response (PARylation) and *pme/PARP* mRNA levels

We assessed levels of 8-oxoguanine (8oxodG), which is the most common DNA lesion initialized by RONS [312], as well as poly-(ADP-ribosylation) (PARylation) as a marker for DNA damage response. Data reveal increased 8oxodG levels for ceruloplasmin-deficient worms up to 350% following 2 mM Cu treatment, while wildtype and atox-1-deficient worms remained unaffected (Figure 35A). PAR levels showed no alterations in wildtype and ceruloplasmin mutants due to Cu supplementation. In contrast, untreated atox-1 mutants displayed reduced PAR levels compared to wildtype worms, but increased PARylation following Cu treatment (Figure 35B). Furthermore, mRNA levels of NAD^+-dependent poly

(ADP-ribose) polymerases (PARP), were examined (Figure 29C+D). While *pme-1/PARP1* remained unchanged, *pme-2/PARP2* was downregulated to about 50% in untreated atox-1-deficient mutants compared to wildtype worms, yet it was upregulated in response to Cu treatment.

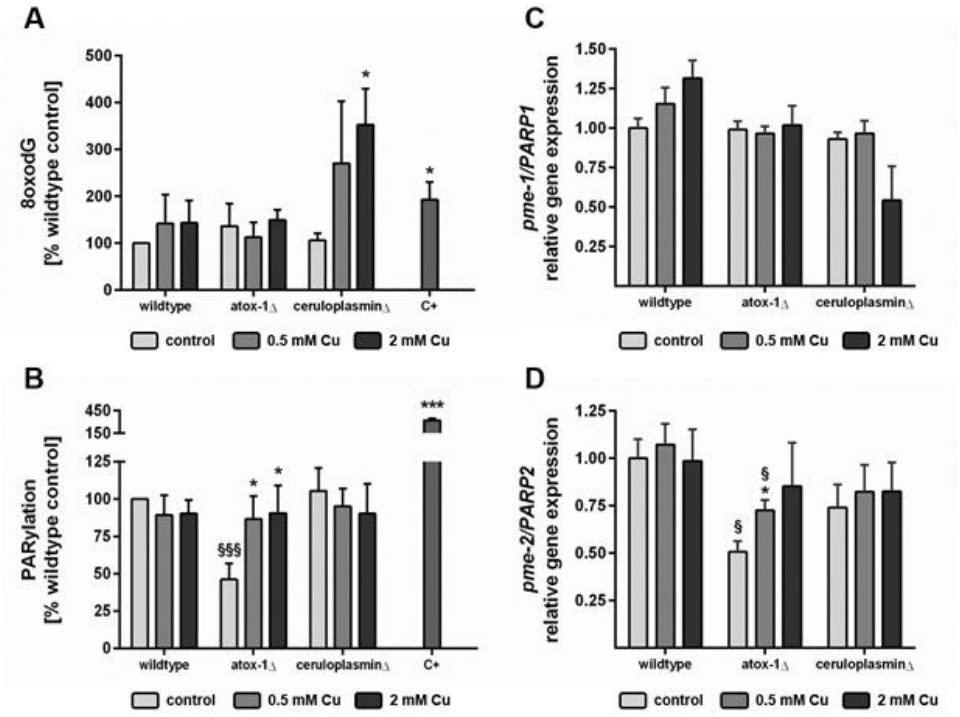

Figure 35. Relative (A) 8oxodG and (B) PARylation levels normalized to wildtype control Relative mRNA levels of (C) pme-1/PARP1 and (D) pme-2/PARP2 following 24 h Cu incubation. Data presented are mean values of n = 4 independent experiments + SEM. [%]. As positive control (C+) *t*-BOOH was used in wildtype worms.

5.3.5. Quantification of neurotransmitters DA, SRT, GABA and ACh levels and aldicarb-induced paralysis assay

HPLC-MS/MS-based quantification of the four neurotransmitters DA, SRT, GABA and ACh revealed different quantities of all analytes in *C. elegans* (Figure 36A-D). Untreated wildtype worms in young adult stage displayed 2.89 ng DA, 0.78 ng SRT, 529 ng GABA and 11.21 ng ACh each per mg of protein. Cu treatment failed to alter levels of all tested neurotransmitters compared to untreated controls in wildtype worms. In addition, in ceruloplasmin-deficient

worms, Cu failed to induce any alterations in neurotransmitter levels, however, mutant strain ceruloplasmin displayed significantly reduced GABA levels compared to the wildtype. In contrast, atox-1-deficient worms had the similar basal levels of neurotransmitters in comparison to wildtype worms, but levels of DA, SRT, GABA and ACh were reduced upon treatment with 2 mM Cu for 24 h. The aldicarb-induced paralysis assay was used to examine alterations in the synaptic transmission rate at the neuromuscular junction in *C. elegans* [311,313]. Results revealed significant differences between wildtype and ceruloplasmin-deficient worms, as they displayed aldicarb resistance starting at 240 min aldicarb treatment compared to wildtype worms (Figure 36E). Cu failed to alter the aldicarb-induced paralysis (Supplementary Figure 55) and thus did not lead to changes in the synaptic transmission rate at the neuromuscular junction.

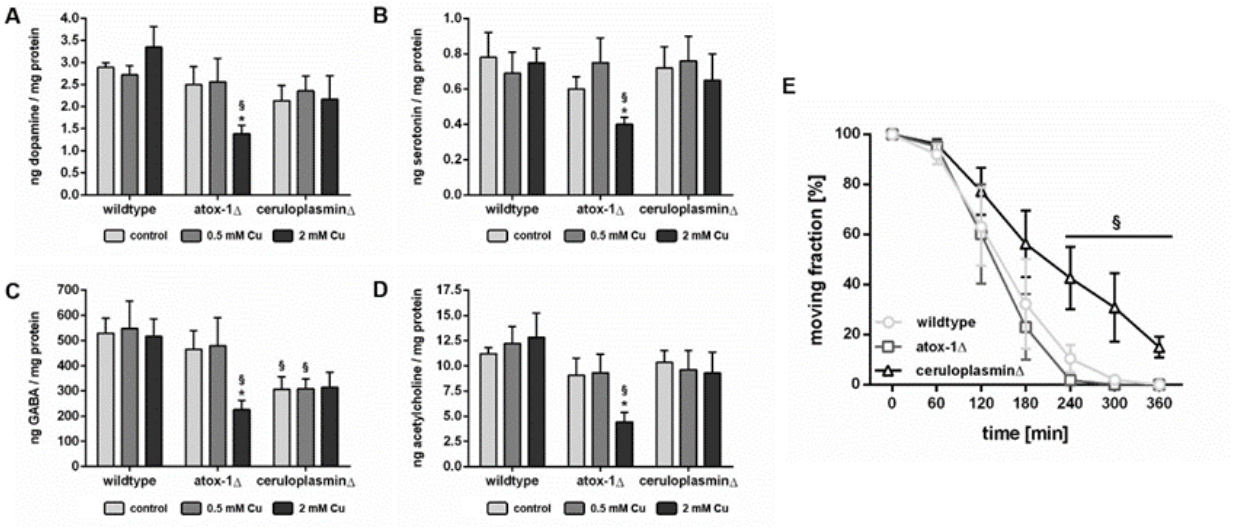

Figure 36. Neurotransmitter levels in ng per mg protein in *C. elegans* quantified via HPLC-MS/MS. Assessed were levels of (A) DA, (B) SRT, (C) acid GABA and (D) ACh. Aldicarb-induced paralysis assay in (E) untreated wildtype (light grey), atox-1Δ (dark grey) and ceruloplasminΔ (black) worms. Plotted are the fraction of moving worms [%] against the assay procedure time [min]. Data presented are mean values of n ≥ 4 independent experiments ± SEM.

5.4. Discussion

Cu is an essential trace element, but is toxic when exceeding the homeostatic range, leading to oxidative stress [314]. Especially labile Cu, namely readily available Cu, is redox active and associated with neurodegenerative diseases, such as Wilson's disease (WD), Alzheimer's disease (AD) and Parkinson's disease (PD) [298,299]. However, the exact underlying mechanisms of Cu toxicity and neurotoxicity are poorly understood. It is therefore of paramount importance to shed light on molecular mechanisms of (labile) Cu-induced oxidative stress and neurotoxicity, which was addressed herein. We used *C. elegans* mutants with a disrupted Cu homeostasis and quantified, by a variety of highly specific and sensitive techniques, oxidative stress-related metabolites. Worm mutants lacking Cu chaperone atox-1 or Cu storage protein ceruloplasmin display elevated labile Cu levels, which was characterized in detail in our previous work [188].

MAP kinases induced by, among others, oxidative stress activate transcription factors like skn-1/NRF2 or daf-16/FOXO4, which then translocate into the nucleus to induce apoptosis, antioxidative defense or DNA repair [315]. Cu treatment led to a significant activation and translocalization of daf-16/FOXO4 in a concentration-dependent manner, corroborating earlier studies [316] and similar effects by other divalent metals like manganese (Mn) [317]. mRNA levels of *daf-16/FOXO4* remained unaffected after 24 h. However, as this is one of the first pathways affected by RONS, mRNA levels may have returned to normal. Urban et al. investigated gene expression levels of the antioxidant defense system over a time period of 10 days and display different time frames of up- and downregulation of genes related to oxidative stress [318]. Other studies reported Mn- and zinc-induced oxidative stress and neurotoxicity, but in that scenario *daf-16/FOXO4* mRNA levels were unaffected as well [224]. Gene expression studies of representatives of the MAPK family revealed Cu-induced increase in *mpk-1/MAPK1* levels in wildtype worms, as well as altered basal

levels in both deletion mutants of atox-1 and ceruloplasmin. He et al. corroborate these findings by displaying Cu-mediated cell death via p38 MAPK activation in vascular endothelial cells [319], while Wang et al. report the absence of Cu-induced apoptosis in *C. elegans* loss-of-function mutants of JNK and p38 MAP kinases [320], indicating the participation of MAPKs in the regulation of Cu-induced oxidative stress.

Cu overload increases the formation of RONS and leads to oxidative stress, which alters, among others, SOD or GPX activity, which then leads to oxidative stress [296,297]. It was shown that the GSH/GSSG ratio is reduced by Cu nanoparticles [319], supporting our data of reduced GSH and increased GSSG levels following Cu treatment. Notably, GSH levels were reduced by 23% in wildtype worms, whereas by 38% in ceruloplasmin-deficient worms, indicating a higher demand or consumption. A higher demand results in an increased synthesis [321], mediated by increased mRNA levels of *gcs-1/GCLC* in ceruloplasmin- and atox-1-deficient mutants. As stated above, Cu mediates p38 downstream activation of transcription factors like daf-16/FOXO4 or skn-1/NRF2, which activates gcs-1/GCLC expression [197]. GSH synthesis is ATP-dependent [322], potentially reducing ATP levels in ceruloplasmin-deficient worms, which are even further lowered by Cu treatment. Baldissera et al. also showed reduced hepatic ATP levels by Cu in *Cichlasoma amazonarum* [323]. In turn, levels of ADP and AMP, which are formed during ATP consumption [324], are increased by Cu supplementation in atox-1- and ceruloplasmin-deficient worms. In addition to GSH, Cu also alters GSSG levels in wildtype and atox-1 mutants, but significantly less in ceruloplasmin-deficient worms. This may indicate a higher rate of recycling or reducing GSSG back to GSH. This process is, among several others, NADPH-dependent, and is decreased in ceruloplasmin-deficient worms. Although this could be a possible explanation, it is noteworthy that energy-related nucleotides take part in other metabolic pathways as well. Thus, NAD^+ is formed in the GSH/GSSG cycling, which gets

elevated by Cu treatment in ceruloplasmin-deficient worms. The Cu-sensing transcription factor Mac1 activates BNA expression and in turn quinolinic acid synthesis which results in *de novo* NAD^+ synthesis, which has been demonstrated in yeast [325,326]. Furthermore, Li et al. described a Cu-dependent S-Adenosylhomocysteine hydrolase inhibition, which results in a shift towards NAD^+ in the NADH/NAD^+ pool [327].

Recent studies have uncovered a rise in MDA levels subsequent to Cu treatment across various organisms [319,328,329], including *C. elegans* [296]. Our findings in wildtype worms demonstrated no alterations in either bound or unbound MDA levels, potentially attributed to our administration of (in wildtype worms) non-lethal Cu concentrations. Surprisingly, mutants deficient in atox-1 and ceruloplasmin exhibited comparable baseline levels of unbound MDA, yet notably heightened levels post-Cu treatment compared to wildtype worms. This suggests an increased hypersensitivity to Cu-induced oxidative stress or impaired antioxidative response under conditions of disrupted Cu homeostasis. CLs are vulnerable to oxidative damage due to their exclusive location within the inner mitochondrial membrane, where RONS are generated as byproduct of cellular respiration [330]. Oxidative stress can result in lipid oxidation and therefore in the formation of oxidized CL species [243]. Our findings indicate no observable formation of oxidized cardiolipins following Cu incubation (data not shown). Blume et al. demonstrated a slight reduction in the total CL content following iron or manganese treatment, but no formation of oxidation products in *C. elegans* [331]. Furthermore, the distribution of individual CL species, known as the CL profile, remains unaffected by Cu exposure or the genetic makeup of the worms. It is noteworthy, however, that our analysis may not quantify all existing CL species, thus limiting our analysis to those above the detection threshold. Moreover, the data presented herein were solely in reference to untreated wildtype worms, as the establishment of improved standards and normalization procedures was essential for facilitating quantitative assessments.

Nevertheless, the total sum of analyzed CL reveals a notable reduction in ceruloplasmin-deficient worms compared to the wildtype. Monteiro-Cardoso et al. stated that the total CL content drops significantly in the brain of an AD mouse model [305]. Several studies have also indicated that the dysregulation of CL content, as well as alterations of its structure and distribution, mediated neuronal dysfunction. These abnormalities are associated with the aging process and play a pivotal role in the pathogenesis of various neurodegenerative disorders, including AD and PD [304]. Aberrant levels of CLs have been linked to mitochondrial dysfunction, oxidative stress and impaired synaptic transmission, which are all hallmarks of AD and PD pathology. Understanding the mechanisms underlying cardiolipin-mediated neurodegeneration may offer novel therapeutic strategies aimed at preserving mitochondrial function and mitigating oxidative stress-related neuronal damage [304,305,332].

Cu and Cu nanoparticles have been shown to disrupt genomic integrity by causing oxidative DNA damage and DNA strand breaks [333,334]. Thus, it is surprising that Cu failed to induce PARylation. This leads to a first assumption that possible DNA damages may already be repaired and that PAR was already degraded in our chronic exposure scenario of 24 h. However, 8oxodG, which is the most common DNA lesion [312], was significantly increased in ceruloplasmin-deficient worms following 24 h Cu incubation, refuting our first assumption. Like wildtype worms, ceruloplasmin mutants exhibited no alterations of PARylation levels, also this strain revealed Cu-induced DNA damage observed characterized by increased 8oxodG levels. PARylation is one of the largest consumers of NAD^+ [335]. Our data reveal normal levels of NAD^+ in wildtype worms and even further increased levels in ceruloplasmin mutants. At first glance, this indicates that NAD^+ deficiency can be ruled out as cause for normal PARylation levels. But it must be noted, that our data only reflect the total NAD^+ content instead of organell-specific selective NAD^+ levels. mRNA levels of *pme-1/PARP1* and *pme-2/PARP2* also remained unchanged in wildtype and

ceruloplasmin-deficient worms. Taken together, these findings suggest that Cu inhibited PARylation, as previously hypothesized by Schwerdtle et al. [336]. Basal levels of PARylation were reduced in atox-1 mutants, possibly due to reduced Cu transport into the nucleus by the lack atox-1, but partially compensated by P-type ATPase ATP7B [337]. In addition, atox-1 interacts with PARPs in a detoured manner. Atox-1 induced the expression of MDC1, a crucial protein for double strand repair [338]. MDC1 interacts with aprataxin [339], which in turn works in concert with PARP's [340], which could explain lowered PARylation and *pme-2/PARP2* mRNA levels in atox-1-deficient mutants compared to wildtype worms. This needs to be further elucidated in *C. elegans*. Although 8oxodG levels were not altered in atox-1-deficient worms, Cu appeared to adversely affect the genomic stability of this mutants, as Cu treatment increased both PARylation and *pme-2/PARP2* mRNA levels. The low basal PARylation raise further concerns, since inhibited PAR has been linked to cellular toxicity as well as neurological dysfunction [341]. Although herein excess Cu failed to cause genotoxicity in wildtype worms, our data underline the importance of a properly functioning Cu homeostasis for genomic integrity.

The loss of proper antioxidant capacity and energy production as well as impaired genomic integrity may cause neuronal death [298,342]. Cu is known to cause neurotoxicity and is associated with neurodegenerative diseases, such as WD [343,344]. Labile bound Cu is commonly mentioned in the context of Cu-induced neurotoxicity [299,345], but knowledge on underlying mechanisms is scarce. Ceruloplasmin-deficient worms revealed aldicarb-resistance, reflecting decreased synaptic transmission rate at the neuromuscular junction [313]. Dabbish et al. demonstrated a correlation between aldicarb-sensitivity and reduced GABA levels [346]. This is contrary to our findings, as ceruloplasmin mutants displayed, next to aldicarb-resistance, reduced GABA levels compared to wildtype worms, indicating that further unknown factors may be involved. One likely mechanism of reduced GABA levels in ceruloplasmin-deficient worms

might be that excess Cu, as described by D'Ambrosi et al. [347], reduces GABA receptor activity, resulting in altered GABA levels. Atox-1 deletion mutant's basal levels of neurotransmitters remained unchanged compared to wildtype worms but were reduced due to 2 mM Cu treatment. Kelner et al. noted that atox-1 suppressed oxidative damage and promoted neuronal survival [348]. Furthermore, atox-1 is known to interact with α-synuclein and inhibit amyloid formation [349]. This is in agreement with our findings on Cu-mediated reduction in neurotransmitter levels due to the lack of atox-1, reflecting Cu-induced neurodegeneration upon loss of atox-1. Our data support that the dysregulation of Cu homeostasis leads to oxidative stress and subsequent detrimental effects on neurocellular pathways, underlining the importance of a properly working Cu homeostasis.

5.5. Conclusion

A comprehensive approach was adopted, employing specific and sensitive techniques to quantify metabolites related to oxidative stress with special focus on mitochondria, oxidative DNA damage, DNA damage response as well as neurodegeneration in the context of disrupted Cu homeostasis. Loss-of-function mutants of Cu chaperone atox-1 and Cu storage protein ceruloplasmin displayed increased labile Cu levels despite lowered total Cu uptake [188] concomitant with increased oxidative stress, reduced mitochondrial ATP levels and CL content, as well as oxidative DNA damage and impaired neuronal health. Our data underline the essentiality of a proper Cu homeostasis and the importance of valuable markers, such as labile Cu, to diagnose Cu dyshomeostasis. Furthermore, our study highlights the importance of mitochondrial integrity for genomic and neuronal health. As a future perspective, understanding the intricate interplay of CL dysregulation and neurodegenerative processes holds significant promise for the development of therapeutic interventions preserving genomic and neuronal stability.

5.6. Funding information

This work was supported by the DFG Research Unit TraceAge (FOR 2558, BO4103/4-2) and the DFG (INST 218/81-1 FUGG).

5.7. Author's contributions

Conceptualization: A.W., J.B.; Investigation/Experiments: A.W., A.G., T.M., V.S., K.S.; Methodology: A.W., A.G., V.S., A.T.; Supervision: J.B.; H.H.; Funding acquisition: J.B.; Visualization: A.W.; Writing-original draft and revision: A.W.; Writing-review and editing: A.G., T.M., V.S., K.S., A.T., T.S., M.A., H.H., J.B.; All authors have read and agreed this version of the manuscript.

5.8. Acknowledgement

Wildtype worms (N2) and TJ356 were provided by CGC, which is funded by NIH Office Research Infrastructure Programs. Atox-1 and ceruloplasmin deletion mutants were provided by S. Mitani Lab (NBRP, Tokyo Women's Medical University, Japan).

Chapter 6 – Final Discussion and Future Perspectives

Chapter 6 – Final Discussion and Future Perspectives

As the most abundant trace element in numerous organisms, Fe is an essential key component in crucial biological processes. Due to the ubiquitous presence of Fe in food, drinking water, and food supplements, Fe is mostly ingested in bound or complexed forms in a variety of Fe species. The most biologically relevant oxidation states are Fe(II) and Fe(III). The redox interconversion between these forms is essential for Fe-dependent biological processes, but also the mode of action for the catalysis of RONS via Fenton reaction. Thus, both Fe deficiency and Fe overload in organisms may lead to adverse consequences and are associated with several diseases. Those associated with Fe overload include hemochromatosis, the most common genetic disorder worldwide, as well as neurodegenerative diseases, which often occur in aging. The latter is associated with accumulation of Fe in the brain, while additional risk factors may include weakened biological processes such as Fe homeostasis or antioxidative defense.

The underlying mechanistic consequences of excess Fe, both induced by different Fe species and in combination with a weakened antioxidant system, are not fully understood. To shed more light on these topics, we worked with the nematode *C. elegans* as a well-established model organism for mechanistic and toxicological studies. In order to gain more mechanistic insights into the consequences of overdosing by different Fe species, we not only investigated bioavailability but also the effects on cellular processes such as Fe homeostasis, oxidative stress, and cell death. In addition, investigations in a model with elevated Fe and low GSH levels provided us with some mechanistic insights into Fe homeostasis, mitochondria, lipidome, and neurological endpoints, in conditions which are associated with the cell death ferroptosis and neurodegenerative diseases. We also investigated both acute and long-lasting effects in this model, as well as initial indications of whether these conditions could lead to ferroptotic cell death. Through the optimization and validation of

an HPLC-FLD method for investigating MDA levels, it was possible to examine whether lipid peroxidation is caused by elevated Fe and decreased GSH levels. Furthermore, this method was applied in a study focusing on dysfunctional Cu homeostasis regarding oxidative stress, mitochondrial, genomic, and neuronal integrity. In chapters 3 – 5, the results of these studies were already discussed in relation to the existing literature; this discussion is further expanded in the next chapters.

6.1 The Impact of Different Fe Species on Several Biological Endpoints

It is well known that heme Fe is absorbed more efficiently than nonheme Fe, and that Fe(II) is more bioavailable than Fe(III).[235,247,350] With growing interest in vegan and vegetarian diets, food supplements, and fortified foods, nonheme Fe is becoming increasingly important in nutrition.[216,247,351] Several studies are showing that different Fe species vary in their bioavailability.[235,350] However, studies investigating cellular consequences beyond bioavailability caused by different Fe species are limited, and these either examine intravenously applied Fe or use liver cells as a model.[237,252,352] To examine a more realistic scenario in our study, we treated an organism with additional Fe through its diet. We treated L4 *C. elegans* with FAC, FeGlu, and $FeCl_2$ for 5 h and 24 h to obtain data for food-relevant Fe species and short-term as well as long-term effects within the same model. According to Commission Regulation (EC) No 1170/2009, FAC and FeGlu are permitted to be added to food and food supplements in the European Union.[217] In chapter 3, we showed that bioavailability can depend on the oxidation state and ligand of the Fe species, but that the impact on Fe homeostasis, oxidative stress, and cell death is similar. By including two treatment periods, it was possible to examine both counter-regulatory responses and long-lasting effects. Although Fe homeostasis in *C. elegans* has been well studied and reviewed by Anderson et al., not all of the genes involved and their functions have been fully elucidated.[190] Using deletion mutants and gene expression measurements, we were able to obtain further

insights into the function of genes associated with Fe homeostasis after treatment with the three Fe species.

By enriching *E. coli* with the Fe species, we provided the compounds via food, although a certain amount was probably also absorbed through the worms' cuticle. The doses and treatment times of Fe species applied were non-lethal, and no behavioral changes of the worms could be observed. While the total Fe content increased similarly across all Fe species after 5 h treatment, the Fe content differed significantly after 24 h treatment. Since the total Fe concentration after treatment of 0.5 mM and 1 mM FAC was similar after 24 h compared to after 5 h, a counter-regulation may have occurred that limited the uptake of Fe by FAC. Treatment with 1 mM FeGlu and $FeCl_2$ resulted in significantly increased Fe contents after 24 h than after 5 h treatment. Since only the Fe content from the Fe(III) species is limited in time, this could suggest a counter-regulation or limitation of the reductive capacity in the worm. After 24 h treatment, Fe contents were twice as high following FeGlu treatment and five times higher following $FeCl_2$ treatment compared to FAC. Our study also revealed that *smf-3*, *f55h2.5* (*dcytb*), *ftn-1, ftn-2*, and *f21d5.3* (*cp*) are involved in the homeostasis of Fe provided by FAC, FeGlu, and $FeCl_2$, with regulatory changes already evident after 5 h. After 5 h of treatment, gene expression of the importer *smf-3* was decreased upon treatment with each species, and the Fe content in *smf-3Δ* was significantly reduced after 24 h compared to wild type. In this strain, both in untreated control and after treatment with all Fe species, more than 50% less Fe was measured compared to wild type. This indicates that SMF-3 could be the main transport protein for Fe from Fe(III) and Fe(II) species in the intestine, but it is probably not the only pathway. Since SMF-1 is also expressed in the anterior and posterior intestine, it should be investigated in future studies.[175] The gene expression of the reductase *dcytb* was only decreased by 0.5 mM $FeCl_2$ after 5 h, while Fe content in *dcytb*Δ was decreased after administration of each species for 24 h. However, Fe content after

treatment with each Fe species was increased compared to untreated control of this strain. This suggests additional enzymes or compounds that reduce Fe(III), or the involvement of other transport pathways that enable the import of Fe(III). Although treatment with all Fe species did not result in any alterations in the gene expression of the Fe storage protein *ftn-2*, they increased *ftn-1* gene expression after 5 h and decreased total Fe levels in *ftn-1;ftn-2*ΔΔ after 24 h. The altered gene expression indicates a counter-regulation to protect the organism from reactive Fe(II) after treatment with each species. Low Fe levels in *ftn-1;ftn-2*ΔΔ additionally suggest counter-regulation of the Fe import, as there is no known active excretion mechanism for Fe. These findings demonstrate the importance of the storage proteins in Fe homeostasis after treatment with the used Fe species, maintaining low Fe levels within the organism already after 5 h of treatment. The gene expression of the Cu storage protein *cp* was slightly decreased by all species, and FeGlu and $FeCl_2$ led to lower Fe levels in *cp*Δ compared to wild type. Since CP is involved in the oxidation of Fe(II) to Fe(III) extracellularly and presumably also intracellularly, *cp*Δ may have regulated Fe import to limit the Fe content. In mammals, the ferroxidase activity of CP and hephaestin enables Fe(III) to be bound and transported by TF through the plasma.[28] However, it is unknown how Fe is systematically distributed in *C. elegans*, as the worm lacks both TF and plasma.

After both treatment times, all three Fe species led to alterations in markers associated with oxidative stress and apoptotic cell death. Although the total Fe content varied considerably, treatment with all Fe species led to increased mitochondrial RONS, translocation of DAF-16, and apoptotic germ cells to a similar extent. While SOD activity was increased by FAC and FeGlu after both treatment times, $FeCl_2$ only led to an increase after 5 h of treatment. These findings demonstrated the impact of each tested Fe species on the antioxidant defense system, as evidenced by counter-regulatory responses such as DAF-16 translocation, increased SOD activity, and altered gene expression of

important Fe homeostasis-associated genes. The altered mitochondrial RONS and apoptotic germ line cells level can be seen even after 24 h of treatment, although counter-regulatory responses are already detected after 5 h of treatment. FAC was the only Fe species that led to increased GSH levels after 24 h treatment compared to untreated control. Although GSH acts as a radical scavenger, it is an important co-enzyme of the GPX family, which inhibits lipid peroxidation, and the GST family, which catalyze the binding of GSH to toxic metabolites and xenobiotics. The enhanced antioxidant defense may prevent more severe damage that would otherwise need to be neutralized by GSH-dependent enzymes. Consequently, despite alterations in other oxidative stress markers, no differences in GSH levels were detected. However, as with most studies, it should be noted that the effects were assessed only at the specific time points investigated. It cannot be excluded that processes are regulated differently earlier or between the 5 h and 24 h treatment.

However, some limitations of this study must be considered for the interpretation of the findings. Firstly, it must be taken into account that the Fe species on the agar plates are in constant contact with oxygen. The compounds were freshly weighed before each experiment, dissolved in bidistilled water, mixed into *E. coli* suspension, and dried on the plates for as short as possible (1 – 2 h). Nevertheless, it cannot be excluded that the oxidation state of the Fe species may have changed to some extent, as may also be the case during liquid treatment. Even though we have already investigated two treatment times, both shorter and longer treatment periods would be very interesting to include. For example, Blume et al. showed that a 30 min treatment with $FeSO_4$ in L1 worms increased Fe levels and affected the cardiolipidome, thereby impacting mitochondrial integrity.[331] Shorter treatment times could help determine when Fe uptake reaches a plateau after FAC treatment, as no difference was observed between 5 h and 24 h treatment, and could also provide insights into the timing of early gene regulation and oxidative stress responses. Longer

treatment periods could provide more insights into long-lasting effects. It would also be interesting to examine the effects of aging if no further Fe is administered after the 24 h of treatment, especially regarding life span, oxidative stress, and cell death. A study by Baesler et al. demonstrated that the Fe content in day 2 adult worms increased sixfold by day 12.[224] In addition, James et al. showed that the administration of FAC to *C. elegans* led to increased ferritin-bound Fe and that this fraction decreased in ageing worms.[177] If the similar effects of different Fe species on oxidative stress and cell death are due to Fe being stored redox-inactive in FTN, aging may increase the availability of redox-active Fe(II). Since Fe accumulation is associated with neurodegenerative diseases, neuronal endpoints such as neurotransmitters or the morphology of neurons should be investigated directly after Fe treatment, but also at a later stage in ageing worms. Capillary electrophoresis-ICP-MS (CE-ICP-MS) could be used to investigate how much of the Fe is present as Fe(II) and Fe(III), or the Fe(II) level could be determined by more available dye assays such as FerroOrange.[353,354] Furthermore, it would be interesting to localize the Fe in the entire worm as well as at cellular level. Since mitochondrial RONS were observed as a consequence of the Fe treatment, isolating these organelles and subsequently determining their Fe content could be an option.[355] In addition, further investigations into apoptosis, but also other types of cell death, should be carried out. The investigations with CED-1::GFP only focus on the engulfment of germ line cells. Using Differential Interference Contrast (DIC) microscopy, apoptotic and necrotic cells could be observed throughout the worm and in all developmental stages.[356]

6.2 The Impact of an Unbalanced Redox System due to Elevated Fe Content and Decreased GSH Level

Both Fe accumulation and a weakened antioxidative system are associated with aging and neurodegenerative diseases. The population is aging, and understanding the mechanistic pathways of diseases is getting more important for disease prevention and therapy.[357] To investigate the consequences of Fe excess and GSH depletion, we treated *C. elegans* with FAC for 24 h and/or DEM for 2 h or 24 h. Since the Fe species had similar effects on the tested endpoints in the previous study (chapter 3), and FAC as Fe(III) species is more stable in contact with atmospheric oxygen, we decided to use this Fe species for our further investigations. Since Fe accumulation presumably takes place over a longer period of time, during which the organism can partially counteract this process, we decided on a 24 h FAC treatment. The two treatment periods of DEM were intended to investigate both acute and long-lasting effects. Endpoints related to mitochondrial integrity, the lipidome, and the neurological system, which are associated with neurodegenerative diseases, were investigated.

DEM is widely used in the literature for investigating consequences associated with GSH depletion. According to my knowledge, the product GSH-DEM was only characterized by Kubal et al. in 1995 using H^1 NMR.[83] To measure GSH-DEM in *C. elegans*, the existing method developed by Thiel et al. for measuring GSH/GSSG using HPLC-MS/MS was modified in this thesis. We were able to detect GSH-DEM using the modified method both after *in vitro* synthesis and in worm suspension. This ensured that DEM binds to GSH in *C. elegans,* and we were able to calculate altered GSH/GSH-DEM ratios.

FAC treatment led to a fivefold increase in total Fe levels compared to untreated control, regardless of the DEM concentration. The upregulated gene expression of *ftn-1* and the unchanged Fe(II) levels compared to untreated control indicate a storage as Fe(III) in the Fe storage protein, whereby *ftn-2* is also expected to play a role despite unchanged gene expression.[177] The low variance between

untreated control and FAC-treated samples of PCA analysis indicates a well-buffered Fe homeostasis, which requires only minor alterations in gene expression. FAC treatment did not affect GSH levels, but it led to decreased GSSG levels. Although increased mitochondrial RONS were measured in the study from chapter 3 after treatment with 0.5 mM and 1 mM FAC for 24 h, treatment with 20 mM FAC did not alter mitochondrial mass or CL levels. While FAC treatment led to slightly increased acetylcholine levels, it appeared not to affect the synaptic transmission rate of acetylcholine in the neuromuscular junction. In addition to its function as a neurotransmitter in the neuromuscular junction, acetylcholine acts as a neuromodulator and is therefore involved in changes of a neuron or group of neurons linked to neurotransmitter release or neuronal excitability.[284] 24 h after FAC treatment and without further FAC application during DEM treatment period, the Fe content was three times higher than in untreated control. This demonstrates that high levels of Fe remain in *C. elegans* over a prolonged period, which is presumably due to the absence of an active excretion mechanism of Fe. At this point, long-term effects on the lipidome could be detected, like elevated levels of numerous PL and SL. Alterations in the lipidome are often discussed in context of neurodegenerative diseases, as PL and SL in particular are essential for the function and integrity of cellular membranes.[279] This is also associated with lipid peroxidation, which can be catalyzed by Fe. In our study, no evidence of elevated lipid peroxidation after FAC treatment could be detected by measuring the byproduct MDA. This could be linked to Fe being stored in ferritin in a redox inert state. Nevertheless, another endpoint for lipid peroxidation, such as the direct measurement of oxidized lipids, should be included to confirm this finding.[358]

Short-term treatment with DEM decreased GSH levels to 30% and resulted in a GSH-DEM/GSH ratio between 1 and 2. DEM treatment had no impact on GSSG levels. Although long-term treatment with 75 mM DEM did not lead to any alterations in GSH levels, GSH-DEM was detected, and a GSH-DEM/GSH ratio

of between 0.01 and 0.04 was observed. In addition, 75 mM DEM led to decreased GSSG levels. However, it should be noted that while 6.2 ± 0.7 ng GSH/µg protein was measured in untreated control after 2 h treatment (day 1 adults) and 1.4 ± 0.3 – 2.3 ± 0.3 ng GSH/µg protein after DEM treatment, GSH level after 24 h treatment in the untreated control (day 2 adults) was only at 1.6 ± 0.2 ng GSH/µg protein. GSSG levels, on the other hand, were similarly in untreated controls at both measurement points. Jenkins et al. demonstrated in *C. elegans* that GSH levels decreased by almost 50% from day 1 adults to day 10 adults.[206] Since the difference in GSH levels observed in our study was greater, the type of DEM treatment in the buffer may also have impacted GSH levels. Transcriptomic analysis revealed that after 2 h DEM treatment, *gcs-1*, *e01a2.1*, and *gss-1* associated with GSH synthesis, were upregulated. 24 h DEM treatment also resulted in upregulated expression of *gcs-1*, which is one of the limiting factors of GSH synthesis. This indicates that the nematode presumably counteracts the DEM treatment through increased GSH synthesis and that altered *gcs-1* expression plays a long-lasting role in this process. Short-term treatment with 20 mM DEM decreased the survival rate to 80%. Even though the antioxidative system comprises many molecules, enzymes, and pathways, this suggests that a certain amount of GSH is crucial for survival. Additionally, Fe(II) levels were increased, and gene expressions of *smf-2*, *smf-3*, *cp*, *fpn-1.1*, and *fpn-1.2* were altered, which demonstrates the impact of DEM on Fe homeostasis. These effects were not observed after long-term DEM treatment, but the increased gene expression of *ftn-1* at this time point indicates a counter-regulation in response to possibly previously elevated Fe(II) formation. One reason for the increased Fe(II) levels detected could be that GSH is less available for complexation of Fe(II) in the LIP, resulting in more reactive Fe(II) being present intracellularly. It is assumed that at pH 7, over 80% of Fe(II) in the LIP is complexed to GSH.[359] Since the pH value in intestinal cells of adult worms is 7.6, Fe(II) may be mainly complexed to GSH also in this organism.[214] This raises the question of how Fe(II) must be present to react with

FerroOrange, because it is always said that the dye detects labile Fe(II).[274] However, if an increased amount of Fe(II) reacts with FerroOrange, the Fe(II) will be present in such a form that it can also react with other molecules. Nevertheless, determining Fe(II) levels of the LIP is of great importance, as they are considered drivers of lipid peroxidation and ferroptosis.[3] Future studies could investigate whether Fe(II) levels also increase after 2 h treatment with 15 mM DEM, as this concentration depleted GSH to a similar extent as 20 mM DEM but did not decrease the survival rate. After both treatment periods, decreased mitochondrial masses were observed, with slight trends toward lower CL levels and altered distributions of CL species measured after long-term treatment. In addition, the upregulated gene expression of *hsp-6* indicated mitochondrial stress after short-term treatment with DEM. In future studies, it would be interesting to isolate the mitochondria and measure total Fe, Fe(II), and GSH levels. In addition, mitochondria-specific antioxidants such as MitoQ could be used to investigate whether the decreased mitochondrial mass is a consequence of mitochondrial oxidative stress.[360] Long-term treatment with DEM led to increased PE-O, LPE, LPC, SM, Cer, and HexCer levels in the lipidome and increased expression of genes involved in SL (*lagr-1*) and PC (*ckb-2*) biosynthesis. Although no alterations in PL and SL levels were measured after short-term treatment, genes involved in SL (*sptl-2*, *sms-5*, *cgt-1*, *gba-2*) and PE (*pcyt-2.1*) biosynthesis were upregulated. PLs are the main component of cellular membranes, and increased biosynthesis could indicate an increased requirement for membrane biogenesis or membrane remodeling. In addition, PLs are increasingly associated with the regulation of cellular and nuclear processes, such as generating signaling molecules or involvement in mechanisms against oxidative stress.[361] While short-term treatment with DEM led to increased serotonin levels, long-term treatment additionally resulted in increased acetylcholine levels. The approx. 20% of worms that died after short-term treatment made an interpretation of the transmission rate of acetylcholine unfeasible. However, after 24 h of treatment, the worms showed slowed

paralysis, indicating a decreased transmission rate of acetylcholine in the neuromuscular junction. After short-term treatment, transcriptomic analysis revealed altered expression of genes involved in acetylcholine homeostasis and serotonin biosynthesis. These involved downregulation of *unc-13* (involved in vesicle exocytosis), *ace-2* (acetylcholine degradation), and *eat-2* (post-synaptic receptor subunit involved in pharyngeal pumping), and upregulation of *acr-18* (post-synaptic receptor with unknown function), *acr-23* (post-synaptic receptor involved in muscle contraction), and *tph-1* (serotonin biosynthesis). In order to confirm the effect on the neurological system through a further endpoint, future studies could investigate the effect on the basal and enhanced slowing response in contact with food. While basal slowing is controlled by dopamine-containing neural circuits, the enhanced slowing response of food-deprived worms in contact with food is mediated by serotonergic neurons.[362]

The combined treatment with FAC and DEM and the associated combination of elevated Fe levels and decreased GSH levels did not alter any of the effects observed with FAC or DEM alone. One possible explanation for this could be that Fe is stored sufficiently in a redox-inactive form within the 24 h treatment period, so that an alteration in antioxidative capacity due to GSH depletion in our endpoints does not enhance these effects. Nevertheless, slight variations in the PCA analysis can be noted after both treatment periods between DEM alone and combined with FAC treatment. In the pathways we focused on, there are some differences in gene expression after long-term treatment. DEM alone led to changes in gene expression of *gpx-2*, *ftn-1*, and *lagr-1*, while the combined treatment lowered the gene expression of *gpx-3* and enhanced that of *fpn-1.1*. The relevance of these genes in our exposure scenario could be investigated in future studies using deletion mutants or RNAi silencing of the respective gene.[363]

Lip-1 slightly increased the survival rate in combination with FAC and DEM, but it was still significantly lower than in untreated control. This suggests that

ferroptosis may be at least partially a consequence of FAC and DEM treatment, but further markers such as oxidized lipids or GPX activity should be investigated. In addition, Lip-1 did not rescue the effects caused by FAC and DEM. Jenkins et al. showed that the Fe chelator salicylaldehyde isonicotinoyl hydrazone (SIH) increased the survival rate more effectively than Lip-1 after DEM treatment.[206] Since SIH binds to Fe(II) of the LIP, and increased Fe(II) levels were measured in our study after DEM treatment, future studies may reveal whether SIH could rescue the effects of DEM observed in our experiments.[364] Further investigations into other types of cell death could provide insights into the pathways that led to a decreased survival rate after treatment with DEM alone and combined with FAC.

Even though we have deliberately chosen these treatment scenarios, treatments at other worm stages, different treatment orders, or times may lead to other results. The two treatment times in this study are not directly comparable, as we used different DEM concentrations and different forms of treatment. Treatment in buffer is suitable for investigating the mechanistic consequences following acute exposure, as only the investigated substance is taken up by the worm in addition to NaCl, and the preparation time until pelletizing and freezing of the worms can be kept to a minimum. Washing off worms treated on NGM plates would take too long in relation to the short treatment time, and this could potentially negate possible effects. Long-term treatment on NGM plates ensures that the worms have sufficient food and, through absorption via *E. coli*, offers a more realistic form of treatment. Since the measurements were taken in the entire worm, no conclusions can be made about the localization of the increased Fe(II) and decreased GSH level regarding the worms organs and cellular organelles. This knowledge would help to investigate possible pathways more specifically, even if initial investigations indicate the involvement of mitochondria. To enable further investigations into this organelle, the involvement of mitoferrin (required for Fe delivery into

mitochondria) could be examined. Huang et al. showed that knockdown of mitoferrin-1 decreased mitochondrial Fe levels and RONS in *C. elegans* Alzheimer's models.[365] In this study, it would also be interesting to investigate long-lasting effects in aging worms, as regulated Fe homeostasis appears to play an important role here as well, both after FAC and after DEM treatment. Since both Fe accumulation and low GSH levels are associated with neurodegenerative diseases, the mechanistic consequences in *C. elegans* models of Alzheimer's or Parkinson's disease could be investigated as well.[79,366]

6.3 The Consequences of Dysfunctional Cu Homeostasis

Findings from both Fe studies suggest that metal homeostasis plays an important role in the prevention of reactive Fe species, but that despite gene regulation of Fe homeostasis-associated genes, Fe can lead to changes in endpoints associated with oxidative stress, cell death, and neuronal alterations. In a previous study, Weishaupt et al. showed in *C. elegans* that deletion of the intracellular Cu chaperone *atox-1* led to increased labile Cu levels after L4 worms were treated for 24 h with 2 mM $CuSO_4$ and that the basal level of labile Cu was increased in *cp*-deficient worms. In wild type worms, the total Cu level was increased six-fold, in *atox-1*Δ five-fold, and in *cp*Δ three-fold. The *atox-1*Δ and *cp*Δ strains showed a slight trend toward lower survival rates compared to wild type worms, which decreased significantly after 2 mM Cu treatment for 24 h, whereas the survival rate remained unchanged in wild type worms.[188]

Through investigations of endpoints associated with oxidative stress and mitochondrial, genomic, and neuronal integrity, further consequences of dysfunctional Cu homeostasis with the same treatment conditions were demonstrated in Chapter 5. In this study, 2 mM $CuSO_4$ in wild type worms led to increased GSH and decreased GSSG levels, but energy-related nucleotides, MDA, CL, and neurotransmitter levels remained unchanged. GSH and GSSG levels in *atox-1*Δ were similarly altered by $CuSO_4$ compared to wild type, but the treatment led to altered ADP, AMP, NADPH, unbound MDA, dopamine,

γ-aminobutyric acid, serotonin, and acetylcholine levels in this mutant. In *cp*Δ, following $CuSO_4$ treatment, GSH levels were also decreased, and GSSG levels were increased, while Cu treatment led to alterations in all investigated nucleotides, unbound MDA, and CL levels. In addition, compared to wild type, the basal level of γ-aminobutyric acid in *cp*Δ was lower, and the untreated mutant showed an aldicarb-resistance. These findings underscore the importance of regulated metal homeostasis, as already discussed in chapters 6.1 and 6.2 with regard to Fe homeostasis. This, and especially the interaction between Cu and Fe, is underscored by the characteristic clinical symptoms of aceruloplasminemia patients. This disease is caused by a mutation in the *cp* gene, resulting in cellular Fe accumulation, including in the brain, and is associated with neurodegenerative diseases as well as other clinical symptoms.[53] In Chapter 3, decreased total Fe levels were measured in untreated *cp*Δ worms (Supplementary Figure 37), but it could not be investigated whether Fe was distributed similarly to wild type worms or whether there was enhanced cellular Fe accumulation. In future studies, it would be interesting to investigate the consequences of combined Fe and Cu treatment in *cp*Δ, particularly with regard to neuronal endpoints.

In the study from Chapter 3, lower basal levels of Fe, Mn, and Zn were measured in *cp*Δ, and lower basal levels of Fe, Mn, Zn, and Cu were measured in *ftn-1;ftn-2*ΔΔ compared to wild type (Supplementary Figure 37). In addition, significantly decreased total Fe and Cu levels were measured after $FeCl_2$ treatment in *cp*Δ compared to wild type. These results show that although the storage proteins are mainly associated with Cu or Fe homeostasis, they can impact other trace elements such as Mn and Zn. The most discussed interactions are those between trace elements during absorption or cellular import, which is an important aspect due to their coexistence in food and food supplements. A study in human epithelial Caco-2 cells showed that treatment with Fe(III) nitrilotriacetate decreased intracellular Cu and Zn content, while

treatment with Cu-histidin decreased intracellular Fe levels. Further investigations revealed competitive uptake interactions at the apical site: elevated Zn or Cu concentrations decreased Fe uptake, elevated Fe concentrations decreased Cu uptake, while elevated Zn concentrations had no effect on Cu absorption.[140] It would be interesting to conduct such studies in *C. elegans* to investigate how trace elements affect the content of other trace elements in a whole organism, and also in context of dysfunctional Fe or Cu homeostasis.

The measurement of MDA via reaction with TBA is widely used in a variety of studies.[367] The optimization and validation of MDA measurement via HPLC-FLD in this study enabled reliable measurement of unbound and bound MDA levels in *C. elegans* samples. Therefore, the method could be used in both the Fe and Cu studies (chapters 4 and 5). Due to the high reactivity of MDA, the extraction from the worm pellets had to be adapted. The antioxidant BHA was added before the pellets were frozen for storage and the storage stability of MDA was verified. The recovery rate revealed that the samples should not be frozen at -80 °C for longer than one week. Furthermore, due a LOQ of 30 nM, pellets of 1500 adult nematodes were sufficient to reliably determine MDA levels.

In sum, this thesis enabled a comparison of the Fe species FAC, FeGlu, and $FeCl_2$ in the same organism, demonstrating that bioavailability depends on the oxidation state and ligand of the Fe species. This study also demonstrated how early and important the regulation of Fe homeostasis genes are and provided new insights into the function of *f55h2.5* (*dcytb*) and *f21d5.3* (*cp*) in *C. elegans*. In both Fe studies from chapters 3 and 4, the gene regulation of *ftn-1* indicates that it is an important factor in antioxidative defense. The regulation of Fe homeostasis also plays a role after treatment with DEM and presumably due to the resulting GSH depletion. The product of GSH and DEM that led to the depletion of GSH could be detected using HPLC-MS/MS. In addition, GSH depletion was associated with alterations in mitochondria, PL, SL, and

neurotransmitter levels. Furthermore, dysfunctional Cu homeostasis demonstrated the importance of a well-functioning metal homeostasis. To a limited extent, this study also addressed the interaction between trace elements and their respective homeostatic regulation. Nevertheless, many questions remain unanswered, and these studies may provide initial insights into potential answers.

Appendix – Supplementary Material

Appendix – Supplementary Material

Supplementary for Chapter 3: Is Ferric the Same as Ferrous? Effect of Nutritionally Relevant Iron Species in *C. elegans*: Bioavailability, Iron Homeostasis, Oxidative Stress, and Cell Death

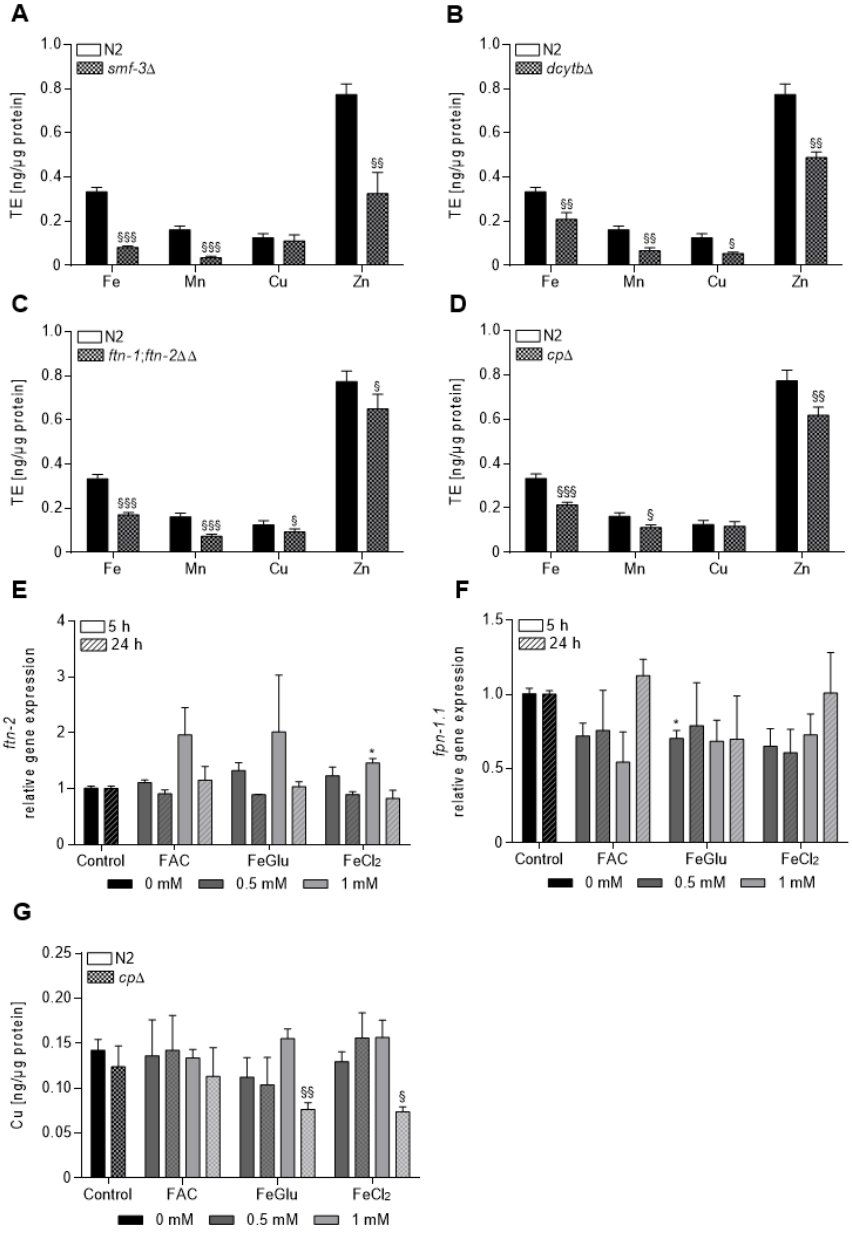

Figure 37. Bioavailability of Fe, Mn, Cu and Zn in (A) *smf-3*Δ, (B) *dcytb*Δ, (C) *ftn-1;ftn-2*ΔΔ, (D) *cp*Δ after treatment for 24 h with Fe species [ng/µg protein]. Relative gene expression of (E) *ftn-2* and (F) *fpn-1.1* after treatment for 5 or 24 h with Fe species. (G) Bioavailability of Cu in N2 and *cp*Δ after treatment for 24 h with Fe species [ng/µg protein]. Shown are mean + SEM of n ≥ 3 independet experiments. Significance are depicted as * compared to untreated control and § compared to wild type.

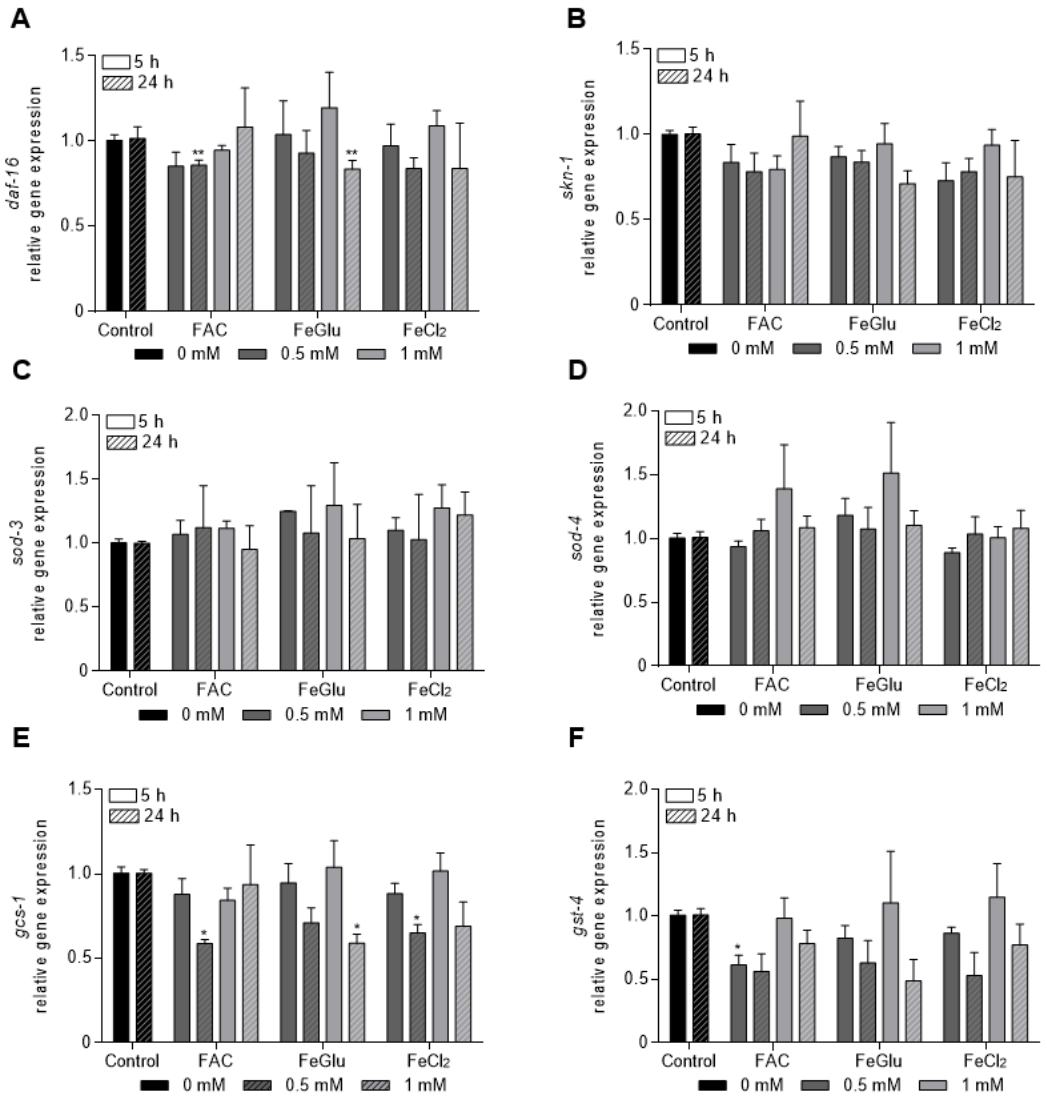

Figure 38. Relative gene expression of (A) *daf-16*, (B) *skn-1*, (C) *sod-3*, (D) *sod-4*, (E) *gcs-1* and (F) *gst-4* after treatment for 5 or 24 h with Fe species. Shown are mean + SEM of n ≥ 3 independet experiments. Significance are depicted as * compared to untreated control.

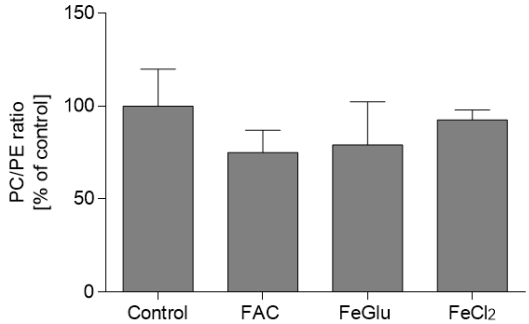

Figure 39. PC/PE ratio compared to untreated control [% of control]. Shown are mean + SEM of n ≥ 3 independet experiments.

Table 4. Areas normalized to protein of PC and PE species used for determination of the distribution by degree of saturation and PC/PE ratio. Listed are mean ± SEM of n ≥ 3 independet experiments.

Lipid	Sum Formula	Area/Protein			
		Control	FAC	FeGlu	$FeCl_2$
PC 32:0	$C_{40}H_{80}NO_8P$	1.2.E+07 ± 2.6.E+06	1.5.E+07 ± 1.9.E+06	1.2.E+07 ± 2.8.E+06	1.3.E+07 ± 1.0.E+06
PC 32:1	$C_{40}H_{78}NO_8P$	4.2.E+07 ± 7.1.E+06	5.6.E+07 ± 6.5.E+06	4.0.E+07 ± 2.2.E+06	4.3.E+07 ± 3.1.E+06
PC 32:2	$C_{40}H_{76}NO_8P$	2.2.E+07 ± 6.1.E+06	2.7.E+07 ± 1.1.E+06	2.4.E+07 ± 3.6.E+06	2.6.E+07 ± 6.2.E+05
PC 33:1	$C_{41}H_{80}NO_8P$	6.7.E+07 ± 1.3.E+07	9.0.E+07 ± 9.7.E+06	7.0.E+07 ± 7.9.E+06	7.1.E+07 ± 5.5.E+06
PC 33:2	$C_{41}H_{78}NO_8P$	7.1.E+07 ± 2.0.E+07	8.4.E+07 ± 5.5.E+06	7.5.E+07 ± 1.3.E+07	7.7.E+07 ± 5.3.E+06
PC 34:1	$C_{42}H_{82}NO_8P$	8.0.E+07 ± 1.7.E+07	9.6.E+07 ± 6.8.E+06	7.1.E+07 ± 5.8.E+06	7.9.E+07 ± 6.1.E+06
PC 34:2	$C_{42}H_{80}NO_8P$	7.1.E+07 ± 6.6.E+06	1.4.E+08 ± 3.8.E+07	9.4.E+07 ± 2.3.E+07	1.0.E+08 ± 2.4.E+07
PC 35:1	$C_{43}H_{84}NO_8P$	9.7.E+07 ± 2.7.E+07	1.1.E+08 ± 6.7.E+06	8.4.E+07 ± 9.2.E+06	6.1.E+07 ± 9.1.E+06
PC 35:2	$C_{43}H_{82}NO_8P$	2.8.E+08 ± 3.0.E+07	3.6.E+08 ± 2.5.E+07	2.7.E+08 ± 3.5.E+06	3.0.E+08 ± 2.1.E+07
PC 36:2	$C_{44}H_{84}NO_8P$	3.0.E+08 ± 1.9.E+07	4.3.E+08 ± 4.2.E+07	3.1.E+08 ± 3.4.E+06	3.4.E+08 ± 3.1.E+07
PC 36:3	$C_{44}H_{82}NO_8P$	1.9.E+08 ± 2.9.E+07	2.3.E+08 ± 1.8.E+07	2.1.E+08 ± 1.9.E+07	2.2.E+08 ± 5.5.E+06
PC 36:7	$C_{44}H_{74}NO_8P$	1.1.E+07 ± 2.2.E+06	1.6.E+07 ± 1.8.E+06	1.1.E+07 ± 1.1.E+06	1.1.E+07 ± 2.1.E+06
PC 37:2	$C_{45}H_{86}NO_8P$	2.4.E+08 ± 1.4.E+07	3.1.E+08 ± 1.5.E+07	2.3.E+08 ± 6.5.E+06	2.6.E+08 ± 1.4.E+07
PC 37:6	$C_{45}H_{78}NO_8P$	2.2.E+08 ± 1.8.E+07	3.1.E+08 ± 2.1.E+07	2.1.E+08 ± 5.1.E+06	2.3.E+08 ± 1.4.E+07
PC 38:2	$C_{46}H_{88}NO_8P$	7.6.E+07 ± 6.8.E+06	9.5.E+07 ± 6.7.E+06	6.4.E+07 ± 5.9.E+06	7.8.E+07 ± 3.0.E+06
PC 38:4	$C_{46}H_{84}NO_8P$	1.2.E+08	1.6.E+08	1.2.E+08	1.3.E+08

		± 1.5.E+07	± 1.6.E+07	± 7.9.E+06	± 8.5.E+06
PC 38:6	$C_{46}H_{80}NO_8P$	6.3.E+08 ± 6.3.E+07	8.9.E+08 ± 1.0.E+08	6.8.E+08 ± 2.2.E+07	7.2.E+08 ± 4.4.E+07
PC 40:4	$C_{48}H_{88}NO_8P$	7.7.E+06 ± 2.2.E+06	8.5.E+06 ± 6.9.E+05	7.6.E+06 ± 7.7.E+05	7.8.E+06 ± 4.9.E+05
PC 40:6	$C_{48}H_{84}NO_8P$	5.0.E+07 ± 1.0.E+07	6.2.E+07 ± 6.7.E+06	5.2.E+07 ± 4.6.E+06	5.2.E+07 ± 4.2.E+06
PC 40:8	$C_{48}H_{80}NO_8P$	1.9.E+08 ± 2.1.E+07	2.6.E+08 ± 2.1.E+07	1.9.E+08 ± 8.2.E+06	2.0.E+08 ± 5.7.E+06
PE 32:1	$C_{37}H_{72}NO_8P$	3.2.E+06 ± 3.6.E+05	6.9.E+06 ± 7.6.E+05	5.2.E+06 ± 1.8.E+06	4.1.E+06 ± 7.1.E+05
PE 32:2	$C_{37}H_{70}NO_8P$	9.8.E+05 ± 7.2.E+04	2.3.E+06 ± 3.4.E+05	1.5.E+06 ± 4.4.E+05	1.5.E+06 ± 2.9.E+05
PE 33:1	$C_{38}H_{74}NO_8P$	6.4.E+06 ± 1.1.E+06	1.1.E+07 ± 2.1.E+06	7.9.E+06 ± 4.1.E+06	7.5.E+06 ± 1.1.E+06
PE 33:2	$C_{38}H_{72}NO_8P$	2.1.E+06 ± 4.1.E+05	4.4.E+06 ± 5.0.E+05	3.3.E+06 ± 9.9.E+05	2.4.E+06 ± 4.2.E+05
PE 34:1	$C_{39}H_{76}NO_8P$	1.2.E+07 ± 2.6.E+06	2.1.E+07 ± 2.4.E+06	1.8.E+07 ± 6.0.E+06	1.3.E+07 ± 2.0.E+06
PE 34:2	$C_{39}H_{74}NO_8P$	6.8.E+06 ± 6.9.E+05	1.3.E+07 ± 1.9.E+06	1.0.E+07 ± 3.2.E+06	8.7.E+06 ± 2.3.E+06
PE 34:4	$C_{39}H_{70}NO_8P$	6.4.E+05 ± 9.9.E+04	1.6.E+06 ± 3.3.E+05	1.0.E+06 ± 1.6.E+05	1.0.E+06 ± 1.5.E+05
PE 36:1	$C_{41}H_{80}NO_8P$	1.4.E+07 ± 4.6.E+06	2.2.E+07 ± 1.5.E+06	2.1.E+07 ± 7.7.E+06	1.4.E+07 ± 1.8.E+06
PE 36:2	$C_{41}H_{78}NO_8P$	2.8.E+07 ± 6.6.E+06	4.9.E+07 ± 4.3.E+06	4.4.E+07 ± 1.5.E+07	3.4.E+07 ± 6.2.E+06
PE 36:3	$C_{41}H_{76}NO_8P$	1.4.E+07 ± 3.2.E+06	2.7.E+07 ± 2.7.E+06	2.3.E+07 ± 7.9.E+06	1.8.E+07 ± 3.7.E+06
PE 36:4	$C_{41}H_{74}NO_8P$	6.4.E+06 ± 8.5.E+05	1.4.E+07 ± 1.9.E+06	9.0.E+06 ± 1.7.E+06	7.9.E+06 ± 1.5.E+06
PE 37:1	$C_{42}H_{82}NO_8P$	4.4.E+06 ± 1.0.E+06	6.6.E+06 ± 4.6.E+05	6.2.E+06 ± 1.9.E+06	4.0.E+06 ± 9.0.E+05
PE 37:2	$C_{42}H_{80}NO_8P$	1.8.E+07	3.0.E+07	2.6.E+07	2.0.E+07

		± 4.4.E+06	± 2.4.E+06	± 8.3.E+06	± 3.8.E+06
PE 37:6	$C_{42}H_{72}NO_8P$	1.7.E+06 ± 4.0.E+05	2.9.E+06 ± 7.2.E+04	2.0.E+06 ± 3.4.E+05	1.7.E+06 ± 3.9.E+05
PE 38:1	$C_{43}H_{84}NO_8P$	2.2.E+06 ± 6.9.E+05	3.7.E+06 ± 3.7.E+05	3.5.E+06 ± 1.5.E+06	2.4.E+06 ± 3.0.E+05
PE 38:3	$C_{43}H_{80}NO_8P$	3.6.E+06 ± 1.2.E+05	6.4.E+06 ± 1.1.E+06	5.7.E+06 ± 8.3.E+05	5.9.E+06 ± 2.8.E+05
PE 38:6	$C_{43}H_{74}NO_8P$	1.5.E+07 ± 3.5.E+06	2.9.E+07 ± 3.8.E+06	2.2.E+07 ± 5.4.E+06	1.9.E+07 ± 4.2.E+06
PE 39:1	$C_{44}H_{86}NO_8P$	1.3.E+06 ± 4.5.E+05	1.8.E+06 ± 1.1.E+05	2.0.E+06 ± 8.1.E+05	1.4.E+06 ± 2.3.E+05
PE 39:5	$C_{44}H_{78}NO_8P$	4.7.E+06 ± 1.7.E+06	6.6.E+06 ± 1.4.E+06	4.3.E+06 ± 1.7.E+06	5.2.E+06 ± 1.2.E+06
PE 40:1	$C_{45}H_{88}NO_8P$	1.0.E+06 ± 3.6.E+05	1.4.E+06 ± 1.3.E+05	1.6.E+06 ± 6.6.E+05	1.1.E+06 ± 2.2.E+05
PE 40:2	$C_{45}H_{86}NO_8P$	1.1.E+06 ± 5.5.E+05	1.3.E+06 ± 2.2.E+05	1.4.E+06 ± 6.5.E+05	1.0.E+06 ± 2.1.E+05
PE 40:3	$C_{45}H_{84}NO_8P$	7.2.E+05 ± 9.9.E+04	1.3.E+06 ± 1.9.E+05	1.1.E+06 ± 1.6.E+05	9.9.E+05 ± 4.2.E+04
PE 40:5	$C_{45}H_{80}NO_8P$	2.2.E+06 ± 8.7.E+05	4.2.E+06 ± 3.2.E+05	3.5.E+06 ± 1.6.E+06	2.5.E+06 ± 1.4.E+05

Supplementary for Chapter 4: Iron Up and Glutathione Down: An Imbalance Impacting Iron Homeostasis, Mitochondria, Lipidome, and Neurotransmitters in *C. elegans*

S1. Method parameters for GSH-DEM determination

To identify the product GSH-DEM and its fragments by LC-MS/MS, the reaction of GSH and DEM was carried out *in vitro* based on Kubal et al. [83] For the stock solutions, DEM was diluted in DMSO and GSH was weighed in freshly and dissolved in 0.2 M phosphate buffer. The reaction was performed at equimolar amounts of both reagents (5 mM) and 1% DMSO in phosphate buffer for 3.5 h at 20 °C. Figure S1 shows the structure of GSH-DEM with the fragmentation

patterns measured in this study. The used collision energy, collision cell exit potential, and declustering potential are shown in Table S1. Figure S2 shows representative chromatograms of the synthesized GSH-DEM standard (Fig. S2A) and a *C. elegans* sample after 2 h DEM treatment (Fig S2B).

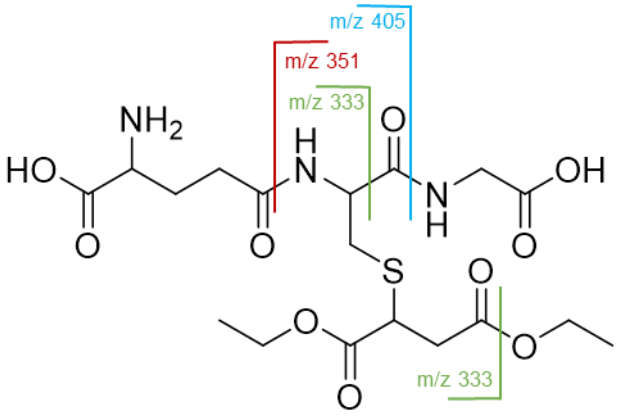

Figure 40. Structural formula of the GSH-DEM product with the fragmentation patterns and the corresponding m/z.

Table 5. Parameters for detection of the fragments of GSH-DEM. Quantifier is marked with an asterisk.

Fragmentation [m/z]	Collision energy [V]	Collision cell exit potential [V]	Declustering potential [V]
480 > 333	23	10	25
480 > 351*	21	10	25
480 > 405	26	10	25

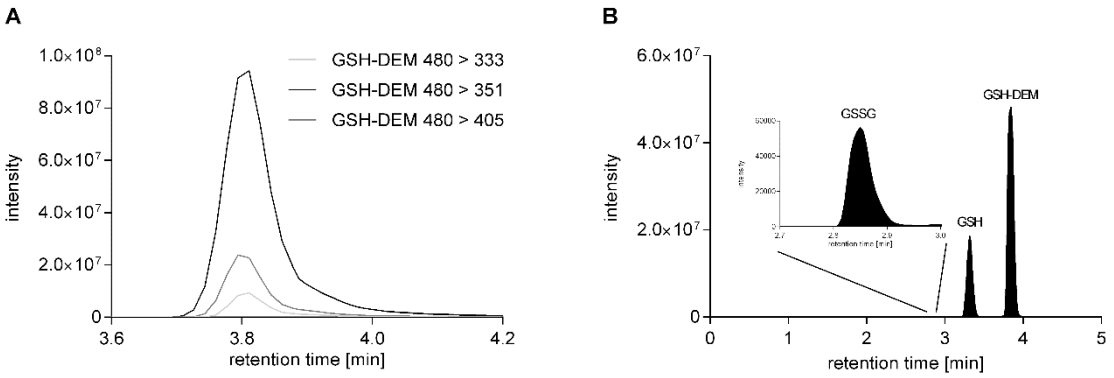

Figure 41. Representative MRM chromatograms of A) mass transitions of GSH-DEM in phosphate buffer and B) GSSG, GSH, and GSH-DEM in *C. elegans* treated with 20 mM DEM for 2 h.

S2. Chemicals

The isotopically labeled lipid standard 1,2-dipalmitoyl-d62-*sn*-glycero-3-phosphocholine (PC 32:0-d62 [PC 16:0 / 16:0 - d62]) was obtained from Biomol GmbH (Hamburg, Germany, PN 28751). 16:1 cardiolipin (CL 64:4), ammonium formate (pur. ≥99.995%) and ammonium acetate (≥99.99%) were purchased from Sigma-Aldrich Corporation (Steinheim, Germany). Butylhydroxytoluene was acquired from Fisher Scientific GmbH (Schwerte, Germany). LC grade chloroform and methyl-*tert*-butylether (MTBE) were obtained from Merck KGaA (Darmstadt, Germany). LC-MS grade acetonitrile (ACN), methanol (MeOH) and 2-propanol (IPA) as well as acetic (≥99.8%) and formic acid (≥99%) were obtained from VWR International GmbH (Darmstadt, Germany). Water was purified utilizing a Milli-Q EQ 7000 system purchased from Merck KGaA (Molsheim, France).

S3. Lipid extraction

For lipid extraction of *C*. *elegans* samples (4500 adult day 1 and 2 nematodes each), an extraction according to the protocol by Matyash *et al*. was performed as follows.[243,270] The pellets were resuspended with 200 µL of water and three freeze-thaw cycles utilizing liquid nitrogen were applied. Afterwards, 20 µL of a 40 µM solution of PC 32:0-d62 was added prior to extraction. The solution was adapted to a final concentration of 2 µM for phospholipid (PL) and sphingolipid (SL) determination. This isotopically labeled internal standard was utilized to ensure proper extraction. Additionally, 20 µL of a 65 mM butylhydroxytoluene solution as antioxidant were added. Before sonication in an ultrasonic processor (20 min, P = 20 W, C = 50 %, A = 80 %; UP200St, Hielscher Ultrasonic GmbH, Germany), 750 µL of ice cold MeOH were added. Subsequently, 750 µL of MeOH and 5 mL of MTBE were added and samples incubated for 1 h under agitation (700 rpm, MULTI-TX5, VELP Scientifica Srl, Italy) at room temperature. Furthermore, 1.25 mL of water were added and samples were incubated for 15 min. Phase separation was supported by centrifugation at

5000 rpm for 5 min (Centrifuge 5804, Eppendorf AG, Germany). After collection of the upper organic phase, another extraction cycle of the remaining aqueous phase was performed by adding 2 mL of MTBE/MeOH/Water (10/3/2.5, *v*/*v*). Combined organic phases were evaporated under a gentle nitrogen stream at 40°C. The residue was reconstituted in 1000 µL of MTBE/MeOH (3/1, *v*/*v*) and subsequently aliquoted for the analysis of cardiolipins (800 µL) as well as PL and SL (200 µL). For PL and SL determination, 200 µL of sample extract were dried under a gentle nitrogen stream at 40°C and the residue reconstituted with 80 µL of IPA. For cardiolipin analysis all 800 µL of sample extract was resuspended in 80 µL of IPA containing CL 64:4 (0.5 M), after drying under a gentle nitrogen stream at 40°C.

S4. Lipid Nomenclature

Lipid denomination is based on the shorthand notation established by Liebisch *et al*.[234,368] Phospholipids are described by their respective subclass notation, followed by the total number of carbon atoms (X) and double bonds (Y) found in the fatty acyl chains, e.g. PC X:Y. For sphingolipid species the total number of carbon atoms (X) and double bonds (Y) between the sphingoid base and fatty acyl chain are given, similar to phospholipid nomenclature. Additionally, the number of hydroxy groups (Z) is given, e.g. SM X:Y;OZ.

S5. Chromatographic setup for determination of CL composition

For 2D chromatographic separation of CL, a Vanquish Flex Duo UHPLC-system (Thermo Scientific, Dionex, Dreieich, Germany; Dual Split Sampler FT, Dual Pump F, Column Compartments H) incorporating a 6-port valve was utilized. Xcalibur 4.1 software and the SII Chromeleon plugin were used for instrument operation. Phospholipid classes were separated in the first dimension using an iHILIC Fusion(+) column (250 x 2.1 mm, 3.5 µm, 100 Å, HILICON AB, Umeå, Sweden) and a gradient based on our previous work, comprising an ammonium formate buffer (20 mM, pH 3.5, 5% ACN, A1) and ACN (B1).[243] Before a series

of measurements, a 20-minute equilibration step at 60% B1 was employed to attain a reproducible HILIC separation and retention times. Additional chromatographic parameters included a flow rate of 0.4 mL/min, an injection volume of 2 µL and a column temperature maintained at 40°C. The HILIC gradient was initiated at 95% B1 for two minutes, followed by a linear decrease to 60% B1 within 15 min. This mobile phase composition was maintained for six minutes before being increased to 95% B1 where it was held for the remainder of the method (33 min total run time). Intra-class separation of CL species in the second chromatographic dimension was achieved utilizing a RP-HPLC XSelect Premier CSH C18 column (100 x 2.1 mm, 2.5 µm, 100 Å; Waters Corporation, Milford, MA, USA) under gradient elution. The gradient system was composed of an aqueous ammonium acetate buffer (10 mM, pH 3.5, 5% MeOH) (A2) and MeOH/IPA (60/40, *v*/*v*, containing 10 mM ammonium acetate buffer, 0.01% acetic acid; B2). Further HPLC parameters included a flow rate of 0.3 mL/min at 40°C column temperature. The RP-HPLC gradient started at 80% B2 and was held for 14 min, then linearly increased to 92% B2 in one minute. Subsequently, B2 was further increased to 98% over 14 min, followed by an increase to 100% B2 within 0.5 min. After maintaining this composition for 2.5 min, B2 was decreased to 80% within 0.4 min and held until the end of the run. In the 2D-LC heart-cut setup, both chromatographic dimensions were connected through a 6-port valve and a valve configuration as previously described.[243] The timing of the 6-port valve switching was determined by the elution window of the CL-class (heart-cut window: 12.1-12.7 min). To enable separation in the second dimension, the heart-cut fraction was collected in a 500 µL sample loop.

S6. Mass spectrometric setup for determination of CL composition

For CL analysis via 2D-HPLC heart-cut MS/MS, mass spectrometric detection was carried out using a Q Exactive Plus mass spectrometer and a heated electrospray ionization source (HESI-II, Thermo Scientific, Bremen, Germany). Electrospray ionization was conducted in negative ionization mode, and HESI-

II probe parameters were set as follows: source voltage -3.5 kV, probe heater temperature 300 °C, sheath gas flow rate 45 arbitrary units, auxiliary gas flow rate 10 arbitrary units, spare gas flow rate 1 arbitrary unit, and capillary temperature 325 °C. The s-lens rf level was set to 85. Full MS measurements were performed with a resolution of 140,000 (FWHM at *m/z* 200), an AGC target set to $3e^6$ and a maximum C-trap injection time of 100 ms. For structural elucidation, data-dependent MS/MS acquisitions were obtained at a normalized collision energy of 24 eV (based on a *m*/*z* of 500) and a resolution of 17.500 (at *m*/*z* 200). The isolation window for precursors was set to 1.5 Da. For MS/MS experiments, a maximum C-trap injection time of 50 ms was applied.

S7. Chromatographic setup for determination of PL and SL composition

Chromatographic separation of phospholipid (PL) and sphingolipid (SL) species was performed utilizing an UltiMate3000 UHPLC system (Thermo Fisher Scientific GmbH, Dreieich, Germany) consisting of the following modules. A DGP-3600RS dual gradient pump module, WPS-3000TRS autosampler, SRD-3600 degasser and TCC-3000SD column oven. RP separation was carried out with an XSelect Premier CSH C18 column (100 x 2.1 mm, 2.5 µm, 100 Å; Waters Corporation, Milford, MA, USA). With this, a binary gradient of A: H_2O/MeOH (95/5, *v*/*v*) and B: IPA/MeOH (85/15, *v*/*v*) with a total runtime of 28.5 min was applied as depicted in Table S2. A constant flow rate of 0.3 mL/min, column oven temperature of 40°C and injection volume of 3 µL were maintained.

Table 6. Binary gradient for RP separation of phospholipids with A: H_2O/MeOH (95/5, *v*/*v*) and B: IPA/MeOH (85/15, *v*/*v*).

time [min]	0.0	1.0	2.0	16.0	18.0	24.0	24.5	28.5
% B	60	60	72	80	100	100	60	60

S8. Mass spectrometric setup for determination of PL and SL composition

Mass spectrometric measurements for PL and SL determination including ion mobility spectrometry were carried out on a timsTOF fleX mass spectrometer (Bruker Daltonics GmbH, Bremen, Germany). Parameters for electrospray ionization (ESI) -trapped ion mobility spectrometry (TIMS) -tandem mass spectrometry (MS/MS) were adapted from Rudt *et al*. and tailored to the here required conditions.[369]

All measurements were performed in negative ionization mode with these following ESI source settings: end plate offset 500 V, capillary voltage 3500 V, nebulizer pressure 2.0 bar, dry gas flow rate 9.0 l/min, and dry gas temperature 220 °C.

For ion mobility spectrometry measurements via TIMS, a mobility range of 0.8 – 1.65 Vs/cm^2 in combination with a ramp time of 300 ms was applied. The utilized tunnel voltages were set as following: Δt1 20.0 V, Δt2 120.0 V, Δt3 -80.0 V, Δt4 -100.0 V, Δt5 0.0 V, Δt6 -100.0 V, collision cell in -220.0 V. Additionally the accumulation was locked to the mobility range and ion accumulation was limited to a target value of 7.5 million via ion charge control for reduction of overcharge effects.

A mass range of *m*/*z* 100 – 1350 combined with the following ion transfer parameters was applied: deflection 1 delta -80.0 V, funnel 1 RF 360.0 Vpp, isCID energy -0.0 eV, funnel 2 RF 250.0 Vpp, multipole RF 200.0 Vpp. Collision cell energy and RF were set to 10.0 eV and 1100.0 Vpp respectively. Quadrupole ion energy and low mass settings were 5.0 eV and *m*/*z* 150.0. Transfer time and pre pulse storage for pre TOF focus were set to 65.0 µs and 7.0 µs respectively.

For MS/MS experiments, data dependent acquisition (dda) with parallel accumulation serial fragmentation (PASEF) was utilized. Fragmentation via

dda-PASEF was applied with a collision energy of 40 eV for ions between a charge range of 0 – 1 and a *m*/*z* range of 300 – 1350. Quadrupole ion selection was based on an isolation width of *m*/*z* 1.75 with an intensity threshold of 100 and a target intensity of 4000. Selected ions were actively excluded and released from selection after 0.1 min. For each cycle two PASEF ramps were applied.

Initial mass calibration was performed according to sodium formate clusters utilizing a 5 mM solution of sodium formate in IPA/H_2O (1/1, *v*/*v*). For initial ion mobility calibration, a tuning mix (ESI-L Low Concentration Tuning Mix; Agilent Technologies Inc., Santa Clara, CA, USA) was used with calibration points depicted in Table S3. Additionally, an online calibration has been applied after each measurement utilizing a mixed mass and mobility calibrant solution (1/1, *v*/*v*). Therefore a 20 µL sample loop was connected to the six-port valve of the timsTOF fleX instrument and continuously filled with calibrant solution via the integrated syringe pump and a flow rate of 1 µL/min. Valve switching at minute 26.5 of the LC run introduced the calibrant into the timsTOF fleX instrument via LC flow.

Table 7. Calibration for mass spectrometric measurements utilizing a 5 mM sodium formate solution (left) and mobility calibration with ESI-L Low Concentration Tuning Mix (right).

Calibration point	Mass Calibration	Mobility Calibration	
	m/z	*m/z*	Mobility [V/cm^2]
1	112.9856	601.9790	0.8824
2	180.9731	1033.9881	1.2582
3	248.9605	1333.9689	1.4073
4	316.9479		
5	384.9353		
6	452.9227		
7	520.9102		
8	588.8976		
9	656.885		
10	724.8724		
11	792.8599		
12	860.8473		
13	928.8347		
14	996.8221		
15	1064.8096		
16	1132.797		
17	1200.7844		
18	1268.7718		
19	1336.7593		

S9. Data Processing and Lipid Identification for determination of CL composition

Chromatographic data processing and identification of CLs were performed using the open-source software MZmine 4 (version 4.2.0; mzio GmbH, Bremen, Germany).[271] The annotation of CL species was based on accurate mass and matching MS/MS spectra. A batch processing method was created for negative ionization mode with noise levels set at 5000 for MS1 and 250 for MS2,

respectively. For the ADAP chromatogram builder a mass tolerance of 15 ppm was set.

S10. Data Processing and Lipid Identification for determination of PL and SL composition

The data processing, annotation and identification workflow was performed utilizing Metaboscape 2023b software (Bruker Daltonics GmbH, Bremen, Germany). For data processing the following parameters were applied. Features were extracted between a retention time of 0.5 – 24.5 min and a *m*/*z* of 100 – 1350. Furthermore, a minimum 4D peak size of 50 data points, recursive feature extraction of 25 data points and intensity threshold of 200 counts was required. Primary ions were selected as $[M-H]^-$ while seed ions were $[M+CH_3COO]^-$, $[M+Cl]^-$, $[M-2H]^{2-}$ and common ions were $[M-H-H_2O]^-$ all with a 0.8 EIC correlation. For annotation of extracted features, the integrated rule-based lipid annotation as well as external MSDIAL-TandemMassSpectralAtlas-VS68-Neg library were applied.[370,371] Respective narrow and wide tolerances were set as CCS 2% and 5%, *m*/*z* 2.0 ppm and 5.0 ppm, MS/MS score 800 and 500, 85 mSigma (isotopic pattern matching). Annotated features were revised manually utilizing lipid-class specific 4D-Kendrick mass plots (KMD (CH_2), *m*/*z*, t_R, CCS) and considering deviation values calculated by Metaboscape software.[372]

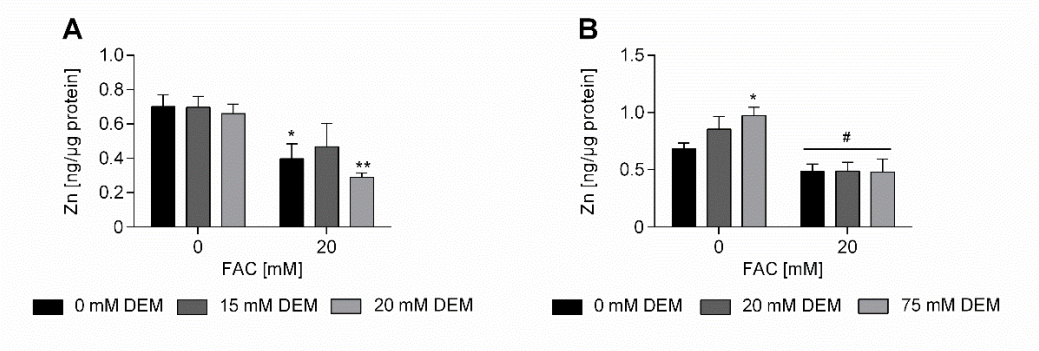

Figure 42. Zn levels after treatment with FAC and 2 h (A) or 24 h (B) DEM. Shown are mean + SEM of ≥ 3 independent experiments. Significance is depicted as * compared to untreated control and # to DEM treatment only.

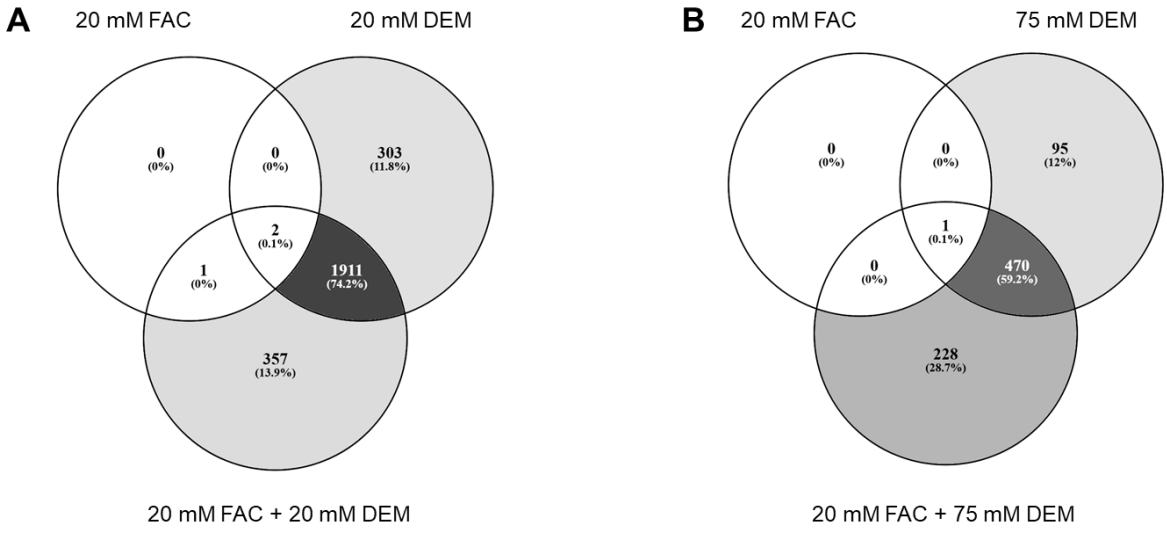

Figure 43. Number of up- and down-regulated DEGs after treatment with FAC and 2 h (A) and 24 h (B) DEM. Visualized using Venny. [373]

Table 8. List of GO terms with corresponding GO numbers.

GO name	GO number
ABC-type transporter activity	GO:0140359
acyl-CoA hydrolase activity	GO:0016289
alcohol dehydrogenase (NAD+) activity	GO:0004022
alcohol dehydrogenase [NADP)+] activity	GO:0018455
alcohol dehydrogenase [NADP+] activity	GO:0018455
binding	GO:0005488
catalytic activity	GO:0003824
cation binding	GO:0043169
DNA-binding transcription factor activity	GO:0003700
fatty acid elongase activity	GO:0009922
flavin adenine dinucleotide binding	GO:0050660
FMN binding	GO:0010181
G protein-coupled receptor activity	GO:0004930
galactoside binding	GO:0016936
glucuronosyltransferase activity	GO:0015020
glutathione disulfide oxidoreductase activity	GO:0015038
glutathione transferase activity	GO:0004364
glycosyltransferase activity	GO:0016757
heme binding	GO:0020037
hexose transmembrane transporter activity	GO:0015149
hexosyltransferase activity	GO:0016758
hypotaurine monooxygenase activity	GO:0047822
ion binding	GO:0043167
iron ion binding	GO:0005506

Continuation of Table 8.

GO name	GO number
lysozyme activity	GO:0003796
metal ion binding	GO:0046872
molecular function	GO:0003674
molecular transducer activity	GO:0060089
monooxygenase activity	GO:0004497
mRNA 5'-diphosphatase activity	GO:0034353
N,N-dimethylaniline monooxygenase activity	GO:0004499
NAD(P)H oxidase H2O2-forming activity	GO:0016174
oxidoreductasae activity	GO:0016491
oxidoreductasae activity, acting on CH-OH group of donors	GO:0016614
oxidoreductase activity, acting on NAD(P)H, oxygen as acceptor	GO:0050664
oxidoreductase activty, acting on paired donors, with incorporation or reduction of molecular oxygen, reduced flavin or flavoprotein as one donor, and incorporation of one atom of oxygen	GO:0016712
oxidoreductase activity, acting on the CH-OH group of donors, NAD or NADP as acceptor	GO:0016616
sequence-specific DNA binding	GO:0043565
signaling receptor activity	GO:0038023
small molecule binding	GO:0036094
sodium ion transmembrane transporter activity	GO:0015081
structural constituent of chromatin	GO:0030527
tetrapyrrole binding	GO:0046906
transcription regulator activity	GO:0140110
transferase activity	GO:0016740
transferase activity, transferring alkyl or aryl (other than methyl) groups	GO:0016765
transition metal ion binding	GO:0046914
transmembrane transporter activity	GO:0022857
transporter activity	GO:0005215
UDP-glycosyltransferase activity	GO:0008194
zinc ion binding	GO:0008270

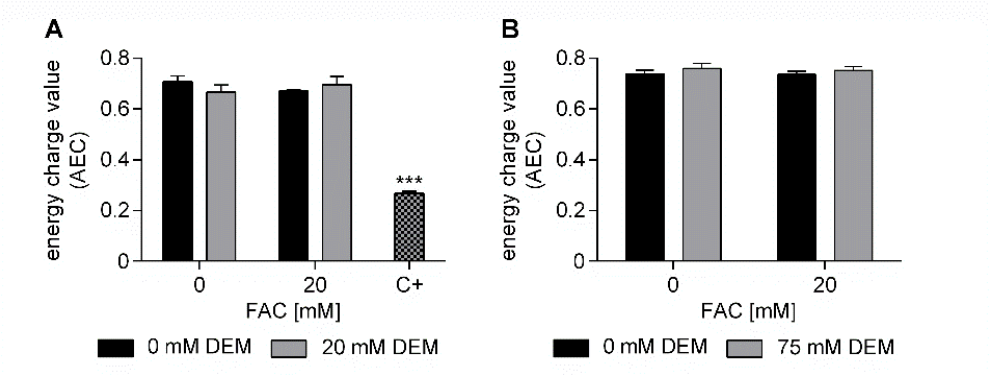

Figure 44. Cellular energy charge value after treatment with FAC and 2h (A) or 24 h (B) DEM. Shown are mean + SEM of ≥ 3 independent experiments. Significance is depicted as * compared to untreated control. C+: 1 h treatment with 100 µM sodium azide as positive control.

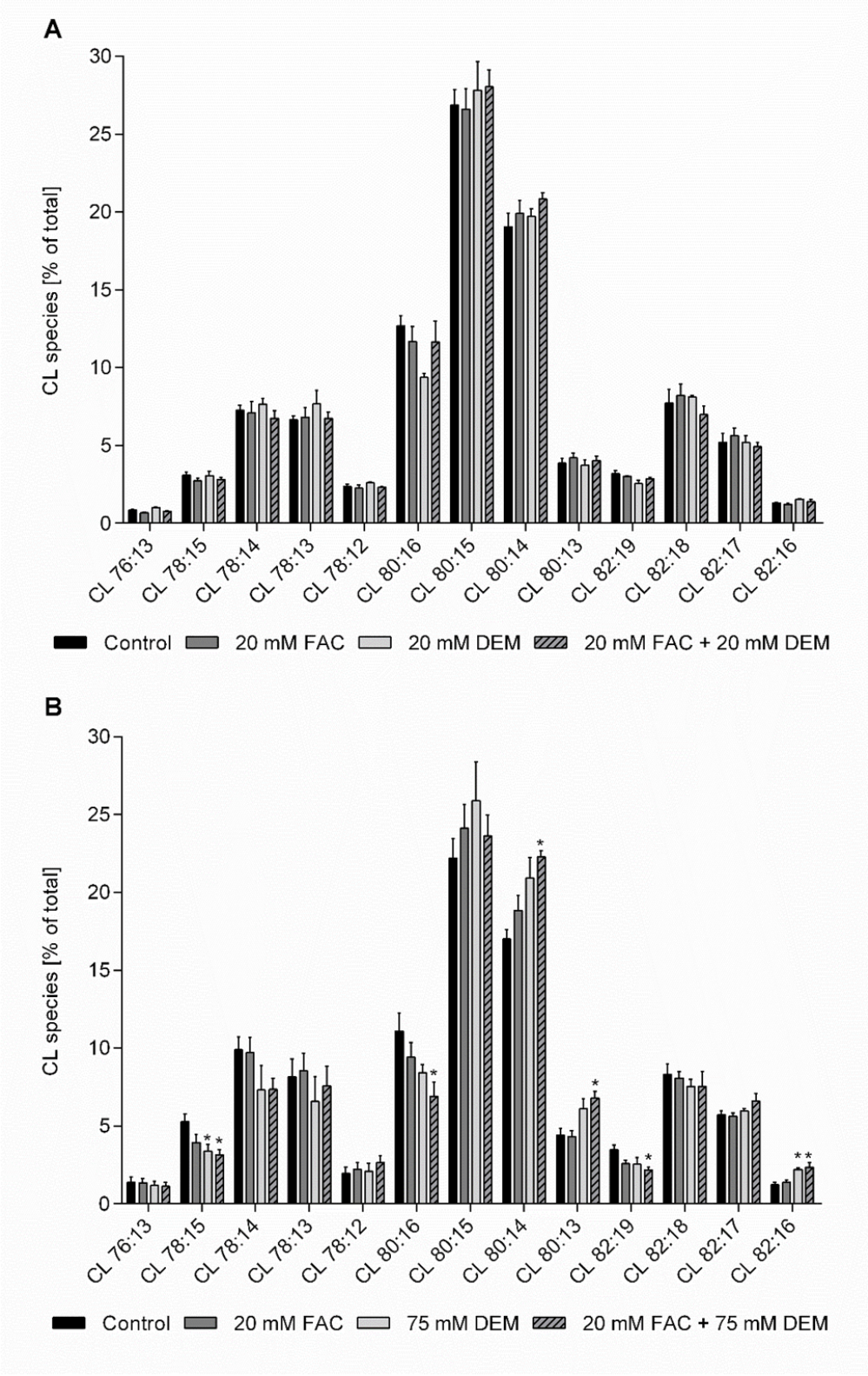

Figure 45. Distribution of CL species after treatment with FAC and 2 h (A) or 24 h (B) DEM. Shown are mean + SEM of ≥ 3 (2h DEM n = 2) independent experiments. Significance is depicted as * compared to untreated control.

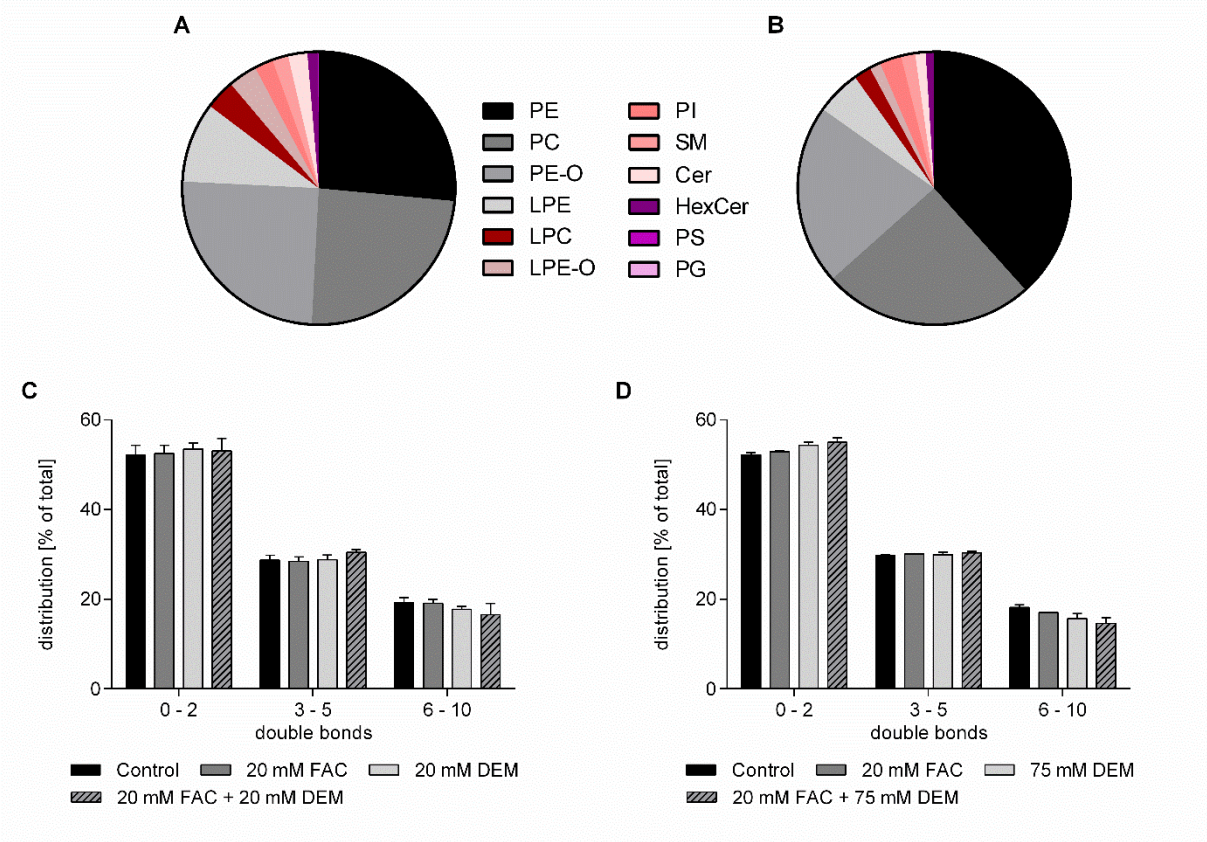

Figure 46. Distribution of phospho- and sphingolipids determined from peak areas in d1 adult (A) and d2 adult (B) untreated controls. Distribution of phospho- and sphingolipids based on the degree of saturation after treatment with FAC and 2 h (C) or 24 h (D) DEM. Shown are mean + SEM of ≥ 3 independent experiments.

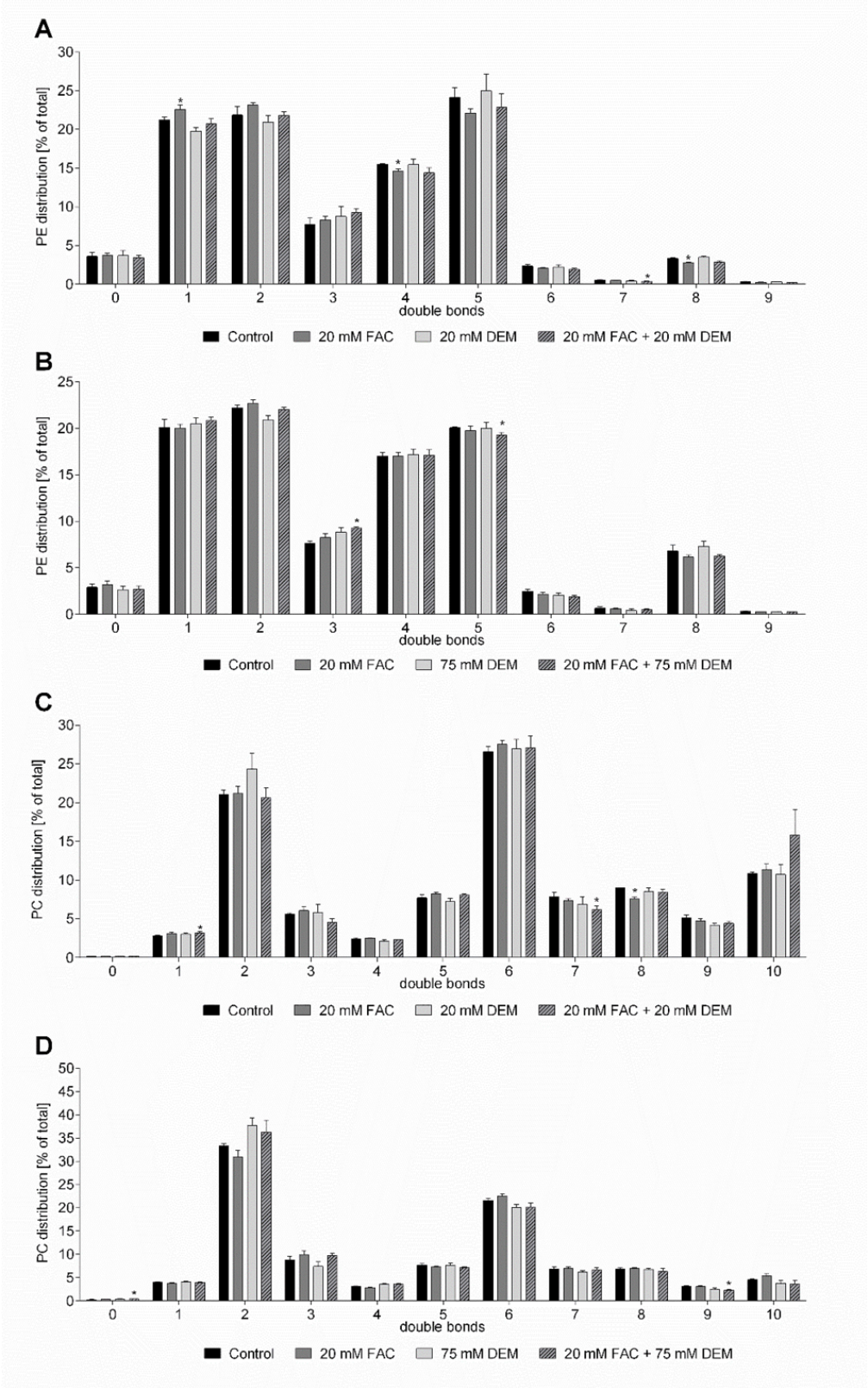

Figure 47. Distribution of PE (A, B) and PC (C, D) based on the degree of saturation after treatment with FAC and 2 h (A, C) or 24 h (B, D) DEM. Shown are mean + SEM of ≥ 3 independent experiments. Significance is depicted as * compared to untreated control.

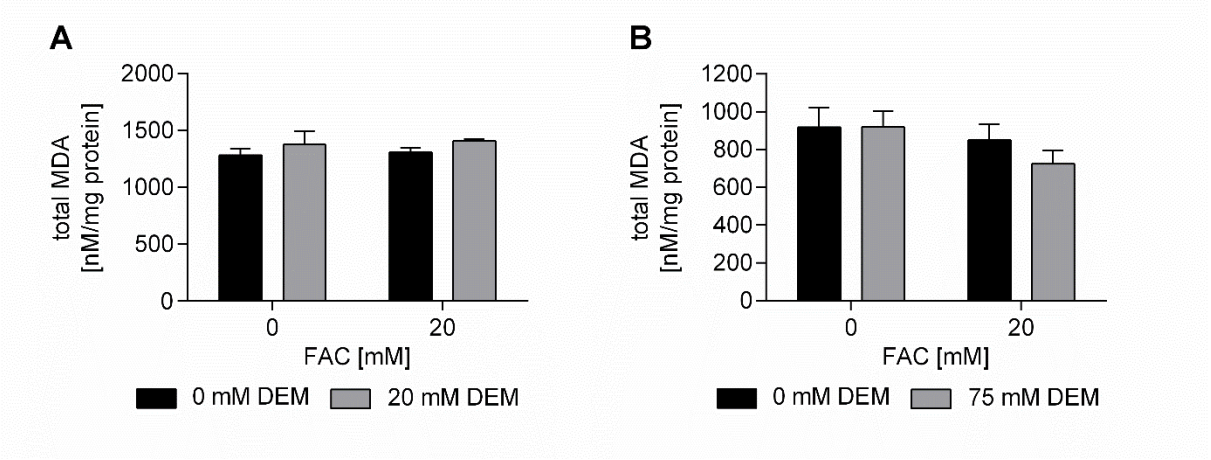

Figure 48. Total MDA content after treatment with FAC and 2 h (A) or 24 h (B) DEM. Shown are mean + SEM of ≥ 3 independent experiments.

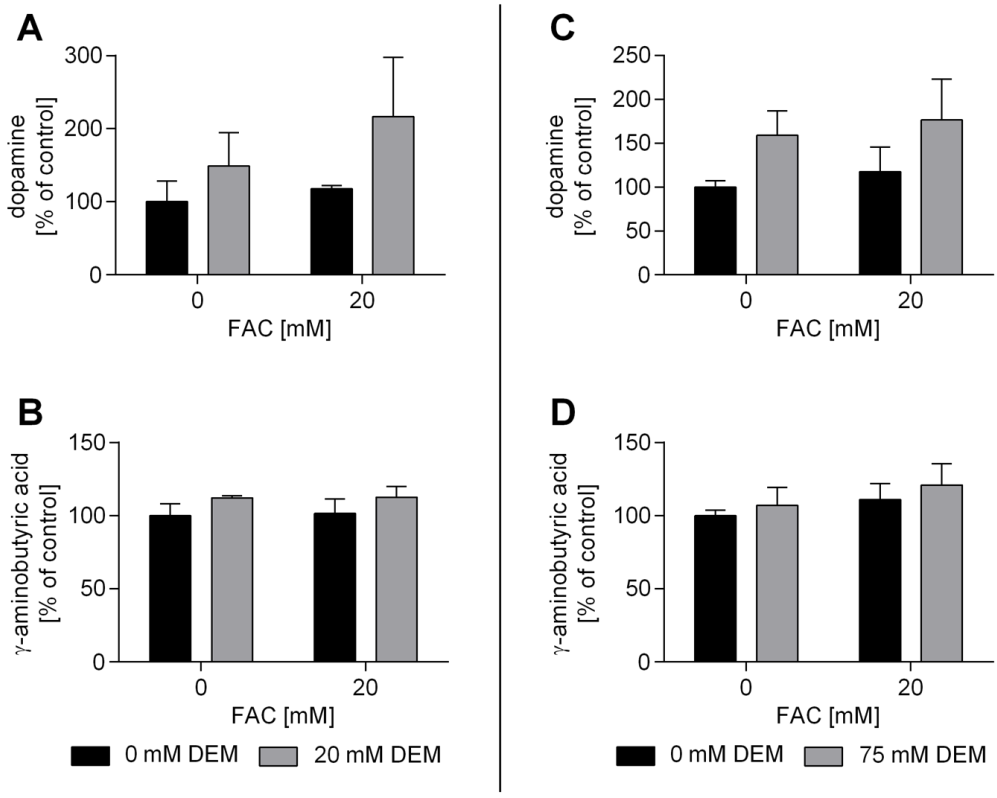

Figure 49. Dopamine (A, C) and γ-aminobutyric acid (B, D) content normalized to protein amount and untreated control after treatment with FAC and 2 h (A, B) or 24 h (C, D) DEM. Shown are mean + SEM of ≥ 3 independent experiments.

Supplementary for Chapter 5: Dysfunctional Copper Homeostasis in *Caenorhabditis elegans* affects genomic and neuronal stability

S11. MDA: Settings for LC-FLD analysis and method validation parameters

LC-FLD parameters for MDA quantification

Analysis was performed by LC-FLD using an Agilent 1260 Infinity II liquid chromatography system. The chromatographic separation was performed using a Chromolith Performance RP-18 100 x 4.6 mm column at 40 °C. 5 mM KH_2PO_4 (pH 7) and MeOH were used as eluents. At a flow rate of 0.7 mL/min, the total run time was 9 min. The measurement started with 0 – 100% of MeOH in 1 min, 100% MeOH for 5 min, 100 – 0% in 2 min and 1 min equilibration at 0% MeOH. Detection was performed by a FLD at extinction of 515 nm and emission of 553 nm.

Method validation parameters

The method for determination of MDA using LC-FLD was validated according to the “ICH guideline Q2(R2) on a validation of analytical procedures” of the European Medicines Agency. All samples and standards were derivatized with 2-Thiobarbituric acid (TBA) before the measurements. The linearity, limit of detection (LOD) and limit of quantification (LOQ) were determined by adding a defined amount of homogenized worm (wild type) matrix to TMP standards before derivatization with TBA. The concentration range of the standards was between 0 – 500 nM TMP. The LOD and LOQ were determined using following formulas: LOD = 3 x SD_y/b and LOQ = 10 x SD_y/b (SD_y = standard deviation of analyte concentration in 4 blank measurements, b = slope of calibration curve). To determine the accuracy, 20 nM, 200 nM and 500 nM TMP were analyzed five times each. The ratio of the measured concentration to the expected concentration was calculated to determine the accuracy. The recovery was determined by analyzing four samples with a defined amount of worm matrix,

four samples with a defined TMP concentration and four samples containing both. To calculate the recovery, the ratio of the measured standard with matrix and the quantity of the standard without matrix was determined. To determine the intraday precision, five samples were pelletized on one day and for interday determination, five samples were pelletized on five different days. The unbound and bound MDA concentrations of these samples were normalized to protein content and the precision is stated as the relative standard deviation of the samples in percent (RSD%).

Table 9. Overview of linearity, LOD, LOQ, accuracy and recovery of the MDA method validation.

Correlation coefficient [R^2]	0.9995		
LOD [nM]	9		
LOQ [nM]	30		
Accuracy [%]	20 nM TMP 134 ± 13	200 nM TMP 98 ± 10	500 nM TMP 100 ± 6
Recovery [%]	98 ± 8		

Table 10. Overview of intraday and interday of unbound and bound MDA.

	unbound MDA	bound MDA
intraday	16 %	10 %
interday	19 %	29 %

S12. Experimental procedure for cardiolipin analysis

Chemicals and materials

Methanol (MeOH), acetonitrile (ACN), 2-propanol (LC/MS grade), formic acid (99-100% p.a.) and acetic acid (≥99.99%) were obtained from VWR International GmbH (Darmstadt, Germany). Methyl-*tert*-butylether (MtBE)

(LC grade) was purchased from Merck KGaA (Darmstadt, Germany). Ammonium formate (≥99.995%) was purchased from Sigma Aldrich (Steinheim, Germany). Ammonium acetate (≥99.99%) was delivered by Honeywell (Seelze, Germany). 18:2 Cardiolipin-d5 (> 99%) (d5-CL 72:8) was obtained from Avanti Polar Lipids (Birmingham, AL, USA). Water was purified by a Milli-Q EQ 7000-System (18.2 MΩcm; 0.2 µm filter; Millipore, Molsheim, France). All chemicals were used as received.

Lipid extraction

Lipid extraction of *C. elegans* samples was carried out according to a modified protocol of Matyash et al. [270] including an additional extraction cycle previously described by Helmer et al [243]. *C. elegans* nematodes in the fourth larvae stadium (L4) were extracted in pellets of 4500 worms. For resuspension of the pellet, 100 µL of water was added. Additionally, 20 µL of 65 mM BHT as an antioxidant was added before three freeze-thaw cycles in liquid nitrogen were performed. This step was followed by sonication (UP200St, Hielscher Ultrasonics GmbH, Germany) of the sample after adding 1.5 mL MeOH and 20 µL 5 µM d5-CL 72:8 as internal standard (IS). Lipid extraction was induced by adding 5 mL MtBE to the sample in 12 mL glass vials with Teflon caps. The sample was shaken for 1 h at 600 rpm at room temperature. For phase separation, 1.25 mL water was added to the extraction mixture followed by an additional 10 min incubation at room temperature. After centrifugation of the sample for 10 min at 2500 rpm (Centrifuge 5804, Eppendorf SE, Germany), the upper organic phase was collected. A second extraction cycle was then applied to the aqueous phase by adding 2 mL MtBE/MeOH/water (10:3:2.5; v/v/v). Pooled organic supernatants were dried utilizing a gentle nitrogen flow. The residue was resuspended in 200 µL of 2-propanol, resulting in a concentration of 0.5 µM IS and 6.5 mM BHT. Lipid extracts were then directly used for analysis.

Cardiolipin analysis via 2D-LC-HRMS

2D-LC-HRMS analysis was carried out utilizing a Thermo Scientific Vanquish Flex Duo UHPLC-system (Thermo Fisher Scientific, Dreieich, Germany) hyphenated to a Q Exactive Plus mass spectrometer (Thermo Fisher Scientific, Bremen, Germany). The instrument setup was controlled via the XCalibur 4.1 software using the SII plug-in. The instrument and heart-cut setup was applied as previously described by Blume et al. [331] and Helmer et al. [243,374]. In first dimension (^{1}D) HILIC separation of phospholipid classes was performed utilizing an iHILIC Fusion(+) column (20 x 2.1 mm, 5 µm, 100 Å) (HILICON AB, Umeå, Sweden). Gradient elution was performed using an aqueous ammonium formate buffer (35 mM, pH 3.5, 5% ACN) (A) and ACN (B) as organic solvent [374]. Equilibration of the stationary phase at 60% B for 20 min took place beforehand to ensure reproducible retention times. In second dimension (^{2}D) RP separation was optimized for efficient separation of CL species on an Xselect Premier CSH C18 column (100 x 2.1 mm, 2,5 µm) (Waters Corporation, France). For gradient elution, aqueous ammonium acetate buffer (10 mM, 0.01% acetic acid, 5% MeOH) (A) and MeOH/2-isopropanol (60:40 (*v*/*v*), 10 mM ammonium acetate, 0.01% acetic acid). The gradient started at 80% B with an equilibration step during the HILIC separation in first dimension [243]. Table 9 gives a detailed gradient overview of ^{1}D HILIC and ^{2}D RP separation. For the heart-cut approach, a transfer window from 5.8 min to 6.4 min was applied. A six-port valve integrated into the column compartment was equipped with a 400 µL stainless-steel sample loop for the heart-cut setup as described earlier [243,331]. Analyte transfer onto the RP column in ^{2}D was carried out by back-flushing the sample loop. Gradient elution as described in Table 9 started simultaneously. The total run time including both separation dimensions was 28 min with a sample injection volume set to 5 µL.

Table 11. Gradient overview containing both gradients for the HILIC separation in the first and the RP separation in the second dimension and the switching positions of the six-port-valve for the heart-cut setup.

^{1}D HILIC gradient			**^{2}D RP gradient**			**Valve set-up**	
time /min	**flow /mLmin^{-1}**	**%B**	**time /min**	**flow /mLmin^{-1}**	**%B**	**time /min**	**position**
0.00	0.3	97	0.00	0.3	80	0.00	2_1
0.2	0.3	97	7.70	0.3	80	5.80	1_6
0.5	0.3	93	8.70	0.3	92	6.40	2_1
2.75	0.3	93	22.70	0.3	98	7.70	1_6
7.50	0.3	60	23.10	0.3	100	25.00	2_1
11.00	0.3	60	26.90	0.3	100		
11.50	0.3	97	27.40	0.3	80		
14.00	0.3	97	28.00	0.3	80		
14.10	0.05	97					
24.50	0.05	97					
28.00	0.3	97					

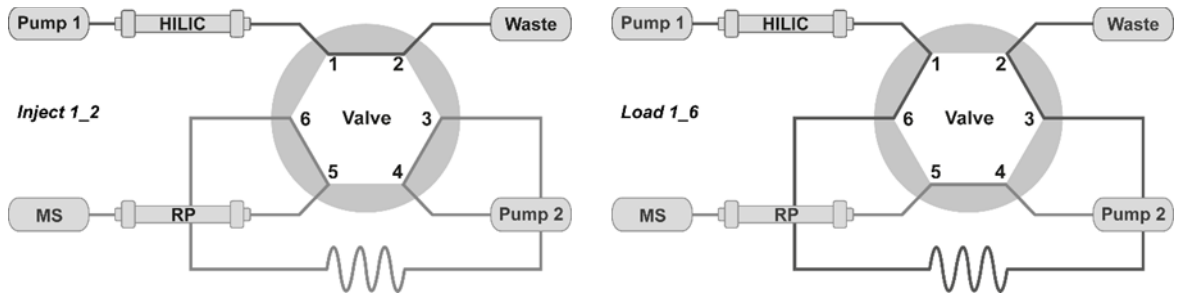

Figure 50. Six-port-valve positions for the heart-cut setup.

Negative electrospray ionization (ESI) was performed by a HESI-II probe (Thermo Fisher Scientific, Bremen, Germany) prior mass spectrometric detection. Probe parameters were set to the following values: source voltage -3.5 kV, probe heater 300 °C, sheath gas flow rate 45 arbitrary units, auxiliary

gas flow rate 10 arbitrary units, spare gas flow rate 1 arbitrary unit, capillary temperature 325 °C. The s-lens rf level was set to 85. Data-dependent MS/MS experiments for structural elucidation were performed at a normalized collision energy of 24 eV (based on a *m*/*z* of 500) by HCD with a resolution of 17,500 (at *m*/*z* 200). Full scan resolution was set to 140,000. An isolation window of 1.5 Da for precursors was set to avoid isotopic interferences. The maximum C-trap injection time was set to 100 ms in full scan mode and 50 ms for MS/MS experiments.

Data processing

For data processing of the HRMS data, the open source software MZmine 3 [271] (version 3.4.21) was utilized. CL annotation was performed by the lipid search module based on accurate mass and matching MS^2 spectra. A batch processing method was created using the processing wizard. The UHPLC-Orbitrap-DDA setup was chosen. Polarity was set to negative with a noise level of 5000 for MS^1 and 1000 for MS^2 level. A mass tolerance of 10 ppm was set for the ADAP chromatogram builder [375]. Subsequently, the created feature lists were aligned and gap filled.

For the analysis of the CL distribution, all peak areas of identified CL species were normalized to the peak area of the IS (0.5 µM d5-CL 72:8) in addition to the protein content. Subsequently, all normalized peak areas of identified CL species were summed up and the relative abundance of all CL species in comparison to the overall CL amount was calculated. An absolute quantification was not carried out. Due to the normalization of the data set, comparable results in wild-type and mutant samples could be observed.

Lipid nomenclature

Lipids were named according to the shorthand notation proposed by Liebisch et al. [234] The total number of carbon atoms in the fatty acyl residues is given together with the number of double bonds i.e. CL 72:8.

Supplementary Figures

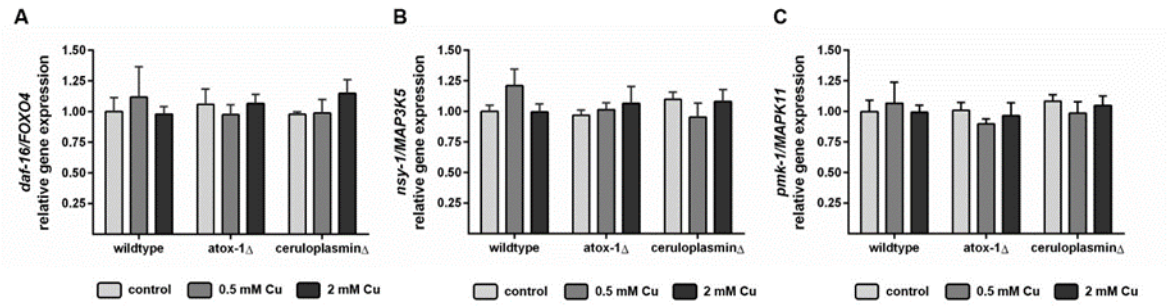

Figure 51. Relative mRNA levels of (A) daf-16/FOXO4, (B) nsy-1/MAP3K5 and (C) pmk-1/MAPK11 following 24 h Cu incubation. Data presented are mean values of n = 4 independent experiments + SEM.

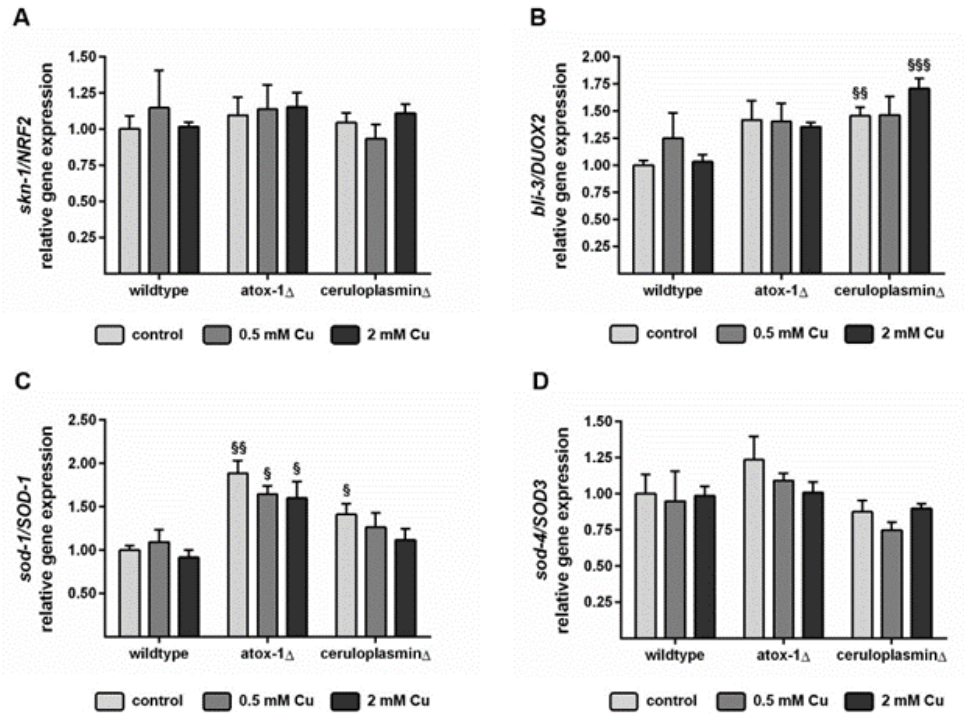

Figure 52. Relative mRNA levels of (A) skn-1/NRF2, (B) bli-3/DUOX2, (C) sod-1/SOD-1 and (D) sod-4/SOD-3 following 24 h Cu incubation. Data presented are mean values of n = 4 independent experiments + SEM.

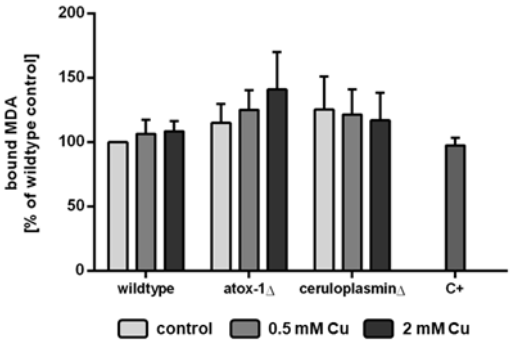

Figure 53. MDA levels (bound) normalized to wildtype control [%]. PQ was used as positive control (C+) in wildtype worms. Data presented are mean values of n = 4 independent experiments + SEM.

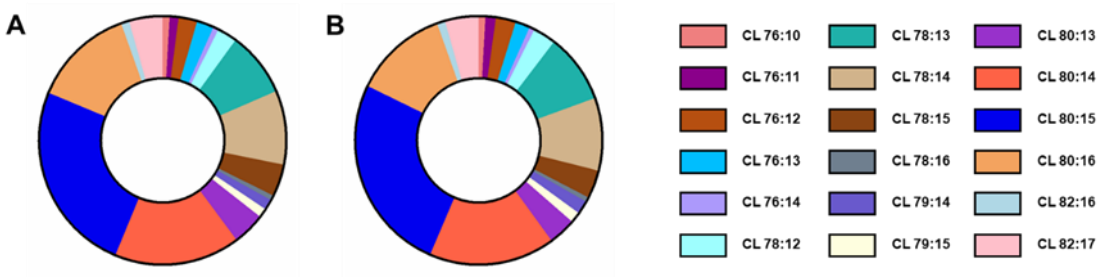

Figure 54. Representative distribution of CL species in terms of chain length and degree of saturation for untreated (A) atox-1 and (B) ceruloplasmin deletion mutants.

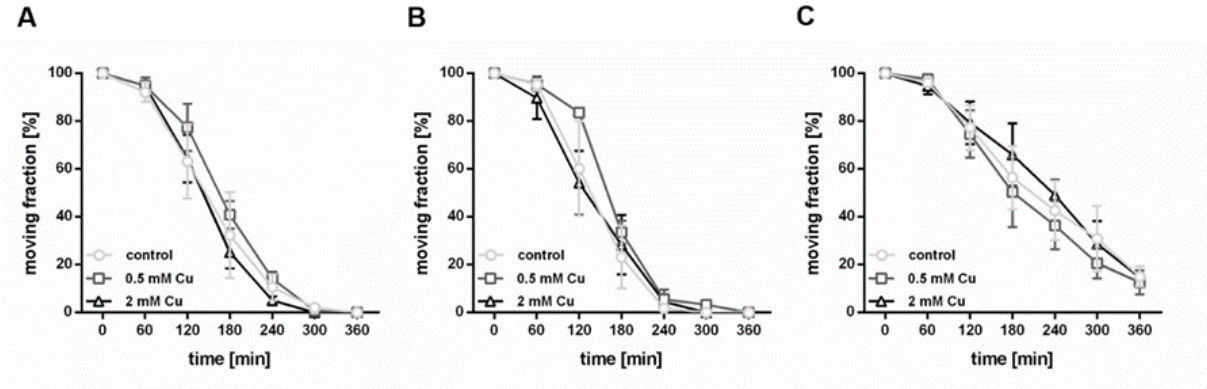

Figure 55. Aldicarb-induced paralysis assay in (A) wildtype, (B) atox-1Δ and (C) ceruloplasminΔ worms treated with 0 mM (light grey), 0.5 mM (dark grey) or 2 mM (black) $CuSO_4$ for 24 h. Plotted are the fraction of moving worms [%] against the assay procedure time [min]. Data presented are mean values of n = 3 independent and blinded experiments ± SEM.

References

(1) Fenton, H. J. H. Oxidation of tartaric acid in the presence of iron. *J. Chem. Soc* **1894**, 899–910.

(2) EFSA Panel on Nutrition, Novel Foods and Food Allergens; Turck, D.; Bohn, T.; Castenmiller, J.; Henauw, S. de; Hirsch-Ernst, K.-I.; Knutsen, H. K.; Maciuk, A.; Mangelsdorf, I.; McArdle, H. J.; Pentieva, K.; Siani, A.; Thies, F.; Tsabouri, S.; Vinceti, M.; Aggett, P.; Fairweather-Tait, S.; Sesmaisons Lecarré, A. de; Fabiani, L.; Karavasiloglou, N.; Saad, R. M.; Sofroniou, A.; Titz, A.; Naska, A. Scientific opinion on the tolerable upper intake level for iron. *EFSA Journal* **2024**, *22*.

(3) Stockwell, B. R. Ferroptosis turns 10: Emerging mechanisms, physiological functions, and therapeutic applications. *Cell* **2022**, *185*, 2401–2421.

(4) Hider, R. C.; Kong, X. L. Glutathione: a key component of the cytoplasmic labile iron pool. *Biometals an international journal on the role of metal ions in biology, biochemistry, and medicine* **2011**, *24*, 1179–1187.

(5) Frey, P. A.; Reed, G. H. The Ubiquity of Iron. *ACS Chemical Biology* **2012**, *7*, 1477–1481.

(6) Al-Fartusie, F. S.; Mohssan, S. N. Essential trace elements and their vital roles in human body. *Indian J Adv Chem Sci* **2017**, *5*, 127–136.

(7) Beard, J. L. Iron Biology in Immune Function, Muscle Metabolism and Neuronal Functioning. *The Journal of Nutrition* **2001**, *131*, 568–580.

(8) Puig, S.; Ramos-Alonso, L.; Romero, A. M.; Martínez-Pastor, M. T. The elemental role of iron in DNA synthesis and repair. *Metallomics.* **2017**, *9*, 1483–1500.

(9) Sánchez, M.; Sabio, L.; Gálvez, N.; Capdevila, M.; Dominguez-Vera, J. M. Iron chemistry at the service of life. *IUBMB Life* **2017**, *69*, 382–388.

(10) German Research Centre for Food Chemistry, Ed. *Food Composition and Nutrition Tables,* 2015.

(11) German Nutrition Society (DGE). Reference values for iron **2023** https://www.dge.de/wissenschaft/referenzwerte/eisen/ (accessed Jun 02, 2025).

(12) Piskin, E.; Cianciosi, D.; Gulec, S.; Tomas, M.; Capanoglu, E. Iron Absorption: Factors, Limitations, and Improvement Methods. *ACS Omega* **2022**, *7*, 20441–20456.

(13) Roughead, Z. K.; Zito, C. A.; Hunt, J. R. Initial uptake and absorption of nonheme iron and absorption of heme iron in humans are unaffected by the addition of calcium as cheese to a meal with high iron bioavailability123. *The American Journal of Clinical Nutrition* **2002**, *76*, 419–425.

(14) Gibson, R. S.; Raboy, V.; King, J. C. Implications of phytate in plant-based foods for iron and zinc bioavailability, setting dietary requirements, and formulating programs and policies. *Nutrition reviews* **2018**, *76*, 793–804.

(15) Man, Y.; Xu, T.; Adhikari, B.; Zhou, C.; Wang, Y.; Wang, B. Iron supplementation and iron-fortified foods: a review. *Critical Reviews in Food Science and Nutrition* **2022**, *62*, 4504–4525.

(16) Siquier-Coll, J.; Bartolomé, I.; Perez-Quintero, M.; Grijota, F. J.; Muñoz, D.; Maynar-Mariño, M. Effects of exposure to high temperatures on serum, urine and sweat concentrations of iron and copper. *Journal of Thermal Biology* **2020**, *89*, 102536.

(17) Green, R.; Charlton, R.; Seftel, H.; Bothwell, T.; Mayet, F.; Adams, B.; Finch, C.; Layrisse, M. Body iron excretion in man: A collaborative study. *The American Journal of Medicine* **1968**, *45*, 336–353.

(18) Ngo, P. A.; Neurath, M. F.; López-Posadas, R. Impact of Epithelial Cell Shedding on Intestinal Homeostasis. *International Journal of Molecular Sciences* **2022**, *23*.

(19) Fuqua, B. K.; Vulpe, C. D.; Anderson, G. J. Intestinal iron absorption. *Journal of trace elements in medicine and biology organ of the Society for Minerals and Trace Elements (GMS)* **2012**, *26*, 115–119.

(20) Dutt, S.; Hamza, I.; Bartnikas, T. B. Molecular Mechanisms of Iron and Heme Metabolism. *Annual Review of Nutrition* **2022**, *42*, 311–335.

(21) Jian, N.; Dowle, M.; Horniblow, R. D.; Tselepis, C.; Palmer, R. E. Morphology of the ferritin iron core by aberration corrected scanning transmission electron microscopy. *Nanotechnology* **2016**, *27*, 46LT02.

(22) van Eden, M. E.; Aust, S. D. Intact Human Ceruloplasmin Is Required for the Incorporation of Iron into Human Ferritin. *Archives of biochemistry and biophysics* **2000**, *381*, 119–126.

(23) Liu, M.-Z.; Kong, N.; Zhang, G.-Y.; Xu, Q.; Xu, Y.; Ke, P.; Liu, C. The critical role of ferritinophagy in human disease. *Frontiers in pharmacology* **2022**, *Volume 13 - 2022*.

(24) Philpott, C. C.; Protchenko, O.; Wang, Y.; Novoa-Aponte, L.; Leon-Torres, A.; Grounds, S.; Tietgens, A. J. Iron-tracking strategies: Chaperones capture iron in the cytosolic labile iron pool. *Frontiers in molecular biosciences* **2023**, *10*.

(25) Paradkar, P. N.; Zumbrennen, K. B.; Paw, B. H.; Ward, D. M.; and Kaplan, J. Regulation of Mitochondrial Iron Import through Differential Turnover of Mitoferrin 1 and Mitoferrin 2. *Molecular and Cellular Biology* **2009**, *29*, 1007–1016.

(26) Galy, B.; Conrad, M.; Muckenthaler, M. Mechanisms controlling cellular and systemic iron homeostasis. *Nature Reviews Molecular Cell Biology* **2024**, *25*, 133–155.

(27) Levi, S.; Ripamonti, M.; Dardi, M.; Cozzi, A.; Santambrogio, P. Mitochondrial Ferritin: Its Role in Physiological and Pathological Conditions. *Cells* **2021**, *10*.

(28) Musci, G.; Polticelli, F.; Bonaccorsi di Patti, Maria Carmela. Ceruloplasmin-ferroportin system of iron traffic in vertebrates. *World journal of biological chemistry* **2014**, *5*, 204–215.

(29) Petrak, J.; Vyoral, D. Hephaestin—a ferroxidase of cellular iron export. *The International Journal of Biochemistry & Cell Biology* **2005**, *37*, 1173–1178.

(30) Fisher, J.; Devraj, K.; Ingram, J.; Slagle-Webb, B.; Madhankumar, A. B.; Liu, X.; Klinger, M.; Simpson, I. A.; Connor, J. R. Ferritin: a novel mechanism for delivery of iron to the brain and other organs. *American Journal of Physiology-Cell Physiology* **2007**, *293*, C641-C649.

(31) Frazer, D. M.; Anderson, G. J. The regulation of iron transport. *BioFactors* **2014**, *40*, 206–214.

(32) Brissot, P.; Ropert, M.; Le Lan, C.; Loréal, O. Non-transferrin bound iron: A key role in iron overload and iron toxicity. *Biochimica et Biophysica Acta (BBA) - General Subjects* **2012**, *1820*, 403–410.

(33) Wang, C.-Y.; Jenkitkasemwong, S.; Duarte, S.; Sparkman, B. K.; Shawki, A.; Mackenzie, B.; Knutson, M. D. ZIP8 Is an Iron and Zinc Transporter Whose Cell-surface Expression Is Up-regulated by Cellular Iron Loading *. *Journal of Biological Chemistry* **2012**, *287*, 34032–34043.

(34) Nam, H.; Wang, C.-Y.; Zhang, L.; Zhang, W.; Hojyo, S.; Fukada, T.; Knutson, M. D. ZIP14 and DMT1 in the liver, pancreas, and heart are differentially regulated by iron deficiency and overload: implications for tissue iron uptake in iron-related disorders. *Haematologica* **2013**, *98*, 1049–1057.

(35) Muckenthaler, M. U.; Galy, B.; Hentze, M. W. Systemic Iron Homeostasis and the Iron-Responsive Element/Iron-Regulatory Protein (IRE/IRP) Regulatory Network. *Annual Review of Nutrition* **2008**, *28*, 197–213.

(36) Nemeth, E.; Ganz, T. Hepcidin and Iron in Health and Disease. *Annual Review of Medicine* **2023**, *74*, 261–277.

(37) Ganz, T. Hepcidin and Its Role in Regulating Systemic Iron Metabolism. *Hematology Am Soc Hematol Educ Program* **2006**, *2006*, 29–35.

(38) Peyssonnaux, C.; Nizet, V.; and Johnson, R. S. Role of the hypoxia inducible factors HIF in iron metabolism. *Cell Cycle* **2008**, *7*, 28–32.

(39) Mastrogiannaki, M.; Matak, P.; Peyssonnaux, C. The gut in iron homeostasis: role of HIF-2 under normal and pathological conditions. *Blood* **2013**, *122*, 885–892.

(40) Paoli, M.; Marles-Wright, J.; Smith, A. Structure–Function Relationships in Heme-Proteins. *DNA and Cell Biology* **2002**, *21*, 271–280.

(41) Mairbäurl, H.; Weber, R. E. Oxygen Transport by Hemoglobin. *Comprehensive Physiology* **2012**, *2*, 1463–1489.

(42) Wittenberg, J. B.; Wittenberg, B. A. Myoglobin function reassessed. *J Exp Biol* **2003**, *206*, 2011–2020.

(43) Yoshikawa, S.; Shimada, A. Reaction Mechanism of Cytochrome c Oxidase. *Chemical Reviews* **2015**, *115*, 1936–1989.

(44) Read, A. D.; Bentley, R. E.; Archer, S. L.; Dunham-Snary, K. J. Mitochondrial iron-sulfur clusters: Structure, function, and an emerging role in vascular biology. *Redox biology* **2021**, *47*, 102164.

(45) Zhang, C. Essential functions of iron-requiring proteins in DNA replication, repair and cell cycle control. *Protein & cell* **2014**, *5*, 750–760.

(46) Pasricha, S.-R.; Tye-Din, J.; Muckenthaler, M. U.; Swinkels, D. W. Iron deficiency. *The Lancet* **2021**, *397*, 233–248.

(47) Georgieff, M. K. Iron deficiency in pregnancy. *American Journal of Obstetrics and Gynecology* **2020**, *223*, 516–524.

(48) Chatard, J.-C.; Mujika, I.; Guy, C.; Lacour, J.-R. Anaemia and Iron Deficiency in Athletes. *Sports Medicine* **1999**, *27*, 229–240.

(49) Saboor, M.; Zehra, A.; Qamar, K.; Moinuddin. Disorders associated with malabsorption of iron: A critical review. *Pakistan journal of medical sciences* **2015**, *31*, 1549–1553.

(50) Camaschella, C. Iron-deficiency anemia. *The New England journal of medicine* **2015**, *372*, 1832–1843.

(51) Pietrangelo, A. Hereditary Hemochromatosis: Pathogenesis, Diagnosis, and Treatment. *Gastroenterology* **2010**, *139*, 393-408.e2.

(52) Brissot, P.; Pietrangelo, A.; Adams, P. C.; Graaff, B. de; McLaren, C. E.; Loréal, O. Haemochromatosis. *Nature Reviews Disease Primers* **2018**, *4*, 18016.

(53) Marchi, G.; Busti, F.; Lira Zidanes, A.; Castagna, A.; Girelli, D. Aceruloplasminemia: A Severe Neurodegenerative Disorder Deserving an Early Diagnosis. *Frontiers in neuroscience* **2019**, *13*, 325.

(54) Hsu, C. C.; Senussi, N. H.; Fertrin, K. Y.; Kowdley, K. V. Iron overload disorders. *Hepatology communications* **2022**, *6*, 1842–1854.

(55) Parlesak, A.; Masino, T. T.; Reis, K. D.; Petersen, C. F.; Christensen, J. J.; Olsen, T.; Tetens, I. Preparatory work for the update of the tolerable upper intake levels for iron. *EFSA Supporting Publications* **2024**, *21*, 8661E.

(56) World Health Organization (WHO). WHO guideline on use of ferritin concentrations to assess iron status in individuals and populations **2020**.

(57) Ameta, R.; K. Chohadia, A.; Jain, A.; Punjabi, P. B. Chapter 3 - Fenton and Photo-Fenton Processes. In *Advanced Oxidation Processes for Waste Water Treatment;* Ameta, S. C.; Ameta, R., Eds.; Academic Press, 2018; pp 49–87.

(58) Poli, G.; Leonarduzzi, G.; Biasi, F.; Chiarpotto, E. Oxidative Stress and Cell Signalling. *Current Medicinal Chemistry* **2004**, *11*, 1163–1182.

(59) Weidinger, A.; Kozlov, A. V. Biological Activities of Reactive Oxygen and Nitrogen Species: Oxidative Stress versus Signal Transduction. *Biomolecules* **2015**, *5*, 472–484.

(60) Brieger, K.; Schiavone, S.; Miller, F. J., JR; Krause, K.-H. Reactive oxygen species: from health to disease. *Swiss medical weekly* **2012**, *142*, w13659.

(61) Liu, Y.; Wang, J. Multivalent metal catalysts in Fenton/Fenton-like oxidation system: A critical review. *Chemical Engineering Journal* **2023**, *466*, 143147.

(62) Pamplona, R.; Costantini, D. Molecular and structural antioxidant defenses against oxidative stress in animals. *American Journal of Physiology-Regulatory, Integrative and Comparative Physiology* **2011**, *301*, R843-R863.

(63) Preiser, J.-C. Oxidative Stress. *Journal of Parenteral and Enteral Nutrition* **2012**, *36*, 147–154.

(64) Liguori, I.; Russo, G.; Curcio, F.; Bulli, G.; Aran, L.; Della-Morte, D.; Gargiulo, G.; Testa, G.; Cacciatore, F.; Bonaduce, D.; Abete, P. Oxidative stress, aging, and diseases. *Clinical Interventions in Aging* **2018**, *13*, 757–772.

(65) Meng, X.; Zhang, X.; Liu, M.; Cai, B.; He, N.; Wang, Z. Fenton reaction-based nanomedicine in cancer chemodynamic and synergistic therapy. *Applied Materials Today* **2020**, *21*, 100864.

(66) Arosio, P.; Ingrassia, R.; Cavadini, P. Ferritins: A family of molecules for iron storage, antioxidation and more. *Biochimica et Biophysica Acta (BBA) - General Subjects* **2009**, *1790*, 589–599.

(67) Hirotsu, Y.; Katsuoka, F.; Funayama, R.; Nagashima, T.; Nishida, Y.; Nakayama, K.; Douglas Engel, J.; Yamamoto, M. Nrf2–MafG heterodimers contribute globally to antioxidant and metabolic networks. *Nucleic acids research* **2012**, *40*, 10228–10239.

(68) Perry, J.; Shin, D. S.; Getzoff, E. D.; Tainer, J. A. The structural biochemistry of the superoxide dismutases. *Biochimica et Biophysica Acta (BBA) - Proteins and Proteomics* **2010**, *1804*, 245–262.

(69) Goyal, M. M.; Basak, A. Human catalase: looking for complete identity. *Protein & cell* **2010**, *1*, 888–897.

(70) Abreu, I. A.; Cabelli, D. E. Superoxide dismutases—a review of the metal-associated mechanistic variations. *Biochimica et Biophysica Acta (BBA) - Proteins and Proteomics* **2010**, *1804*, 263–274.

(71) Forcina, G. C.; Dixon, S. J. GPX4 at the Crossroads of Lipid Homeostasis and Ferroptosis. *Proteomics* **2019**, *19*, 1800311.

(72) Sharma, R.; Yang, Y.; Sharma, A.; Awasthi, S.; Awasthi, Y. C. Antioxidant Role of Glutathione S-Transferases: Protection Against Oxidant Toxicity and Regulation of Stress-Mediated Apoptosis. *Antioxidants & redox signaling* **2004**, *6*, 289–300.

(73) Krafczyk, N.; Klotz, L.-O. FOXO transcription factors in antioxidant defense. *IUBMB Life* **2022**, *74*, 53–61.

(74) Deponte, M. Glutathione catalysis and the reaction mechanisms of glutathione-dependent enzymes. *Biochimica et Biophysica Acta (BBA) - General Subjects* **2013**, *1830*, 3217–3266.

(75) Lu, S. C. Glutathione synthesis. *Biochimica et Biophysica Acta (BBA) - General Subjects* **2013**, *1830*, 3143–3153.

(76) Lewerenz, J.; Hewett, S. J.; Huang, Y.; Lambros, M.; Gout, P. W.; Kalivas, P. W.; Massie, A.; Smolders, I.; Methner, A.; Pergande, M.; Smith, S. B.; Ganapathy, V.; Maher, P. The Cystine/Glutamate Antiporter System xc− in Health and Disease: From Molecular Mechanisms to Novel Therapeutic Opportunities. *Antioxidants & redox signaling* **2012**, *18*, 522–555.

(77) Santacroce, G.; Gentile, A.; Soriano, S.; Novelli, A.; Lenti, M. V.; Di Sabatino, A. Glutathione: Pharmacological aspects and implications for clinical use in non-alcoholic fatty liver disease. *Frontiers in Medicine* **2023**, *10*.

(78) Couto, N.; Wood, J.; Barber, J. The role of glutathione reductase and related enzymes on cellular redox homoeostasis network. *Free Radical Biology and Medicine* **2016**, *95*, 27–42.

(79) Johnson, W. M.; Wilson-Delfosse, A. L.; Mieyal, J. J. Dysregulation of glutathione homeostasis in neurodegenerative diseases. *Nutrients* **2012**, *4*, 1399–1440.

(80) Ballatori, N.; Krance, S. M.; Notenboom, S.; Shi, S.; Tieu, K.; Hammond, C. L. Glutathione dysregulation and the etiology and progression of human diseases **2009**, *390*, 191–214.

(81) Emir, U. E.; Raatz, S.; McPherson, S.; Hodges, J. S.; Torkelson, C.; Tawfik, P.; White, T.; Terpstra, M. Noninvasive quantification of ascorbate and glutathione concentration in the elderly human brain. *NMR Biomed.* **2011**, *24*, 888–894.

(82) Sekhar, R. V.; Patel, S. G.; Guthikonda, A. P.; Reid, M.; Balasubramanyam, A.; Taffet, G. E.; Jahoor, F. Deficient synthesis of glutathione underlies oxidative stress in aging and

can be corrected by dietary cysteine and glycine supplementation1234. *The American Journal of Clinical Nutrition* **2011**, *94*, 847–853

(83) Kubal, G.; Meyer, D. J.; Norman, R. E.; Sadler, P. J. Investigations of glutathione conjugation in vitro by 1H NMR spectroscopy. Uncatalyzed and glutathione transferase-catalyzed reactions. *Chemical research in toxicology* **1995**, *8*, 780–791.

(84) Drew, R.; Miners, J. O. The effects of buthionine sulphoximine (BSO) on glutathione depletion and xenobiotic biotransformation. *Biochemical Pharmacology* **1984**, *33*, 2989–2994

(85) Martínez-Reyes, I.; Chandel, N. S. Mitochondrial TCA cycle metabolites control physiology and disease. *Nature Communications* **2020**, *11*, 102.

(86) Bhatti, J. S.; Bhatti, G. K.; Reddy, P. H. Mitochondrial dysfunction and oxidative stress in metabolic disorders - A step towards mitochondria based therapeutic strategies. *Biochimica et biophysica acta. Molecular basis of disease* **2017**, *1863*, 1066–1077.

(87) Brillo, V.; Chieregato, L.; Leanza, L.; Muccioli, S.; Costa, R. Mitochondrial Dynamics, ROS, and Cell Signaling: A Blended Overview. *Life* **2021**, *11*.

(88) Chen, Y.; Guo, X.; Zeng, Y.; Mo, X.; Hong, S.; He, H.; Li, J.; Fatima, S.; Liu, Q. Oxidative stress induces mitochondrial iron overload and ferroptotic cell death. *Scientific Reports* **2023**, *13*, 15515.

(89) Jovaisaite, V.; Auwerx, J. The mitochondrial unfolded protein response—synchronizing genomes. *Current Opinion in Cell Biology* **2015**, *33*, 74–81

(90) Hara, H.; Kuwano, K.; Araya, J. Mitochondrial Quality Control in COPD and IPF. *Cells* **2018**, *7*.

(91) Cowan, K.; Anichtchik, O.; Luo, S. Mitochondrial integrity in neurodegeneration. *CNS Neurosci Ther* **2019**, *25*, 825–836.

(92) Ott, M.; Gogvadze, V.; Orrenius, S.; Zhivotovsky, B. Mitochondria, oxidative stress and cell death. *Apoptosis* **2007**, *12*, 913–922.

(93) Ansenberger-Fricano, K.; Ganini, D.; Mao, M.; Chatterjee, S.; Dallas, S.; Mason, R. P.; Stadler, K.; Santos, J. H.; Bonini, M. G. The peroxidase activity of mitochondrial superoxide dismutase. *Free Radical Biology and Medicine* **2013**, *54*, 116–124

(94) Gaschler, M. M.; Stockwell, B. R. Lipid peroxidation in cell death. *Biochemical and biophysical research communications* **2017**, *482*, 419–425

(95) Rao, M.; Mayor, S. Active organization of membrane constituents in living cells. *Current Opinion in Cell Biology* **2014**, *29*, 126–132

(96) Casares, D.; Escribá, P. V.; Rosselló, C. A. Membrane Lipid Composition: Effect on Membrane and Organelle Structure, Function and Compartmentalization and Therapeutic Avenues. *International Journal of Molecular Sciences* **2019**, *20*.

(97) Horton, A. A.; Fairhurst, S.; and Bus, J. S. Lipid Peroxidation and Mechanisms of Toxicity. *CRC Critical Reviews in Toxicology* **1987**, *18*, 27–79.

(98) Niki, E.; Yoshida, Y.; Saito, Y.; Noguchi, N. Lipid peroxidation: Mechanisms, inhibition, and biological effects. *Biochemical and biophysical research communications* **2005**, *338*, 668–676

(99) Pizzimenti, S.; Ciamporcero, E. S.; Daga, M.; Pettazzoni, P.; Arcaro, A.; Cetrangolo, G.; Minelli, R.; Dianzani, C.; Lepore, A.; Gentile, F.; Barrera, G. Interaction of aldehydes derived from lipid peroxidation and membrane proteins. *Frontiers in Physiology* **2013**, *Volume 4 - 2013*

(100) Ayala, A.; Muñoz, M. F.; Argüelles, S. Lipid Peroxidation: Production, Metabolism, and Signaling Mechanisms of Malondialdehyde and 4-Hydroxy-2-Nonenal. *Oxidat Med and Cellu Longevi* **2014**, *2014*, 360438.

(101) Niki, E.; Noguchi, N. Dynamics of Antioxidant Action of Vitamin E. *Accounts of Chemical Research* **2004**, *37*, 45–51.

(102) Houtkooper, R. H.; Vaz, F. M. Cardiolipin, the heart of mitochondrial metabolism. *Cellular and Molecular Life Sciences* **2008**, *65*, 2493–2506.

(103) Brill, A.; Torchinsky, A.; Carp, H.; Toder, V. The Role of Apoptosis in Normal and Abnormal Embryonic Development. *Journal of Assisted Reproduction and Genetics* **1999**, *16*, 512–519.

(104) Lockshin, R. A.; Zakeri, Z. Cell death in health and disease. *Journal of cellular and molecular medicine* **2007**, *11*, 1214–1224.

(105) Kroemer, G.; Petit, P.; Zamzami, N.; Vayssière, J.-L.; Mignotte, B. The biochemistry of programmed cell death. *The FASEB Journal* **1995**, *9*, 1277–1287.

(106) Newton, K.; Strasser, A.; Kayagaki, N.; Dixit, V. M. Cell death. *Cell* **2024**, *187*, 235–256.

(107) Hajibabaie, F.; Abedpoor, N.; Mohamadynejad, P. Types of Cell Death from a Molecular Perspective. *Biology* **2023**, *12*.

(108) Bertheloot, D.; Latz, E.; Franklin, B. S. Necroptosis, pyroptosis and apoptosis: an intricate game of cell death. *Cellular & molecular immunology* **2021**, *18*, 1106–1121.

(109) Hengartner, M. O.; Horvitz, H. R. Activation of C. elegans cell death protein CED-9 by an ammo-acid substitution in a domain conserved in Bcl-2. *Nature* **1994**, *369*, 318–320.

(110) Gross, A.; McDonnell, J. M.; Korsmeyer, S. J. BCL-2 family members and the mitochondria in apoptosis. *Genes & development* **1999**, *13*, 1899–1911.

(111) Boatright, K. M.; Salvesen, G. S. Mechanisms of caspase activation. *Current Opinion in Cell Biology* **2003**, *15*, 725–731

(112) Polyak, K.; Xia, Y.; Zweier, J. L.; Kinzler, K. W.; Vogelstein, B. A model for p53-induced apoptosis. *Nature* **1997**, *389*, 300–305.

(113) Nagata, S. Fas Ligand-Induced Apoptosis. *Annual Review of Genetics* **1999**, *33*, 29–55

(114) Maderna, P.; Godson, C. Phagocytosis of apoptotic cells and the resolution of inflammation. *Biochimica et biophysica acta. Molecular basis of disease* **2003**, *1639*, 141–151.

(115) Kari, S.; Subramanian, K.; Altomonte, I. A.; Murugesan, A.; Yli-Harja, O.; Kandhavelu, M. Programmed cell death detection methods: a systematic review and a categorical comparison. *Apoptosis* **2022**, *27*, 482–508.

(116) Yang, W. S.; Stockwell, B. R. Synthetic Lethal Screening Identifies Compounds Activating Iron-Dependent, Nonapoptotic Cell Death in Oncogenic-RAS-Harboring Cancer Cells. *Chemistry & Biology* **2008**, *15*, 234–245.

(117) Berndt, C.; Lillig, C. H. Glutathione, Glutaredoxins, and Iron. *Antioxidants & redox signaling* **2017**, *27*, 1235–1251.

(118) Latunde-Dada, G. O. Ferroptosis: Role of lipid peroxidation, iron and ferritinophagy. *Biochimica et Biophysica Acta (BBA) - General Subjects* **2017**, *1861*, 1893–1900.

(119) Mazhar, M.; Din, A. U.; Ali, H.; Yang, G.; Ren, W.; Wang, L.; Fan, X.; Yang, S. Implication of ferroptosis in aging. *Cell death discovery* **2021**, *7*, 149.

(120) Gao, H.; Bai, Y.; Jia, Y.; Zhao, Y.; Kang, R.; Tang, D.; Dai, E. Ferroptosis is a lysosomal cell death process. *Biochemical and biophysical research communications* **2018**, *503*, 1550–1556

(121) Gao, M.; Yi, J.; Zhu, J.; Minikes, A. M.; Monian, P.; Thompson, C. B.; Jiang, X. Role of Mitochondria in Ferroptosis. *Molecular Cell* **2019**, *73*, 354-363.e3.

(122) Cañeque, T.; Baron, L.; Müller, S.; Carmona, A.; Colombeau, L.; Versini, A.; Solier, S.; Gaillet, C.; Sindikubwabo, F.; Sampaio, J. L.; Sabatier, M.; Mishima, E.; Picard-Bernes, A.; Syx, L.; Servant, N.; Lombard, B.; Loew, D.; Zheng, J.; Proneth, B.; Thoidingjam, L. K.; Grimaud, L.; Fraser, C. S.; Szylo, K. J.; Der Kazarian, E.; Bonnet, C.; Charafe-Jauffret, E.; Ginestier, C.; Santofimia-Castaño, P.; Estaras, M.; Dusetti, N.; Iovanna, J. L.; Cunha, A. S.; Pittau, G.; Hammel, P.; Tzanis, D.; Bonvalot, S.; Watson, S.; Gandon, V.; Upadhyay, A.; Pratt, D. A.; Freitas, F. P.; Friedmann Angeli, J. P.; Stockwell, B. R.; Conrad, M.; Ubellacker, J. M.; Rodriguez, R. Activation of lysosomal iron triggers ferroptosis in cancer. *Nature* **2025**, *642*, 492–500.

(123) Yang, W. S.; SriRamaratnam, R.; Welsch, M. E.; Shimada, K.; Skouta, R.; Viswanathan, V. S.; Cheah, J. H.; Clemons, P. A.; Shamji, A. F.; Clish, C. B. Regulation of ferroptotic cancer cell death by GPX4. *Cell* **2014**, *156*, 317–331.

(124) Seibt, T. M.; Proneth, B.; Conrad, M. Role of GPX4 in ferroptosis and its pharmacological implication. *Free Radical Biology and Medicine* **2019**, *133*, 144–152

(125) Conrad, M.; Proneth, B. Selenium: Tracing Another Essential Element of Ferroptotic Cell Death. *Cell Chemical Biology* **2020**, *27*, 409–419.

(126) Ingold, I.; Berndt, C.; Schmitt, S.; Doll, S.; Poschmann, G.; Buday, K.; Roveri, A.; Peng, X.; Porto Freitas, F.; Seibt, T.; Mehr, L.; Aichler, M.; Walch, A.; Lamp, D.; Jastroch, M.; Miyamoto, S.; Wurst, W.; Ursini, F.; Arnér, E. S.; Fradejas-Villar, N.; Schweizer, U.; Zischka, H.; Friedmann Angeli, J. P.; Conrad, M. Selenium Utilization by GPX4 Is Required to Prevent Hydroperoxide-Induced Ferroptosis. *Cell* **2018**, *172*, 409-422.e21.

(127) Angeli, J. P. F.; Shah, R.; Pratt, D. A.; Conrad, M. Ferroptosis Inhibition: Mechanisms and Opportunities. *Trends in Pharmacological Sciences* **2017**, *38*, 489–498.

(128) Zilka, O.; Shah, R.; Li, B.; Friedmann Angeli, J. P.; Griesser, M.; Conrad, M.; Pratt, D. A. On the Mechanism of Cytoprotection by Ferrostatin-1 and Liproxstatin-1 and the Role of Lipid Peroxidation in Ferroptotic Cell Death. *ACS Central Science* **2017**, *3*, 232–243.

(129) Aschner, M.; Skalny, A. V.; Martins, A. C.; Sinitskii, A. I.; Farina, M.; Lu, R.; Barbosa, F., JR; Gluhcheva, Y. G.; Santamaria, A.; Tinkov, A. A. Ferroptosis as a mechanism of non-ferrous metal toxicity. *Archives of toxicology* **2022**, *96*, 2391–2417.

(130) Bazira, P. J. An overview of the nervous system. *Surgery (Oxford)* **2021**, *39*, 451–462.

(131) Lovinger, D. M. *Communication networks in the brain: neurons, receptors, neurotransmitters, and alcohol:* United States, 2008.

(132) Bennett, M. K.; Scheller, R. H. A molecular description of synaptic vesicle membrane trafficking. *Annual review of biochemistry* **1994**, *63*, 63–100.

(133) Gether, U.; Andersen, P. H.; Larsson, O. M.; Schousboe, A. Neurotransmitter transporters: molecular function of important drug targets. *Trends in Pharmacological Sciences* **2006**, *27*, 375–383.

(134) Nimgampalle, M.; Chakravarthy, H.; Sharma, S.; Shree, S.; Bhat, A. R.; Pradeepkiran, J. A.; Devanathan, V. Neurotransmitter systems in the etiology of major neurological disorders: Emerging insights and therapeutic implications. *Ageing research reviews* **2023**, *89*, 101994.

(135) Rossi, S.; Zanier, E. R.; Mauri, I.; Columbo, A.; Stocchetti, N. Brain temperature, body core temperature, and intracranial pressure in acute cerebral damage. *Journal of neurology, neurosurgery, and psychiatry* **2001**, *71*, 448–454.

(136) Trigo, D.; Avelar, C.; Fernandes, M.; Sá, J.; Da Cruz e Silva, O. Mitochondria, energy, and metabolism in neuronal health and disease. *FEBS Letters* **2022**, *596*, 1095–1110.

(137) Moujalled, D.; Strasser, A.; Liddell, J. R. Molecular mechanisms of cell death in neurological diseases. *Cell Death & Differentiation* **2021**, *28*, 2029–2044.

(138) Jellinger, K. A. Basic mechanisms of neurodegeneration: a critical update. *Journal of cellular and molecular medicine* **2010**, *14*, 457–487.

(139) Ryan, K. C.; Ashkavand, Z.; Norman, K. R. The Role of Mitochondrial Calcium Homeostasis in Alzheimer's and Related Diseases. *International Journal of Molecular Sciences* **2020**, *21*.

(140) ARREDONDO, M.; Martínez, R.; Núñez, M. T.; RUZ, M.; OLIVARES, M. Inhibition of iron and copper uptake by iron, copper and zinc. *Biological Research* **2006**, *39*, 95–102.

(141) Pan Chen, Julia B Bornhorst, Michael Aschner. Manganese metabolism in humans. *FBL* **2018**, *23*, 1655–1679.

(142) Whittaker, J. W. Non-heme manganese catalase – The 'other' catalase. *Archives of biochemistry and biophysics* **2012**, *525*, 111–120

(143) Miriyala, S.; Spasojevic, I.; Tovmasyan, A.; Salvemini, D.; Vujaskovic, Z.; St. Clair, D.; Batinic-Haberle, I. Manganese superoxide dismutase, MnSOD and its mimics. *Biochimica et biophysica acta. Molecular basis of disease* **2012**, *1822*, 794–814

(144) Chua, A. C. G.; Morgan, E. H. Effects of iron deficiency and iron overload on manganese uptake and deposition in the brain and other organs of the rat. *Biological Trace Element Research* **1996**, *55*, 39–54.

(145) Erikson, K. M.; Shihabi, Z. K.; Aschner, J. L.; Aschner, M. Manganese accumulates in iron-deficient rat brain regions in a heterogeneous fashion and is associated with neurochemical alterations. *Biological Trace Element Research* **2002**, *87*, 143–156.

(146) Qin Li; Haobin Chen; Xi Huang; Max Costa. Effects of 12 metal ions on iron regulatory protein 1 (IRP-1) and hypoxia-inducible factor-1 alpha (HIF-1α) and HIF-regulated genes. *Toxicology and Applied Pharmacology* **2006**, *213*, 245–255.

(147) Yin, Z.; Jiang, H.; Lee, E.-S. Y.; Ni, M.; Erikson, K. M.; Milatovic, D.; Bowman, A. B.; Aschner, M. Ferroportin is a manganese-responsive protein that decreases manganese cytotoxicity and accumulation. *Journal of Neurochemistry* **2010**, *112*, 1190–1198.

(148) Bjørklund, G.; Dadar, M.; Peana, M.; Rahaman, M. S.; Aaseth, J. Interactions between iron and manganese in neurotoxicity. *Archives of toxicology* **2020**, *94*, 725–734.

(149) John B. Vincent; Sharifa Love. The binding and transport of alternative metals by transferrin. *Biochimica et Biophysica Acta (BBA) - General Subjects* **2012**, *1820*, 362–378.

(150) Angelova, M.; Asenova, S.; Nedkova, V.; Koleva-Kolarova, R. Copper in the human organism. *Trakia journal of sciences* **2011**, *9*, 88–98.

(151) Collins, J. F.; Prohaska, J. R.; Knutson, M. D. Metabolic crossroads of iron and copper. *Nutrition reviews* **2010**, *68*, 133–147.

(152) Wang, X.; Flores, S. R.; Ha, J.-H.; Doguer, C.; Woloshun, R. R.; Xiang, P.; Grosche, A.; Vidyasagar, S.; Collins, J. F. Intestinal DMT1 Is Essential for Optimal Assimilation of Dietary Copper in Male and Female Mice with Iron-Deficiency Anemia. *The Journal of Nutrition* **2018**, *148*, 1244–1252.

(153) Badria, F. A.; Ibrahim, A. S.; Badria, A. F.; Elmarakby, A. A. Curcumin Attenuates Iron Accumulation and Oxidative Stress in the Liver and Spleen of Chronic Iron-Overloaded Rats. *PloS one* **2015**, *10*, e0134156.

(154) Lim, K. H. C.; Riddell, L. J.; Nowson, C. A.; Booth, A. O.; Szymlek-Gay, E. A. Iron and Zinc Nutrition in the Economically-Developed World: A Review. *Nutrients* **2013**, *5*, 3184–3211.

(155) Skalny, A. V.; Aschner, M.; Tinkov, A. A. Zinc. *Advances in food and nutrition research* **2021**, *96*, 251–310.

(156) Kondaiah, P.; Aslam, M. F.; Mashurabad, P. C.; Sharp, P. A.; Pullakhandam, R. Zinc induces iron uptake and DMT1 expression in Caco-2 cells via a PI3K/IRP2 dependent mechanism. *Biochemical Journal* **2019**, *476*, 1573–1583.

(157) Goldberg, E. K.; Neogi, S.; Lal, A.; Higa, A.; Fung, E. Nutritional Deficiencies Are Common in Patients with Transfusion-Dependent Thalassemia and Associated with Iron Overload. *Journal of food and nutrition research (Newark, Del.)* **2018**, *6*, 674–681.

(158) Niles, B. J.; Clegg, M. S.; Hanna, L. A.; Chou, S. S.; Momma, T. Y.; Hong, H.; Keen, C. L. Zinc Deficiency-induced Iron Accumulation, a Consequence of Alterations in Iron Regulatory Protein-binding Activity, Iron Transporters, and Iron Storage Proteins *. *Journal of Biological Chemistry* **2008**, *283*, 5168–5177.

(159) Mousa, S. O.; Abd Alsamia, E. M.; Moness, H. M.; Mohamed, O. G. The effect of zinc deficiency and iron overload on endocrine and exocrine pancreatic function in children with transfusion-dependent thalassemia: a cross-sectional study. *BMC Pediatrics* **2021**, *21*, 468.

(160) Brenner, S. The genetics of Caenorhabditis elegans. *Genetics* **1974**, *77*, 71–94.

(161) Hubrecht, R. C.; Carter, E. The 3Rs and Humane Experimental Technique: Implementing Change. *Animals* **2019**, *9*.

(162) Meneely, P. M.; Dahlberg, C. L.; Rose, J. K. Working with Worms: Caenorhabditis elegans as a Model Organism. *Current Protocols Essential Laboratory Techniques* **2019**, *19*, e35.

(163) Sulston, J. E.; Horvitz, H. R. Post-embryonic cell lineages of the nematode, Caenorhabditis elegans. *Developmental biology* **1977**, *56*, 110–156.

(164) Ward, S.; Carrel, J. S. Fertilization and sperm competition in the nematodeCaenorhabditis elegans. *Developmental biology* **1979**, *73*, 304–321

(165) The C. elegans Sequencing Consortium*. Genome Sequence of the Nematode *C. elegans*: A Platform for Investigating Biology. *Science* **1998**, *282*, 2012–2018.

(166) Jones, M. R.; Lohn, Z.; Rose, A. M. Chapter 2 - Specialized Chromosomes and Their Uses in Caenorhabditis elegans. In *Methods in Cell Biology Caenorhabditis elegans: Molecular Genetics and Development;* Rothman, J. H.; Singson, A., Eds.; Academic Press, 2011; Vol. 106, pp 23–64.

(167) Kaletta, T.; Hengartner, M. O. Finding function in novel targets: C. elegans as a model organism. *Nature Reviews Drug Discovery* **2006**, *5*, 387–399.

(168) Nance, J.; Frøkjær-Jensen, C. The Caenorhabditis elegans Transgenic Toolbox. *Genetics* **2019**, *212*, 959–990.

(169) Aschner, M.; Palinski, C.; Sperling, M.; Karst, U.; Schwerdtle, T.; Bornhorst, J. Imaging metals in Caenorhabditis elegans. *Metallomics integrated biometal science* **2017**, *9*, 357–364.

(170) Hartman, J. H.; Widmayer, S. J.; Bergemann, C. M.; King, D. E.; Morton, K. S.; Romersi, R. F.; Jameson, L. E.; Leung, M. C. K.; Andersen, E. C.; Taubert, S.; Meyer, J. N. Xenobiotic metabolism and transport in Caenorhabditis elegans. *Journal of toxicology and environmental health. Part B, Critical reviews* **2021**, *24*, 51–94.

(171) Kimble, J.; Nüsslein-Volhard, C. The great small organisms of developmental genetics: Caenorhabditis elegans and Drosophila melanogaster. *Developmental biology* **2022**, *485*, 93–122.

(172) Porta-de-la-Riva, M.; Fontrodona, L.; Villanueva, A.; Cerón, J. Basic Caenorhabditis elegans methods: synchronization and observation. *Journal of visualized experiments JoVE* **2012**, e4019.

(173) Fielenbach, N.; Antebi, A. C. elegans dauer formation and the molecular basis of plasticity. *Genes & development* **2008**, *22*, 2149–2165.

(174) Chen, C.; Hamza, I. Notes from the Underground: Heme Homeostasis in C. elegans. *Biomolecules* **2023**, *13*.

(175) Au, C.; Benedetto, A.; Anderson, J.; Labrousse, A.; Erikson, K.; Ewbank, J. J.; Aschner, M. SMF-1, SMF-2 and SMF-3 DMT1 orthologues regulate and are regulated differentially by manganese levels in C. elegans. *PloS one* **2009**, *4*, e7792.

(176) Romney, S. J.; Newman, B. S.; Thacker, C.; Leibold, E. A. HIF-1 regulates iron homeostasis in Caenorhabditis elegans by activation and inhibition of genes involved in iron uptake and storage. *PLoS genetics* **2011**, *7*, e1002394.

(177) James, S. A.; Roberts, B. R.; Hare, D. J.; Jonge, M. D. de; Birchall, I. E.; Jenkins, N. L.; Cherny, R. A.; Bush, A. I.; McColl, G. Direct in vivo imaging of ferrous iron dyshomeostasis in ageing Caenorhabditis elegans. *Chem. Sci.* **2015**, *6*, 2952–2962.

(178) van den Ecker, D.; Hoffmann, M.; Müting, G.; Maglioni, S.; Herebian, D.; Mayatepek, E.; Ventura, N.; Distelmaier, F. Caenorhabditis elegans ATAD-3 modulates mitochondrial iron and heme homeostasis. *Biochemical and biophysical research communications* **2015**, *467*, 389–394.

(179) Valentini, S.; Cabreiro, F.; Ackerman, D.; Alam, M. M.; Kunze, M. B. A.; Kay, C. W. M.; Gems, D. Manipulation of in vivo iron levels can alter resistance to oxidative stress without affecting ageing in the nematode C. elegans. *Mechanisms of ageing and development* **2012**, *133*, 282–290.

(180) Sayers, E. W.; Bolton, E. E.; Brister, J. R.; Canese, K.; Chan, J.; Comeau, D. C.; Connor, R.; Funk, K.; Kelly, C.; Kim, S.; Madej, T.; Marchler-Bauer, A.; Lanczycki, C.; Lathrop, S.; Lu, Z.; Thibaud-Nissen, F.; Murphy, T.; Phan, L.; Skripchenko, Y.; Tse, T.; Wang, J.; Williams, R.; Trawick, B. W.; Pruitt, K. D.; Sherry, S. T. Database resources of the national center for biotechnology information. *Nucleic acids research* **2022**, *50*, 20-26.

(181) Rajagopal, A.; Rao, A. U.; Amigo, J.; Tian, M.; Upadhyay, S. K.; Hall, C.; Uhm, S.; Mathew, M. K.; Fleming, M. D.; Paw, B. H.; Krause, M.; Hamza, I. Haem homeostasis is regulated by the conserved and concerted functions of HRG-1 proteins. *Nature* **2008**, *453*, 1127–1131.

(182) Lewandowski, J.; Komur, A. A.; Sobańska, D. Structural and functional relationship of mammalian and nematode ferritins. *Biotechnologia* **2021**, *102*, 457–471.

(183) Gourley, B. L.; Parker, S. B.; Jones, B. J.; Zumbrennen, K. B.; Leibold, E. A. Cytosolic aconitase and ferritin are regulated by iron in Caenorhabditis elegans. *Journal of Biological Chemistry* **2003**, *278*, 3227–3234.

(184) Mubarak, S. S. M.; Malcolm, T. R.; Brown, H. G.; Hanssen, E.; Maher, M. J.; McColl, G.; Jameson, G. N. L. Biochemical Characterization of Caenorhabditis elegans Ferritins. *Biochemistry* **2023**, *62*, 1484–1496.

(185) Kim, Y.-I.; Cho, J. H.; Yoo, O. J.; Ahnn, J. Transcriptional regulation and life-span modulation of cytosolic aconitase and ferritin genes in C.elegans. *Journal of molecular biology* **2004**, *342*, 421–433.

(186) Chakraborty, S.; Chen, P.; Bornhorst, J.; Schwerdtle, T.; Schumacher, F.; Kleuser, B.; Bowman, A. B.; Aschner, M. Loss of pdr-1/parkin influences Mn homeostasis through altered ferroportin expression in C. elegans. *Metallomics.* **2015**, *7*, 847–856.

(187) Patel, D.; Xu, C.; Nagarajan, S.; Liu, Z.; Hemphill, W. O.; Shi, R.; Uversky, V. N.; Caldwell, G. A.; Caldwell, K. A.; Witt, S. N. Alpha-synuclein inhibits Snx3–retromer-mediated retrograde recycling of iron transporters in S. cerevisiae and C. elegans models of Parkinson's disease. *Human Molecular Genetics* **2018**, *27*, 1514–1532.

(188) Weishaupt, A.-K.; Lamann, K.; Tallarek, E.; Pezacki, A. T.; Matier, C. D.; Schwerdtle, T.; Aschner, M.; Chang, C. J.; Stürzenbaum, S. R.; Bornhorst, J. Dysfunction in atox-1 and ceruloplasmin alters labile Cu levels and consequently Cu homeostasis in C. elegans. *Frontiers in molecular biosciences* **2024**, *11*, 1354627.

(189) Gremme, A.; Al-Timimi Safa Flaih, Z.; Scholz, J.; Gerisch, E.; Thiel, A.; McColl, G.; Hayen, H.; Michalke, B.; Bornhorst, J. Is Ferric the Same as Ferrous? Effect of Nutritionally Relevant Iron Species in C. elegans: Bioavailability, Iron Homeostasis, Oxidative Stress, and Cell Death. *Journal of Agricultural and Food Chemistry* **2025**.

(190) Anderson, C. P.; Leibold, E. A. Mechanisms of iron metabolism in Caenorhabditis elegans. *Frontiers in pharmacology* **2014**, *5*, 113.

(191) Romney, S. J.; Thacker, C.; Leibold, E. A. An iron enhancer element in the FTN-1 gene directs iron-dependent expression in Caenorhabditis elegans intestine. *Journal of Biological Chemistry* **2008**, *283*, 716–725.

(192) Ackerman, D.; Gems, D. Insulin/IGF-1 and Hypoxia Signaling Act in Concert to Regulate Iron Homeostasis in Caenorhabditis elegans. *PLoS genetics* **2012**, *8*, e1002498.

(193) Moreno-Arriola, E.; Cárdenas-Rodríguez, N.; Coballase-Urrutia, E.; Pedraza-Chaverri, J.; Carmona-Aparicio, L.; Ortega-Cuellar, D. Caenorhabditis elegans: A Useful Model for Studying Metabolic Disorders in Which Oxidative Stress Is a Contributing Factor. *Oxidat Med and Cellu Longevi* **2014**, *2014*, 705253.

(194) Dilberger, B.; Baumanns, S.; Schmitt, F.; Schmiedl, T.; Hardt, M.; Wenzel, U.; Eckert, G. P. Mitochondrial Oxidative Stress Impairs Energy Metabolism and Reduces Stress Resistance and Longevity of C. elegans. *Oxidat Med and Cellu Longevi* **2019**, *2019*, 6840540.

(195) Doonan, R.; McElwee, J. J.; Matthijssens, F.; Walker, G. A.; Houthoofd, K.; Back, P.; Matscheski, A.; Vanfleteren, J. R.; Gems, D. Against the oxidative damage theory of aging: superoxide dismutases protect against oxidative stress but have little or no effect on life span in Caenorhabditis elegans. *Genes & development* **2008**, *22*, 3236–3241.

(196) Oleh I. Petriv; Richard A. Rachubinski. Lack of Peroxisomal Catalase Causes a Progeric Phenotype in Caenorhabditis elegans*. *Journal of Biological Chemistry* **2004**, *279*, 19996–20001.

(197) Ferguson, G. D.; Bridge, W. J. The glutathione system and the related thiol network in Caenorhabditis elegans. *Redox biology* **2019**, *24*, 101171.

(198) Dancy, B. M.; Brockway, N.; Ramadasan-Nair, R.; Yang, Y.; Sedensky, M. M.; Morgan, P. G. Glutathione S-transferase mediates an ageing response to mitochondrial dysfunction. *Mechanisms of ageing and development* **2016**, *153*, 14–21.

(199) Hengartner, M. O.; Horvitz, H. R. The ins and outs of programmed cell death during C. elegans development. *Philosophical Transactions of the Royal Society of London. Series B: Biological Sciences* **1994**, *345*, 243–246.

(200) Lant, B.; Derry, W. B. Analysis of apoptosis in Caenorhabditis elegans. *Cold Spring Harbor protocols* **2014**, *2014*.

(201) W. Brent Derry; Aaron P. Putzke; Joel H. Rothman. *Caenorhabditis elegans* p53: Role in Apoptosis, Meiosis, and Stress Resistance. *Science* **2001**, *294*, 591–595.

(202) Yee, C.; Yang, W.; Hekimi, S. The Intrinsic Apoptosis Pathway Mediates the Pro-Longevity Response to Mitochondrial ROS in *C. elegans*. *Cell* **2014**, *157*, 897–909.

(203) Perez, M. A.; Watts, J. L. Worms, Fat, and Death: Caenorhabditis elegans Lipid Metabolites Regulate Cell Death. *Metabolites* **2021**, *11*, 125.

(204) Zhou, Z.; Hartwieg, E.; Horvitz, H. R. CED-1 is a transmembrane receptor that mediates cell corpse engulfment in C. elegans. *Cell* **2001**, *104*, 43–56.

(205) Sakamoto, T.; Maebayashi, K.; Nakagawa, Y.; Imai, H. Deletion of the four phospholipid hydroperoxide glutathione peroxidase genes accelerates aging in Caenorhabditis elegans. *Genes to cells devoted to molecular & cellular mechanisms* **2014**, *19*, 778–792.

(206) Jenkins, N. L.; James, S. A.; Salim, A.; Sumardy, F.; Speed, T. P.; Conrad, M.; Des Richardson, R.; Bush, A. I.; McColl, G.; Gruber, J.; Tyler, J. K. Changes in ferrous iron and glutathione promote ferroptosis and frailty in aging Caenorhabditis elegans. *eLife* **2020**, *9*, e56580.

(207) Zhang, Y.; Zou, X.; Ding, Y.; Wang, H.; Wu, X.; Liang, B. Comparative genomics and functional study of lipid metabolic genes in Caenorhabditis elegans. *BMC genomics* **2013**, *14*, 164.

(208) Witting, M.; Schmitt-Kopplin, P. The Caenorhabditis elegans lipidome: A primer for lipid analysis in Caenorhabditis elegans. *Archives of biochemistry and biophysics* **2016**, *589*, 27–37

(209) Watts, J. L.; Ristow, M. Lipid and Carbohydrate Metabolism in Caenorhabditis elegans. *Genetics* **2017**, *207*, 413–446.

(210) White, J. G.; Southgate, E.; Thomson, J. N.; Brenner, S. The structure of the nervous system of the nematode Caenorhabditis elegans. *Philosophical Transactions of the Royal Society of London. Series B: Biological Sciences* **1986**, *314*, 1–340.

(211) Varshney, L. R.; Chen, B. L.; Paniagua, E.; Hall, D. H.; Chklovskii, D. B. Structural Properties of the Caenorhabditis elegans Neuronal Network. *PLOS Computational Biology* **2011**, *7*, e1001066.

(212) Wang, C.; Vidal, B.; Sural, S.; Loer, C.; Aguilar, G. R.; Merritt, D. M.; Toker, I. A.; Vogt, M. C.; Cros, C. C.; Hobert, O.; Zimmer, M.; Cardona, A. A neurotransmitter atlas of C. elegans males and hermaphrodites. *eLife* **2024**, *13*, RP95402.

(213) Weishaupt, A.-K.; Kubens, L.; Ruecker, L.; Schwerdtle, T.; Aschner, M.; Bornhorst, J. A Reliable Method Based on Liquid Chromatography-Tandem Mass Spectrometry for the Simultaneous Quantification of Neurotransmitters in Caenorhabditis elegans. *Molecules (Basel, Switzerland)* **2023**, *28*.

(214) Nehrke, K. A Reduction in Intestinal Cell pH i Due to Loss of the Caenorhabditis elegans Na+/H+ Exchanger NHX-2 Increases Life Span*. *Journal of Biological Chemistry* **2003**, *278*, 44657–44666.

(215) Fallingborg, J. Intraluminal pH of the human gastrointestinal tract. *Dan Med Bull* **1999**, *46*, 183–196.

(216) Schäfer, A. C.; Boeing, H.; Conrad, J.; Watzl B. für die DGE Arbeitsgruppe Lebensmittelbezogene Ernährungsempfehlungen: Wissenschaftliche Grundlagen der lebensmittelbezogenen Ernährungsempfehlungen für Deutschland. Methodik und Ableitungskonzepte. *Ernährungs Umschau* **2024**, 5–7.

(217) European Comission. Comission Regulation (EC) No 1170/2009 of 30 November 2009 amending Directive 2002/46/EC of the European Parliament and of Council and Regulation (EC) No 1925/2006 of the European Parliament and of the Council as regards the lists of vitamin and minerals and their forms that can be added to foods, including food supplements. *Official Journal of the European Union* **2009**, *L 314*, 36–42.

(218) Dev, S.; Babitt, J. L. Overview of iron metabolism in health and disease. *Hemodialysis international. International Symposium on Home Hemodialysis* **2017**, *21*, S6–S20.

(219) Fraga, C. G.; Oteiza, P. I. Iron toxicity and antioxidant nutrients. *Toxicology* **2002**, *180*, 23–32.

(220) Winterbourn, C. C. Toxicity of iron and hydrogen peroxide: the Fenton reaction. *Toxicology Letters* **1995**, *82-83*, 969–974.

(221) Ryter, S. W.; Kim, H. P.; Hoetzel, A.; Park, J. W.; Nakahira, K.; Wang, X.; Choi, A. M. K. Mechanisms of Cell Death in Oxidative Stress. *Antioxidants & redox signaling* **2006**, *9*, 49–89.

(222) Fiser, B.; Jójárt, B.; Csizmadia, I. G.; Viskolcz, B. Glutathione--hydroxyl radical interaction: a theoretical study on radical recognition process. *PloS one* **2013**, *8*, e73652.

(223) Scholz, J.; Rudt, E.; Gremme, A.; Gaßmöller, C. M.; Bornhorst, J.; Hayen, H. Hyphenation of supercritical fluid chromatography and trapped ion mobility-mass spectrometry for quantitative lipidomics. *Analytica Chimica Acta* **2024**, *1317*, 342913.

(224) Baesler, J.; Michaelis, V.; Stiboller, M.; Haase, H.; Aschner, M.; Schwerdtle, T.; Sturzenbaum, S. R.; Bornhorst, J. Nutritive Manganese and Zinc Overdosing in Aging C. elegans Result in a Metallothionein-Mediated Alteration in Metal Homeostasis. *Molecular nutrition & food research* **2021**, *65*, e2001176.

(225) Kubens, L.; Weishaupt, A.-K.; Michaelis, V.; Rohn, I.; Mohr, F.; Bornhorst, J. Exposure to the environmentally relevant fungicide Maneb: Studying toxicity in the soil nematode Caenorhabditis elegans. *Environment international* **2024**, *183*, 108372.

(226) Bornhorst, J.; Chakraborty, S.; Meyer, S.; Lohren, H.; Brinkhaus, S. G.; Knight, A. L.; Caldwell, K. A.; Caldwell, G. A.; Karst, U.; Schwerdtle, T.; Bowman, A.; Aschner, M. The effects of pdr1, djr1.1 and pink1 loss in manganese-induced toxicity and the role of α-synuclein in C. elegans. *Metallomics integrated biometal science* **2014**, *6*, 476–490.

(227) Livak, K. J.; Schmittgen, T. D. Analysis of relative gene expression data using real-time quantitative PCR and the 2(-Delta Delta C(T)) Method. *Methods (San Diego, Calif.)* **2001**, *25*, 402–408.

(228) Neumann, C.; Baesler, J.; Steffen, G.; Nicolai, M. M.; Zubel, T.; Aschner, M.; Bürkle, A.; Mangerich, A.; Schwerdtle, T.; Bornhorst, J. The role of poly(ADP-ribose) polymerases in manganese exposed Caenorhabditis elegans. *Journal of trace elements in medicine and biology organ of the Society for Minerals and Trace Elements (GMS)* **2020**, *57*, 21–27.

(229) Henderson, S. T.; Johnson, T. E. daf-16 integrates developmental and environmental inputs to mediate aging in the nematode Caenorhabditis elegans. *Current Biology* **2001**, *11*, 1975–1980.

(230) Chen, J.; Su, Y.; Lin, F.; Iqbal, M.; Mehmood, K.; Zhang, H.; Shi, D. Effect of paraquat on cytotoxicity involved in oxidative stress and inflammatory reaction: A review of mechanisms and ecological implications. *Ecotoxicology and Environmental Safety* **2021**, *224*, 112711.

(231) Zhang, J.; Chen, R.; Yu, Z.; Xue, L. Superoxide Dismutase (SOD) and Catalase (CAT) Activity Assay Protocols for Caenorhabditis elegans. *Bio-protocol* **2017**, *7*, e2505.

(232) Thiel, A.; Weishaupt, A.-K.; Nicolai, M. M.; Lossow, K.; Kipp, A. P.; Schwerdtle, T.; Bornhorst, J. Simultaneous quantitation of oxidized and reduced glutathione via LC-MS/MS to study the redox state and drug-mediated modulation in cells, worms and animal tissue. *Journal of chromatography. B, Analytical technologies in the biomedical and life sciences* **2023**, *1225*, 123742.

(233) Folch, J.; Lees, M.; Stanley, G. S. A SIMPLE METHOD FOR THE ISOLATION AND PURIFICATION OF TOTAL LIPIDES FROM ANIMAL TISSUES. *Journal of Biological Chemistry* **1957**, *226*, 497–509.

(234) Liebisch, G.; Vizcaíno, J. A.; Köfeler, H.; Trötzmüller, M.; Griffiths, W. J.; Schmitz, G.; Spener, F.; Wakelam, M. J. Shorthand notation for lipid structures derived from mass spectrometry. *Journal of Lipid Research* **2013**, *54*, 1523–1530.

(235) Caballero Valcárcel, A. M.; Martínez Graciá, C.; Martínez Miró, S.; Madrid Sánchez, J.; González Bermúdez, C. A.; Domenech Asensi, G.; López Nicolás, R.; Santaella Pascual, M. Iron bioavailability of four iron sources used to fortify infant cereals, using anemic weaning pigs as a model. *Eur J Nutr* **2019**, *58*, 1911–1922.

(236) Kriplani, A.; Pal, B.; Bhat, V.; Swami, O. Ferrous Ascorbate: Current Clinical Place of Therapy in the Management of Iron Deficiency Anemia. *Journal of South Asian Federation of Obstetrics and Gynaecology* **2021**, *13*, 103–109.

(237) Scheiber-Mojdehkar, B.; Sturm, B.; Plank, L.; Kryzer, I.; Goldenberg, H. Influence of parenteral iron preparations on non-transferrin bound iron uptake, the iron regulatory protein and the expression of ferritin and the divalent metal transporter DMT-1 in HepG2 human hepatoma cells. *Biochemical Pharmacology* **2003**, *65*, 1973–1978.

(238) Ceballos, M. P.; Parody, J. P.; Quiroga, A. D.; Casella, M. L.; Francés, D. E.; Larocca, M. C.; Carnovale, C. E.; Alvarez, M. d. L.; Carrillo, M. C. FoxO3a nuclear localization and its association with β-catenin and Smads in IFN-α-treated hepatocellular carcinoma cell lines. *Journal of interferon & cytokine research the official journal of the International Society for Interferon and Cytokine Research* **2014**, *34*, 858–869.

(239) McCord, J. M.; Fridovich, I. Superoxide Dismutase: AN ENZYMIC FUNCTION FOR ERYTHROCUPREIN (HEMOCUPREIN). *Journal of Biological Chemistry* **1969**, *244*, 6049–6055.

(240) Marrocco, I.; Altieri, F.; Peluso, I. Measurement and Clinical Significance of Biomarkers of Oxidative Stress in Humans. *Oxidat Med and Cellu Longevi* **2017**, 6501046.

(241) van der Veen, J. N.; Kennelly, J. P.; Wan, S.; Vance, J. E.; Vance, D. E.; Jacobs, R. L. The critical role of phosphatidylcholine and phosphatidylethanolamine metabolism in

health and disease. *Biochimica et biophysica acta. Biomembranes* **2017**, *1859*, 1558–1572.

(242) Koyiloth, M.; Gummadi, S. N. Regulation and functions of membrane lipids: Insights from Caenorhabditis elegans. *BBA advances* **2022**, *2*, 100043.

(243) Helmer, P. O.; Nicolai, M. M.; Schwantes, V.; Bornhorst, J.; Hayen, H. Investigation of cardiolipin oxidation products as a new endpoint for oxidative stress in C. elegans by means of online two-dimensional liquid chromatography and high-resolution mass spectrometry. *Free Radical Biology and Medicine* **2021**, *162*, 216–224.

(244) Salinas, L. S.; Maldonado, E.; Navarro, R. E. Stress-induced germ cell apoptosis by a p53 independent pathway in Caenorhabditis elegans. *Cell Death & Differentiation* **2006**, *13*, 2129–2139.

(245) Santiago, P. Ferrous versus ferric oral iron formulations for the treatment of iron deficiency: a clinical overview. *TheScientificWorldJournal* **2012**, 846824.

(246) Katsarou, A.; Pantopoulos, K. Basics and principles of cellular and systemic iron homeostasis. *Molecular aspects of medicine* **2020**, *75*, 100866.

(247) Dawczynski, C.; Weidauer, T.; Richert, C.; Schlattmann, P.; Dawczynski, K.; Kiehntopf, M. Nutrient Intake and Nutrition Status in Vegetarians and Vegans in Comparison to Omnivores - the Nutritional Evaluation (NuEva) Study. *Frontiers in Nutrition* **2022**, *9*, 819106.

(248) Jenkitkasemwong, S.; Wang, C.-Y.; Mackenzie, B.; Knutson, M. D. Physiologic implications of metal-ion transport by ZIP14 and ZIP8. *Biometals an international journal on the role of metal ions in biology, biochemistry, and medicine* **2012**, *25*, 643–655.

(249) Kohgo, Y.; Ikuta, K.; Ohtake, T.; Torimoto, Y.; Kato, J. Body iron metabolism and pathophysiology of iron overload. *International Journal of Hematology* **2008**, *88*, 7–15.

(250) Miyajima, H. Aceruloplasminemia. *Neuropathology official journal of the Japanese Society of Neuropathology* **2015**, *35*, 83–90.

(251) Abbasi, U.; Abbina, S.; Gill, A.; Kizhakkedathu, J. N. Development of an iron overload HepG2 cell model using ferrous ammonium citrate. *Scientific Reports* **2023**, *13*.

(252) Sturm, B.; Steinkellner, H.; Ternes, N.; Goldenberg, H.; Scheiber-Mojdehkar, B. In vitro study on the effects of iron sucrose, ferric gluconate and iron dextran on redox-active iron and oxidative stress. *Arzneimittel-Forschung* **2010**, *60*, 459–465.

(253) Piloni, N. E.; Vargas, R.; Fernández, V.; Videla, L. A.; Puntarulo, S. Effects of acute iron overload on Nrf2-related glutathione metabolism in rat brain. *Biometals an international journal on the role of metal ions in biology, biochemistry, and medicine* **2021**, *34*, 1017–1027.

(254) Lyamzaev, K. G.; Huan, H.; Panteleeva, A. A.; Simonyan, R. A.; Avetisyan, A. V.; Chernyak, B. V. Exogenous Iron Induces Mitochondrial Lipid Peroxidation, Lipofuscin Accumulation, and Ferroptosis in H9c2 Cardiomyocytes. *Biomolecules* **2024**, *14*, 730.

(255) Senchuk, M. M.; Dues, D. J.; Schaar, C. E.; Johnson, B. K.; Madaj, Z. B.; Bowman, M. J.; Winn, M. E.; van Raamsdonk, J. M. Activation of DAF-16/FOXO by reactive oxygen species contributes to longevity in long-lived mitochondrial mutants in Caenorhabditis elegans. *PLoS genetics* **2018**, *14*, e1007268.

(256) Ghadery, C.; Pirpamer, L.; Hofer, E.; Langkammer, C.; Petrovic, K.; Loitfelder, M.; Schwingenschuh, P.; Seiler, S.; Duering, M.; Jouvent, E.; Schmidt, H.; Fazekas, F.; Mangin, J.-F.; Chabriat, H.; Dichgans, M.; Ropele, S.; Schmidt, R. R2* mapping for brain iron: associations with cognition in normal aging. *Neurobiology of Aging* **2015**, *36*, 925–932.

(257) Detcheverry, F.; Senthil, S.; Narayanan, S.; Badhwar, A. Changes in levels of the antioxidant glutathione in brain and blood across the age span of healthy adults: A systematic review. *NeuroImage: Clinical* **2023**, *40*, 103503.

(258) Conrad, M.; Kagan, V. E.; Bayir, H.; Pagnussat, G. C.; Head, B.; Traber, M. G.; Stockwell, B. R. Regulation of lipid peroxidation and ferroptosis in diverse species. *Genes & development* **2018**, *32*, 602–619.

(259) Lill, R.; Hoffmann, B.; Molik, S.; Pierik, A. J.; Rietzschel, N.; Stehling, O.; Uzarska, M. A.; Webert, H.; Wilbrecht, C.; Mühlenhoff, U. The role of mitochondria in cellular iron–sulfur protein biogenesis and iron metabolism. *Biochimica et biophysica acta. Molecular cell research* **2012**, *1823*, 1491–1508.

(260) Federico, A.; Cardaioli, E.; Da Pozzo, P.; Formichi, P.; Gallus, G. N.; Radi, E. Mitochondria, oxidative stress and neurodegeneration. *Journal of the Neurological Sciences* **2012**, *322*, 254–262.

(261) Cheng, R.; Dhorajia, V. V.; Kim, J.; Kim, Y. Mitochondrial iron metabolism and neurodegenerative diseases. *Neurotoxicology* **2022**, *88*, 88–101.

(262) Martin, M. Cutadapt removes adapter sequences from high-throughput sequencing reads. *EMBnet.journal* **2011**, 10–12.

(263) Love, M. I.; Huber, W.; Anders, S. Moderated estimation of fold change and dispersion for RNA-seq data with DESeq2. *Genome Biology* **2014**, *15*, 550.

(264) Ashburner, M.; Ball, C. A.; Blake, J. A.; Botstein, D.; Butler, H.; Cherry, J. M.; Davis, A. P.; Dolinski, K.; Dwight, S. S.; Eppig, J. T.; Harris, M. A.; Hill, D. P.; Issel-Tarver, L.; Kasarskis, A.; Lewis, S.; Matese, J. C.; Richardson, J. E.; Ringwald, M.; Rubin, G. M.; Sherlock, G. Gene Ontology: tool for the unification of biology. *Nature Genetics* **2000**, *25*, 25–29.

(265) The Gene Ontology Consortium; Aleksander, S. A.; Balhoff, J.; Carbon, S.; Cherry, J. M.; Drabkin, H. J.; Ebert, D.; Feuermann, M.; Gaudet, P.; Harris, N. L.; Hill, D. P.; Lee, R.; Mi, H.; Moxon, S.; Mungall, C. J.; Muruganugan, A.; Mushayahama, T.; Sternberg, P. W.; Thomas, P. D.; van Auken, K.; Ramsey, J.; Siegele, D. A.; Chisholm, R. L.; Fey, P.; Aspromonte, M. C.; Nugnes, M. V.; Quaglia, F.; Tosatto, S.; Giglio, M.; Nadendla, S.; Antonazzo, G.; Attrill, H.; dos Santos, G.; Marygold, S.; Strelets, V.; Tabone, C. J.; Thurmond, J.; Zhou, P.; Ahmed, S. H.; Asanitthong, P.; Luna Buitrago, D.; Erdol, M. N.; Gage, M. C.; Ali Kadhum, M.; Li, K. Y. C.; Long, M.; Michalak, A.; Pesala, A.; Pritazahra, A.; Saverimuttu, S. C. C.; Su, R.; Thurlow, K. E.; Lovering, R. C.; Logie, C.; Oliferenko, S.; Blake, J.; Christie, K.; Corbani, L.; Dolan, M. E.; Ni, L.; Sitnikov, D.; Smith, C.; Cuzick, A.; Seager, J.; Cooper, L.; Elser, J.; Jaiswal, P.; Gupta, P.; Naithani, S.; Lera-Ramirez, M.; Rutherford, K.; Wood, V.; Pons, J. L. de; Dwinell, M. R.; Hayman, G. T.; Kaldunski, M. L.; Kwitek, A. E.; Laulederkind, S. J. F.; Tutaj, M. A.; Vedi, M.; Wang, S.-J.; D'Eustachio, P.; Aimo, L.; Axelsen, K.; Bridge, A.; Hyka-Nouspikel, N.; Morgat, A.; Engel, S. R.; Karra, K.; Miyasato, S. R.; Nash, R. S.; Skrzypek, M. S.; Weng, S.; Wong, E. D.; Bakker, E.; Berardini, T. Z.; Reiser, L.; Auchincloss, A.; Argoud-Puy, G.; Blatter, M.-C.; Boutet, E.; Breuza, L.; Casals-Casas, C.; Coudert, E.; Estreicher, A.; Livia Famiglietti, M.; Gos, A.; Gruaz-Gumowski, N.; Hulo, C.; Jungo, F.; Le Mercier, P.; Lieberherr, D.; Masson, P.; Pedruzzi, I.; Pourcel, L.; Poux, S.; Rivoire, C.; Sundaram, S.; Bateman, A.; Bowler-Barnett, E.; Bye-A-Jee, H.; Denny, P.; Ignatchenko, A.; Ishtiaq, R.; Lock, A.; Lussi, Y.; Magrane, M.; Martin, M. J.; Orchard, S.; Raposo, P.; Speretta, E.; Tyagi, N.; Warner, K.; Zaru, R.; Diehl, A. D.; Chan, J.; Diamantakis, S.; Raciti, D.; Zarowiecki, M.; Fisher, M.; James-Zorn, C.; Ponferrada, V.; Zorn, A.; Ramachandran, S.; Ruzicka, L.; Westerfield, M. The Gene Ontology knowledgebase in 2023. *Genetics* **2023**, *224*, iyad031.

(266) Thomas, P. D.; Ebert, D.; Muruganujan, A.; Mushayahama, T.; Albou, L.-P.; Mi, H. PANTHER: Making genome-scale phylogenetics accessible to all. *Protein science a publication of the Protein Society* **2022**, *31*, 8–22.

(267) Bonnot, T.; Gillard, M.; Nagel, D. A Simple Protocol for Informative Visualization of Enriched Gene Ontology Terms. *Bio-protocol* **2019**, *9*.

(268) Morton, K. S.; Wahl, A. K.; Meyer, J. N. The effect of common paralytic agents used for fluorescence imaging on redox tone and ATP levels in Caenorhabditis elegans. *PloS one* **2024**, *19*, e0292415.

(269) Bornhorst, J.; Ebert, F.; Lohren, H.; Humpf, H.-U.; Karst, U.; Schwerdtle, T. Effects of manganese and arsenic species on the level of energy related nucleotides in human cells. *Metallomics.* **2012**, *4*, 297–306.

(270) Matyash, V.; Liebisch, G.; Kurzchalia, T. V.; Shevchenko, A.; Schwudke, D. Lipid extraction by methyl-tert-butyl ether for high-throughput lipidomics. *Journal of Lipid Research* **2008**, *49*, 1137–1146.

(271) Schmid, R.; Heuckeroth, S.; Korf, A.; Smirnov, A.; Myers, O.; Dyrlund, T. S.; Bushuiev, R.; Murray, K. J.; Hoffmann, N.; Lu, M.; Sarvepalli, A.; Zhang, Z.; Fleischauer, M.; Dührkop, K.; Wesner, M.; Hoogstra, S. J.; Rudt, E.; Mokshyna, O.; Brungs, C.; Ponomarov, K.; Mutabdžija, L.; Damiani, T.; Pudney, C. J.; Earll, M.; Helmer, P. O.; Fallon, T. R.; Schulze, T.; Rivas-Ubach, A.; Bilbao, A.; Richter, H.; Nothias, L.-F.; Wang, M.; Orešič, M.; Weng, J.-K.; Böcker, S.; Jeibmann, A.; Hayen, H.; Karst, U.; Dorrestein, P. C.; Petras, D.; Du, X.; Pluskal, T. Integrative analysis of multimodal mass spectrometry data in MZmine 3. *Nature biotechnology* **2023**, *41*, 447–449.

(272) Weishaupt, A.-K.; Gremme, A.; Meiners, T.; Schwantes, V.; Sarnow, K.; Thiel, A.; Schwerdtle, T.; Aschner, M.; Hayen, H.; Bornhorst, J. Dysfunctional copper homeostasis in Caenorhabditis elegans affects genomic and neuronal stability. *Redox Biochemistry and Chemistry* **2024**, *10*, 100043.

(273) Mahoney, T. R.; Luo, S.; Nonet, M. L. Analysis of synaptic transmission in Caenorhabditis elegans using an aldicarb-sensitivity assay. *Nature Protocols* **2006**, *1*, 1772–1777.

(274) Hirayama, T.; Niwa, M.; Hirosawa, S.; Nagasawa, H. High-Throughput Screening for the Discovery of Iron Homeostasis Modulators Using an Extremely Sensitive Fluorescent Probe. *ACS Sensors* **2020**, *5*, 2950–2958.

(275) Presley, A. D.; Fuller, K. M.; Arriaga, E. A. MitoTracker Green labeling of mitochondrial proteins and their subsequent analysis by capillary electrophoresis with laser-induced fluorescence detection. *Journal of Chromatography B* **2003**, *793*, 141–150.

(276) Cornell, R.; Cao, W.; Harradine, B.; Godini, R.; Handley, A.; Pocock, R. Neuro-intestinal acetylcholine signalling regulates the mitochondrial stress response in Caenorhabditis elegans. *Nature Communications* **2024**, *15*, 6594.

(277) James, S. A.; Hare, D. J.; Jenkins, N. L.; Jonge, M. D. de; Bush, A. I.; McColl, G. φXANES: In vivo imaging of metal-protein coordination environments. *Scientific Reports* **2016**, *6*, 20350.

(278) Luo, H.; Zhao, X.; Wang, Z.-D.; Wu, G.; Xia, Y.; Dong, M.-Q.; Ma, Y. Sphingolipid profiling reveals differential functions of sphingolipid biosynthesis isozymes of Caenorhabditis elegans. *Journal of Lipid Research* **2024**, *65*, 100553.

(279) Kosicek, M.; Hecimovic, S. Phospholipids and Alzheimer's Disease: Alterations, Mechanisms and Potential Biomarkers. *International Journal of Molecular Sciences* **2013**, *14*, 1310–1322.

(280) Wang, H.; Jiang, X.; Wu, J.; Zhang, L.; Huang, J.; Zhang, Y.; Zou, X.; Liang, B. Iron Overload Coordinately Promotes Ferritin Expression and Fat Accumulation in Caenorhabditis elegans. *Genetics* **2016**, *203*, 241–253.

(281) Tian, Y.; Tian, Y.; Yuan, Z.; Zeng, Y.; Wang, S.; Fan, X.; Yang, D.; Yang, M. Iron Metabolism in Aging and Age-Related Diseases. *International Journal of Molecular Sciences* **2022**, *23*.

(282) Perez, V. P.; de Lima, Maria Noêmia Martins; Da Silva, R. S.; Dornelles, A. S.; Vedana, G.; Bogo, M. R.; Bonan, C. D.; Schröder, N. Iron leads to memory impairment that is associated with a decrease in acetylcholinesterase pathways. *Current neurovascular research* **2010**, *7*, 15–22.

(283) Pohanka, M. Copper, aluminum, iron and calcium inhibit human acetylcholinesterase in vitro. *Environmental toxicology and pharmacology* **2014**, *37*, 455–459.

(284) Picciotto, M. R.; Higley, M. J.; Mineur, Y. S. Acetylcholine as a neuromodulator: cholinergic signaling shapes nervous system function and behavior. *Neuron* **2012**, *76*, 116–129.

(285) Dixon, S. J.; Stockwell, B. R. The Hallmarks of Ferroptosis. *Annual Review of Cancer Biology* **2019**, *3*, 35–54.

(286) Zhang, B.; Chen, X.; Ru, F.; Gan, Y.; Li, B.; Xia, W.; Dai, G.; He, Y.; Chen, Z. Liproxstatin-1 attenuates unilateral ureteral obstruction-induced renal fibrosis by inhibiting renal tubular epithelial cells ferroptosis. *Cell Death & Disease* **2021**, *12*, 843.

(287) Friedmann Angeli, J. P.; Schneider, M.; Proneth, B.; Tyurina, Y. Y.; Tyurin, V. A.; Hammond, V. J.; Herbach, N.; Aichler, M.; Walch, A.; Eggenhofer, E.; Basavarajappa, D.; Rådmark, O.; Kobayashi, S.; Seibt, T.; Beck, H.; Neff, F.; Esposito, I.; Wanke, R.; Förster, H.; Yefremova, O.; Heinrichmeyer, M.; Bornkamm, G. W.; Geissler, E. K.; Thomas, S. B.; Stockwell, B. R.; O'Donnell, V. B.; Kagan, V. E.; Schick, J. A.; Conrad, M. Inactivation of the ferroptosis regulator Gpx4 triggers acute renal failure in mice. *Nature cell biology* **2014**, *16*, 1180–1191.

(288) Li, Y.; Sun, M.; Cao, F.; Chen, Y.; Zhang, L.; Li, H.; Cao, J.; Song, J.; Ma, Y.; Mi, W.; Zhang, X. The Ferroptosis Inhibitor Liproxstatin-1 Ameliorates LPS-Induced Cognitive Impairment in Mice. *Nutrients* **2022**, *14*.

(289) Chen, X.; Zhang, B.; Liu, T.; Feng, M.; Zhang, Y.; Zhang, C.; Yao, W.; Wan, L. Liproxstatin-1 Attenuates Morphine Tolerance through Inhibiting Spinal Ferroptosis-like Cell Death. *ACS Chemical Neuroscience* **2019**, *10*, 4824–4833.

(290) Mortensen, M. S.; Ruiz, J.; Watts, J. L. Polyunsaturated Fatty Acids Drive Lipid Peroxidation during Ferroptosis. *Cells* **2023**, *12*.

(291) Watts, J. L.; Browse, J. Genetic dissection of polyunsaturated fatty acid synthesis in Caenorhabditis elegans. *Proceedings of the National Academy of Sciences* **2002**, *99*, 5854–5859.

(292) Eto, S.; Matsumura, R.; Shimane, Y.; Fujimi, M.; Berhanu, S.; Kasama, T.; Kuruma, Y. Phospholipid synthesis inside phospholipid membrane vesicles. *Communications Biology* **2022**, *5*, 1016.

(293) Yong, Y.-Y.; Yan, L.; Wang, B.-D.; Fan, D.-S.; Guo, M.-S.; Yu, L.; Wu, J.-M.; Qin, D.-L.; Law, B. Y.-K.; Wong, V. K.-W.; Yu, C.-L.; Zhou, X.-G.; Wu, A.-G. Penthorum chinense Pursh inhibits ferroptosis in cellular and Caenorhabditis elegans models of Alzheimer's disease. *Phytomedicine international journal of phytotherapy and phytopharmacology* **2024**, *127*, 155463.

(294) Sarparast, M.; Pourmand, E.; Hinman, J.; Vonarx, D.; Reason, T.; Zhang, F.; Paithankar, S.; Chen, B.; Borhan, B.; Watts, J. L.; Alan, J.; Lee, K. S. S. Dihydroxy-Metabolites of Dihomo-γ-linolenic Acid Drive Ferroptosis-Mediated Neurodegeneration. *ACS Central Science* **2023**, *9*, 870–882.

(295) Chen, L.; Min, J.; Wang, F. Copper homeostasis and cuproptosis in health and disease. *Signal transduction and targeted therapy* **2022**, *7*, 378.

(296) Zhang, Y.; Zhao, C.; Zhang, H.; Liu, R.; Wang, S.; Pu, Y.; Yin, L. Integrating transcriptomics and behavior tests reveals how the C. elegans responds to copper induced aging. *Ecotoxicology and Environmental Safety* **2021**, *222*, 112494.

(297) Song, S.; Zhang, X.; Wu, H.; Han, Y.; Zhang, J.; Ma, E.; Guo, Y. Molecular basis for antioxidant enzymes in mediating copper detoxification in the nematode Caenorhabditis elegans. *PloS one* **2014**, *9*, e107685.

(298) Squitti, R.; Faller, P.; Hureau, C.; Granzotto, A.; White, A. R.; Kepp, K. P. Copper Imbalance in Alzheimer's Disease and Its Link with the Amyloid Hypothesis: Towards a Combined Clinical, Chemical, and Genetic Etiology. *Journal of Alzheimer's disease JAD* **2021**, *83*, 23–41.

(299) Borchard, S.; Raschke, S.; Zak, K. M.; Eberhagen, C.; Einer, C.; Weber, E.; Müller, S. M.; Michalke, B.; Lichtmannegger, J.; Wieser, A.; Rieder, T.; Popowicz, G. M.; Adamski, J.; Klingenspor, M.; Coles, A. H.; Viana, R.; Vendelbo, M. H.; Sandahl, T. D.; Schwerdtle, T.; Plitz, T.; Zischka, H. Bis-choline tetrathiomolybdate prevents copper-induced blood-brain barrier damage. *Life science alliance* **2022**, *5*.

(300) Maares, M.; Haupt, A.; Schüßler, C.; Kulike-Koczula, M.; Hackler, J.; Keil, C.; Mohr, I.; Schomburg, L.; Süssmuth, R. D.; Zischka, H.; Merle, U.; Haase, H. A fluorometric assay to determine labile copper(II) ions in serum. *Scientific Reports* **2023**, *13*, 12807.

(301) Tassone, G.; Kola, A.; Valensin, D.; Pozzi, C. Dynamic Interplay between Copper Toxicity and Mitochondrial Dysfunction in Alzheimer's Disease. *Life (Basel, Switzerland)* **2021**, *11*.

(302) Kim, G. H.; Kim, J. E.; Rhie, S. J.; Yoon, S. The Role of Oxidative Stress in Neurodegenerative Diseases. *Experimental neurobiology* **2015**, *24*, 325–340.

(303) Grotto, D.; Santa Maria, L. D.; Boeira, S.; Valentini, J.; Charão, M. F.; Moro, A. M.; Nascimento, P. C.; Pomblum, V. J.; Garcia, S. C. Rapid quantification of malondialdehyde in plasma by high performance liquid chromatography-visible detection. *Journal of pharmaceutical and biomedical analysis* **2007**, *43*, 619–624.

(304) Falabella, M.; Vernon, H. J.; Hanna, M. G.; Claypool, S. M.; Pitceathly, R. D. S. Cardiolipin, Mitochondria, and Neurological Disease. *Trends in endocrinology and metabolism: TEM* **2021**, *32*, 224–237.

(305) Monteiro-Cardoso, V. F.; Oliveira, M. M.; Melo, T.; Domingues, M. R. M.; Moreira, P. I.; Ferreiro, E.; Peixoto, F.; Videira, R. A. Cardiolipin profile changes are associated to the early synaptic mitochondrial dysfunction in Alzheimer's disease. *Journal of Alzheimer's disease JAD* **2015**, *43*, 1375–1392.

(306) Yurkova, I. L.; Arnhold, J.; Fitzl, G.; Huster, D. Fragmentation of mitochondrial cardiolipin by copper ions in the Atp7b-/- mouse model of Wilson's disease. *Chemistry and physics of lipids* **2011**, *164*, 393–400.

(307) Wandt, V. K.; Winkelbeiner, N.; Bornhorst, J.; Witt, B.; Raschke, S.; Simon, L.; Ebert, F.; Kipp, A. P.; Schwerdtle, T. A matter of concern - Trace element dyshomeostasis and genomic stability in neurons. *Redox biology* **2021**, *41*, 101877.

(308) Porta-de-la-Riva, M.; Fontrodona, L.; Villanueva, A.; Cerón, J. Basic Caenorhabditis elegans methods: synchronization and observation. *Journal of visualized experiments JoVE* **2012**, e4019.

(309) Grintzalis, K.; Zisimopoulos, D.; Grune, T.; Weber, D.; Georgiou, C. D. Method for the simultaneous determination of free/protein malondialdehyde and lipid/protein hydroperoxides. *Free radical biology & medicine* **2013**, *59*, 27–35.

(310) Nicolai, M. M.; Weishaupt, A.-K.; Baesler, J.; Brinkmann, V.; Wellenberg, A.; Winkelbeiner, N.; Gremme, A.; Aschner, M.; Fritz, G.; Schwerdtle, T.; Bornhorst, J. Effects of Manganese on Genomic Integrity in the Multicellular Model Organism Caenorhabditis elegans. *International Journal of Molecular Sciences* **2021**, *22*.

(311) Mahoney, T. R. Analysis of synaptic transmission in Caenorhabditis elegans using an aldicarb-sensitivity assay. *Nature Protocols* **2006**.

(312) Poetsch, A. R. The genomics of oxidative DNA damage, repair, and resulting mutagenesis. *Computational and structural biotechnology journal* **2020**, *18*, 207–219.

(313) Weishaupt, A.-K.; Kubens, L.; Ruecker, L.; Schwerdtle, T.; Aschner, M.; Bornhorst, J. A Reliable Method Based on Liquid Chromatography–Tandem Mass Spectrometry for the Simultaneous Quantification of Neurotransmitters in Caenorhabditis elegans. *Molecules* **2023**, *28*, 5373.

(314) Ge, E. J.; Bush, A. I.; Casini, A.; Cobine, P. A.; Cross, J. R.; DeNicola, G. M.; Dou, Q. P.; Franz, K. J.; Gohil, V. M.; Gupta, S.; Kaler, S. G.; Lutsenko, S.; Mittal, V.; Petris, M. J.; Polishchuk, R.; Ralle, M.; Schilsky, M. L.; Tonks, N. K.; Vahdat, L. T.; van Aelst, L.; Xi, D.; Yuan, P.; Brady, D. C.; Chang, C. J. Connecting copper and cancer: from transition metal signalling to metalloplasia. *Nature reviews. Cancer* **2022**, *22*, 102–113.

(315) Peres, T. V.; Arantes, L. P.; Miah, M. R.; Bornhorst, J.; Schwerdtle, T.; Bowman, A. B.; Leal, R. B.; Aschner, M. Role of Caenorhabditis elegans AKT-1/2 and SGK-1 in Manganese Toxicity. *Neurotoxicity research* **2018**, *34*, 584–596.

(316) Hamann, I.; Petroll, K.; Grimm, L.; Hartwig, A.; Klotz, L.-O. Insulin-like modulation of Akt/FoxO signaling by copper ions is independent of insulin receptor. *Archives of biochemistry and biophysics* **2014**, *558*, 42–50.

(317) Gubert, P.; Puntel, B.; Lehmen, T.; Bornhorst, J.; Avila, D. S.; Aschner, M.; Soares, F. A. A. Reversible reprotoxic effects of manganese through DAF-16 transcription factor activation and vitellogenin downregulation in Caenorhabditis elegans. *Life sciences* **2016**, *151*, 218–223.

(318) Urban, N.; Tsitsipatis, D.; Hausig, F.; Kreuzer, K.; Erler, K.; Stein, V.; Ristow, M.; Steinbrenner, H.; Klotz, L.-O. Non-linear impact of glutathione depletion on C. elegans life span and stress resistance. *Redox biology* **2017**, *11*, 502–515.

(319) He, H.; Zou, Z.; Wang, B.; Xu, G.; Chen, C.; Qin, X.; Yu, C.; Zhang, J. Copper Oxide Nanoparticles Induce Oxidative DNA Damage and Cell Death via Copper Ion-Mediated P38 MAPK Activation in Vascular Endothelial Cells. *International journal of nanomedicine* **2020**, *15*, 3291–3302.

(320) Wang, S.; Wu, L.; Wang, Y.; Luo, X.; Lu, Y. Copper-induced germline apoptosis in Caenorhabditis elegans: the independent roles of DNA damage response signaling and the dependent roles of MAPK cascades. *Chemico-biological interactions* **2009**, *180*, 151–157.

(321) Franco, R.; Schoneveld, O. J.; Pappa, A.; Panayiotidis, M. I. The central role of glutathione in the pathophysiology of human diseases. *Archives of physiology and biochemistry* **2007**, *113*, 234–258.

(322) Cui, C.; Kong, M.; Wang, Y.; Zhou, C.; Ming, H. Characterization of polyphosphate kinases for the synthesis of GSH with ATP regeneration from AMP. *Enzyme and microbial technology* **2021**, *149*, 109853.

(323) Baldissera, M. D.; Souza, C. F.; Barroso, D. C.; Pereira, R. S.; Alessio, K. O.; Bizzi, C.; Baldisserotto, B.; Val, A. L. Acute exposure to environmentally relevant concentrations of copper affects branchial and hepatic phosphoryl transfer network of Cichlasoma amazonarum: Impacts on bioenergetics homeostasis. *Comparative Biochemistry and Physiology Part C: Toxicology & Pharmacology* **2020**, *238*, 108846.

(324) Bonora, M.; Patergnani, S.; Rimessi, A.; Marchi, E. de; Suski, J. M.; Bononi, A.; Giorgi, C.; Marchi, S.; Missiroli, S.; Poletti, F.; Wieckowski, M. R.; Pinton, P. ATP synthesis and storage. *Purinergic signalling* **2012**, *8*, 343–357.

(325) Croft, T.; Venkatakrishnan, P.; Lin, S.-J. NAD+ Metabolism and Regulation: Lessons From Yeast. *Biomolecules* **2020**, *10*.

(326) James Theoga Raj, C.; Croft, T.; Venkatakrishnan, P.; Groth, B.; Dhugga, G.; Cater, T.; Lin, S.-J. The copper-sensing transcription factor Mac1, the histone deacetylase Hst1, and nicotinic acid regulate de novo NAD+ biosynthesis in budding yeast. *The Journal of biological chemistry* **2019**, *294*, 5562–5575.

(327) Li, M.; Li, Y.; Chen, J.; Wei, W.; Pan, X.; Liu, J.; Liu, Q.; Leu, W.; Zhang, L.; Yang, X.; Lu, J.; Wang, K. Copper ions inhibit S-adenosylhomocysteine hydrolase by causing dissociation of NAD+ cofactor. *Biochemistry* **2007**, *46*, 11451–11458.

(328) Anadozie, S. O.; Aduma, A. U.; Adewale, O. B. Alkaloid-rich extract of Buchholzia coriacea seed mitigate the effect of copper-induced toxicity in Drosophila melanogaster. *Vegetos* **2023**.

(329) Rehman, M.; Maqbool, Z.; Peng, D.; Liu, L. Morpho-physiological traits, antioxidant capacity and phytoextraction of copper by ramie (Boehmeria nivea L.) grown as fodder in copper-contaminated soil. *Environmental science and pollution research international* **2019**, *26*, 5851–5861.

(330) Kowalczyk, P.; Sulejczak, D.; Kleczkowska, P.; Bukowska-Ośko, I.; Kucia, M.; Popiel, M.; Wietrak, E.; Kramkowski, K.; Wrzosek, K.; Kaczyńska, K. Mitochondrial Oxidative Stress-A Causative Factor and Therapeutic Target in Many Diseases. *International Journal of Molecular Sciences* **2021**, *22*.

(331) Blume, B.; Schwantes, V.; Witting, M.; Hayen, H.; Schmitt-Kopplin, P.; Helmer, P. O.; Michalke, B. Lipidomic and Metallomic Alteration of Caenorhabditis elegans after Acute and Chronic Manganese, Iron, and Zinc Exposure with a Link to Neurodegenerative Disorders. *Journal of Proteome Research* **2023**, *22*, 837–850.

(332) Pope, S.; Land, J. M.; Heales, S. J. R. Oxidative stress and mitochondrial dysfunction in neurodegeneration; cardiolipin a critical target? *Biochimica et biophysica acta* **2008**, *1777*, 794–799.

(333) Sadiq, R.; Khan, Q. M.; Mobeen, A.; Hashmat, A. J. In vitro toxicological assessment of iron oxide, aluminium oxide and copper nanoparticles in prokaryotic and eukaryotic cell types. *Drug and chemical toxicology* **2015**, *38*, 152–161.

(334) Husain, N.; Mahmood, R. Copper(II) generates ROS and RNS, impairs antioxidant system and damages membrane and DNA in human blood cells. *Environmental science and pollution research international* **2019**, *26*, 20654–20668.

(335) Bürkle, A. Poly(ADP-ribose). The most elaborate metabolite of NAD+. *The FEBS journal* **2005**, *272*, 4576–4589.

(336) Schwerdtle, T.; Hamann, I.; Jahnke, G.; Walter, I.; Richter, C.; Parsons, J. L.; Dianov, G. L.; Hartwig, A. Impact of copper on the induction and repair of oxidative DNA damage, poly(ADP-ribosyl)ation and PARP-1 activity. *Molecular nutrition & food research* **2007**, *51*, 201–210.

(337) Karginova, O.; Weekley, C. M.; Raoul, A.; Alsayed, A.; Wu, T.; Lee, S. S.-Y.; He, C.; Olopade, O. I. Inhibition of Copper Transport Induces Apoptosis in Triple-Negative Breast Cancer Cells and Suppresses Tumor Angiogenesis. *Molecular cancer therapeutics* **2019**, *18*, 873–885.

(338) Jin, J.; Ma, M.; Shi, S.; Wang, J.; Xiao, P.; Yu, H.-F.; Zhang, C.; Guo, Q.; Yu, Z.; Lou, Z.; Teng, C.-B. Copper enhances genotoxic drug resistance via ATOX1 activated DNA damage repair. *Cancer letters* **2022**, *536*, 215651.

(339) Becherel, O. J.; Jakob, B.; Cherry, A. L.; Gueven, N.; Fusser, M.; Kijas, A. W.; Peng, C.; Katyal, S.; McKinnon, P. J.; Chen, J.; Epe, B.; Smerdon, S. J.; Taucher-Scholz, G.; Lavin, M. F. CK2 phosphorylation-dependent interaction between aprataxin and MDC1 in the DNA damage response. *Nucleic acids research* **2010**, *38*, 1489–1503.

(340) Harris, J. L.; Jakob, B.; Taucher-Scholz, G.; Dianov, G. L.; Becherel, O. J.; Lavin, M. F. Aprataxin, poly-ADP ribose polymerase 1 (PARP-1) and apurinic endonuclease 1 (APE1) function together to protect the genome against oxidative damage. *Human Molecular Genetics* **2009**, *18*, 4102–4117.

(341) Bornhorst, J.; Meyer, S.; Weber, T.; Böker, C.; Marschall, T.; Mangerich, A.; Beneke, S.; Bürkle, A.; Schwerdtle, T. Molecular mechanisms of Mn induced neurotoxicity: RONS generation, genotoxicity, and DNA-damage response. *Molecular nutrition & food research* **2013**, *57*, 1255–1269.

(342) Hegde, M. L.; Hegde, P. M.; Holthauzen, L. M. F.; Hazra, T. K.; Rao, K. S. J.; Mitra, S. Specific Inhibition of NEIL-initiated repair of oxidized base damage in human genome by copper and iron: potential etiological linkage to neurodegenerative diseases. *The Journal of biological chemistry* **2010**, *285*, 28812–28825.

(343) Minniti, A. N.; Rebolledo, D. L.; Grez, P. M.; Fadic, R.; Aldunate, R.; Volitakis, I.; Cherny, R. A.; Opazo, C.; Masters, C.; Bush, A. I.; Inestrosa, N. C. Intracellular amyloid formation in muscle cells of Abeta-transgenic Caenorhabditis elegans: determinants and physiological role in copper detoxification. *Molecular neurodegeneration* **2009**, *4*, 2.

(344) Metaxas, A. Imbalances in Copper or Zinc Concentrations Trigger Further Trace Metal Dyshomeostasis in Amyloid-Beta Producing Caenorhabditis elegans. *Frontiers in neuroscience* **2021**, *15*, 755475.

(345) Squitti, R.; Cataldi, C.; Gigante, L.; Marianetti, M.; Rosari, M.; Mariani, S.; Bucossi, S.; Mastromoro, G.; Ventriglia, M.; Simonelli, I.; Tondolo, V.; Singh, P.; Kumar, A.; Pal, A.; Rongioletti, M. Non-Ceruloplasmin Copper Identifies a Subtype of Alzheimer's Disease (CuAD): Characterization of the Cognitive Profile and Case of a CuAD Patient Carrying an RGS7 Stop-Loss Variant. *International Journal of Molecular Sciences* **2023**, *24*.

(346) Dabbish, N. S.; Raizen, D. M. GABAergic synaptic plasticity during a developmentally regulated sleep-like state in C. elegans. *The Journal of neuroscience the official journal of the Society for Neuroscience* **2011**, *31*, 15932–15943.

(347) D'Ambrosi, N.; Rossi, L. Copper at synapse: Release, binding and modulation of neurotransmission. *Neurochemistry international* **2015**, *90*, 36–45.

(348) Kelner, G. S.; Lee, M.; Clark, M. E.; Maciejewski, D.; McGrath, D.; Rabizadeh, S.; Lyons, T.; Bredesen, D.; Jenner, P.; Maki, R. A. The copper transport protein Atox1 promotes neuronal survival. *The Journal of biological chemistry* **2000**, *275*, 580–584.

(349) Horvath, I.; Blockhuys, S.; Šulskis, D.; Holgersson, S.; Kumar, R.; Burmann, B. M.; Wittung-Stafshede, P. Interaction between Copper Chaperone Atox1 and Parkinson's Disease Protein α-Synuclein Includes Metal-Binding Sites and Occurs in Living Cells. *ACS Chemical Neuroscience* **2019**, *10*, 4659–4668.

(350) Milman, N.; Jønsson, L.; Dyre, P.; Pedersen, P. L.; Larsen, L. G. Ferrous bisglycinate 25 mg iron is as effective as ferrous sulfate 50 mg iron in the prophylaxis of iron deficiency and anemia during pregnancy in a randomized trial. *Journal of perinatal medicine* **2014**, *42*, 197–206.

(351) Man, Y.; Xu, T.; Adhikari, B.; Zhou, C.; Wang, Y.; and Wang, B. Iron supplementation and iron-fortified foods: a review. *Critical Reviews in Food Science and Nutrition* **2022**, *62*, 4504–4525.

(352) Pai, A. B.; Boyd, A. V.; McQuade, C. R.; Harford, A.; Norenberg, J. P.; Zager, P. G. Comparison of oxidative stress markers after intravenous administration of iron dextran, sodium ferric gluconate, and iron sucrose in patients undergoing hemodialysis. *Pharmacotherapy* **2007**, *27*, 343–350.

(353) Michalke, B.; Willkommen, D.; Venkataramani, V. Iron Redox Speciation Analysis Using Capillary Electrophoresis Coupled to Inductively Coupled Plasma Mass Spectrometry (CE-ICP-MS). *Frontiers in Chemistry* **2019**, *Volume 7 - 2019*.

(354) Pandey, T.; Wang, B.; Wang, C.; Zu, J.; Deng, H.; Shen, K.; do Vale, G. D.; McDonald, J. G.; Ma, D. K. LPD-3 as a megaprotein brake for aging and insulin-mTOR signaling in C. elegans. *Cell reports* **2024**, *43*, 113899.

(355) Grad, L. I.; Sayles, L. C.; Lemire, B. D. Isolation and Functional Analysis of Mitochondria From the Nematode Caenorhabditis elegans. In *Mitochondria: Practical Protocols;* Leister, D.; Herrmann, J. M., Eds.; Humana Press: Totowa, NJ, 2007; pp 51–66.

(356) Li, Z.; Lu, N.; He, X.; Zhou, Z. Monitoring the clearance of apoptotic and necrotic cells in the nematode Caenorhabditis elegans. *Methods in molecular biology (Clifton, N.J.)* **2013**, *1004*, 183–202.

(357) Hou, Y.; Dan, X.; Babbar, M.; Wei, Y.; Hasselbalch, S. G.; Croteau, D. L.; Bohr, V. A. Ageing as a risk factor for neurodegenerative disease. *Nature Reviews Neurology* **2019**, *15*, 565–581.

(358) Rund, K. M.; Heylmann, D.; Seiwert, N.; Wecklein, S.; Oger, C.; Galano, J.-M.; Durand, T.; Chen, R.; Gueler, F.; Fahrer, J.; Bornhorst, J.; Schebb, N. H. Formation of trans-epoxy fatty acids correlates with formation of isoprostanes and could serve as biomarker of oxidative stress. *Prostaglandins & other lipid mediators* **2019**, *144*, 106334.

(359) Hider, R.; Aviles, M. V.; Chen, Y.-L.; Latunde-Dada, G. O. The Role of GSH in Intracellular Iron Trafficking. *International Journal of Molecular Sciences* **2021**, *22*.

(360) Ng, L. F.; Gruber, J.; Cheah, I. K.; Goo, C. K.; Cheong, W. F.; Shui, G.; Sit, K. P.; Wenk, M. R.; Halliwell, B. The mitochondria-targeted antioxidant MitoQ extends lifespan and improves healthspan of a transgenic Caenorhabditis elegans model of Alzheimer disease. *Free Radical Biology and Medicine* **2014**, *71*, 390–401.

(361) Qiu, H.; Ye, C. Phospholipid Biosynthesis: An Unforeseen Modulator of Nuclear Metabolism. *Biol. Cell.* **2025**, *117*, e70002.

(362) Sawin, E. R.; Ranganathan, R.; Horvitz, H. C. elegans Locomotory Rate Is Modulated by the Environment through a Dopaminergic Pathway and by Experience through a Serotonergic Pathway. *Neuron* **2000**, *26*, 619–631.

(363) Fire, A.; Xu, S.; Montgomery, M. K.; Kostas, S. A.; Driver, S. E.; Mello, C. C. Potent and specific genetic interference by double-stranded RNA in Caenorhabditis elegans. *Nature* **1998**, *391*, 806–811.

(364) Jansová, H.; Kubeš, J.; Reimerová, P.; Štěrbová-Kovaříková, P.; Roh, J.; Šimůnek, T. 2,6-Dihydroxybenzaldehyde Analogues of the Iron Chelator Salicylaldehyde Isonicotinoyl Hydrazone: Increased Hydrolytic Stability and Cytoprotective Activity against Oxidative Stress. *Chemical research in toxicology* **2018**, *31*, 1151–1163.

(365) Huang, J.; Chen, S.; Hu, L.; Niu, H.; Sun, Q.; Li, W.; Tan, G.; Li, J.; Jin, L.; Lyu, J.; Zhou, H. Mitoferrin-1 is Involved in the Progression of Alzheimer's Disease Through Targeting Mitochondrial Iron Metabolism in a Caenorhabditis elegans Model of Alzheimer's Disease. *Neuroscience* **2018**, *385*, 90–101.

(366) Martins, A. C.; Virgolini, M. B.; Tinkov, A. A.; Skalny, A. V.; Tirumala, R. P.; Farina, M.; Santamaria, A.; Lu, R.; Aschner, M. Iron overload and neurodegenerative diseases: What can we learn from Caenorhabditis elegans? *Toxicology Research and Application* **2022**, *6*, 23978473221091852.

(367) Grotto, D.; Maria, L. S.; Valentini, J.; Paniz, C.; Schmitt, G.; Garcia, S. C.; Pomblum, V. J.; Rocha, J. B. T.; Farina, M. Importance of the lipid peroxidation biomarkers and methodological aspects FOR malondialdehyde quantification. *Quím. Nova* **2009**, *32*, 169–174.

(368) Liebisch, G.; Fahy, E.; Aoki, J.; Dennis, E. A.; Durand, T.; Ejsing, C. S.; Fedorova, M.; Feussner, I.; Griffiths, W. J.; Köfeler, H.; Merrill, A. H., JR; Murphy, R. C.; O'Donnell, V. B.; Oskolkova, O.; Subramaniam, S.; Wakelam, M. J. O.; Spener, F. Update on LIPID MAPS classification, nomenclature, and shorthand notation for MS-derived lipid structures. *Journal of Lipid Research* **2020**, *61*, 1539–1555.

(369) Rudt, E.; Feldhaus, M.; Margraf, C. G.; Schlehuber, S.; Schubert, A.; Heuckeroth, S.; Karst, U.; Jeck, V.; Meyer, S. W.; Korf, A.; Hayen, H. Comparison of Data-Dependent Acquisition, Data-Independent Acquisition, and Parallel Reaction Monitoring in Trapped Ion Mobility Spectrometry-Time-of-Flight Tandem Mass Spectrometry-Based Lipidomics. *Analytical Chemistry* **2023**, *95*, 9488–9496.

(370) Kind, T.; Liu, K.-H.; Lee, D. Y.; DeFelice, B.; Meissen, J. K.; Fiehn, O. LipidBlast in silico tandem mass spectrometry database for lipid identification. *Nature methods* **2013**, *10*, 755–758.

(371) Tsugawa, H.; Ikeda, K.; Takahashi, M.; Satoh, A.; Mori, Y.; Uchino, H.; Okahashi, N.; Yamada, Y.; Tada, I.; Bonini, P.; Higashi, Y.; Okazaki, Y.; Zhou, Z.; Zhu, Z.-J.; Koelmel,

J.; Cajka, T.; Fiehn, O.; Saito, K.; Arita, M.; Arita, M. A lipidome atlas in MS-DIAL 4. *Nature biotechnology* **2020**, *38*, 1159–1163.

(372) Korf, A.; Vosse, C.; Schmid, R.; Helmer, P. O.; Jeck, V.; Hayen, H. Three-dimensional Kendrick mass plots as a tool for graphical lipid identification. *Rapid communications in mass spectrometry RCM* **2018**, *32*, 981–991.

(373) Oliveros, J. C. Venny. An interactive tool for comparing lists with Venn's diagrams. *https://bioinfogp.cnb.csic.es/tools/venny/index.html* **2007 - 2015**.

(374) Helmer, P. O.; Wienken, C. M.; Korf, A.; Hayen, H. Mass spectrometric investigation of cardiolipins and their oxidation products after two-dimensional heart-cut liquid chromatography. *Journal of chromatography. A* **2020**, *1619*, 460918.

(375) Myers, O. D.; Sumner, S. J.; Li, S.; Barnes, S.; Du, X. One Step Forward for Reducing False Positive and False Negative Compound Identifications from Mass Spectrometry Metabolomics Data: New Algorithms for Constructing Extracted Ion Chromatograms and Detecting Chromatographic Peaks. *Analytical Chemistry* **2017**, *89*, 8696–8703.

CCV